UNIVERSITY OF LIVERPOOL

School of Engineering

Characterisation of the Damage of Bituminous Materials Prepared with Warm Mix Asphalt Additives

Thesis submitted in accordance with the requirements of

University of Liverpool for the degree of Doctor in Philosophy by

Mohammed Adnan S. Sadeq

B.Sc., M.Sc.

July 2017

Abstract

Warm mix asphalt (WMA) is a relatively new technology that allows asphalt mixtures to be mixed and compacted at lower temperatures than the conventional hot mix asphalt (HMA). Previous WMA investigations have predominantly been limited to basic performance indicators and properties, especially in the Middle East region. Implementing the WMA technology in the asphalt pavement industry in the State of Qatar requires investigation of material properties and performance under the prevailing climatic conditions in the country. This study provides a fundamental material evaluation of WMA material damage using advanced testing and analysis approaches. The results led to a conceptual understanding of the impact of WMA additives on asphalt materials' performance. It was found that Sasobit is the most effective WMA additive, as it increases the material's (bitumen and mastic) stiffness, enhances resistance to rutting, and causes a reduction in the ageing effect on fatigue.

The study also evaluated the impact of ageing on WMA material damage. Fine Aggregate Mix (FAM) samples were placed in an accelerated weathering machine that was controlled to simulate the climatic condition in Qatar (UV light and heat). The samples showed significant changes after ageing in the weathering instrument. The aged FAM samples were then subjected to repeated creep and recovery testing and the performance of the material at different ageing levels was studied. The results showed that the Sasobit mix had the highest ability to recover damage induced during the loading period. The results showed a high correlation between the recovery modulus of the material and the reduced damage captured during the unloading. In order to further characterise damage, air void sizes in the asphalt mixture before and after adopting the repeated creep and recovery test were examined by scanning them using the X-Ray CT system. The air voids of the control mix (without any WMA additives)

showed a remarkable change after the repeated creep and recovery test; however, all WMA samples had lower air void sizes and minor changes after testing. The CT imaging also confirmed that ageing using the UV light has an insignificant impact on air void changing before and after the repeated loading test.

The results confirmed the benefits of implementing the WMA technology in the asphalt industry in the State of Qatar. This is particularly the case for Sasobit, which showed significant improvement in the performance testing results in comparison with the control mix and other WMA additives.

Dedication

To my father, mother, wife, and my country, ‘Palestine’.

Acknowledgements

Before all, no words can describe my gratefulness and appreciation to my Lord (Allah) for giving me the opportunity, patience, knowledge and strength to achieve my goals.

I take this opportunity to express my sincere gratitude to my generous supervisors, Dr Hussain Al-Khalid and Dr Eyad Masad. Their continuous support and advice has had a huge role in me reaching this point in my life and submitting this work. I consider myself fortunate to have had them as my advisors. It was an honour to work under their supervision and learn from their vast research expertise.

Moreover, I sincerely acknowledge the invaluable care and support from my parents, Adnan Sadek and Samia Dahlan, who gave me everything that made me what I am today and I wish I could make them proud of me.

Furthermore, I would like to acknowledge my beloved wife, Rana Jamous, for her patience and encouragement, and for believing in me to complete my research project. She has brought joy into my life and I hope I can return the same to her one day.

Finally, many thanks to my brothers, Husam and Haytham, and sister, Lubna. Husam has been by my side since the first day in my research journey and he has never let me down. His guidance has always been helpful to me, and I will be grateful to him all my life. Special thanks to Haytham for being always available to encourage me to achieve my goals and for helping me look at the world differently; and to my lovely sister, Lubna, who has looked after me consistently and stood by me against the diverse challenges I have encountered.

List of Abbreviations

AASHTO	American Association of State Highway and Transportation Officials
AMPT	Asphalt Mixture Performance Machine
ANOVA	Analysis of Variance
ASTM	American Society for Testing and Materials
BH	Beam Hardening
DE	Dissipated Energy
DNI	Direct Normal Irradiation
DHI	Diffuse Horizontal Irradiation
DIP	Digital Image Processing
DPSE	Dissipated Pseudo Strain Energy
DSC	Differential Scanning Calorimetry
DSR	Dynamic Shear Rheometer
ecdf	Empirical Cumulative Distribution Function
FAM	Fine Aggregate Mix
FTIR	Fourier Transform Infrared Spectroscopy
GHI	Global Horizontal Irradiance
GIS	Geographic Information System
HMA	Hot Mix Asphalt
ICR	Infrastructure Carbon Review
IDT	Indirect Tensile Test
IR	Infrared
ITS	Indirect Tensile Strength
LDH	Layered Double Hydroxides
LVE	Linear Viscoelastic
MET	Minimum Error Thresholding
MSCR	Multiple Stress Creep Recovery
NLVE	Nonlinear Viscoelastic
NMR	Nuclear Magnetic Resonance
NPVE	Nonlinear Plasto-viscoelastic
PAV	Pressurised Ageing Vessel
PG	Performance Grading
PMB	Polymer Modified Bitumen
RAP	Reclaimed Asphalt Pavement
RCDE	Rate of Change of Dissipated Energy
RCRT	Repeated Creep Recovery Test
RM	Recovery Modulus
RTFO	Rolling Thin Film Oven
RV	Rotational Viscometer
SBS	Styrene-Butadiene-Styrene
S-VECD	Simplified Viscoelastic Continuum Damage

TFOT	Thin Film Oven Test
TGA	Thermogravimetric Analysis
UV	Ultra-Violate
VE	Viscoelastic
VECD	Viscoelastic Continuum Damage
VIS	Visible
VP	Viscoplastic
W-FAM	Warm Fine Aggregate Mixture
WMA	Warm Mix Asphalt
X-Ray CT	X-Ray Computed Tomography

Table of Contents

List of Figures

List of Tables

1. Introduction

Warm mix asphalt (WMA) technology was introduced by different European countries in 1995 and has since attracted the attention of practitioners and researchers worldwide (National Center for Asphalt Technology, 2005). Numerous international organisations have started producing WMA additives using different processes and materials. These additives are mixed with bitumen to reduce the mixing and compaction temperatures of asphalt mixtures to 20 to 30ºC lower than the conventional hot mix asphalt (HMA), which usually reach 160-180ºC for mixing and 130-140ºC for compaction. The advantages of using WMA additives extended further by lessening the fuel consumption and smoke emission during construction. These advantages made the WMA technology to be considered as an eco-friendly product and encouraged researchers to study the additive's influence on pavement performance.

Advantages of using WMA can be classified into three categories: environmental aspects, workers' comfort and field performance (Xiao and Amirkhanian, 2010). Using the WMA technologies increases the ability to keep the mixture workable at an acceptable level for longer periods. This allows the mixture to be placed and compacted over longer distances (Caro *et al.*, 2012; Feipeng and Bradley, 2012; Mogawer *et al.*, 2013; Vaiana *et al.*, 2013; Xie *et al.*, 2013; Ates *et al.*, 2015). In addition, it allows the road to be opened to traffic in a shorter period and for more roads to be paved than would be covered by HMA.

The State of Qatar emphasises the environmental aspects of construction through the Qatar Green Building Council and other institutions. These initiatives were established to support more eco-friendly construction activities that consider Qatar's environment

and lower the construction cost through reducing energy consumption sources. Implementing the WMA technology in the asphalt pavement industry would contribute partially to achieving that goal. The public works authority in the State of Qatar announced the expressways programme which cover construction of 800 km of new roads by 2030 (Public Works Authority, 2017).

The implementation of the WMA technology in the construction specifications for the State of Qatar requires an in-depth investigation of its properties and performance when locally available materials are used and under local climatic conditions. However, the current literature is still missing important aspects of using WMA technology that would affect the decision to implement it in the country's specification. The decision to implement WMA technology in the asphalt pavement construction industry should be built on advanced research studies that examine the performance of the WMA material on roads and when experiencing local loading and environmental conditions.

Qatar experiences harsh environmental conditions during the summer that directly affect the performance of its asphalt pavements. The UV index in Qatar is high most of the year (can reach up to 11), which has a significant effect on the physical properties of the materials. Hence, studying the effect of UV light on asphalt material properties would confirm the feasibility of implementing WMA technology in a high UV-index country like Qatar. On the other hand, the current studies and practical outcomes that cover the WMA technology's performance do not exceed the basic properties and performance indicators that explain the performance of WMA pavements. Hence, the execution of a profound and advanced study of the WMA material behaviour is significant and would clarify the practicability of employing the use of WMA technology in the national specifications and construction codes.

In this thesis, the WMA technology was included in an advanced performance testing and evaluation process. The study began with a basic material performance evaluation in order to understand the overall behaviour of WMA material. Then, a new ageing protocol was proposed that simulated Qatar's climate by accounting for the UV light in an accelerated weathering conditioning. The aged WMA materials were later involved in a developed testing protocol and analysis approach that can analytically determine the damage to material. The damage incorporated with the testing was investigated in depth to evaluate changes in crack sizes due to repeated loading.

1.1. Motivation

By going through the literature, several shortcomings were found in the research area that drove the author to conduct the research documented in this thesis. These shortcomings were as follows:

- There have been very few studies in the Middle East about the efficacy of using the WMA technology. These studies were concerned about the basic behaviour of the asphalt material mixed with WMA additives and did not involve in-depth investigations of mechanical behaviour and performance.
- The ageing techniques used with the WMA materials were all limited to the standardised short- and long-term ageing processes. There has been no consideration of the significance of sunlight in physically changing the material properties. This is a critical factor in the Middle East where the UV index is high.
- The majority of fatigue characterisation and analysis approaches relied on explaining the effect of loading on material properties (e.g. reduction in

stiffness). Few studies were concerned with measuring crack sizes in the asphalt mixtures and correlating these to the material's damage.

- Typically, prior research studies investigated permanent deformation behaviour separate from fatigue cracking behaviour. This approach ignores the nature of the asphalt material as being a visco-elasto-plastic material that experiences permanent deformation concurrently with fatigue cracking.
- Studies that used the X-Ray CT system in investigating the air voids in asphalt materials were following a subjective or an experimental method in defining the air void areas. These methods were less reliable, expensive and time-consuming to conduct.

1.2. Objectives

The main purpose of this study is to evaluate the performance and responses of the asphalt materials mixed with WMA technologies and study the feasibility of using that technology in the State of Qatar. The research study is conducted to accomplish the following specific objectives:

- Evaluate the use and performance of WMA additives with material available locally in the State of Qatar.
- Investigate the effect of climatic conditions in Qatar on ageing the WMA materials.
- Examine the WMA material behaviour against repeated loading using advanced testing and analysis approaches.

1.3. Research Contribution

This study is the first to evaluate various WMA additives with the material used locally in the State of Qatar for pavement construction. The study considered local climatic conditions (temperature and sunlight (UV exposure)) in studying the ageing effect on WMA. This research study proposed a new ageing protocol using the UV light and heat to simulate the outdoor ageing of asphalt materials. This protocol uses the meteorological information about the country to estimate the exposure time and intensity to reproduce the effects that would occur over a certain number of years in a designed and shortened time inside the laboratory. Then, the material was included in a developed testing procedure and analysis approach to investigate the damage in WMA materials. The analysis approach can distinguish the damage that evolved in the material due to repeated loads for more accurate interpretation of the results. This study also presents a developed computational tool that uses the X-Ray CT images to measure the air void area sizes and compare them before and after exposing the material to a repeated loading test. The study tries to link the results of the cracks' opening and closing to the material properties and correlate them with the damage analysis.

1.4. Thesis Structure

The thesis is divided into eight chapters that present the evaluation of WMA additives used with bituminous materials (asphalt bitumen and asphalt mix). A summary of each chapter's content is presented as follows:

1.4.1. Chapter 1: Introduction

The thesis starts with an introductory description of the WMA material behaviour and the background. The overall objectives and motivation are listed in this chapter, in

addition to a clarification of the research contribution and details of the thesis structure.

1.4.2. Chapter 2: Studies on the Fundamental Properties of WMA, Ageing and Damage Characterisation

The second chapter provides a literature review relevant to the WMA studies in the Middle East region and approaches presented by earlier studies on the linear and nonlinear viscoelastic analysis of asphalt mixtures. In addition, the chapter reviews the research studies that focused on fatigue resistance and ageing characterisation of asphalt materials. A discussion ensues about air void measurements performed using the X-Ray CT systems and damage characterisation of asphalt mixtures using mechanical testing and analytical approaches.

1.4.3. Chapter 3: Performance Evaluation of Various WMA Technologies

Chapter 3 starts with fundamental testing of bituminous materials mixed with different WMA additives. Standardised analysis approaches are presented to help in understanding the basic material performance and the impact of the WMA additives on the bitumen basic behaviour.

1.4.4. Chapter 4: Fatigue Characterisation of Fine Aggregate Warm Asphalt Mixtures

Fatigue testing of fine aggregate mixtures (FAM) prepared with WMA additives is introduced in Chapter 4 to evaluate the influence of the WMA additives on the fatigue performance. Advanced analysis procedure was presented and showed the effect of using WMA additives on the fatigue life.

1.4.5. Chapter 5: Characterisation of Aged Warm Fine Aggregate Mixtures

A new ageing protocol is presented in Chapter 5 using the accelerated weathering machine. The new protocol was designed to simulate the State of Qatar's climatic conditions in ageing the FAM samples. Chapter 4 also presents the validation of the ageing protocol for further use and evaluation.

1.4.6. Chapter 6: Characterisation of the Creep and Recovery Responses of Fine Aggregate Warm Asphalt Mixtures

Chapter 6 includes a developed testing method and analysis approach that investigate the damage that evolved in the FAM samples prepared with WMA additives. This chapter consists of the newly developed analysis approach that characterises the damage induced by mechanical testing and assesses the ability of the materials to recover that damage.

1.4.7. Chapter 7: Air Void Measurement for W-FAM Samples using X-Ray Computed Tomography Imaging

In order to clarify the cause of material damage, the FAM samples before and after testing were included in the X-Ray CT imaging process to evaluate the change in air void sizes due to loading. The chapter includes the use of digital image processing techniques to measure the air void sizes and evaluate the impact of ageing on these results.

1.4.8. Chapter 8: Conclusions and Recommendations

The final chapter includes the final findings and conclusions that drawn from the research work. It also includes some recommendations that suggest further areas to be investigated by researchers.

2. Studies on the Fundamental Properties of WMA, Ageing and Damage Characterisation

Warm mix asphalt (WMA) is a relatively new technology that allows the asphalt mixture components to be mixed in the asphalt plant, laid down, and compacted in the field at a temperature 20 - 30ºC lower than the conventional hot mix asphalt (HMA). This technology was defined as a mid-point between hot mix asphalt and cold mix asphalt, which is prepared at a low temperature (0ºC - 30ºC). WMA was first introduced in Europe in 1995 and has demonstrated its benefits and performance over the past two decades (Button *et al.*, 2007; Al-Rawashdeh, 2008; Chowdhury and Button, 2008; Sadeq *et al.*, 2015, 2016). Asphalt mixtures can be produced at a low temperature either by reducing the bitumen viscosity or increasing the mixture workability.

Advantages of using WMA can be classified into three categories: environmental, workers' comfort and field performance (Xiao and Amirkhanian, 2010). Fluctuating energy prices, an alarming level of global warming and strict new environmental regulations have increased the interest in WMA technologies because of the need for a decrease in energy consumption and emissions (Ates *et al.*, 2015). Furthermore, of the need to reduce carbon emissions has attracted attention globally after major industry leaders joined governments in signing the Infrastructure Carbon Review (ICR) initiative in 2013 (The Green Construction Board, 2016). The European Practice report mentioned that the reduction in CO_2 emissions was reported to be between 15% and 40% as a result of using WMA technology (Al-Rawashdeh, 2008; D'Angelo *et al.*, 2008; Caro *et al.*, 2012; Vaiana *et al.*, 2013). Additionally, lowering the mixing temperature in the asphalt plant reduces the fuel consumed when heating the bitumen

in storage silos and aggregate drying drum. Studies showed that fuel savings with WMA technologies range from 20% to 35% (Hurley and Prowell, 2006a, 2006b; D'Angelo *et al.*, 2008). It was also mentioned that worker comfort is enhanced by the reduction in asphalt temperature since it lowers the emissions to which workers are exposed by around 30%. Using WMA technologies also increases the ability to keep the mixture workable at an acceptable level for longer periods, and it allows the mixture to be placed and compacted over longer distances (Caro *et al.*, 2012; Feipeng and Bradley, 2012; Mogawer *et al.*, 2013; Vaiana *et al.*, 2013; Xie *et al.*, 2013; Ates *et al.*, 2015). In addition, it allows the road to be opened to traffic in a shorter period and for more roads to be paved than normally covered by HMA.

The WMA technologies involve different types of additives. Table 1 lists some of the WMA additives available on the market classified based on type and application. This information was initially presented in the "Warm-Mix Asphalt: European Practice" report published in 2008 (D'Angelo *et al.*, 2008).

Table 1: List of WMA additives categorised based on type (D'Angelo *et al.*, 2008)

WMA Additive Type	Commercial Name
Organic Additives & Wax	Sasobit
	SonneWarmix
Foaming	Advera
	Aspha-min
	Low Emission Asphalt
	Double Barrel Green
Chemical Additives	Evotherm 3G
	Rediset LQ

There are three major methods to produce asphalt mixtures at a relatively low temperature. The first method is to reduce the bitumen viscosity by using organic additives, such as Sasobit and SonneWarmix. These additives can alter the viscosity of the bitumen and allow it to be mixed with aggregate at a lower temperature. Alternatively, organic additives can be mixed with bitumen initially or by adding it directly to the mixture (i.e. bitumen and aggregate) (Hamzah *et al.*, 2014).

Sasobit is a fine crystalline long-chain aliphatic hydrocarbon which is manufactured by Sasol Wax in South Africa from natural gas using the Fisher Tropsch process of polymerisation (Butz *et al.*, 2001; Hurley and Prowell, 2005; Sasol Wax, 2014). Sasobit is available in three solid forms: a 5-mm diameter prill, 1-mm diameter prill, or 3-mm chips flaked form. Sasobit is used to lower the viscosity of the bitumen and improve its flow. The manufacturer claims that, when Sasobit is in the liquid form, the aggregate moves more freely in the bitumen, while, when it cools down, it forms a uniform linked structure (Sasol Wax, 2014). The manufacturer recommends that the dosage rate of the Sasobit should range from 0.8% up to a maximum of 4.0% of the bitumen weight; it can be added into the bitumen itself or directly to the mixture. Once they are blended, the mixture stays homogeneous with mixing and handling temperatures that are 10°C to 30°C lower than HMA (Cao and Ji, 2011; Sasol Wax, 2014).

The wide dosage range (0.8% to 4.0% of the bitumen weight) is intended to achieve different purposes from using Sasobit. Using a dosage between 1.5% and 2.5% can improve the workability of the asphalt mix, while adding Sasobit up to 3.5% reduces the mixing and compaction temperatures and increases the time in which paving can take place, especially during poor weather conditions. Using high dosages of Sasobit (between 2.5% and 3.5%) improves the stability of the asphalt mix, which enables the

project to be opened to traffic more quickly. However, the maximum recommended dosage (i.e. 4.0%) can be used for a heavy-duty asphalt mixture such as required for dedicated truck routes, industrial areas and airports (Sasol, 2014).

The second method used to prepare the mixture at a lower temperature is to expand the contact surface of the bitumen using foaming technology. Foaming asphalt mixtures can be prepared by injecting steam (1% to 3% by weight of the mixture) into the hot bitumen liquid using a foaming machine (Newcomb *et al.*, 2015).

This injection allows the bitumen to expand through the formation of voids. Mechanical foaming methods are available to disperse water into the bitumen such as mechanical mixing, Venturi mixing, expansion chamber, shear/colloid mill, air-atomised water and high-pressure atomised water. However, the commercially available laboratory methods are air-atomised water or pressurised water (Newcomb *et al.*, 2015). The other way of foaming asphalt bitumen is by using water-bearing agents such as Zeolite. Zeolite is a mineral additive that has entrapped water in its crystalline structure that starts to be emitted at high temperatures, such as Advera and Aspha-min. These products are produced as an aluminosilicate and synthetic zeolite, respectively.

Advera is a free-flowing white to grey powder (100% passing the 0.075 mm (No. 200) sieve). Such a particle size ensures the uniform distribution of the particles within the asphalt mix. The addition of Advera by 0.25% of the asphalt mix (equal to 4.8%-5.0% by weight of bitumen) can lower the bitumen production temperature by 20 to 30°C while no change in the mix design is needed. Advera contains about 21% of entrapped water in its crystalline structure that starts to be emitted at temperatures over 100°C (PQ Corporation, 2014). The emitted water causes a sustained, time-release foaming

of the bitumen. The foaming process temporarily increases the workability and enhances the aggregate coating. Advera is an inorganic material that does not change the performance grade of the bitumen (PQ Corporation, 2014).

The last method by which to prepare asphalt mixtures at a lower temperature is to use chemical additives, such as Rediset LQ and Evotherm. The addition of the chemical additives to the asphalt mixture, specifically Rediset, improves the aggregate-surfaces wetting with binder and reduces the binder viscosity, which increases the workability and allows mixing at a lower temperature (Jamshidi *et al.*, 2013).

Rediset LQ additive was obtained from the AkzoNobel company for this study. It can be added to the bitumen by 0.5%-1.0% of its weight and allows the mixing temperature to be reduced by up to 30ºC. Adding Rediset LQ to bitumen does not require the use of a high shear mixer in the laboratory since it dissolves and blends at a temperature of 85ºC (Hamzah *et al.*, 2014). Figure 1 shows the three types of WMA additives described above.

(a) (b) (c)

Figure 1: (a) Advera WMA additive acquired from PQ Corporation, (b) Sasobit WMA additive acquired from Sasol Company and (c) Rediset LQ acquired from AkzoNobel

Table 2 presents the properties of the WMA additives used in this study.

Table 2: Basic properties of WMA additives used in this study

WMA Additive	Sasobit	Advera	Rediset
Appearance	Off-white to pale brown pastilles or flakes	Powder	Liquid
Colour	White	White	Dark brown
Odour	Practically odourless	Odourless	Slight
Bulk density (g/cm^3)	0.90	0.40-0.48	0.99
Solubility in water	Insoluble	Insoluble	Partly soluble
Viscosity (mPa.s at 20°C)	Not applicable	Not applicable	1.700

2.1. Warm Mix Asphalt Studies in the Middle East

The open literature listed a limited number of studies conducted on WMA in Arab countries. Some studies were conducted to evaluate moisture sensitivity, rutting resistance and long-term performance of WMA in Iran. Khodaii *et al.* (2012) testing matrix included the use of two WMA additives (Aspha-min and Sasobit), two aggregate gradations and two bitumen types. The testing was carried out by following the indirect tensile strength (ITS) test procedure at a temperature of 25ºC. The study investigated the use of hydrated lime with WMA using dense-graded and gap-graded mixtures and showed that the temperature reduction in preparing WMA depends on the type of the WMA additive, bitumen type and aggregate gradation. Moghadas Nejad *et al.* (2014) examined the use of Reclaimed Asphalt Pavement (RAP) materials with WMA additives and their effect on rutting resistance. The study consisted of testing asphalt mixtures prepared with Sasobit and conducting Marshall stability and flow test, dynamic creep test and ITS. The results confirmed that the optimal content of RAP with WMA additives was 50%.

In 2010, cold asphalt mixtures were used in Qatar for some road trials, as mentioned in a published article in the Al Raya newspaper (2010). The article mentioned that the Department of Road Maintenance had constructed several trial sections to test their performance and use them in road maintenance. However, it was also mentioned that the cost of importing this material was high compared to the current existing solution, which led the country to consider producing it locally.

Due to an increase in both awareness of the environmental aspects of construction and the prices of fuel in Arab countries, interest in implementing green construction concepts and enhancing worker comfort has increased during the past few years in Qatar. This awareness has appeared in encouragement to use environmentally friendly materials in construction, to consider energy saving and to monitor human rights regulations within construction companies.

Bitumen in Qatar is imported for asphalt pavement construction from the Kingdom of Bahrain. It arrives in Doha, the capital of Qatar, as unmodified bitumen and is graded by the penetration test presented in AASHTO T49 and ASTM D5 as Pen 60/70. Then, it is modified locally with polymers (styrene-butadiene-styrene, SBS) by Qatar Fuel (Woqod) to be produced as polymer-modified bitumen (PMB). Other companies produce and supply modified bitumen in Doha, but the modification processes are proprietary. Unmodified Pen 60/70 bitumen is usually used for the construction of local roads and lower pavement layers, while the modified bitumen is used in the surface pavement layers for highways that are expected to bear higher traffic loads. It is worth mentioning that the unmodified bitumen Pen 60/70 was previously graded based on the Superpave performance grading system to be PG 64-22 (Masad *et al.*, 2011).

2.2. Linear Viscoelastic Analysis Approaches

Bitumen and asphalt mixtures are typically modelled as viscoelastic materials. That is due to their combined viscous and elastic behaviour under loading. The elastic nature of the asphalt material gives the material the ability to recover its original state after removal of the load. However, part of the deformation remains after load removal due to the viscous nature. Temperature and loading rate are the main factors affecting the behaviour of asphalt materials. The asphalt materials behave in a more elastic manner at lower temperatures and are more viscous at high temperatures. Also, the behaviour of the material is changing based on the loading rate which become more elastic at high loading rate and more viscous at low loading rate (Rahimzadeh, 2002).

Asphalt mixtures exhibit linear viscoelastic (LVE) behaviour when the applied load does not exceed the LVE region of the material as shown in Figure 2. The material at the LVE region can recover the strain completely after the removal of the load. Additionally, the material can recover the strain as long as the load level remains within the nonlinear response region. However, if the material exceeds the nonlinear viscoelastic (NLVE) region and reaches the damage region, some of the strain will be permanent and the material will not recover when the load is removed. The material can still handle more stress and deformation until a certain point where complete failure happens. Figure 2 presents the effect of the strain rate on the stress-strain behaviour. While with increasing the applied strain rate, the responses stress will be higher.

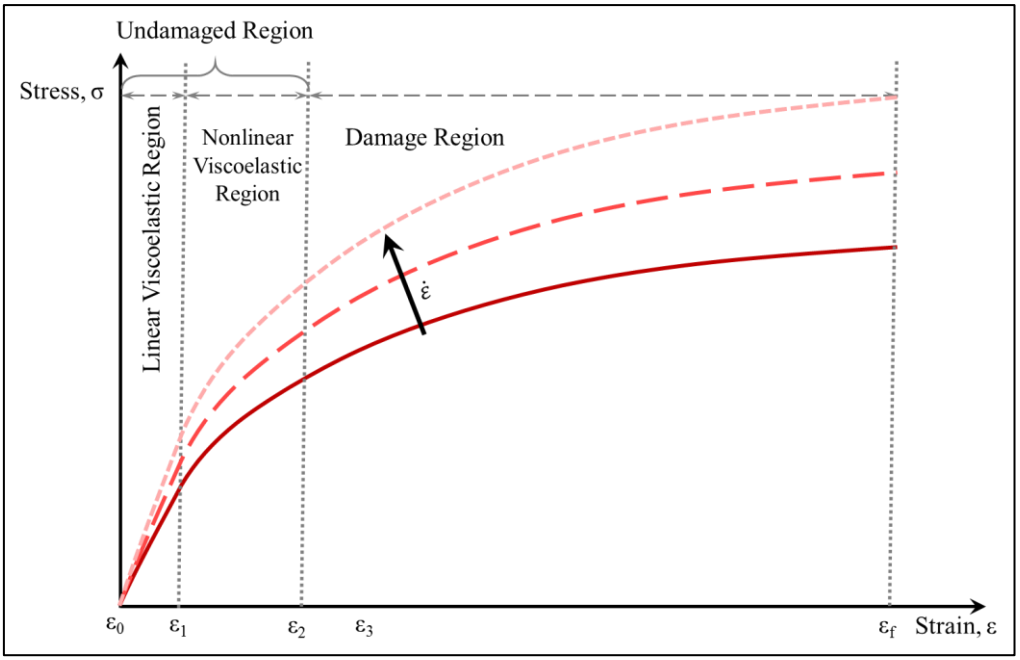

Figure 2: Stress-strain curve for asphalt materials at different strain rate

Usually, testing asphalt mixtures starts by measuring the material properties at the LVE region. This region is used to define the material properties at the undamaged state. The two most commonly used test methods to define material LVE properties are a transient method (such as stress relaxation and creep loading) and an oscillatory method.

Superpave bitumen testing was established to test the bitumen at a linear viscoelastic region at different temperatures and loading rates. Testing of the bitumen involves measuring the dynamic viscosity at a high temperature (135ºC and 165ºC) to evaluate pumping, mixing and workability during production. The test is conducted by using the rotation viscometer (RV) at a constant rotation speed (20 rpm) at a constant temperature (AASHTO T 316 and ASTM D 4402). The machine measures the required torque to maintain the rotation speed to calculate the dynamic viscosity. On the other hand, testing the performance of the bitumen at intermediate and low temperatures is conducted by using the Dynamic Shear Rheometer (DSR), which is

also used for performance grading (PG) of bitumen which is part of the Superpave system. The performance grading (PG) system was established based on the concept that the bitumen's properties is related to its service condition. The grading includes testing the bitumen based on climatic conditions and ageing states. The DSR is used to evaluate the rheological properties of the bitumen at specific temperatures and grade it based on the results. Testing is performed by placing a small capsule of bitumen between two plates and rotating the upper plate in oscillatory mode (stress- or strain-controlled mode). The machine calculates the shear modulus (|G*|) and phase angle (δ) by measuring the torque required to achieve the applied displacement (strain-controlled mode) or measuring the displacement achieved by the applied torque (stress-controlled mode) (AASHTO - T 315, 2009).

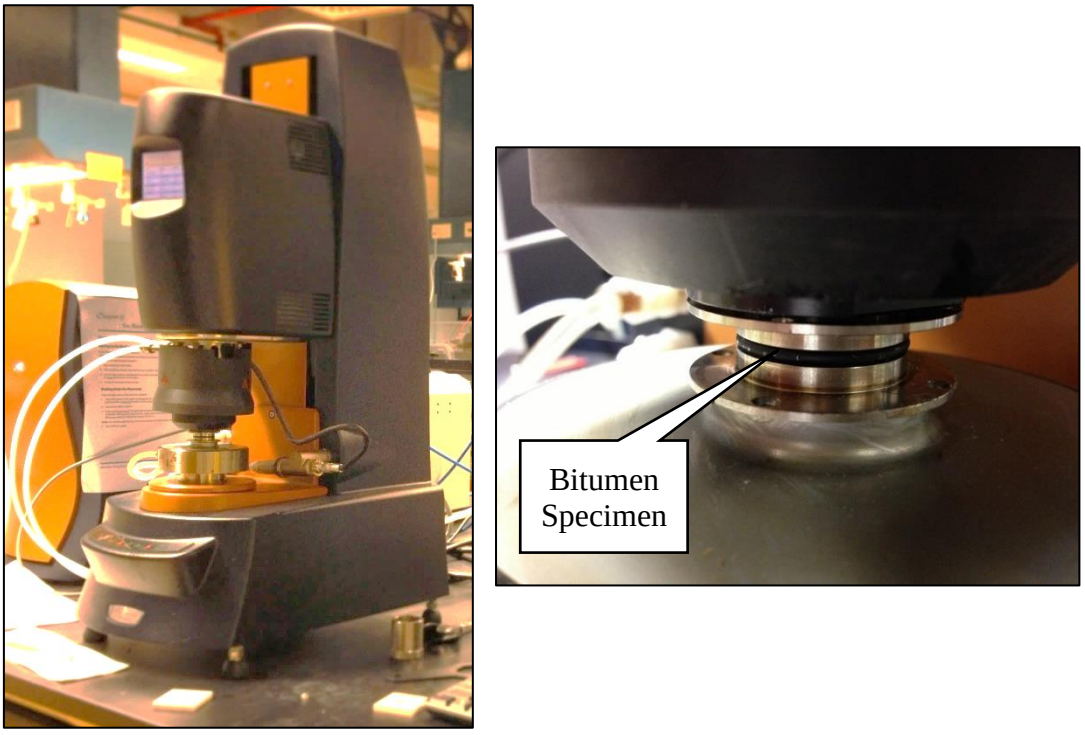

(a) (b)

Figure 3: (a) Dynamic Shear Rheometer (DSR) (b) Parallel plates of DSR and bitumen specimen placed for testing

It has been addressed in many previous studies that, in grading the bitumen using the DSR test, the PG system has some limitations in describing the actual performance of the bitumen. The limitations are because the bitumen is tested at the LVE region and the rutting factor ($|G^*|/\sin(\delta)$) and fatigue factor ($|G^*|.\sin(\delta)$) are defined based on this region (D'Angelo *et al.*, 2007). To overcome this issue, D'Angelo *et al.* (2007) conducted studies to implement the Multiple Stress Creep Recovery (MSCR) test in the performance grading. This test was added to the AASHTO - M 320 (2009) standard and introduced traffic classifications into the bitumen grading.

Several studies have shown that the fatigue factor ($|G^*|.\sin\delta$) has limitations in characterising the fatigue life of asphalt mixtures (Stuart *et al.*, 1999; D'Angelo and Dongre, 2002; Dongre and D'Angelo, 2003). These studies and others recommended various other tests that rely on repeated loading of bitumen and a criterion for fatigue failure.

The LVE testing results can be represented by mathematical models such as the 'Prony Series'. The Prony Series is an effective numerical method that is used to represent the viscoelastic properties of materials (Pacheco *et al.*, 2015). It is a polynomial function that has the ability to fit most of the viscoelastic behaviour by adding more terms to the function. Other function such as the power law can be used for simple viscoelastic material behaviour. Park and Schapery (1999) used the Prony Series to relate the relaxation and creep functions of the viscoelastic polymeric materials. Similarly, several studies adopted the Prony Series to define the viscoelastic coefficients that can be used in material characterisation (Tzikang, 2000; Beake, 2006; Hu *et al.*, 2006; Sorvari and Malinen, 2007; Felhos *et al.*, 2008; Sorvari and Hämäläinen, 2010). In this study, the Prony Series will be effectively used in several types of analysis to represent the material properties for performance evaluation.

2.3. Nonlinear Viscoelastic Analysis Approaches

As mentioned in the previous section, the inaccuracy of Superpave specifications (specifically the PG grading) in measuring the rutting resistance using the rutting factor – especially with modified bitumen – encouraged researchers to investigate other methods. The development of the MSCR test was based on the repeated creep recovery test (RCRT) but with multiple creep stress levels. Initially, one stress level (300 Pa) was used to perform 100 creep cycles in the NCHRP 9-10 project (D'Angelo *et al.*, 2007). This test attempts to model the repeated nature of traffic loading on the road. Then, the FHWA modified the RCRT test by making the stress levels increase with time and renamed it the Multiple Stress Creep Recovery (MSCR) test. The stress level starts at 25 Pa and increases in 11 steps to 25,600 Pa by applying 10 cycles for each stress level. In 2007, D'Angelo *et al.* published a revision of the Superpave high-temperature specification to overcome the limitation of the LVE testing of the PG grading of the bitumen and evaluate the stress dependency of the asphalt material using one test specimen. The study presented the use of non-recoverable creep compliance, 'J_{nr}', which is a normalised term that shows the response of the material and avoids the difficulty of comparing different stress levels. The developed MSCR test protocol consists of applying two stress levels for 10 cycles: 100 Pa and 3200 Pa. The standard test applies 1 second of creep loading followed by 9 seconds of recovery. The high-stress level (3200 Pa) applied to the bitumen is used to expose the material to nonlinearity and damage (Masad *et al.*, 2009). The test results, in terms of unrecoverable compliance, were implemented in the bitumen grading by adding the letter 'S', 'H', 'V' or 'E' next to the PG grading to represent the traffic specification. These letters indicate Standard, Heavy, Very heavy and Extremely heavy traffic, respectively. Masad *et al.* (2009) investigated the MSCR test and claimed that this

method might not show the exactly recoverable strain following 9 seconds of recovery time. They adopted the plasto-viscoelastic analysis approach using Schapery's nonlinear viscoelastic model. The model revealed that the bitumen ranking could change when considering the full recovery of the bitumen, and then the predicted rutting resistance would be more precise. More details about the plasto-viscoelastic approach are presented in Chapter 3.

2.4. Fatigue Characterisation of Asphalt Concrete Mixtures

Fatigue cracking is one of the major distresses that affect asphalt pavements' serviceability. In most cases, it requires an expensive rehabilitation process by milling the surface if the crack is top-down or removing the whole asphalt layers if the crack is generated from the bottom to the surface. Usually, cracks initiate at the top of the asphalt layer and propagate downward because of the localised tensile stresses at the upper layers. Ageing and tyre-pavement interaction are the main reasons why localised tensile stresses develop. On the other hand, cracks that initiate from the bottom of the asphalt layer upwards occur due to high horizontal tensile strain, and then migrate to the surface (Molenaar, 1983).

The characterisation of the fatigue resistance of asphalt materials went through several stages. Some methods focused on determining the elastic behaviour of the bitumen that can prevent brittle failure at low temperatures (Bhasin *et al.*, 2011; Pang *et al.*, 2012; Shan *et al.*, 2013). Other methods evaluate the whole asphalt mixture exposed to a repeated loading test at a certain frequency and stress (or strain) amplitude (Bhasin *et al.* 2008; Pronk 2006; Shen *et al.* 2010; Lancaster and Khalid 2015; Ahmed and Khalid 2015; Artamendi and Khalid 2005). Some studies went further by investigating the crack initiation and propagation at a micro-level and capturing it using a

sophisticated technique (Khan and Collop, 2010; T. Liu *et al.*, 2014; Menapace *et al.*, 2015; Zeng *et al.*, 2015). The analysis of the fatigue test data has been developed from different testing protocols to explain the fatigue resistance performance regardless of the sample shape, geometry, and testing mode (stress- or strain-controlled mode). Several analysis approaches were developed based on that goal, and some of them are summarised below.

Different methods have been developed for testing the fatigue resistance of bitumen, mastics and mixtures. These methods involve different sample geometries, loading rates, frequencies, temperatures and loading modes. Testing methods such as 2-point, 3-point and 4-point bending beam tests as well as the uniaxial tension-compression test were developed based on the repeated sine loading waves being applied to the specimens. Other test methods, such as the indirect tensile test (IDT), were developed based on the concept of combining three different tests (resilient modulus, static creep and strength test) and their results into a fracture mechanics framework to calculate the energy ratio (Das *et al.*, 2012).

The Dissipated Energy (DE) approach was initially developed by Van Dijk and Visser (1977) to calculate the total energy dissipated due to cracking failure. Energy is represented by the area encircled by the stress-strain hysteresis loops. This method has the limitation of being dependent on the loading mode and not differentiating among the various dissipated energy components (viscoelastic, viscoplastic and fracture). Schapery (1984) presented the concept of eliminating the energy dissipated because of the viscoelastic response from the energy dissipated due to damage, and introduced the concept of the pseudo-strain (or pseudo-stress). However, it has been reported that this method underestimated the viscoelastic dissipated energy and overestimated the material damage (Sadek, 2015). Ghuzlan and Carpenter (2000) overcame some of the

DE method limitations by using the rate of change in measuring the dissipated energy (RCDE). A study by Masad *et al.* (2008) presented a method that separated the dissipated pseudo-strain energy into three components associated with a change in phase angle between load cycles, a change in phase angle within a single cycle and a change in stiffness between cycles.

Monismith *et al.* (1985) proposed an empirical equation to predict the fatigue life that was based on testing parameters limited to the geometry of the tested sample and the mode of testing. Also, the method did not consider viscoelastic behaviour in predicting the asphalt fatigue behaviour since it was based on the initial modulus and stress/strain amplitude. Another analysis method was presented based on the hysteresis loops generated by sinusoidal loading (stress or strain). The area inside those loops was calculated and multiplied by the number of cycles to report the dissipated energy due to fatigue (Van Dijk & Visser 1977).

Based on Schapery's viscoelastic theory, the viscoelastic continuum damage (VECD) approach was developed to evaluate the fatigue resistance of asphalt mixtures (Schapery, 1987). This method predicts the internal damage of asphalt mixtures by measuring the material properties from a cyclic loading test. The method claims that, using the internal damage, 'S' is not affected by sample geometry, loading rate or mode. The VECD approach is discussed in detail in Chapter 3.

Several fatigue characterisation studies conducted on WMA were reviewed from the literature and are summarised in this section. Zelelew *et al.* (2013) used the fatigue factor ($|E^*|.\sin\delta$) which combines the dynamic modulus ($|E^*|$) and the phase angle (δ) to study fatigue resistance of WMA. The study investigated the performance of asphalt bitumen and mixtures with the addition of WMA additive. The testing included using

the DSR oscillation testing, asphalt mixture performance testing (AMPT) and Hamburg test. The results showed that the rutting factor is mostly affected by the rheological properties of the asphalt bitumen and the WMA addition dosage. However, the study also concluded that using WMA additives reduced the fatigue resistance of the asphalt mixtures and showed that the control HMA has the highest resistance to cracking. Kim *et al.* (2010) used the Superpave bitumen test programme to evaluate the properties of polymer-modified bitumen using the DSR and RV. The study included mixing the bitumen with two WMA additives: Aspha-min and Sasobit. It was confirmed that using Sasobit decreased the viscosity of the asphalt bitumen. However, using Aspha-min increased the viscosity of the bitumen due to the existence of undissolved filler inside the bitumen. The fatigue factor ($|G^*|.\sin\delta$) of each WMA was compared and it was concluded that WMA additives reduced the fatigue resistance of the bitumen. Haggag *et al.* (2011) tested long-term aged WMA mixtures prepared with three WMA additives: Advera, Sasobit and Evotherm 3G with virgin binder PG64-22. The asphalt mixtures were compacted using 75 gyrations and 100 gyrations to be tested with the uniaxial cyclic direct tension-compression test. The experimental results were analysed using the viscoelastic continuum damage (VECD) approach to evaluate the fatigue resistance. The results showed that there was no significant difference between the HMA and WMA samples in fatigue cracking resistance, except for the WMA prepared using Advera additive. Safaei *et al.* (2014) used 19% of RAP with 9.5 mm nominal maximum aggregate size WMA mixtures. Two types of WMA technologies were used: foaming by water injection and Evotherm 3G. The control HMA mixtures were short-term aged at 135ºC for 4 hours while the WMA mixtures were short-term aged at 117ºC for two hours. However, the long-term ageing of HMA and WMA was conducted by placing the samples in a heating oven at

85ºC for two and eight days. All specimens were tested using the dynamic modulus test and controlled crosshead cyclic direct tension test. The results were analysed using the simplified viscoelastic continuum damage (S-VECD). The results showed that the effect of preparing the WMA at a lower temperature (i.e. short-term ageing is lower) helped in having a reduced mixture stiffness after the long-term ageing. The fatigue resistance due to the difference in mixture preparation was clear until the full eight days long-term ageing of the asphalt mixture, when it became negligible.

2.5. Alternative Ageing Characterisation Studies on Asphalt Concrete Mixtures

The asphalt materials laid down on the roads are subjected to changes leading eventually to damage due to exposure to external factors (heat, moisture and load) over time. Prediction of asphalt mixtures' performance after construction was the main reason for implementing different ageing protocols for bitumen and mixtures. Ageing the whole asphalt mixture samples (bitumen and aggregate) results in a more accurate simulation of outdoor ageing than aging the bitumen alone. Some studies have shown that aggregate affects the bitumen oxidation (Petersen *et al.*, 1974; Wu, 2009). Modelling the ageing in the laboratory has an important role in the design decisions and material selection. The hardening of the asphalt material is related to the loss of volatiles and oxidation which happens during the preparation of the mixture due to the elevated temperature. Most specifications allow up to 1% of volatile loss during production. The standard specifications of ASTM F 2872 and AASHTO - T 240 (2009) present the procedure to simulate the ageing of bitumen that happens in asphalt plants during mixture preparation. During this period, the bitumen is heated in the storage tanks at a high temperature (can reach 180ºC for modified bitumen) and then

mixed with preheated aggregates inside the pugmill. Heating the mixture components to a high temperature is performed to achieve proper bitumen-aggregate coating and prevent segregation and loss of workability. The mixing temperature is usually defined by performing a viscosity test on the bitumen at an elevated temperature to specify at which temperature the viscosity of the bitumen will be adequate for coating the aggregate and being placed on the site. Ageing of bitumen during this stage of pavement construction is called 'short-term ageing' and can be simulated in the laboratory with different techniques. Ageing techniques in the laboratory vary between using extended heating and oxidation procedure. Methods such as Thin Film Oven Test (TFOT), Rolling Thin Film Oven (RTFO) test and the rotating flask test were developed to age bitumen by heating the sample at a high temperature (around 160ºC) for an extended period. The RTFO method improved the TFOT method (and shortened the ageing time) by ensuring that all the material was exposed to the heat and airflow during the ageing process by rolling the bottles during the ageing period (Figure 4).

(a) (b)

Figure 4: RTFO system and bottles

The rolling mechanism of the RTFO ageing helps in dispersing the bitumen modifiers (if any) and inhibits surface skin formation (Airey, 2003). Although the short-term

ageing does not impose a high level of ageing on the asphalt pavements compared to the long-term ageing, testing the rutting resistance of the bitumen during this stage of ageing is more reliable. Asphalt pavement at this stage is still soft and viscous to exhibit deformation due to traffic loading. For the asphalt mixtures, different procedures were developed by Pauls and Welborn (1952), Scholz (1995) and Von Quintus *et al.* (1992), who used intact samples and a loose mix to simulate the short-term ageing in the laboratory. Procedures include heating the mixture sample at an elevated temperature for various periods.

During the service life of the asphalt pavement, the asphalt material ages due to heat and UV light from the sun. Several laboratory ageing protocols have been proposed to simulate the long-term ageing of bitumen. Those protocols included an extended heating and applying high pressure to the material to accompany the hardening and oxidation. The pressurised ageing vessel (PAV) is one of the long-term ageing machines that expose the short-term aged material placed in thin pans to a high temperature (90ºC – 110ºC) and a high air pressure (2.07 MPa - 2.24 MPa) continuously for 20 hours. Samples should be degassed after this procedure to remove the entrapped air bubbles that have occurred due to the high pressure. This procedure causes oxidation and alters the chemical composition of the bitumen and simulates 7 to 10 years of actual ageing on the road. Long-term ageing of asphalt mixtures is performed by placing the intact or loose mixtures inside the oven at a high temperature for an extended period. These standard methods showed that they had been successfully designed as they were able to predict the performance of asphalt pavements over several years. However, a few years ago, new concerns were raised about the accuracy of these methods in simulating the bitumen and mixtures (Wu *et al.*, 2009; Xiao *et al.*, 2013; Fernández-Gómez *et al.*, 2014). More studies were

performed to propose new ageing protocols that include multiple ageing factors and predict the performance of the asphalt material over time.

Nonconventional ageing procedures have been introduced in many studies on asphalt pavements. Including other factors that affect the durability of asphalt materials was to predict and design the material to resist ageing distresses. Ultraviolet (UV) and infrared (IR) light treatments as part of sunlight were introduced in several studies (Davidson *et al.*, 1989; Airey, 2003; Pang *et al.*, 2011; P. F. Liu *et al.*, 2014; Zeng *et al.*, 2015, 2015; Menapace and Masad, 2016). The results showed that the UV radiation is an effective factor that changes the physical properties of the bitumen and causes degradation. Materials that are not UV-stable may crack or disintegrate due to UV radiation. Obviously, continuous exposure to UV radiation can be more severe than sporadic exposure, since damage depends on the extent and degree of exposure (Atlas, 2015).

Weathering is the reaction of a material to the climate that causes undesirable failure. The significant cost of a material's degradation drives the manufacturer to find ways to stop their product from failing due to environmental causes and to increase the durability of the material. There are three main contributors to weathering: solar radiation (light energy), temperature and water (Atlas Electric Devices Company, 2001). The sun sends radiant energy in photons that travel through space to reach Earth. These photons travel in the form of waves that have a wavelength, where having a small wavelength results in higher energy. The sun sends the solar radiation to Earth's surface in a wavelength between 280 and 3000 nanometres divided commonly into three stages: ultraviolet (UV), visible (VIS) and Infrared (IR), as shown in Figure 5 (International Commission on Illumination, 1989). UV light, which has a

wavelength between 200 and 400nm, reserves around 6.8% only from the total percentage of the solar energy.

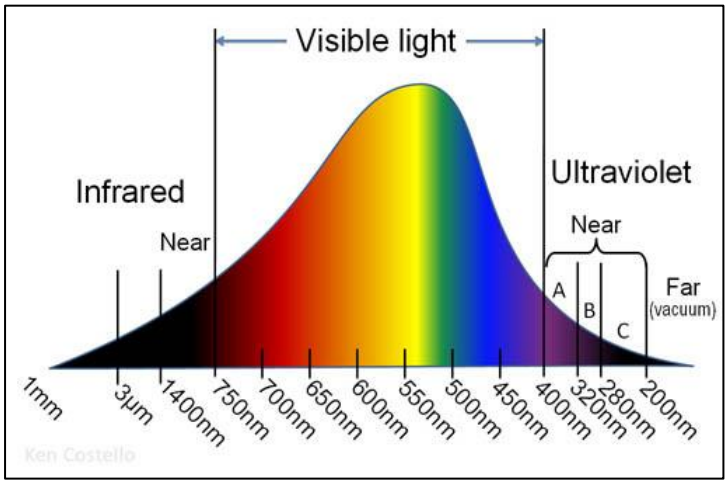

Figure 5: Sunlight Spectrum (ttv gmbh, 2017)

The ozone layer surrounds Earth and helps to prevent the UV-C wavelength from reaching it. However, the UV-A and UV-B can reach the ground surface in different percentages. Some of the UV-B waves are reflected by the clouds, but the UV-A waves totally reach the surface and have a strong effect on human health and material degradation.

Wu *et al.* (2009) investigated the thermal and rheological behaviour of bitumen with different film thicknesses using differential scanning calorimetry (DSC), thermogravimetric analysis (TGA), Fourier transform infrared spectroscopy (FTIR) and the Dynamic Shear Rheometer (DSR). The DSR test was conducted at various temperatures and frequencies to develop master curves of shear modulus (|G*|) and phase angle (δ). It was observed that the |G*| master curve is shifted upwards with more hours of ageing, which indicates a higher stiffness at all frequencies and temperatures than the original bitumen. It was proven that the UV light affects the first 500 µm of the bitumen. It was concluded that UV ageing would increase the glass

transition temperature of the bitumen, which is the temperature that transforms the polymer from the hard and glassy form to a soft and rubbery form (Breen and Stephens, 1967). Increasing the glass transition temperature leads to an improvement in the thermal behaviour of the bitumen. Also, Mouillet *et al.* (2014) conducted a study comparing UV ageing with thermal ageing, RTFO, PAV and field ageing. The bitumen was extracted from aged samples and tested using the DSR. The results presented in the study showed – regarding rutting factors ($|G^*|/\sin \delta$) of bitumen – that the rutting factor increases rapidly from unaged to 600 hours of UV-aged bitumen samples, and then stays almost constant with further ageing. The same idea was observed with the fatigue factor ($|G^*|.\sin \delta$). The study concluded that UV exposure deteriorates the bitumen properties more than the conventional PAV ageing. The study also showed that oxidation increases with UV ageing and has a noteworthy penetration of the top 1 cm of the pavement structure. A study by Menapace and Masad (2016) showed that the combined effect of UV radiation and thermal oxidation causes modification of the surface microstructure of bitumen and improves its stiffness and ductility. It was also noticed that the dynamic modulus ($|G^*|$) increased and phase angle (δ) decreased with ageing (Kane *et al.*, 2013; Xiao *et al.*, 2013; Fernández-Gómez *et al.*, 2014; P. F. Liu *et al.*, 2014).

Since 1985, researchers have been trying to simulate in the laboratory the climatic conditions on the road by using controlled chambers with weathering factors. *Edler et al.* (1985) developed a weathering machine that combines heat, UV light and pressure on a thin film of bitumen (100 micrometres). Montepara *et al.* (1996) followed the same idea and exposed the bitumen to UV-B and UV-C at 140ºC but with a thicker bitumen film (1.5mm). Bitumen samples were then tested using standard tests (penetration, softening point and viscosity), nuclear magnetic resonance (NMR) and

Fourier transform infrared spectroscopy (FTIR). The bitumen samples were aged with the UV light showing volatilisation, oxidation and polymerisation. The term ‘volatilisation’ is used to express the evaporating of the light particles from the bitumen by the effect of an elevated temperature, while the term ‘oxidation’ describes the reaction between the bitumen and the oxygen. Finally, ‘polymerisation’ is a progressive hardening that occurs when the large molecules in the bitumen combine with each other at an elevated temperature (Hagos, 2008). Montepara and Giuliani (2000) then completed the investigation and compared the results with the conventional RTFO and PAV, but showed that the UV ageing did not reach the same ageing level as the conventional standard methods. A study by Bocci and Cerni (2000) concluded that simulating the long-term field ageing might require a combination of thermal-oxidation treatment with the photochemical techniques (UV light). Although the results from Tia *et al.*'s (1988) study on the UV light ageing of asphalt mixtures did not show a significant penetration depth of ageing inside the mixtures, a recommendation was given in the study to use heating with the UV light to enhance the ageing protocol.

2.6. Use of X-Ray CT in Characterisation of Internal Structure and Crack Size Measurement

Since the 1970s and after the introduction of X-Ray computed tomography (CT) to medical screening and preventive medicine, researchers around the world started investigating the use of this technology in other possible applications. Many studies have used the CT technology to investigate the integrity of different civil engineering materials (Manahiloh *et al.*, 2012). Recently, some studies have been performed on asphalt materials to establish evaluation methods for cracks, damage and performance.

An imaging technique includes three stages: image acquisition, processing and analysis. Acquiring images can be done by any X-Ray CT system depending on the system resolution, sample size and range of interest. Images acquired must be of an adequate resolution and quality to be processed using different types of software packages. Processing includes turning the images into quantifiable data for obtaining information about the material. Finally, images become ready for analysis using special software packages to measure parameters such as density, intensity, counts and area (or volume) (Inanc *et al.*, 2007). Several studies have implemented the X-Ray CT system for density measurements of asphalt mixtures and to develop a quality control system for mix design and aggregate gradation (Taniguchi *et al.*, 2012, 2014). Other studies were concerned about the performance of asphalt mixtures against fatigue damage, permeability and micro-damage (Wang *et al.*, 2003; Braz *et al.*, 2004; Khan and Collop, 2010; Kutay and Aydilek, 2010; Shaheen *et al.*, 2016). Any CT system consists of an X-Ray source, detector and turntable that holds the sample and rotates it, as shown in Figure 6.

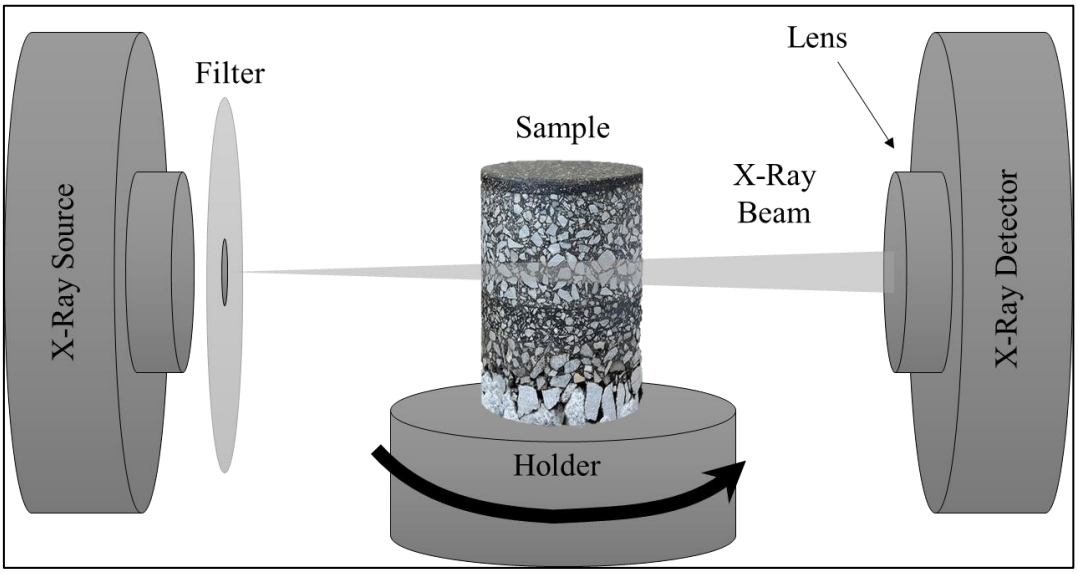

Figure 6: Sketch of a typical X-Ray CT system and its components

The CT system generates an X-Ray beam that is transmitted through the sample and received by the detector, which sends the data to the workstation computer for processing. The sample holder keeps rotating and moving vertically to capture the assigned range of the sample and send the images to the workstation. The detected images are then processed by the software to generate cross-sectional slices that can be used for analysis. An example of an imaged slice is shown in Figure 7.

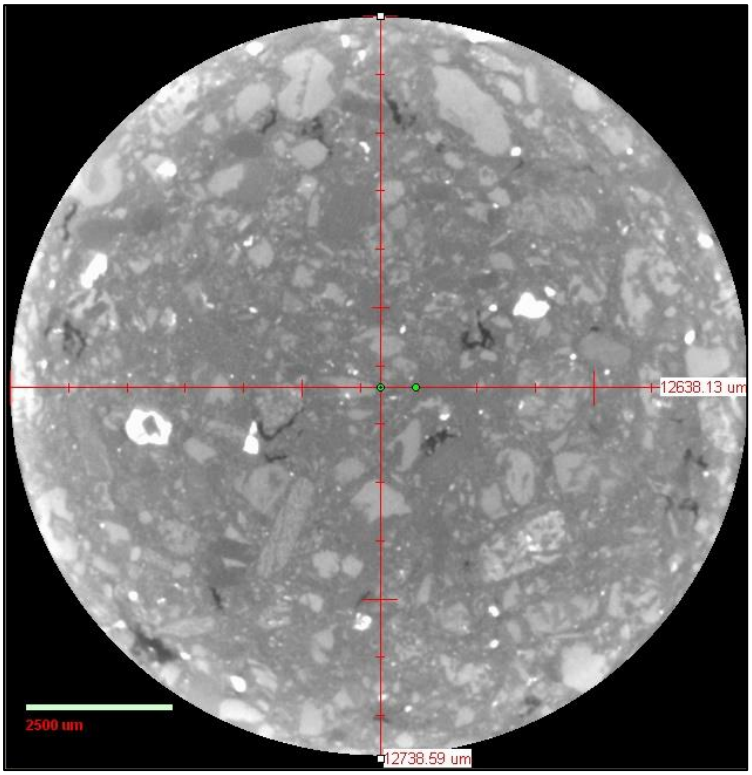

Figure 7: Single slice of asphalt mixture imaged by a typical X-Ray CT system

The workstation computer processes the slices and shows the image components in different levels of brightness. The aggregate has the brightest colours, followed by the mastic (bitumen with fine aggregate), followed by the air voids, which are the darkest black (Inanc *et al.*, 2007).

Images go through several stages of digital image processing (DIP), such as image enhancement, noise removal and edge detection (Zelelew and Papagiannakis, 2011).

Methods such as equalisation are usually used to adjust the grey level intensity to enhance the image contrast. Intensity in digital images are described by bits, which indicate the colour of a single pixel.

Digital Imaging Processing (DIP) is a technique that uses computer algorithms to process digital images. All of the DIP methods are aimed at enhancing the image quality and prepare it for the thresholding technique. A better thresholding technique leads to a better analysis of the quantifiable image information and more accurate volumetric measurements of the material. A few studies have shown practical techniques for defining thresholds of the colour histograms of the sliced images of asphalt mixtures, such as Shaheen *et al.* (2016) and Zelelew and Papagiannakis (2011). They used the laboratory-measured air voids as a reference to calibrate the threshold of image samples before any test. This technique needs some experimental work to measure the air voids in the laboratory (measuring the bulk and maximum specific gravity for the mix). However, other studies decided to define the threshold levels visually by specifying the levels that cover the black area in the images and checking all slices to ensure that all the black areas are covered. This method is considered subjective in many cases and depends on personal judgement. It also includes a high possibility of error since imaging usually generates too many slices and the image intensity alters from sample to sample due to X-Ray intensity and material density. Many studies have concluded that X-Ray CT imaging is a promising tool which can help in understanding the complexity of asphalt materials and their performance against major distresses. Some studies have attempted to link fatigue damage to asphalt mixture cracks and changes in microstructure. Shaheen *et al.* (2016) developed a framework to validate the HMA fatigue characterisation based on X-Ray CT imaging. Masad *et al.* (2002) studied the distribution of the air voids of HMA cores.

The results showed that air voids distribution take the shape of the bathtub, where larger air voids were present at the top and bottom of the specimen than in the middle. The study concluded that compacting the sample above 150 gyrations has an insignificant influence on the air void distribution. Reversibly, the aggregate gradation has a higher influence on the air void sizes and distribution.

2.7. Damage and Healing Characterisation of Asphalt Concrete Mixtures

Asphalt material – like any other material – is affected by different external loading mechanisms. It acts differently against those loads, especially at different loading rates, loading amplitudes and environmental conditions. These loads can – to a certain extent – damage the material and change its behaviour. However, researchers have proven that asphalt material can repair some of this damage and partially restore some of its properties to its original state (Qiu, 2012).

Studying factors that induce damage to asphalt materials was an interesting topic in many research studies decades ago. However, introducing the concept of the material self-healing started during the 1960s. Usually, the term ‘self-healing’ is used to describe the ability of the material to recover its properties by itself without the use of any healing agents. Most studies nowadays refer to the self-healing term only by ‘healing’, to indicate that the material relies on its internal structure to heal itself without any outer support. Several studies have focused on the healing capability in asphalt materials at different component levels: bitumen, asphalt mastic and the asphalt mixture. The studies have used conventional and nonconventional methods to initially identify the healing potential in the asphalt material, and then tried to quantify or qualify it.

As mentioned in the previous section, asphalt materials are time- and temperature-dependent due to their viscoelastic nature. Hence, researchers initially thought that, since the time and the temperature have a major effect on the material's damage, they can also play a major role in its healing. Exposing asphalt materials to creep loading for a certain period might induce damage, but applying relaxation periods can also allow the material to recover part of this damage. On the other hand, the high temperature to which asphalt materials are exposed during the day has a harmful effect on the material's resistance to deformation. However, it also allows the bitumen to lubricate and adhere the cracks.

Studies conducted on asphalt materials have used two types of tests. The first type is by conducting cyclic oscillation loading, which applies a stress (or strain) at sinusoidal or haversine form. Usually, this test lasts for a relatively large number of cycles until the specimen fails or loses 50% of its initial stiffness. The oscillation test can be applied as a stress- or strain-controlled mode. The other type is the creep or relaxation test, which applies a constant stress (or strain) for a continuous period and measures the strain increase (or stress decrease) over time. In evaluating the damage and healing of asphalt materials, both types of tests have been used by several studies. Kim *et al.* (2003) developed a reproducible fatigue relationship that introduced rest periods during oscillation testing. The study used sand-asphalt mixture samples to prepare cylindrical samples of 50 mm height and 12 mm diameter. The strain-controlled test was applied to the samples using the dynamic mechanical analyser (DMA) at three different strain levels: 0.20%, 0.28%, and 0.40% strain amplitude at 10 Hz frequency. The test was conducted at 25ºC temperature since evaluating the fatigue resistance has to be carried out at intermediate and low temperatures. The study showed that using DMA in testing sand-asphalt mixtures is an effective method to evaluate the fatigue

resistance under torsional loading. Furthermore, introducing rest periods during the test increased the fatigue life, which the authors interpreted as indicating the healing potential. Additionally, a study published by Pronk (2006) used the four-point bending beam test to study healing in asphalt materials. The study developed a proposed model related to the rate of dissipated energy and depended only on the sample geometry and loading mode. The study proposed a partial healing model that is unrelated to rest periods used by other researchers. Bhasin *et al.* (2008) also showed that introducing rest periods into fatigue testing has drawbacks in quantifying the healing. Their study proposed a framework to quantify the effect of healing on asphalt materials. The study discussed the healing mechanism due to fracture process and healing zone. The proposed framework was built on the concept of intrinsic healing function and wetting distribution function. The wetting distribution function was related to the rate of fracture process/heal and can be calculated using material properties (creep compliance and Poisson's ratio), while the intrinsic function was divided into instantaneous strength gain by the interfacial cohesion and time-dependent strength gain by the diffusion between crack surfaces. The study suggested using the DSR to measure the intrinsic healing function parameters by bringing two bitumen specimens (28 mm diameter and 3.5 mm thickness) into contact with the DSR's two plates and measuring the shear modulus (Bommavaram *et al.*, 2009). This method was taken one step further by evaluating the effect of ageing on the healing capability (Bhasin *et al.*, 2011). The results showed that, even with aged bitumen, adequate wetting could be achieved to provide overall healing to the material. On the other hand, cylindrical Fine Aggregate Mixtures (FAM) samples were tested using the dynamic mechanical analyser by applying a sinusoidal strain wave at 0.2% amplitude and 10 Hz frequency.

The results were analysed using the dissipated pseudo-strain energy and showed very good correlation with the results developed by the rest periods tests.

Several studies have tried to develop a single index for the healing capability of asphalt materials, and all of them have used one of three methods (Shan *et al.*, 2013). The first method is to test the material with and without rest periods and use the ratio between material properties before and after the test as the healing index. The second method is to evaluate the change in the fatigue life with and without rest periods. The last method is to assess the damage rate after healing. A study by Pang *et al.* (2012) was conducted on bitumen and performed fatigue testing using the DSR by imposing rest periods into the test. The healing index was developed by comparing the degree of damage before and after using the rest periods. The damage degree was derived from the initial shear modulus and the fatigued modulus. On the other hand, the multiple stress creep recovery (MSCR) test was used in a study conducted by Kim and Roque (2006) to test the asphalt mixtures against damage and healing. The creep time was fixed for all cycles to be 6 minutes, but the recovery time changed with cycles (from 4 to 20 minutes). The healing was measured by calculating the slope of the line connecting the last point of creep strain by the last point of the recovery strain. The slope was normalised to establish a healing index that can represent the material's capability to heal. This analysis method assumes that the creep phase (loading phase) includes the steric softening, damage and heating of the asphalt mixture, while the recovery phase (unloading phase) includes the steric hardening, damage recovery and cooling. Also, Shan *et al.* (2013) worked on establishing a universal healing index that can identify the potential of healing in bitumen. The study was conducted using the 8 mm plate in the DSR to perform a fatigue test. The fatigue test was performed in stress- and strain-controlled modes at 10 Hz sinusoidal loading frequency. The study

presented a healing index that reflects the healing performance and concluded that using long rest periods shows a higher healing capability. Similarly, Shen *et al.* (2010) used the DSR to apply a constant shear stress at different temperatures and 10 Hz frequency with rest periods. The test was designed to examine the cohesive healing within the bitumen without including the adhesive healing within the bitumen-aggregate interface. The results were analysed using the dissipated energy (DE) approach and it was concluded that the healing extended the fatigue life of the bitumen. The healing effect was related to the healing rate quantified by a relation that depends on the rest periods.

A study presented by Karki *et al.* (2014) proposed a new technique to measure the fatigue damage and healing potential of asphalt material using a single test specimen. The technique was based on the conventional fatigue testing of FAM samples compacted and cored to be 45 mm in height and 12.25 mm in diameter. The testing protocol was conducted by applying a torsional stress to measure the dynamic shear modulus and impose rest periods at different times during the test. During the rest periods, the material regained some of the stiffness it lost due to the applied stress as shown in Figure 8. It was noticed that, by reapplying the same stress amplitude after the rest period, the material followed the same trend that was interrupted by the rest periods. The interrupted curves were then stitched (i.e. conjoined) together to construct one resultant curve that can be used for analysing the fatigue damage.

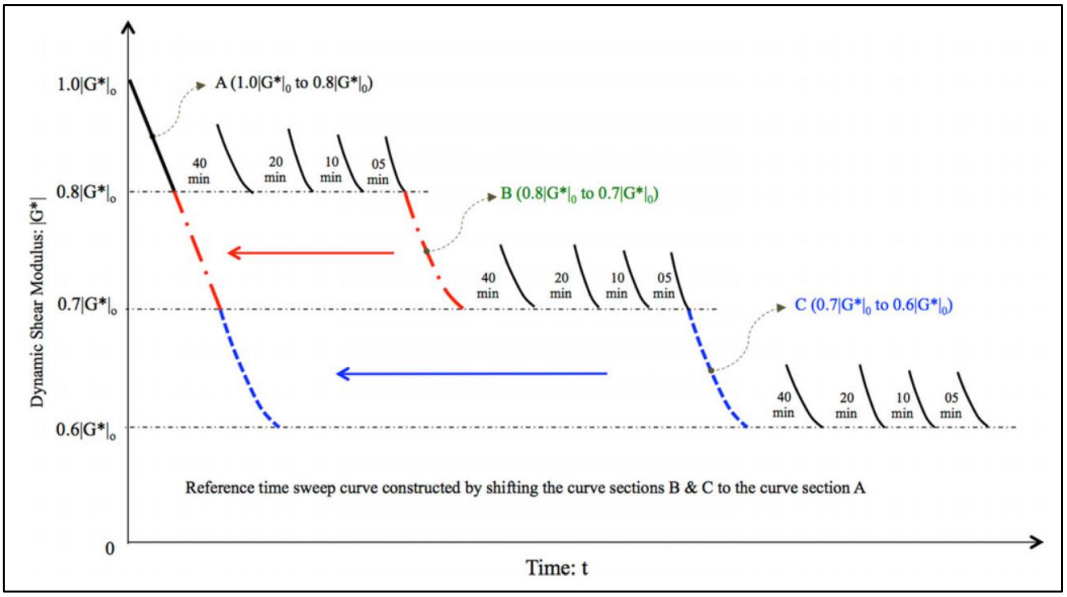

Figure 8: Dynamic shear modulus stitched curve with rest periods (Karki *et al.*, 2014)

The viscoelastic continuum damage (VECD) approach was used to calculate fatigue damage. Then, the same experimental data were used in calculating a healing index based on the internal damage measured by the VECD approach. The analysis of the healing index showed that applying the rest periods at an earlier time during the test increases the healing index. This confirms the dependency of the healing index on time.

A series of studies published by researchers at Texas A&M University presented a continuum mechanic-based viscodamage constitutive relationship to model the fatigue damage and the micro-damage healing (Abu Al-Rub *et al.*, 2010; Darabi *et al.*, 2012, 2013). The model was proposed using the UMAT subroutine in ABAQUS finite element software and validated against laboratory testing. These studies discussed the internal compressive stresses and proved that it helps in the micro-damage healing besides the rest periods.

Some other studies, such as Liu *et al.* (2012) and Tan *et al.* (2012), used sophisticated techniques to measure the healing potential of the asphalt materials. Liu *et al.* (2012) used an infrared camera to measure the healing speed of asphalt mixtures' cores after the addition of steel wool fibres to the asphalt mixture. The study mainly discussed the benefits of adding the steel wool fibres to the healing capability of the asphalt mixture. On the other hand, Tan *et al.* (2012) introduced the use of a digital microscope to monitor the cracks present in the bitumen samples after testing. By microscopic imaging, it was possible to detect hairline cracks at 200 times zoomed images. The study concluded that the bitumen performs better with rest periods and the microstructural configuration of the material has a major effect on the healing potential.

A study by Luo (2012) proposed a new testing protocol using the creep and recovery test on asphalt materials. The analysis concept was based on the crack growth and closure processes due to energy absorbed and dissipated during the loading and recovery phases of the test. Luo discussed the term 'Internal Stresses' presented by many researchers and explained it in her thesis as follows. The internal stresses are driven forces generated by the material itself during the recovery phase of the test. These forces are driving the material to recover when the loading is removed. The internal stresses were measured by applying small stress loads during the recovery phase of the creep and recovery test. The small stress loads are applied at different levels following each other. Step loading can change the residual strain during the recovery phase into one of the following scenarios. The first scenario is when the recovery strain continues to decrease, which indicates that the strain rate has a value less than zero ($\dot{\varepsilon} < 0$). In this case, the applied step load would be lower than the internal stresses generated inside the material to help it to recover. The other scenario

is when the strain becomes constant during the application of the step-loading. This case shows that the applied step-loading would be equal to the internal stresses generated by the material itself ($\dot{\varepsilon} = 0$). In this case, the applied step-loading can be considered as the internal stress of the material at that time of the recovery phase. The last scenario is when the strain changes its trend and increases again during the recovery phase. This case indicates that the step-loading applied imposes a load that is higher than the internal stresses and makes the strain rate above zero ($\dot{\varepsilon} > 0$). Figure 9 explains the concept of the internal stresses described above.

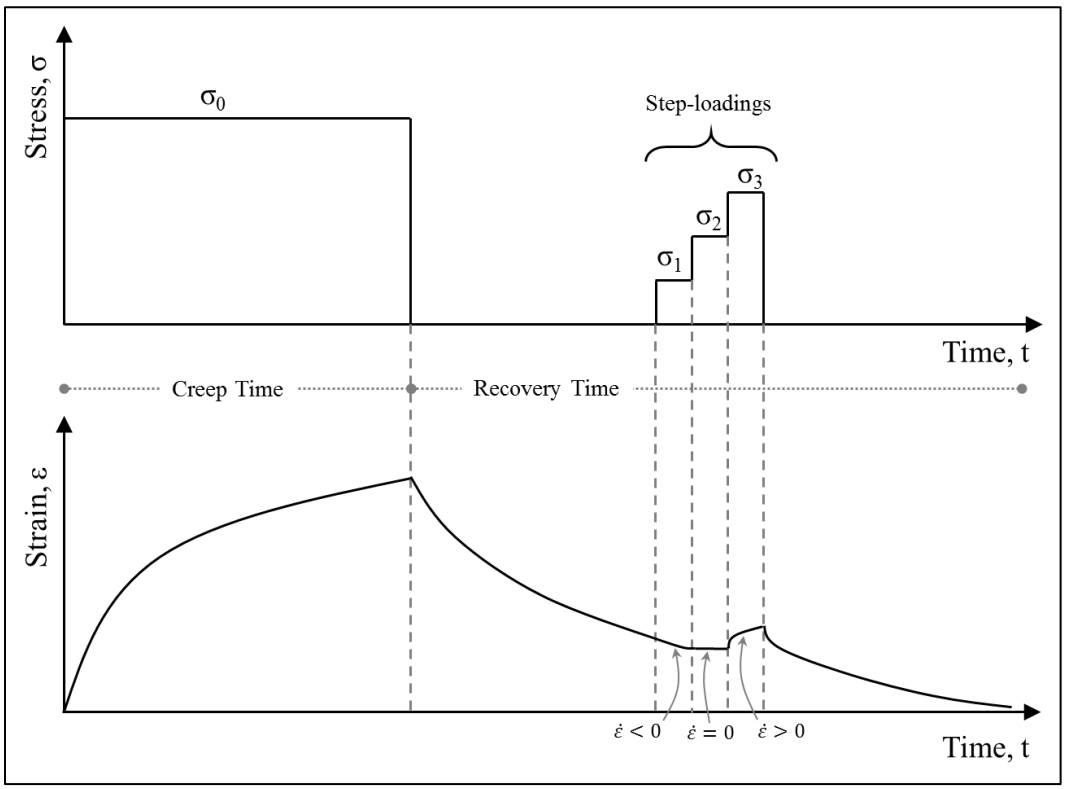

Figure 9: Test protocol for the creep and recovery test with step-loading (Luo, 2012)

To measure the internal stresses, three different step-loadings were selected as a percentage of the original creep load and applied at a different time during the recovery phase. Five step-loadings were applied at the recovery phase in Luo's study, and each step-loading showed a strain rate that is plotted against the time, as shown in Figure 10. The three steps were then fitted with the best-fitting equation and then the stress

that gives a zero strain rate was calculated. This stress was considered as the internal stress at that specific time.

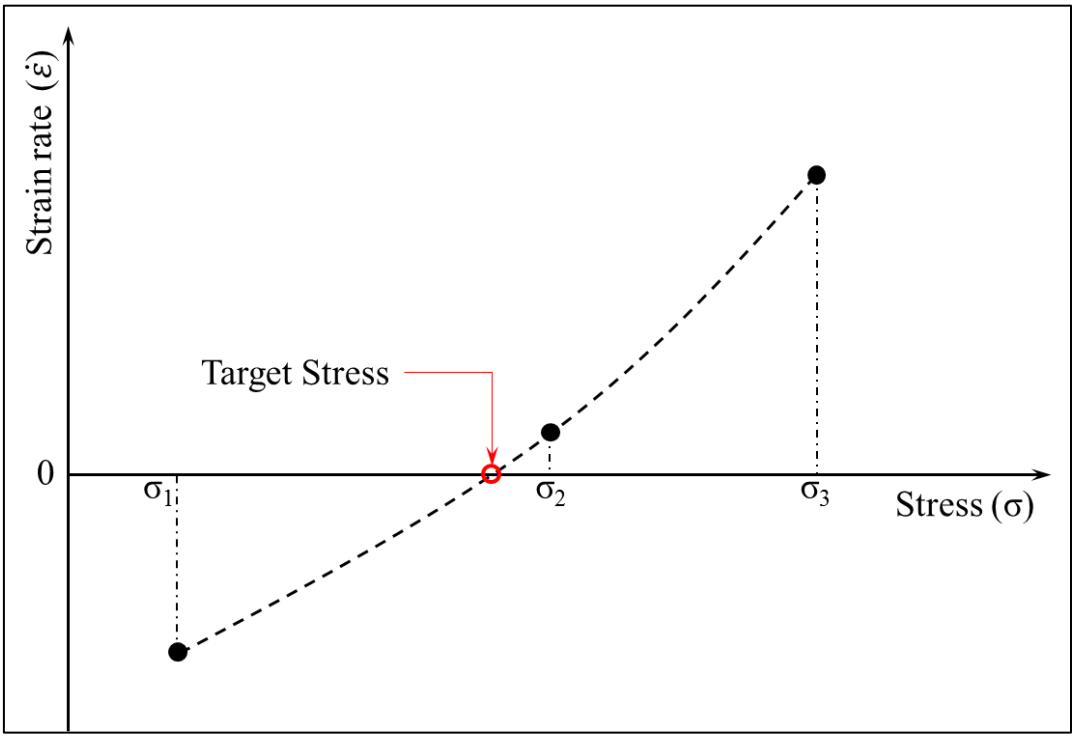

Figure 10: Regression curve to measure the internal stress (Luo, 2012)

Then, the damage and healing characterisation was built based on the balance energy equations that use the apparent (σ^A) and true stress (σ^T) during the creep phase to measure the damage. The true stress indicates the stress that affects the intact material (without the cracks) while the apparent stress is the stress that affects the whole sample (material and cracks). After that, the apparent and true internal stresses were used to calculate the recovery modulus during the recovery phase. Luo (2012) presented the recovery modulus of the material and claimed that it represents the molecules' rearrangement when measured from a non-destructive test.

2.8. Summary

The literature review presented in this chapter showed that only a few studies have been conducted in the Middle East region on the warm mix asphalt (WMA) technology. These studies attempted to highlight the basic benefits of using WMA in the region. However, there are no studies about the performance of WMA under the prevailing climatic conditions in the region, or characterisation of WMA using local materials.

The chapter summarised fatigue characterisation approaches. Moreover, the review covered several related studies on ageing protocols and their viability with the asphalt materials. Investigating UV ageing of asphalt materials has been discussed by many studies. However, they were only investigating the feasibility of the UV ageing with asphalt materials irrespective of the expected climatic conditions. The performance of the UV-aged asphalt materials was discussed in most of the studies that involved the use of weathering machines. The testing was mostly conducted on bitumen and mixtures, but none of the studies has considered the asphalt mastic.

As mentioned in section 2.6, the techniques of measuring the crack size and the change in shape using the X-Ray CT imaging were based on two methods. The first method was to calibrate the thresholding values with experimental measurement of air void percentage, while the second method was based on the individual judgement of the threshold value that covers all air voids in the images. The first method relies on the availability of the material and the tools to measure the air voids in the laboratory to be calibrated with the image sample. The second method has a high risk of error and subjectivity since most of the asphalt mixture images from the X-Ray CT are dark and trying to identify the black spots can be difficult.

Most of the healing studies introduced rest periods in the testing scheme to capture the material regaining some of its stiffness and defined the re-stiffening as healing. The presented testing schemes proposed healing indices which are related to the testing protocol, geometries and testing modes. These indices were not used as universal indices or introduced as a material property to present healing potential. The analysis methods showed a high dependency on the rest periods' duration and application time. These indices can change dramatically from test to test. Luo (2012) tried to overcome this limitation by presenting the idea of internal stresses, crack propagation and healing. However, the study made a few assumptions, which are discussed as follows.

The study performed by Luo (2012) depends on applying only one cycle of creep and recovery to identify healing indices. However, it is well known that one cycle is not enough to show the full material behaviour especially with regard to damage and healing. Also, all the analysis presented in the study was based on the concept of the crack size enlargement and shrinkage during loading and unloading. The study used the recovery modules to define the true and apparent internal stresses which are responsible for the recovery of the intact material and closing the cracks. The equations used in the analysis were considering the crack to have a cone-shaped zone on the top and bottom of it. These zones go through enlargement and shrinkage to absorb and dissipate energy around the crack. It was an interesting concept to present, but it makes many assumptions that could lead to a high risk of the results being misinterpreted.

3. Performance Evaluation of Various WMA Technologies

As mentioned in Chapter 2, WMA technology is relatively new and it was introduced to the asphalt industry for its economic and environmental benefits. The use of WMA technology in the State of Qatar supports the achievement of those benefits that are aligned with the country's recent focus on sustainability and the efficient use of energy. However, implementation of WMA technology in the current practice requires profound technical investigation in order to discern its benefits and performance. This chapter presents the initial assessment conducted on the WMA material in order to develop an initial understanding of its performance. In this stage, testing procedures and analysis approaches were followed in order to characterise the differences in various WMA additives and how they would impact the bituminous material's behaviour.

In this chapter, testing begins by investigating the linear viscoelastic (LVE) behaviour of the bitumen mixed with the selected WMA additives (Advera and Sasobit). This part of the study focused on the rheological properties of the bitumen with WMA additives in terms of their viscosity and Superpave grade. Then, further analysis was conducted to characterise the nonlinear viscoelastic (NLVE) and viscoplastic (VP) properties of the bitumen.

3.1. Linear Viscoelastic Analysis of WMA Bitumen

The LVE response and properties were determined by applying stress or strain and measuring the resultant strain or stress, respectively. The creep compliance, 'D', and the relaxation modulus, 'E_R', are linear viscoelastic properties of the materials that relate the stress and the strain in the time domain, as shown in equation (1).

$$\varepsilon(t) = D(t)\sigma \quad \text{or} \quad \sigma(t) = E_R(t)\varepsilon \tag{1}$$

These parameters, i.e. D(t) and $E_R(t)$, help in predicting the performance of the material under different test modes and amplitudes as long as the material stays within the linear viscoelastic region.

In the frequency domain, when a sinusoidal dynamic stress or strain is applied to the materials, the dynamic modulus (|G*|) is calculated by dividing the maximum applied stress (τ_{max}) over the maximum resultant strain (γ_{max}), while the phase angle (δ) is the time lag between the maximum applied stress and the resultant strain, as shown in Figure 11.

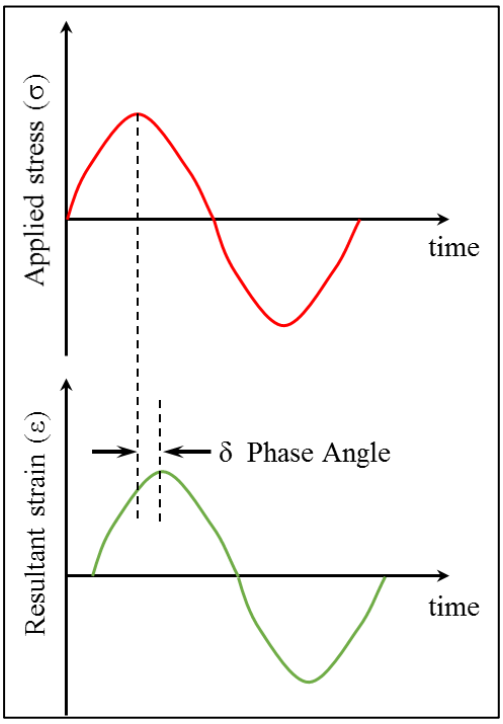

Figure 11: Time lag between maximum applied stress and maximum resultant strain representing the phase angle

Several studies (mentioned in Chapter 2) concluded that using WMA additives altered the rheological properties of the asphalt bitumen. This section includes the measurements of the rheological properties for several WMA additives mixed with

the bitumen. The rheological properties provide standardised parameters that describe the expected performance of WMA during production, at early service life and at long service life. Testing includes assessing the effect of standard ageing processes (RTFO and PAV discussed in Chapter 2) on WMA bitumen's permanent deformation and fatigue-cracking behaviour.

3.1.1. Testing Materials and Methodologies

Several samples of an unmodified bitumen (Pen 60/70) and polymer-modified bitumen (PG 76-22) with and without WMA additives were tested using the Dynamic Shear Rheometer (DSR) and Rotational Viscometer (RV). Both bitumen types were obtained from a local asphalt plant in Qatar. Samples were subjected to standard ageing processes and tested only at low and intermediate temperatures. Standard ageing techniques (i.e. Rolling Thin Film Oven (RTFO) and the Pressurised Ageing Vessel (PAV) procedures) were used for simulating short- and long-term ageing of bitumen, respectively. Three replicate samples were tested as per the experimental matrix shown in Figure 12.

In this study, the Advera additive was mixed with the bitumen at a dosage of 5% of the bitumen weight, while Sasobit was mixed with a 2% dosage based on recommendation stated by the suppliers to achieve lower mixing and compaction temperature.

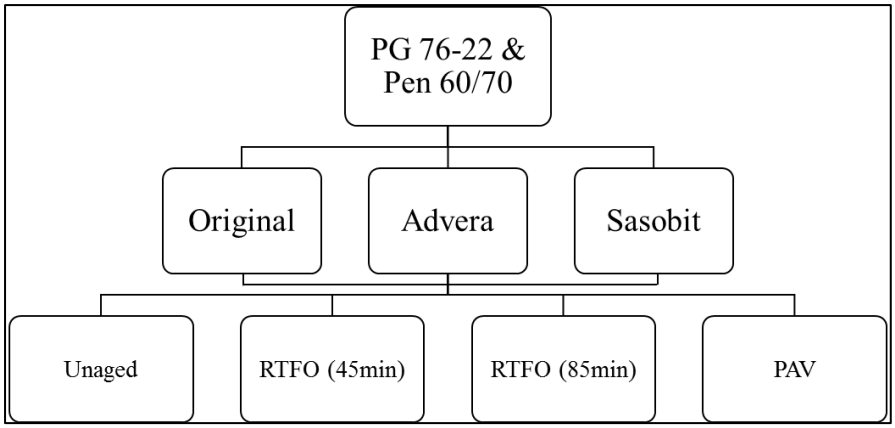

Figure 12: Experimental matrix for modified and unmodified bitumen mixed with WMA additives

The modified bitumen PG 76-22 was heated up to 160°C for 2 hours in the oven and then mixed with the WMA additive using a high shear mixer at 4000 rpm for 10 minutes. A heating bath was used under the sample container at the same temperature to keep the sample heated during mixing. The same procedure was used with unmodified bitumen after heating it up to 130°C for 2 hours. The WMA additives were added to the bitumen in the mentioned dosages while being mixed with a high shear mixer slowly and in portions, as shown in Figure 13. The properties of the WMA additives is mentioned in Table 2.

Figure 13: High shear mixer used in mixing WMA additives with bitumen

Short-term ageing was performed with two different ageing durations: 45 minutes and 85 minutes. The temperature used with both durations was the standard conventional ageing temperature (163°C) as per AASHTO T240 standard. The different durations were used to evaluate the effect of ageing time on the bitumen with different WMA technologies. On the other hand, the long-term ageing process was performed by placing specimens that had already been aged using the RTFO in the pressurised ageing vessel (PAV). The pressure in the PAV is set at 2.10 MPa inside the vessel for 20 hours at 110°C (AASHTO, 2009).

Using the DSR (from TA Instruments, Model DHR-1), the oscillation strain-controlled test was conducted to measure the shear modulus (|G*|) and phase angle (δ) of the bitumen following AASHTO - T 315 (2009). The oscillation strain test was performed at 12% strain amplitude for the unaged bitumen, 10% strain amplitude for the RTFO-

aged bitumen, and 1% strain amplitude for the PAV-aged bitumen. These strain amplitudes were selected based on the target values recommended by the AASHTO standard, which ensured they would be within the linear viscoelastic region. The test was performed by placing the bitumen specimen between the two parallel DSR plates: 25 mm with a 1-mm gap for the unaged and RTFO-aged bitumen, and 8 mm with a 2-mm gap for the PAV-aged bitumen. The test was conducted at PG grade temperatures to assess the performance grading of both bitumen types based on AASHTO - M 320 (2009). Samples of polymer-modified PG 76-22 bitumen were tested at 76ºC to calculate the rutting factor ($|G^*|/\sin(\delta)$) and at 31ºC to calculate the fatigue factor ($|G^*|.\sin(\delta)$), while samples of unmodified Pen 60/70 bitumen (previously graded as PG64-22, as mentioned in Chapter 2) were tested at 64ºC and 25ºC to calculate the rutting factor and the fatigue factor, respectively. The frequency used in these tests was 1.59 Hz (10 rad/sec) as specified in AASHTO T315.

Viscosity measurements were performed using a rotational viscometer from Brookfield by following two methods: rotational speed sweep and temperature sweep. The first method was conducted to evaluate if adding WMA additives would affect the Newtonian behaviour of the bitumen, while the second measurement was performed to evaluate the effect of WMA additives on the bitumen viscosity at mixing and compaction temperatures (Kim *et al.*, 2010). The Newtonian behaviour describes the independency of a fluid's properties on shear rate. Non-Newtonian fluids are the fluids that exhibit different viscosity at different shear rates, while Newtonian fluids keep their viscosity constant regardless of the shear rate, as shown in Figure 14.

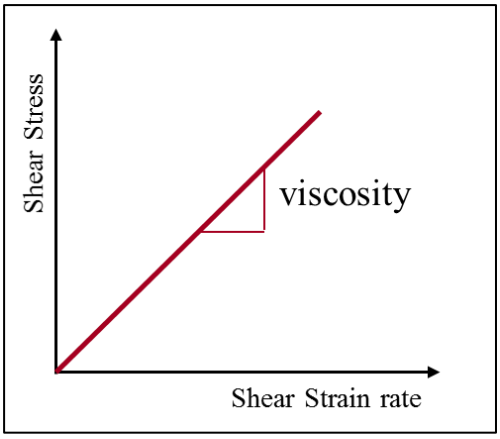

Figure 14: Illustration of Newtonian behaviour of fluids

The current method being used to estimate the mixing and compaction temperatures assumes that the bitumen is a Newtonian fluid. However, Bahia *et al.* (2001) stated in the NCHRP 459 report that most modified bitumens are considered non-Newtonian fluids and their viscosity measurement depends on the shear rate. Hence, the Newtonian behaviour in bitumen mixed with WMA additives should be evaluated prior to measuring the bitumen's viscosity. The viscosity was measured at 20, 40, 60, 80 and 100 rpm at a temperature of 135°C. Then, the viscosity was measured at 165ºC.

3.1.2. Test Results and Discussion

The rutting parameter ($|G^*|/\sin(\delta)$) and fatigue parameter ($|G^*|.\sin(\delta)$) specified in the Superpave specifications were determined using the DSR measurements, and the results are presented in Figure 15 and Figure 16, respectively.

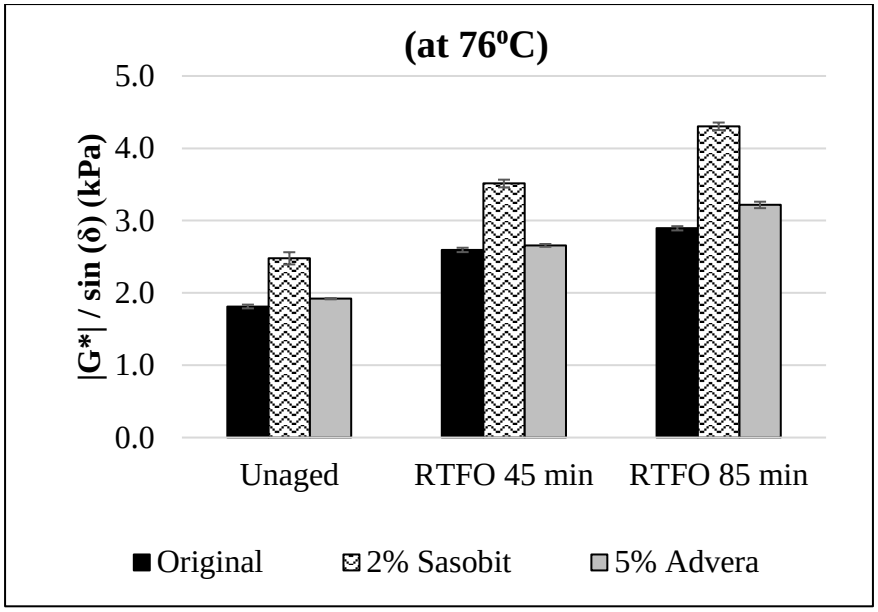

(a) PG76-22

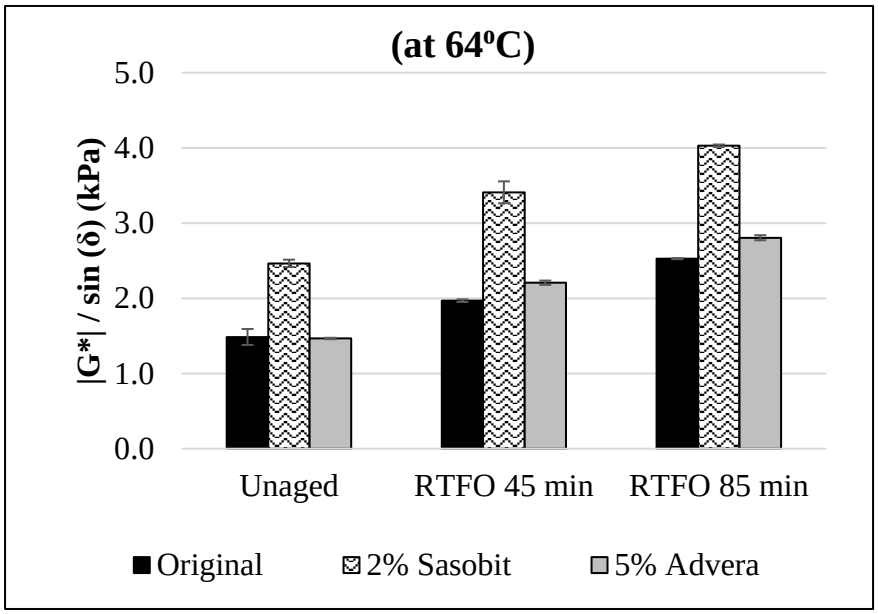

(b) Pen 60/70

Figure 15: Rutting factor (|G*|/sin(δ)) for (a) polymer-modified PG 76-22 bitumen at 76°C and (b) unmodified Pen 60/70 bitumen at 64°C mixed with WMA additives at different ageing processes

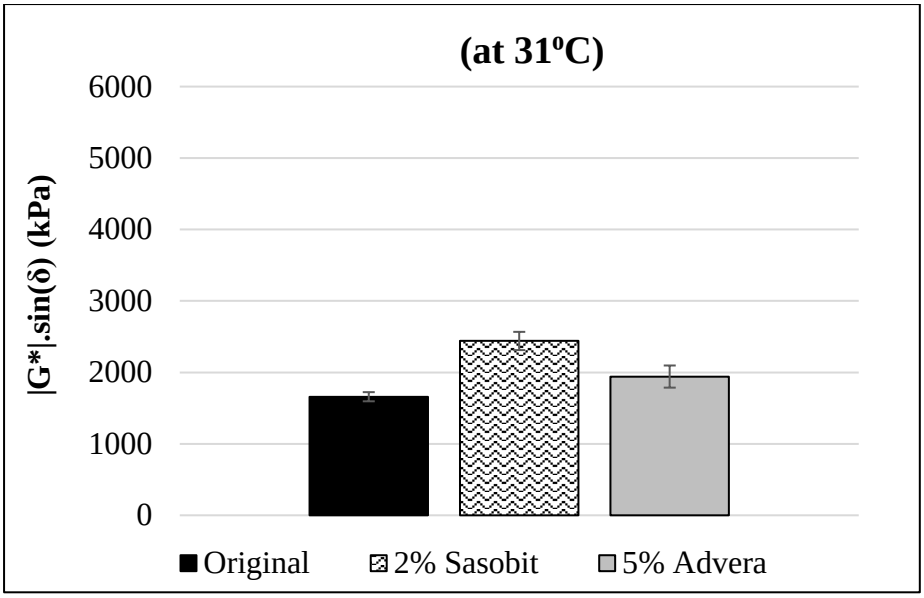

(a) PG76-22

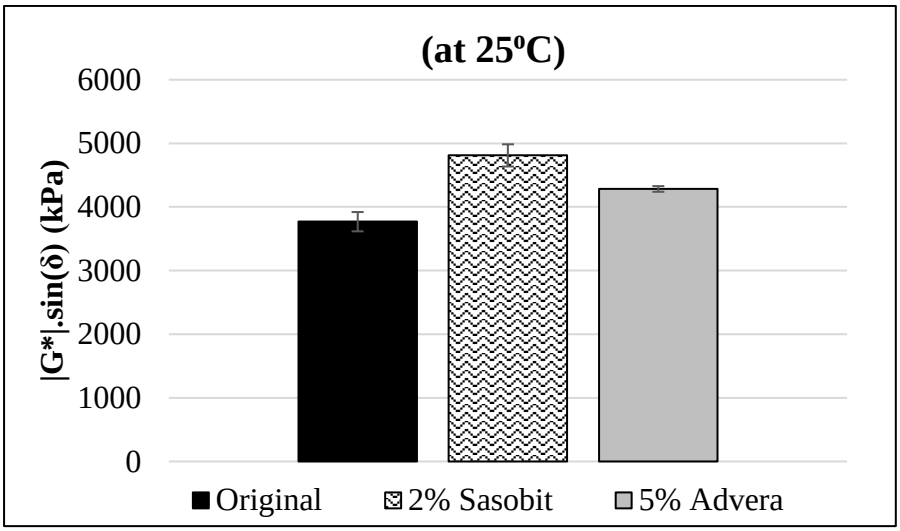

(b) Pen 60/70

Figure 16: Fatigue factor (|G*|.sin(δ)) for (a) polymer-modified PG 76-22 bitumen at 31°C and (b) unmodified Pen 60/70 bitumen at 25°C with different WMA additives and aged by PAV system for long-term ageing

The results show that both bitumen types have similar trends. Adding Sasobit to both bitumen types (PMB and Pen 60/70) increased the rutting and fatigue factors (|G*|/sin δ and |G*|.sin δ). In addition, the rutting and fatigue factors increased with ageing. The rutting factor of the bitumen after adding Sasobit increased at the test temperature (76ºC), which showed that the bitumen with Sasobit could pass the performance grade

specification of PG 82. Similarly, Pen 60/70 with Sasobit can pass the performance grade specification of PG 70.

The effect of adding Advera to both bitumen types was insignificant. The shear modulus and phase angle values remained almost the same before and after adding 5% of Advera. The rutting factor of the original bitumen and the bitumen mixed with Advera did not change before ageing. However, the difference between them was noticeable after the short-term ageing. At a lower temperature, Advera showed minor effect on the binder's fatigue factor compared to Sasobit.

Bitumen samples were tested using the Rotational Viscometer at 135° C with different WMA additives using different rotational speeds (20, 40, 60, 80 and 100 rpm). It can be seen in Figure 17 that the bitumen kept the Newtonian behaviour with various WMA additives and the change in the rotation speed did not change the viscosity of the bitumen significantly at a single temperature. However, it can also be noticed that the viscosity measurement showed small shear thinning behaviour at the beginning of the test (at 20 rpm) which might be related to fluctuation of the measurements.

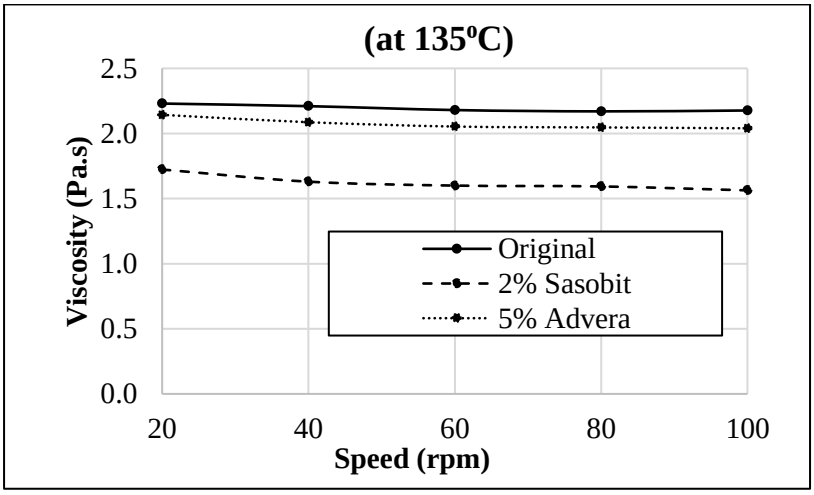

(a) PG76-22

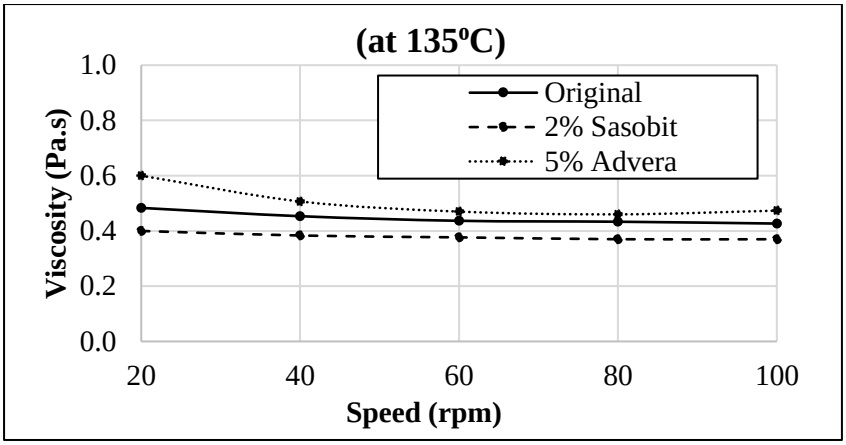

(b) Pen 60/740

Figure 17: Viscosity measurements at different rotational speeds for (a) polymer-modified PG 76-22 bitumen and (b) unmodified Pen 60/70 bitumen mixed with WMA additives

On the other hand, Figure 18 shows that the addition of Sasobit to the polymer-modified PG 76-22 bitumen had a greater effect than adding Advera. Sasobit lowered the viscosity of the bitumen at mixing and compaction temperatures (135ºC and 165ºC). Inversely, adding Advera resulted in a minor reduction in viscosity at both temperatures.

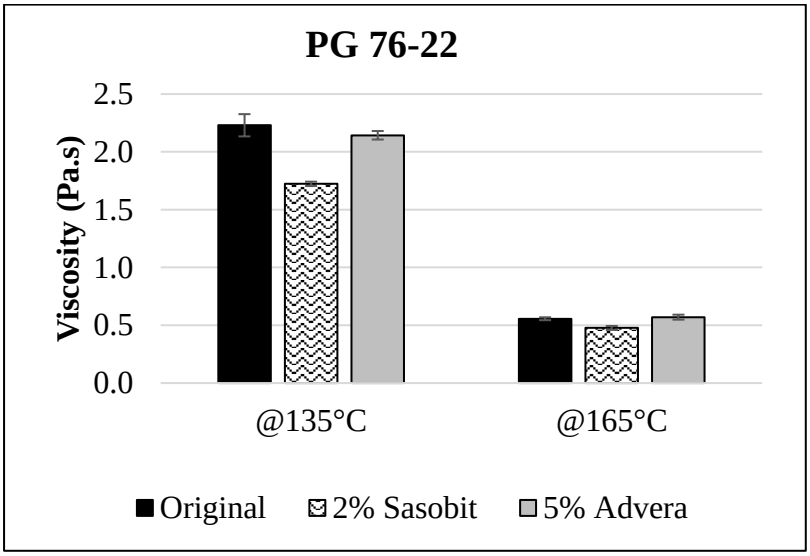

(a)

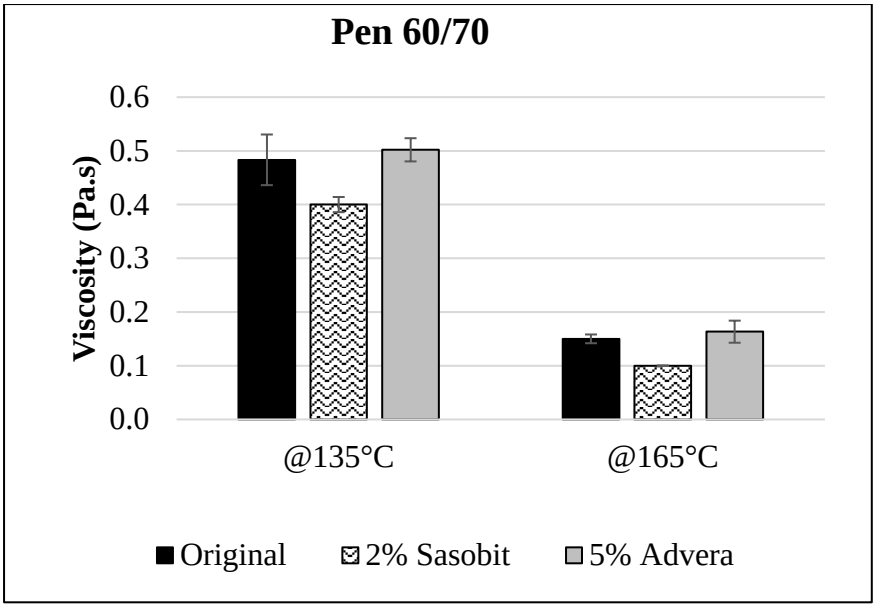

(b)

Figure 18: Viscosity measurements at 20 rpm for (a) PG 76-22 (b) Pen 60/70 bitumen mixed with WMA additives

As mentioned earlier, this section includes a preliminary assessment of the properties of bitumens incorporating WMA additives under alternative ageing processes. Sasobit additive increased the rutting factor and elevated the PG grade of the bitumen by one unit (6° C in PG grading) when added by 2% of the weight of the bitumen. This stiffness increment also affected the fatigue factor, which increases the possibility of fatigue cracking at intermediate service temperatures. Sasobit increased the bitumen stiffness in all ageing processes. Viscosity decreased when using Sasobit at the conventional mixing and compaction temperatures.

Mixed at a dosage rate of 5% of bitumen weight, Advera has a limited effect on bitumen. It had a minor influence on the performance of bitumen against rutting resistance. However, it increased the potential of fatigue cracking at a low temperature.

Viscosity measurements showed that a valuable reduction in viscosity would occur when mixing Sasobit with modified or unmodified bitumen, while the effect of Advera

was negligible with both bitumen types. However, the addition of WMA additives did not influence the Newtonian behaviour of the bitumen, even with the polymer-modified bitumen.

3.2. Nonlinear Viscoelastic and Plasto-Viscoelastic Analysis of WMA Bitumen

The characterisation of bitumen used in WMA has focused in the past primarily on measuring the Superpave parameters that are based on linear viscoelastic responses. However, the Multiple Stress Creep Recovery (MSCR) test is more suitable for characterisation of resistance to permanent deformation because it applies higher strain levels and measures accumulated strains (Golalipour 2011; D'Angelo *et al.* 2007; Shirodkar *et al.* 2012). Many researchers have used the MSCR test in characterising the effect on the bitumen's performance of adding the WMA additives (Adorjányi and Füleki, 2011; Arega *et al.*, 2011; Arega and Bhasin, 2012; Zelelew *et al.*, 2013).

A number of laboratory studies have shown that some WMA additives have an adverse effect on rutting resistance of asphalt mixtures (Arega *et al.*, 2011). However, Zelelew *et al.* (2013) found that Sasobit improved the deformation resistance while Advera reduced it in comparison with the control bitumen. Arega and Bhasin (2012) evaluated the rutting resistance of asphalt bitumen mixed with WMA additives using the MSCR test. They showed that WMA additives (Evotherm, Rediset and Advera) except Sasobit reduced the permanent deformation resistance.

As mentioned in Chapter 2, use of the MSCR test was proposed originally by D'Angelo *et al.* (2007) to evaluate the resistance of bitumen to permanent deformation at high temperatures. In the MSCR analysis method, the non-recoverable creep

compliance (J_{nr}) is calculated by dividing the unrecovered strain by the loading stress, which gives this method the advantage of comparing bitumen's response at different stress levels. However, the use of J_{nr} has the limitation of calculating the unrecovered strain based on the time used in the test for recovery. The unrecovered strain, calculated after 9 seconds of recovery, might include more recoverable strain that did not have enough time to recover within the 9 seconds. Masad *et al.* (2009) developed an analytical approach to analyse the nonlinear plasto-viscoelastic (NPVE) response of bitumen by separating the total strain obtained from the MSCR test into recoverable and irrecoverable components. This analysis approach isolates the effect of time on the recovery response and identifies the amount of irrecoverable strain. This section utilises the approach presented by Masad *et al.* (2009) to analyse the nonlinear plasto-viscoelastic response of bitumen mixed with WMA additives and evaluate its resistance to permanent deformation.

The primary objective of this section is to evaluate the efficacy of different approaches (viscoelastic and plasto-viscoelastic) in characterising the resistance of WMA bitumen to permanent deformation. This objective is achieved by evaluating the non-recoverable creep compliance (J_{nr}) and the unrecovered (permanent) strain determined following the plasto-viscoelastic analysis approach.

3.2.1. Testing Materials and Methodologies

The MSCR test was performed using the DSR at two different stress levels, 0.1 kPa and 3.2 kPa. The creep stress was applied to the sample for 1 second and then released for 9 seconds for relaxation. Ten cycles for both stress levels were applied to the bitumen specimen placed between the 25 mm parallel plates. The plates were heated to 76ºC and 64ºC after placing the bitumen specimen to test the polymer-modified PG 76-22 bitumen and unmodified Pen 60/70 (considered as PG64-22) bitumen,

respectively. Equilibrium time of 10 minutes was given to the specimen to ensure equal temperature distribution within the specimen and the plates. No time gaps were left between stress levels, and the strain was not zeroed after the low-stress level and before the high-stress level. Three replicate samples were tested for each bitumen type and each additive type. The test was performed by following the AASHTO - TP 70 (2009) method on RTFO bitumen residue. However, the test was also executed on unaged samples to consider the effect of the ageing on the bitumen with different WMA additives (Arega *et al.*, 2013).

3.2.1.1. Nonlinear Viscoelastic Analysis and Results

The MSCR test was performed on RTFO-aged bitumen samples to explore their rutting resistance at early stages. Using the MSCR test on an original bitumen (unaged) sample was meant to show the effect of WMA additives on the bitumen's performance before and after the construction process. From the MSCR test, the strain at the beginning of the cycle (ε_0), the strain at the end of creep phase (ε_c), and the strain values at the end of the recovery phase (ε_r) are captured for all cycles and both stress levels as shown in Figure 19.

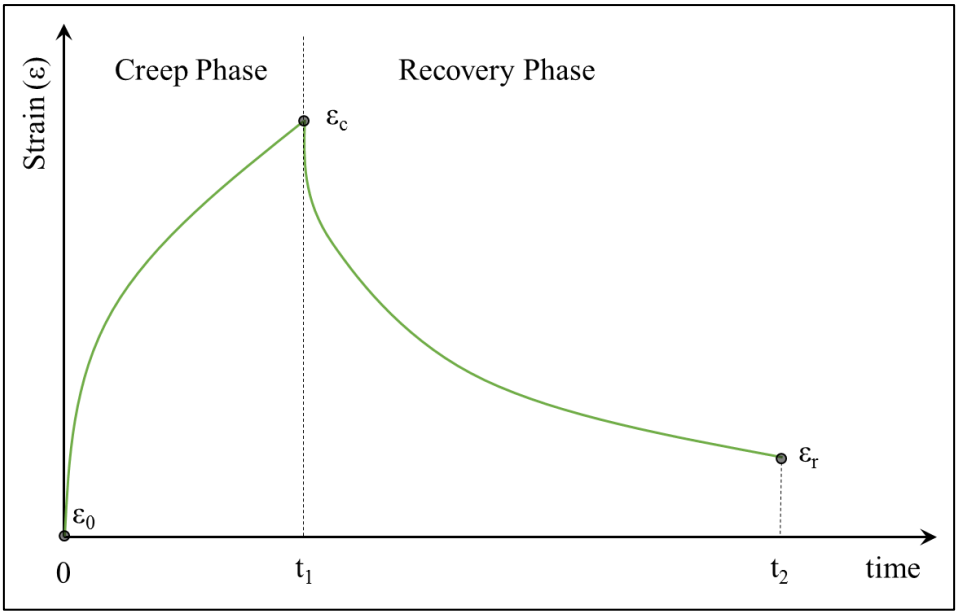

Figure 19: Points of interest to calculate the recovery percentage and the non-recoverable creep compliance from the MSCR test

As shown in Table 3, typical results from MSCR test is listed for both stress levels for the original bitumen (without WMA additive).

Table 3: Typical strain results from MSCR test

Creep Stress Level = 0.1 kPa			
Cycle	**Initial Strain %**	**Creep Stain %**	**Recovery Strain %**
	ε_0	**ε_c**	**ε_r**
1	0.0	33.8	5.5
2	5.5	38.7	8.8
3	8.8	42.0	11.5
4	11.5	44.6	13.8
5	13.8	46.8	15.8
6	15.8	48.7	17.7
7	17.7	50.5	19.4
8	19.4	52.2	21.1
9	21.1	53.8	22.6
10	22.6	55.3	24.2
Creep Stress Level = 3.2 kPa			
Cycle	**initial Strain %**	**Creep Stain %**	**Recovery Strain %**
	ε_0	**ε_c**	**ε_r**
1	0.0	1013.1	347.8
2	347.8	1538.4	858.6

3	858.6	2140.6	1488.2
4	1488.2	2844.9	2235.6
5	2235.6	3657.7	3096.5
6	3096.5	4563.7	4047.4
7	4047.4	5542.6	5064.6
8	5064.6	6581.4	6136.6
9	6136.6	7671.3	7255.4
10	7255.4	8802.3	8413.6

The percentage of recovery and the non-recoverable creep compliance were calculated using equations (2) and (3), respectively:

$$J_{nr}(\text{kPa}^{-1}) = \frac{\varepsilon_r - \varepsilon_0}{\text{Stress Level}} \quad \textbf{(2)}$$

$$R\ (\%) = \frac{\varepsilon_c - \varepsilon_r}{\varepsilon_c - \varepsilon_0} \quad \textbf{(3)}$$

Figure 20 and Figure 21 show the percentage of recovery ($R_{0.1}$ and $R_{3.2}$) and the non-recoverable creep compliance ($J_{nr0.1}$ and $J_{nr3.2}$) at both stress levels (0.1 and 3.2 kPa) and in different ageing processes for PMB bitumen PG76-22.

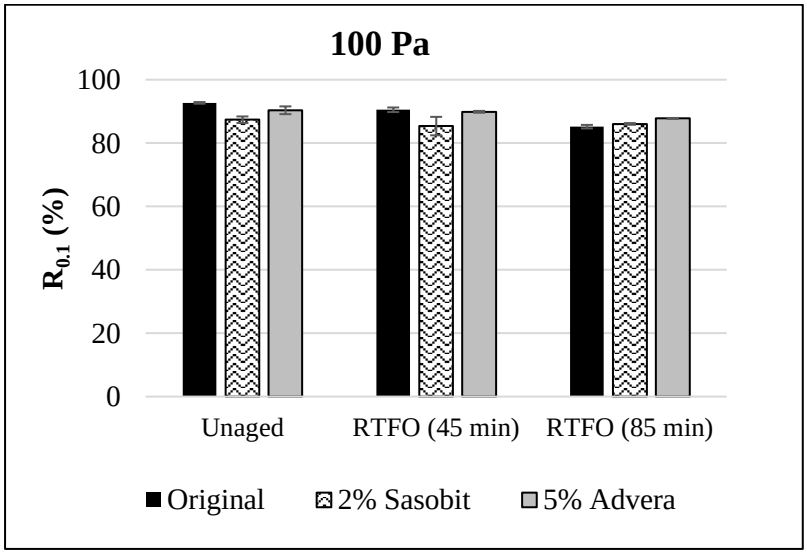

(a)

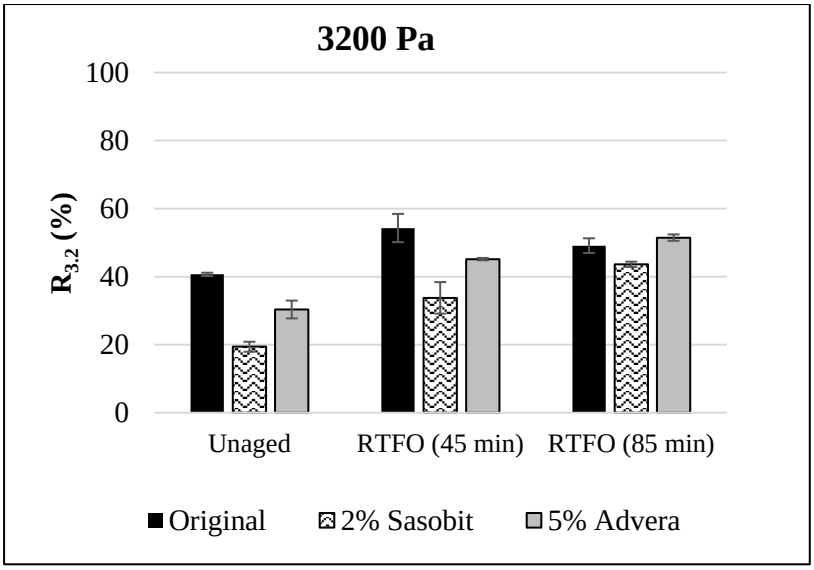

(b)

Figure 20: Percentage recovery results from the MSCR test for polymer-modified PG 76-22 bitumen mixed with WMA additives at different ageing processes

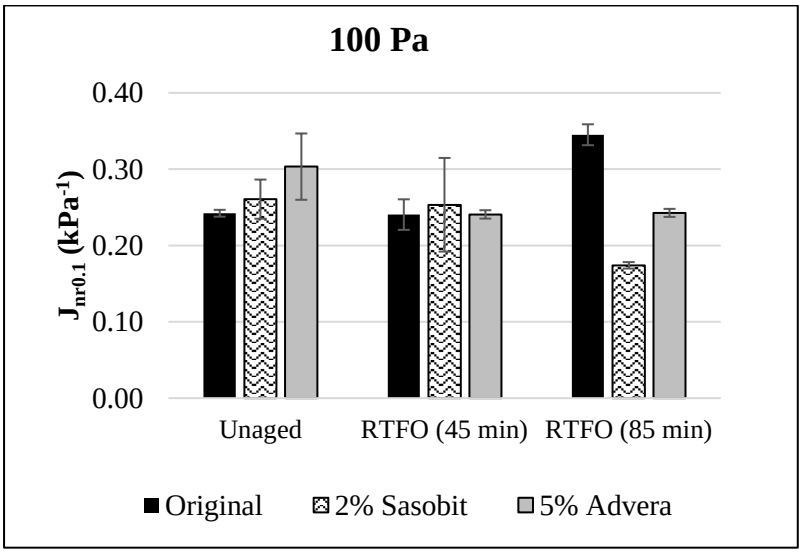

(c)

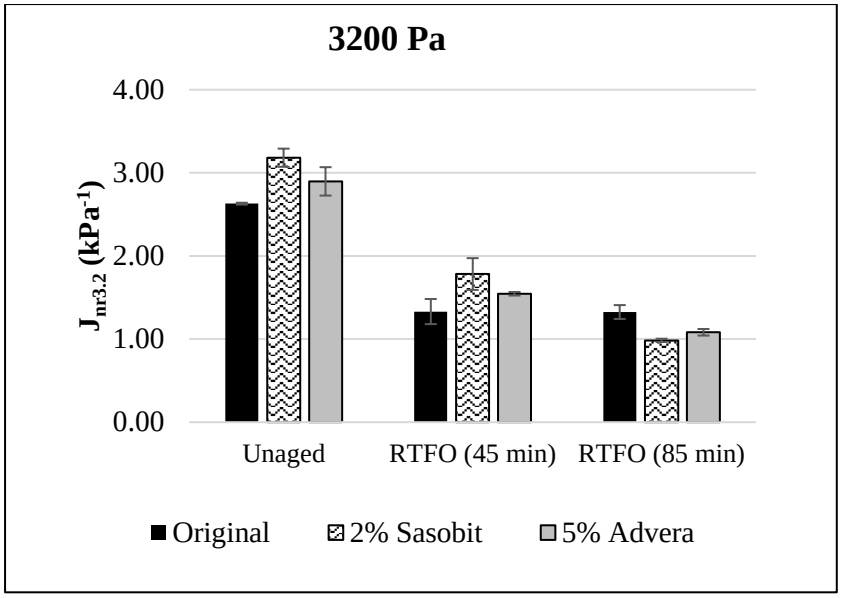

(d)

Figure 21: Non-recoverable creep compliance (J_{nr}) results for polymer-modified PG 76-22 bitumen mixed with WMA additives at different ageing processes

It can be noticed from Figure 20(a) that the difference in the percentage of recovery at 0.1 kPa stress level changed slightly with different ageing and WMA additives. Therefore, the comparison between WMA bitumen types at a low-stress level is insufficient. However, in the case of the high-stress level (3.2 kPa), the percentage of recovery is getting higher - with and without the WMA additives - with more ageing since the material gets stiffer. After the complete short-term ageing (total period of 85 min.), the samples containing either Advera or Sasobit showed a roughly similar percentage of recovery to the original bitumen. Results showed that bitumen mixed with WMA additives would have a similar performance against rutting after the bitumen had been fully RTFO aged. Equally, the non-recoverable creep compliance (J_{nr}) values were very close after the complete short-term ageing, while all $J_{nr3.2}$ values met the heavy traffic 'H' classification (maximum 2.0 kPa^{-1}) for all additives.

The results of the experiments on unmodified Pen 60/70 bitumen shown in Figure 22 and Figure 23 indicate that the Sasobit had a more significant effect on the percentage

of recovery and non-recoverable creep compliance than the polymer-modified bitumen did.

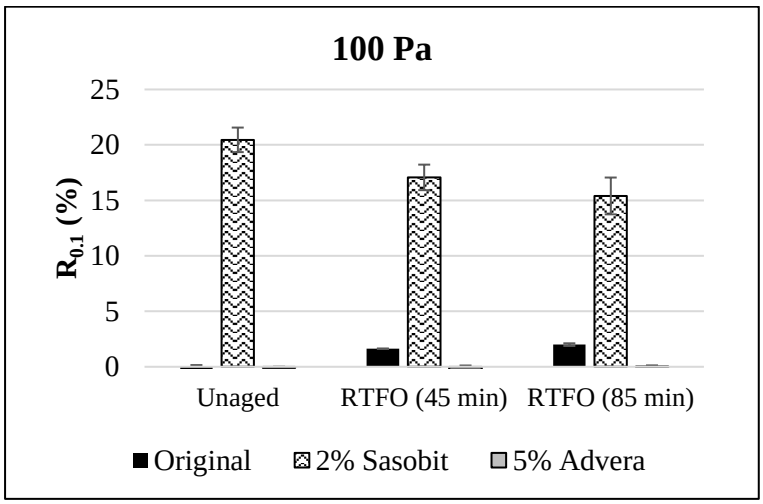

(a)

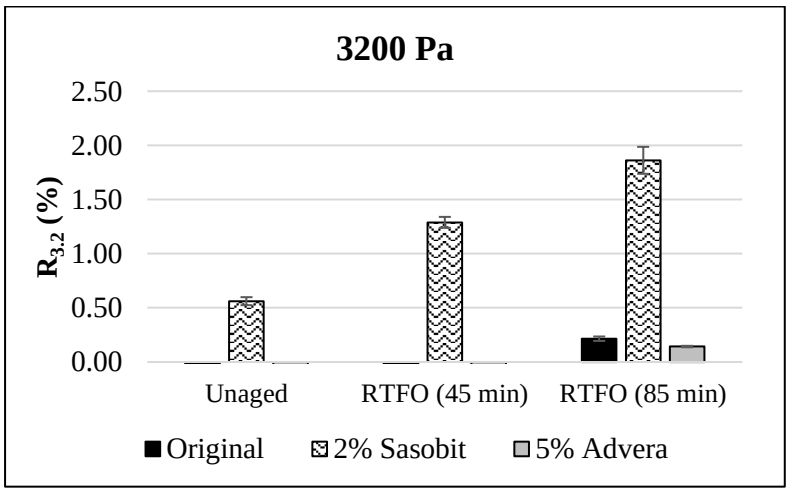

(b)

Figure 22: Percentage of recovery for unmodified Pen 60/70 bitumen mixed with WMA additives at different ageing processes

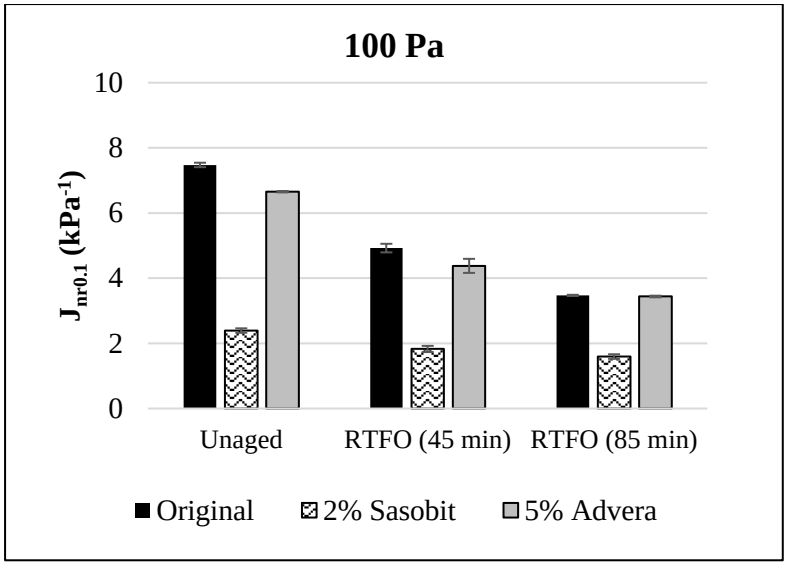

(c)

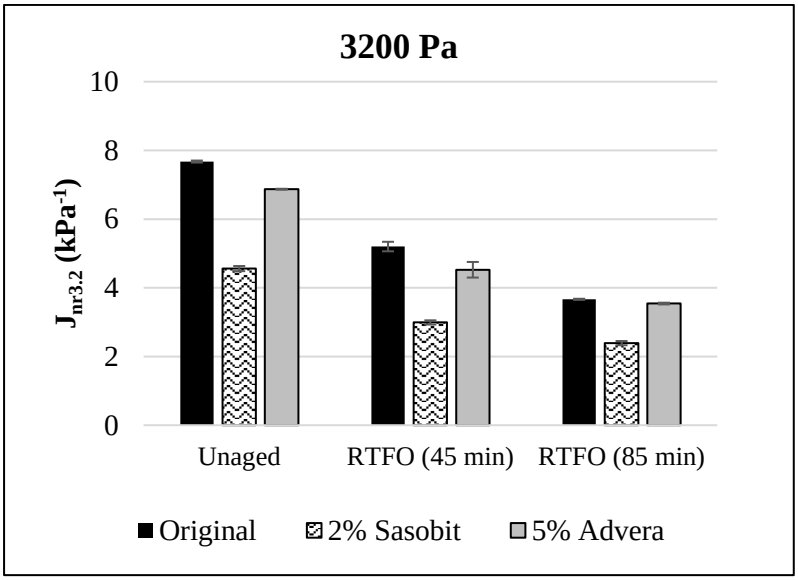

(d)

Figure 23: Non-recoverable creep compliance (J_{nr}) results for unmodified Pen 60/70 bitumen mixed with WMA additives at different ageing processes

The addition of Sasobit increases the percentage of recovery relative to the original bitumen, as shown in Figure 22. The effect of Sasobit on the percentage of recovery appears in both high- and low-stress levels. On the other hand, adding Advera to the Pen 60/70 bitumen did not improve the performance of the bitumen against permanent deformation; inversely, it lowered the recovery over complete short-term ageing. Adding Sasobit significantly lowered the non-recoverable creep compliance of the Pen

60/70 bitumen over ageing at both stress levels, while the effect of the Advera was considered to be very small. However, as shown in Figure 23, this reduction did not change the traffic specification grade for the bitumen, which was standard traffic classification 'S' (maximum of 4.0 kPa^{-1}).

3.2.2. Test Results and Discussion

The approach developed by Masad *et al.* (2009) for the analysis of MSCR test data was used to determine the total permanent strain (rutting). This analysis approach is based on the recovery response of the bitumen that could exhibit nonlinear viscoelastic behaviour. The unrecovered strain of the nonlinear viscoelastic behaviour does not necessarily equate with the total permanent strain. The accumulated strain might also include some viscoelastic strain that was not fully recovered because the recovery time allowed in the test was relatively short.

The MSCR test experimental data were analysed using Schapery's single integral model to define the nonlinear viscoelastic behaviour of the asphalt bitumen (Schapery, 1969). Based on a series of studies, the bitumen showed that it could exhibit a nonlinear viscoelastic behaviour. The nonlinear behaviour appears as a response to high strains developed when the bitumen is within the asphalt mix (Cheung and D Cebon, 1997; Cheung and D. Cebon, 1997; Gordon *et al.*, 2002, 2004; Masad and Somadevan, 2002).

The total accumulated strain (ε^{total}) is the sum of the recoverable and the irrecoverable strains, as shown in equation (4) (Huang *et al.*, 2011):

$$\varepsilon^{total} = \varepsilon^{rec} + \varepsilon^{irrec} \quad \textbf{(4)}$$

Following Schapery's nonlinear viscoelastic model (Schapery, 1969), the nonlinear recoverable strain component can be represented as follows:

$$\varepsilon^{rec} = g_0 D_0 \sigma + g_1 \int_0^t \Delta D(\Psi - \Psi^t) \frac{dg_2 \sigma}{d\tau} d\tau \quad \textbf{(5)}$$

where σ is the stress, Ψ is reduced time, and τ is the time.

The first term of equation (5) represents the instantaneous response of the asphalt bitumen, as shown in Figure 24, while D_0 is the linear instantaneous compliance. This part is discounted in the analysis because, at a high temperature, defining the instantaneous response from the experimental measurement is not feasible.

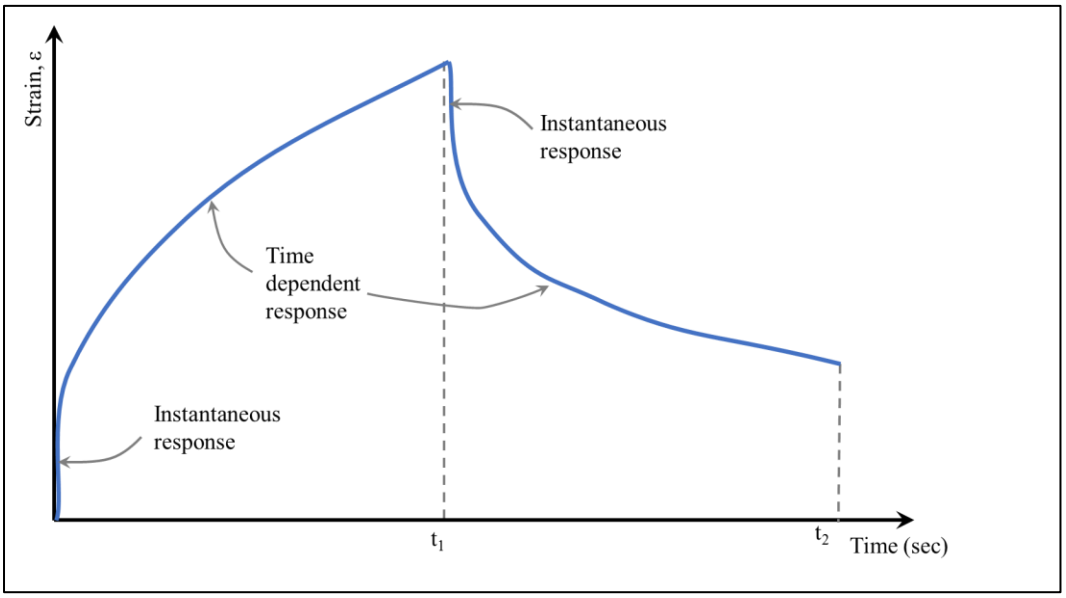

Figure 24: Diagram for the creep and recovery strain response

The second term of equation (5) represents the time-dependent response where ΔD is the transient linear compliance and Ψ^t is the reduced retardation time. The parameters of g_0, g_1, and g_2 quantify the nonlinear response and are affected by the shape of creep and recovery strain curves. An increase in g_2 means that the creep and recovery strains are increasing, which indicates that the material becomes softer (Masad *et al.*, 2009).

An increase in g_1 also indicates that the material becomes softer, but it is affected only by the creep strain.

The transient linear compliance (ΔD) can be signified by using the Prony Series model as follows:

$$\Delta D(\Psi^t) = \sum_{n=1}^{N} D_n(1-e^{(-\lambda_n \Psi^t)}) \quad \textbf{(6)}$$

where D_n and λ_n are coefficients of the Prony Series model. The value of 'n' is the number of Prony's Series used for a specific material to represent its behaviour. Time (ψ^t) was not reduced with shifting factor because the test was performed at a single temperature, so the shifted time (ψ^t) can be replaced with normal time (t). The number of Prony's Series coefficients can be predicted by fitting the recoverable strain during recovery phase at the first cycle which is assumed to have no damage.

Numerical equations for the creep and recovery strains are developed in a systematic pattern for each cycle (total of 20 cycles: 10 for the low-stress level followed by 10 for the high-stress level). The equations were developed based on the Boltzmann superposition integral of equation (5). The principle of the Boltzmann superposition integral (or sometimes called 'Duhamel's integral') can be used for any stress analysis problem where stress (or strain) happens at a different time (Brinson and Brinson, 2008; Gutierrez-Lemini, 2014). It can be applied to find the strain response of variable stress inputs that are expressed by a series of step stresses which begins at a different time as per the Multiple Stress Creep Recovery (MSCR) test protocol.

Equations (7) and (8) present creep and recovery strains for the first cycle, while equations (9) and (10) are for creep and recovery strains for the second cycle. g_1^n, g_2^n

are the nonlinear parameters with 'n' as the cycle number, while $\Delta D(t)$ is the Prony's Series measured at a certain time (t).

$$\varepsilon_1^c(t) = g_1^1 g_2^1 \sigma_1 \Delta D(t) + \varepsilon^{irrec}(t) \quad \textbf{(7)}$$

$$\varepsilon_1^r(t) = \left[g_2^1 \sigma_1 \Delta D(t) - g_2^1 \sigma_1 \Delta D(t-t_a)\right] + \varepsilon^{irrec}(t_a) \quad \textbf{(8)}$$

$$\varepsilon_2^c(t) = g_1^2\left[g_2^1 \sigma_1 \Delta D(t) - g_2^1 \sigma_1 \Delta D(t-t_a) + g_2^2 \sigma_2 \Delta D(t-t_b)\right] + \varepsilon^{irrec}(t) \quad \textbf{(9)}$$

$$\varepsilon_2^r(t) = \left[g_2^1 \sigma_1 \Delta D(t) - g_2^1 \sigma_1 \Delta D(t-t_a) + g_2^2 \sigma_2 \Delta D(t-t_b) - g_2^2 \sigma_2 \Delta D(t-t_c)\right] + \varepsilon^{irrec}(t_c) \quad \textbf{(10)}$$

The Prony's Series (i.e. D_n and λ_n) coefficients were obtained by minimising the error between the experimental recoverable strain ($\Delta\varepsilon_1^r(t)$) shown in Figure 25 at the first cycle (n = 1). The number of Prony's Series 'n' varies and depends on the fitting quality. Using a higher number of coefficients can give an accurate fitting, but the optimisation process becomes complicated. As demonstrated in some previous studies, fixing the retardation time 'λ_n' and determining the compliance coefficients 'D_n' makes the fitting process more efficient (Huang *et al.*, 2011).

In the first cycle, when the stress level is the lowest, the asphalt bitumen exhibits a linear behaviour where g_1 and g_2 parameters are assumed to be equal to unity. In this cycle, coefficients of the Prony Series can be obtained by minimising the error between $\Delta\varepsilon_1^r(t)$ for the experimental data and the numerical model. The $\Delta\varepsilon_1^r(t)$ is the difference between the creep strain at the end of loading (t_a) and recovery strain during the unloading in the first cycle, as it assumes there is no viscoplastic strain during the recovery phase of the first cycle at the lowest stress level, as shown in equation (11) below and Figure 25:

$$\Delta\varepsilon_1^r = \varepsilon_1^c(t_a) - \varepsilon_1^r(t) = \sigma_1[\Delta D(t_a) - \Delta D(t) + \Delta D(t-t_a)] \qquad t \in [t_a, t_b] \tag{11}$$

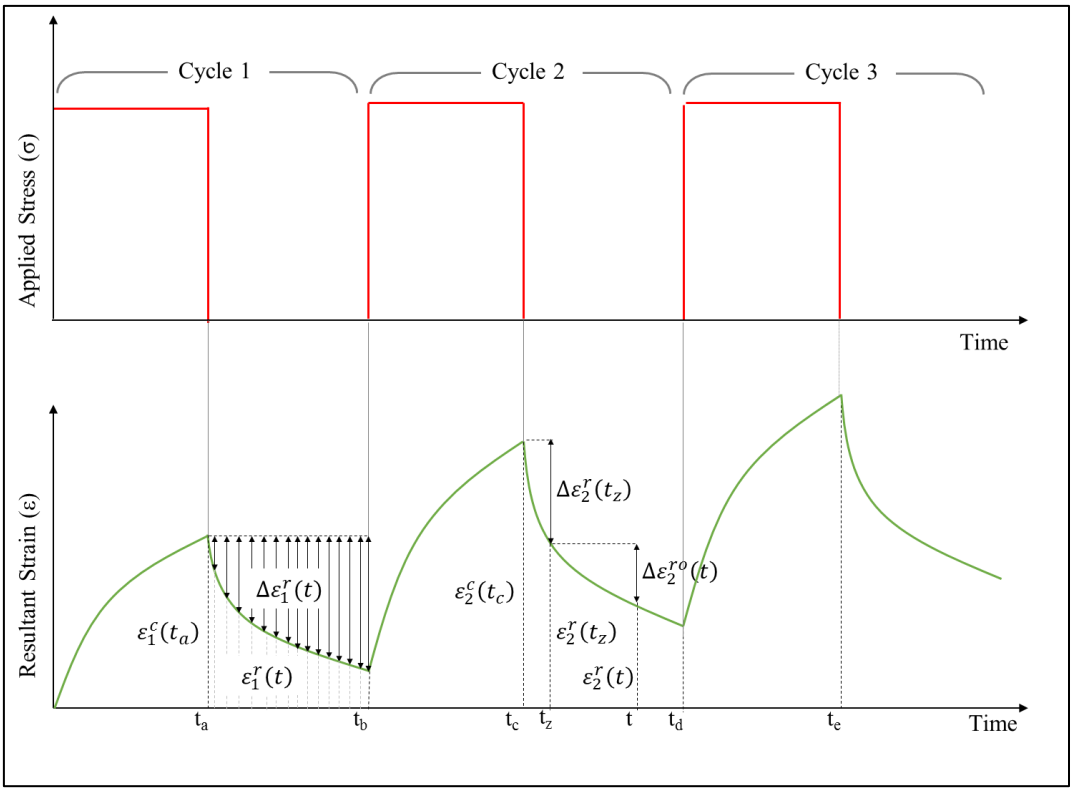

Figure 25: Sketch of the creep and recovery response and points of interest for the optimisation process (Masad *et al.*, 2009)

Once the coefficients of the Prony Series were determined, g_1 and g_2 values were calculated for cycle 2 up to cycle 20. The error between $\Delta\varepsilon^{ro}(t)$ from the experimental data and the numerical model was minimised to optimise g_2 value. $\Delta\varepsilon^{ro}(t)$, as shown in equation (12), is the difference between the recovery strain at a particular time during unloading (t_z) and the recovery strain during unloading. The value of 't_z' in this study was chosen to be the tenth time reading from the experimental data during the unloading for each cycle.

$$\Delta\varepsilon_2^{ro}(t) = \varepsilon_2^r(t_z) - \varepsilon_2^r(t) = \sigma_1 g_2^1[\Delta D(t_z) - \Delta D(t_z - t_a) - \Delta D(t) + \Delta D(t - t_a)] + \sigma_2 g_2^2[\Delta D(t_z - t_b) - \Delta D(t_z - t_c) - \Delta D(t - t_b) + \Delta D(t - t_c)] \tag{12}$$

Once g_2 is determined, g_1 is determined by minimising the error between $\Delta\varepsilon^r(t_z)$ from the experimental data and the numerical model. $\Delta\varepsilon^r(t_z)$ is the difference between the creep strain at the end of loading (t_c) and the recovery strain at the tenth time reading of the experimental data (t_z).

$$\Delta\varepsilon_2^r(t_z) = \varepsilon_2^c(t_c) - \varepsilon_2^r(t_z) = g_1^2[\sigma_1\Delta D(t_c) - \sigma_1\Delta D(t_c - t_a) + g_2^2\sigma_2\Delta D(t_c - t_b)] - [\sigma_1\Delta D(t_z) - \sigma_1\Delta D(t_z - t_a) + g_2^2\sigma_2\Delta D(t_z - t_b) - g_2^2\sigma_2\Delta D(t_z - t_c)] \quad \textbf{(13)}$$

The same procedure was repeated for all cycles in both stress levels to optimise g_1 and g_2 values. Then, the irrecoverable creep and recovery strains were obtained by subtracting the experimental strain values from the recoverable creep and recovery strain values obtained by the numerical equations.

Calculating J_{nr} for each cycle changed from the conventional MSCR analysis (equation (2)) to be as follows:

$$J_{nr}^{irr}(kPa^{-1}) = \frac{\varepsilon_r^{irr} - \varepsilon_0^{irr}}{\text{Stress Level}} \quad \textbf{(14)}$$

where ε_r^{irr} is the irrecoverable strain value at the end of the recovery phase in each cycle and ε_0^{irr} is the initial irrecoverable strain at the beginning of the loading phase in each cycle, as shown in Figure 26.

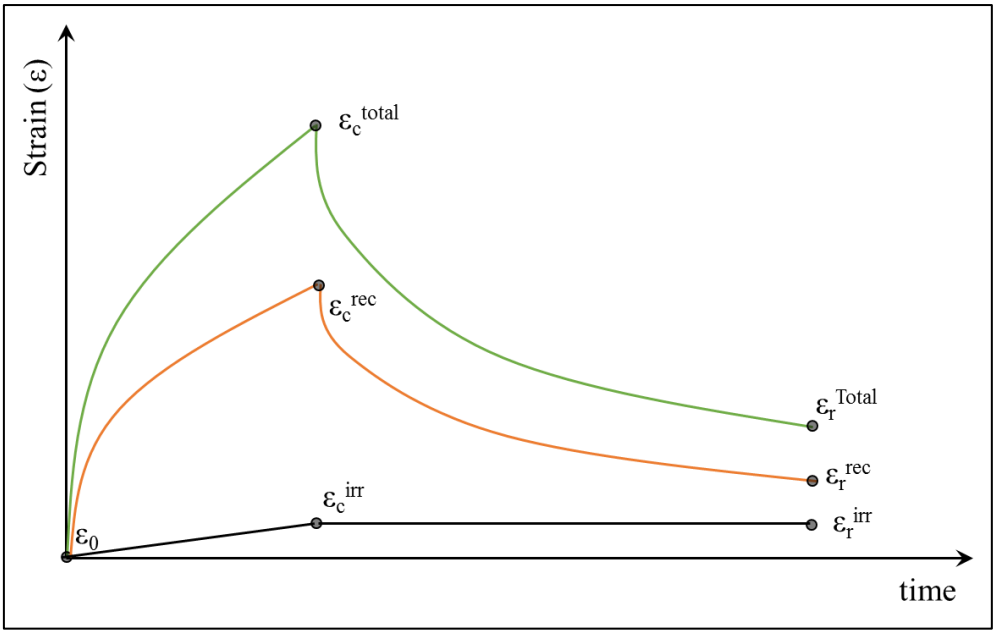

Figure 26: Points of interest for percentage of recovery and non-recoverable creep compliance calculation of the MSCR test using the NPVE approach

Also, calculating the percentage recovery (R) changed from equation (3) to be:

$$R\ (\%)=\frac{\varepsilon_c^{Total}-\varepsilon_r^{irr}}{\varepsilon_c^{Total}-\varepsilon_0^{irr}} \qquad \textbf{(15)}$$

where ε_c^{Total} is the value of the experimental strain at the end of the loading phase in each cycle. Also, irrecoverable creep compliance and percentage recovery are averaged for each stress level.

A MATLAB code (version R2012a) was developed to read all the experimental data, perform the analysis, and optimise the g_1 and g_2 parameters. The first cycle at the lowest stress level (100 Pa) was used to obtain the coefficients of the Prony Series as described earlier. Six coefficients of Prony Series were assigned for the modified bitumen and seven for the unmodified. The retardation time values were fixed to be 0.1, 1.0, 2.0, 5.0, 7.0 and 9.0 sec for the modified bitumen and 0.0005, 0.001, 0.002, 0.0083, 0.02, 0.2 and 2.0 sec for the unmodified bitumen. The optimisation in this process is not unique and can be different if different retardation time is used.

Unmodified Pen 60/70 bitumen mixed with Advera was excluded from the NPVE analysis approach because it did not exhibit any recovery strain. Consequently, nonlinear parameters, g_1 and g_2, were not calculated for this bitumen.

The g_1 and g_2 values for the modified PG76-22 bitumen were calculated and are shown in Figure 27. The g_1 and g_2 values are almost constant at 1.0 at low-stress levels, which is expected since the low-stress level test did not impose nonlinearity on the material. A constant g_1 parameter indicates that the creep strain is not changing with more loading cycles.

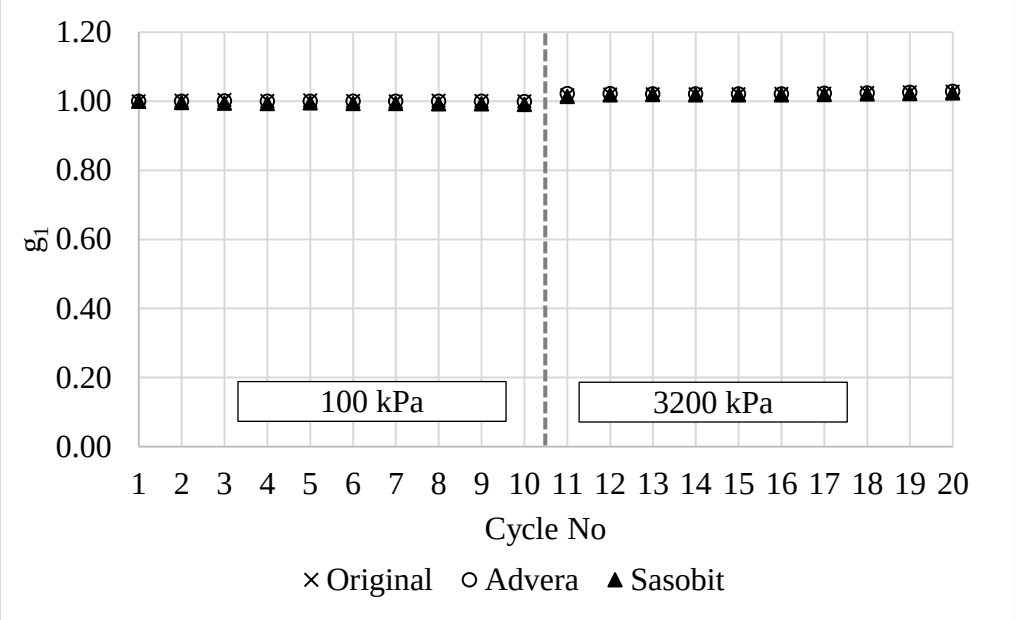

(a) g_1

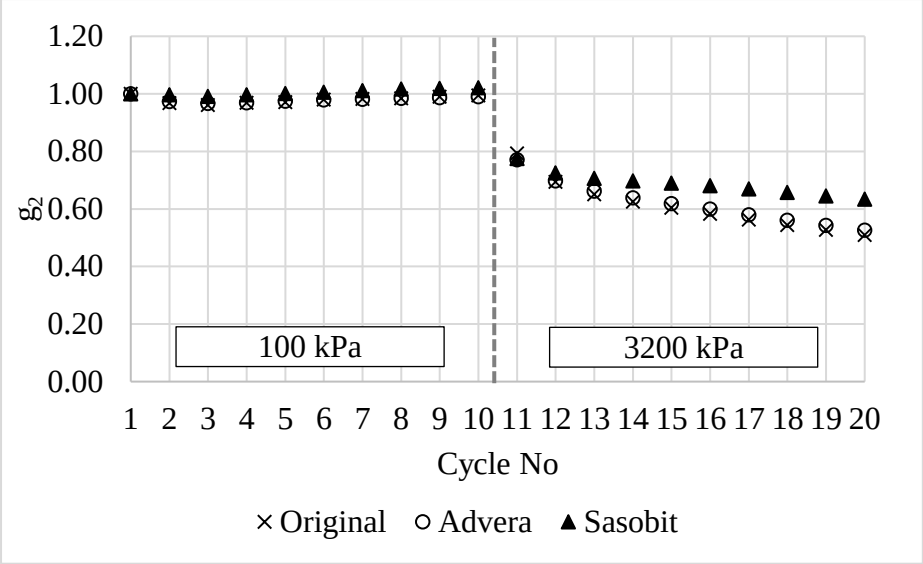

(b) g_2

Figure 27: Nonlinear parameters (a) g_1 and (b) g_2 from the NPVE analysis approach for MSCR test results of polymer-modified bitumen PG76-22

The constant g_2 values for PG76-22 at the low-stress test indicate that the bitumen did not experience softening or hardening. On the other hand, at the high-stress level test, a constant g_1 indicates that introducing the material to nonlinearity did not affect the creep strain with more loading cycles. However, a decreasing g_2 value with more cycles at high-stress level indicates that the bitumen is experiencing strain hardening with time. Sasobit with modified bitumen had the lowest rate of decrease in g_2 at high-stress level.

Masad *et al.* (2009) attributed the hardening behaviour of asphalt bitumen to the accumulation of permanent strain and alteration in the bitumen's internal structure. Accumulation of permanent strain is associated with the development of the normal strain as a result of applying a shear stress (i.e. coupling between shear and volumetric responses in plastic deformation). In the DSR, the development of normal strain is not allowed because of the geometry and fixed gap between the parallel plates. As a result, the bitumen experiences normal stresses to counter its tendency to develop normal

strains; this phenomenon has been discussed in studies by other researchers (Gie and Chan, 1984; Franck, 2014). The normal stress difference on the instrument's upper plate was extracted from the raw data files and is shown in Figure 28.

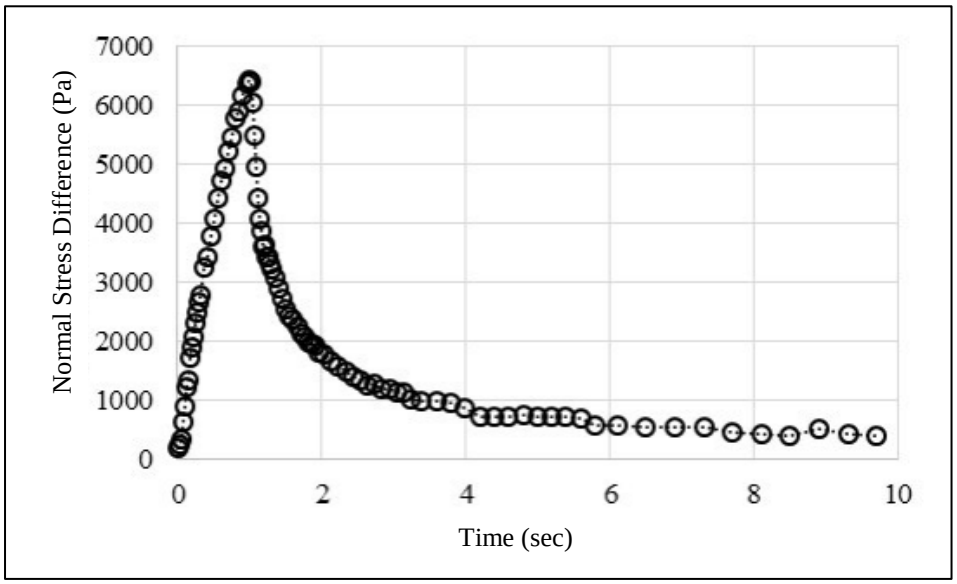

Figure 28: Normal stresses applied to the upper DSR plate during MSCR test

As shown in Figure 28, the bitumen applied relatively high normal stress difference to the upper plate of the DSR instrument. The normal stress difference increased with creep loading and decreased with recovery. Since Schapery's model does not account for the coupling between shear and volumetric responses, accumulation of permanent strain in the bitumen and development of normal stresses manifested itself in a decrease in the g_2 with an increase in loading cycles.

After estimating the nonlinear parameters, the percentage of recovery and irrecoverable creep compliance were calculated as an average of 10 cycles for each stress level. Figure 29 shows typical strain values after the NPVE method for the full test.

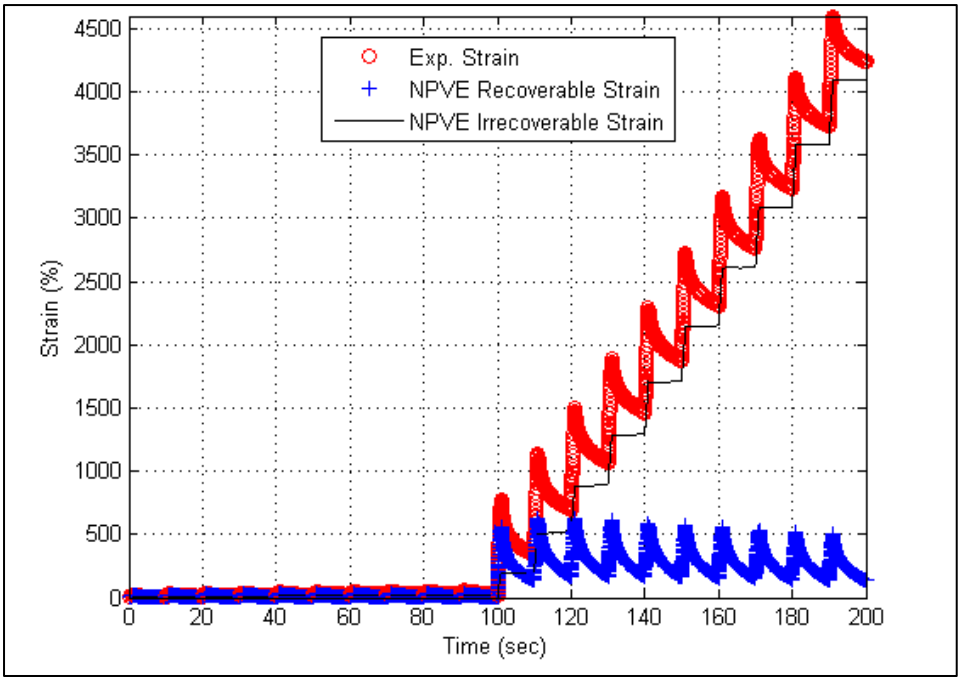

Figure 29: Example for decoupling total strain to recoverable and irrecoverable strain over 20 cycles for polymer-modified bitumen PG 76-22

By examining Figure 30, it can be noticed that the recoverable strain ε_{rec} is smaller than the recoverable strain ε_{rec}^{NPVE} calculated from the NPVE approach. This is also reflected in calculating the irrecoverable strain ε_{irr}^{NPVE}.

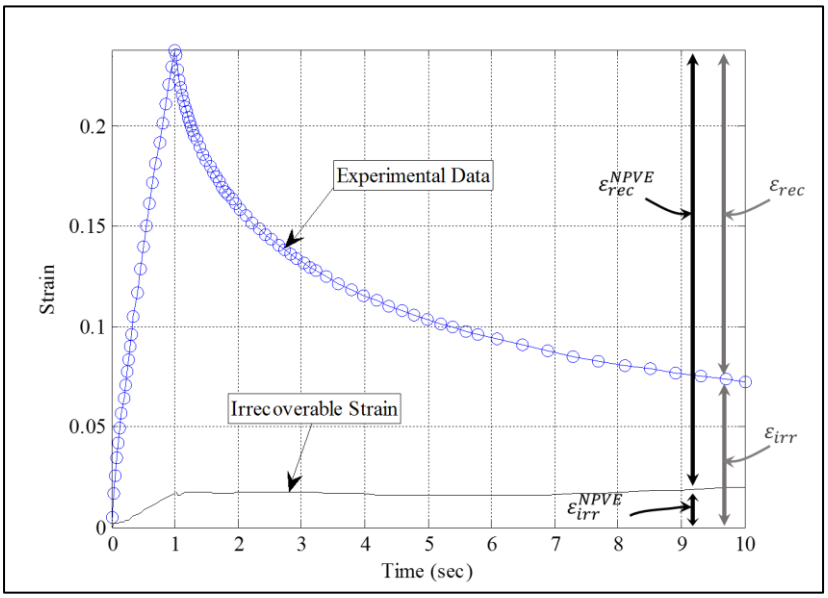

Figure 30: Example of experimental data and irrecoverable strain measured by the nonlinear plasto-viscoelastic approach

Table 4 shows that the average percentage of recovery at the low- and high-stress levels determined using the nonlinear plasto-viscoelastic approach is larger than those determined directly from the data for all types of additives. This suggests that the conventional method of analysing MSCR test results does not necessarily show the full recovery after releasing the creep load. However, normalising all the cycle's non-recoverable creep compliance shows the insignificant difference between the conventional and NPVE analysis methods.

Table 4: Comparison between the percentage of recovery and creep compliance for each stress level for modified PG 76-22 bitumen between the conventional MSCR analysis and plasto-viscoelastic approach

Parameter	Original		Sasobit		Advera	
	Conventional MSCR Approach	Nonlinear Plasto-Viscoelastic Approach	Conventional MSCR Approach	Nonlinear Plasto-Viscoelastic Approach	Conventional MSCR Approach	Nonlinear Plasto-Viscoelastic Approach
$R_{0.1}$ (%)	86.90	91.06	88.64	91.53	89.70	93.00
$R_{3.2}$ (%)	49.98	58.18	44.60	51.54	52.88	60.51
$J_{nr0.1}$ (kPa^{-1})	0.30	0.27	0.14	0.13	0.20	0.18
$J_{nr3.2}$ (kPa^{-1})	1.28	1.28	0.95	0.95	1.03	1.04

Figure 31 shows irrecoverable strain at the end of the recovery phase in each type of bitumen before and after using the NPVE method. The results showed that using WMA additives could yield more recovery than estimated using the conventional percentage of recovery. In both stress levels, Figure 31 shows that Sasobit-modified bitumen has the lowest irrecoverable strain than the other bitumens. A lower irrecoverable strain indicates better resistance to permanent deformation.

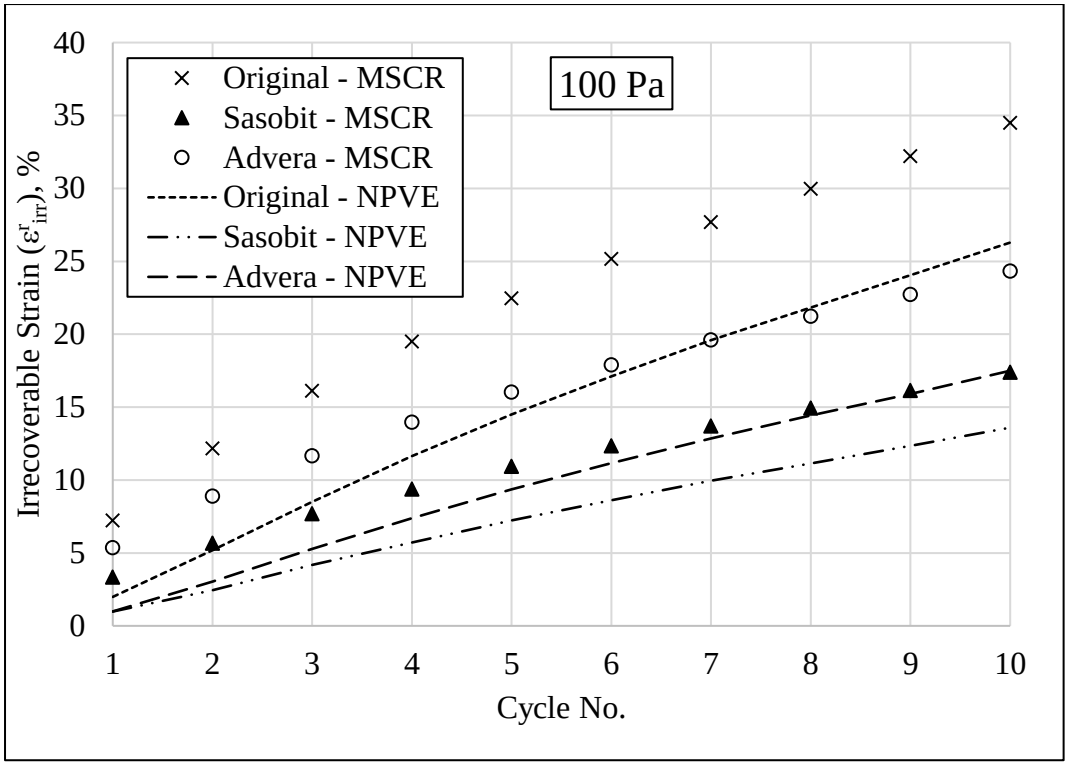

(a)

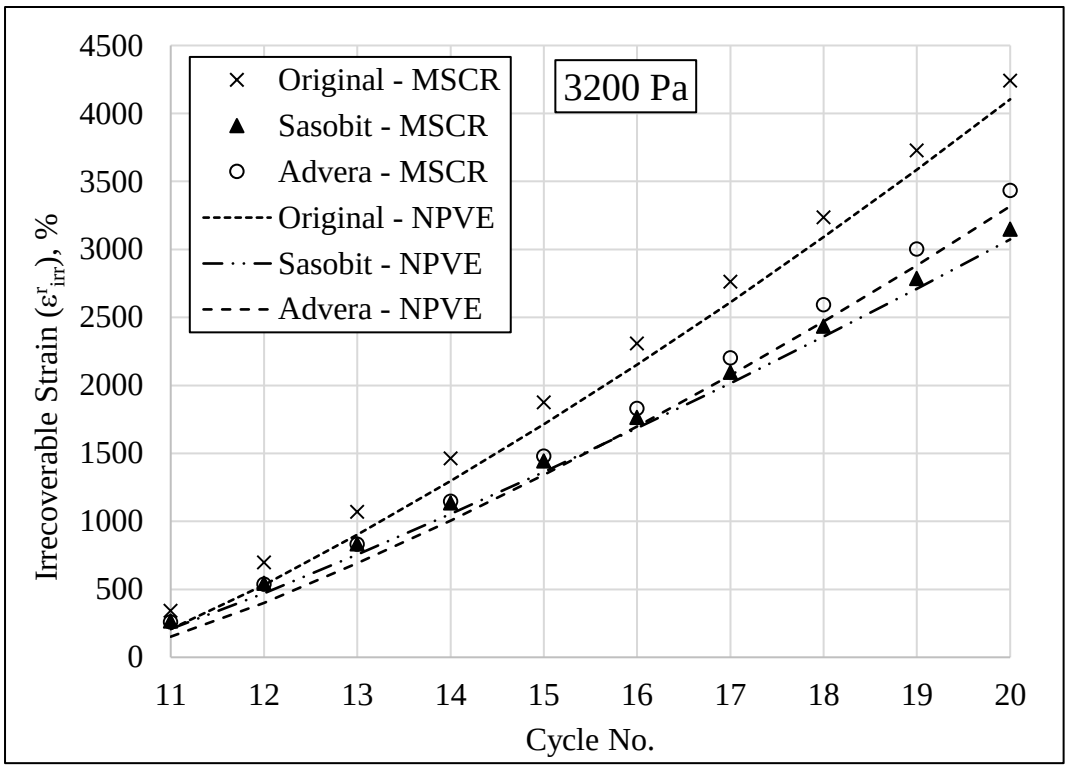

(b)

Figure 31: Comparison of maximum irrecoverable strain (ε_r^{irr}) in (a) 100 Pa (b) 3200 Pa stress level overall cycles for polymer-modified PG 76-22 bitumen with different WMA technologies

As shown in Figure 32, the unmodified Pen 60/70 bitumen exhibited almost constant g_1 value of 1.0, indicating that the creep strain of the asphalt bitumen stayed constant for the whole test. In contrast, the g_2 parameters were decreasing during the low-stress level test, which indicates that, even when the creep loading is small, the material still exhibits nonlinearity. The g_2 parameter for Sasobit-modified bitumen was greater than the original bitumen at the low-stress level and experienced a sharper decrease at high-stress level over cycles. A higher g_2 value at low-stress level means that Sasobit has increased the recoverable strain at each cycle. However, a sharper decrease in the slope indicates that the bitumen with Sasobit was slightly hardening over more cycles of loading compared to the original bitumen.

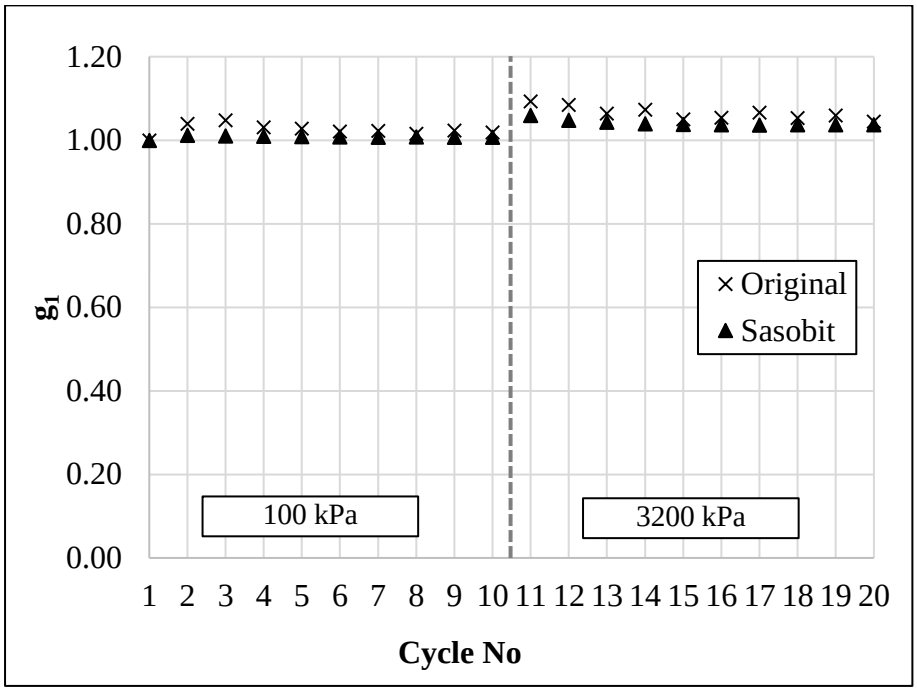

(a) g_1

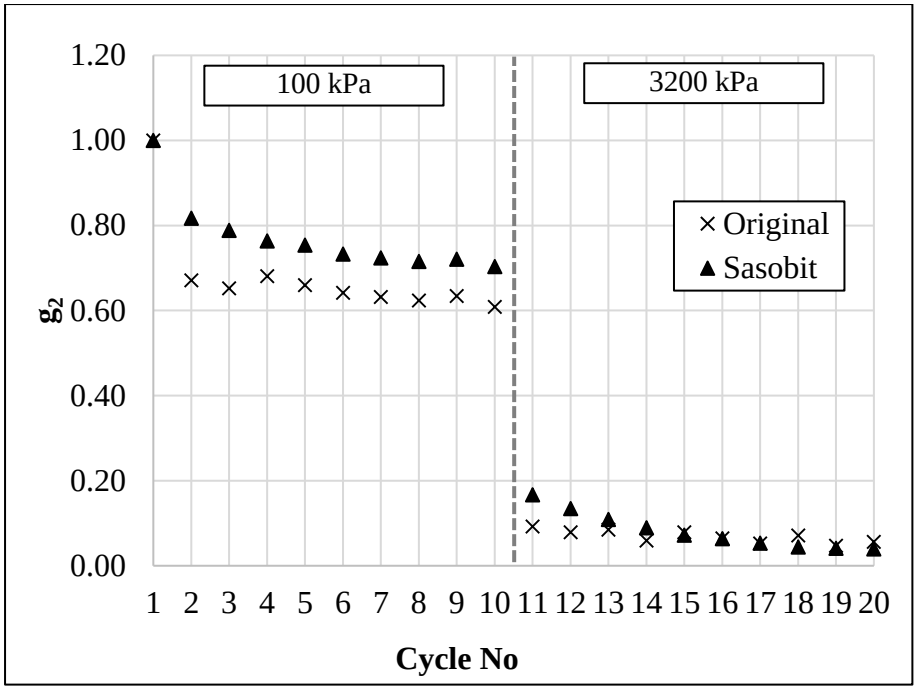

(b) g_2

Figure 32: Plot of nonlinear parameters (a) g_1 and (b) g_2 for 20 cycles for original unmodified bitumen Pen 60/70 and with unmodified bitumen mixed with Sasobit

It is shown in Table 5 that there was no significant difference between the MSCR experimental approach and the nonlinear plasto-viscoelastic approach in determining the non-recoverable creep compliance values. However, the nonlinear plasto-viscoelastic approach provides an insight into the development of recoverable strains for both bitumens.

Table 5: Comparison between the percentage of recovery and creep compliance for each stress level for unmodified Pen 60/70 bitumen between the linear viscoelastic approach and plasto-viscoelastic approach

Parameter	Original		Sasobit		Advera	
	Conventional MSCR Approach	Nonlinear Plasto-Viscoelastic Approach	Conventional MSCR Approach	Nonlinear Plasto-Viscoelastic Approach	Conventional MSCR Approach	Nonlinear Plasto-Viscoelastic Approach
$R_{0.1}$ (%)	2.02	9.36	15.59	20.62	0.01	-
$R_{3.2}$ (%)	0.22	1.26	1.88	2.53	0.14	-

$J_{nr0.1}$ (kPa^{-1})	3.44	3.40	1.57	1.57	3.44	-
$J_{nr3.2}$ (kPa^{-1})	3.63	3.63	2.36	2.37	3.54	-

Figure 33 shows that the addition of Sasobit reduced deformation in comparison with the original bitumen. For the high-stress level (Figure 33b), the nonlinear viscoelastic analysis of the MSCR data and the NPVE approach gave the same results. This behaviour indicates that the unmodified bitumen has recovered all possible deformation during the unloading period of the MSCR test, and would not recover any more strain even if a longer unloading time was used.

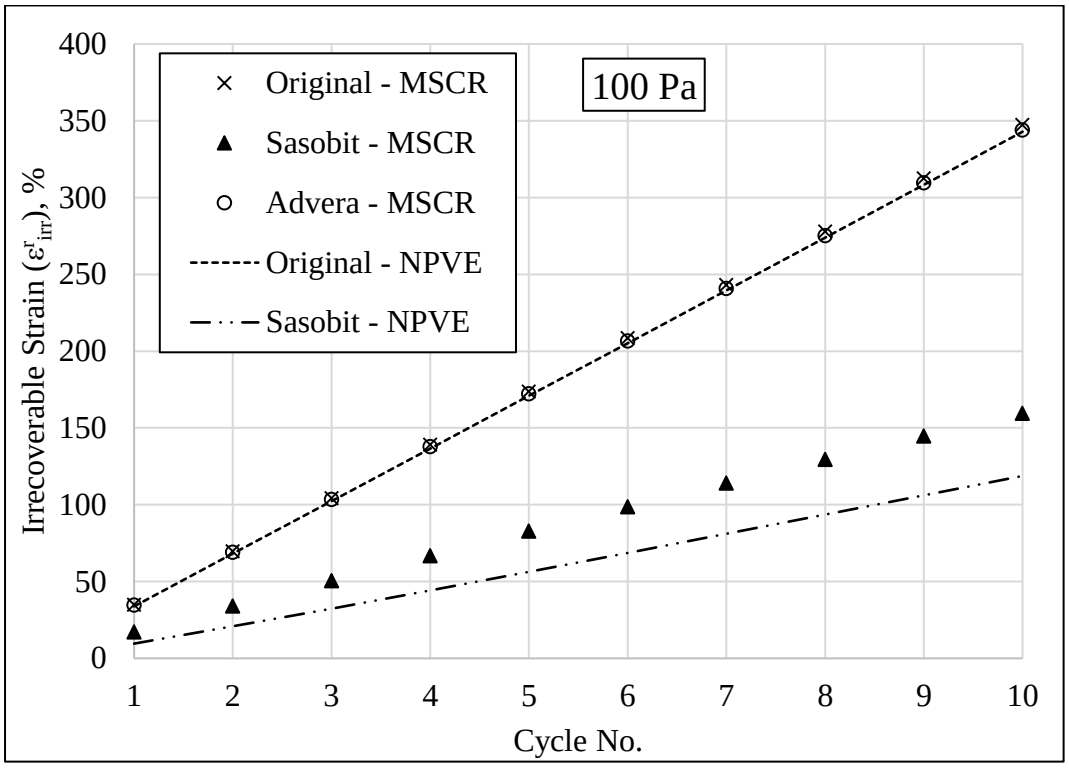

(a)

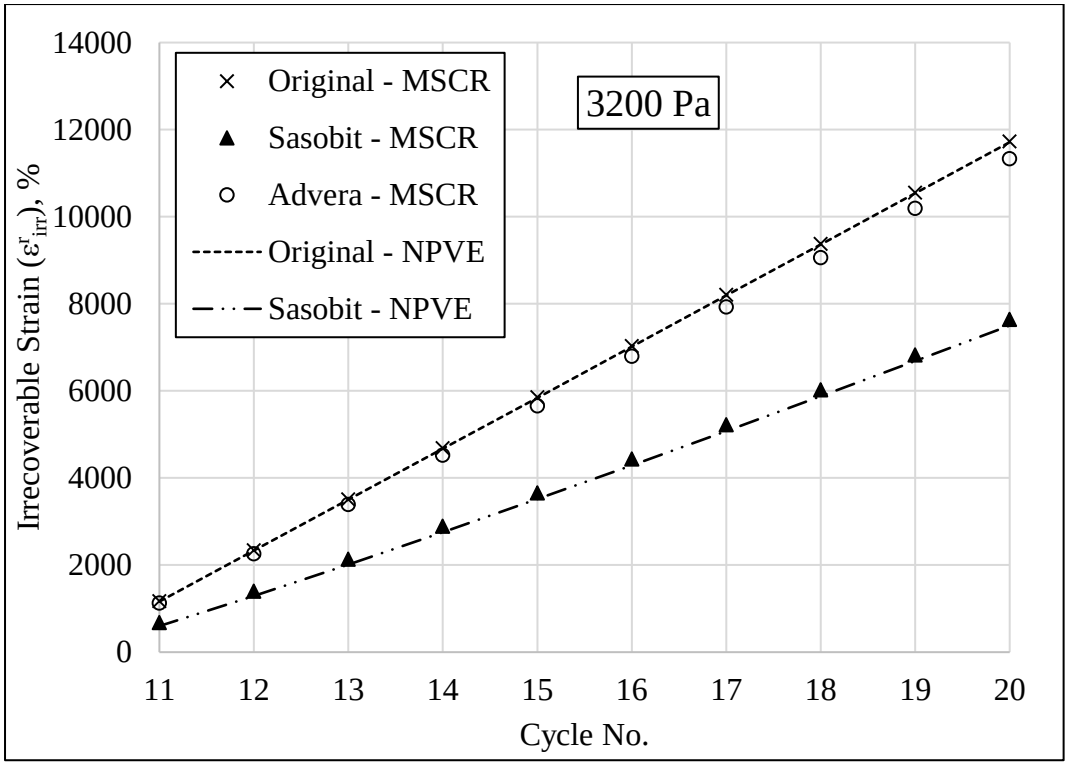

(b)

Figure 33: Comparison of maximum irrecoverable strain (ε_r^{irr}) in (a) 100 Pa and (b) 3200 Pa stress level overall cycles for original unmodified Pen 60/70 bitumen and unmodified bitumen mixed with Sasobit

Based on the results, the conventional analysis of the results from the MSCR test examined the nonlinear viscoelastic behaviour of the bitumen before and after adding WMA additives. The polymer-modified PG76-22 bitumen mixed with Sasobit showed insignificant difference in rutting performance compared to the original bitumen after full short-term ageing. Results indicate that Sasobit would affect the fresh bitumen in lowering the mixing and compaction temperatures, but would perform the same as original bitumen against rutting. However, when Sasobit was mixed with unmodified Pen 60/70 bitumen, it increased the potential to recover the strain to eight times higher than the original bitumen. Consequently, Sasobit decreased the non-recoverable creep compliance, which would lead to lower rutting of asphalt pavement. The effect of using Advera additives on the permanent deformation of polymer-modified and unmodified asphalt bitumen was insignificant and ignorable.

On the other hand, the nonlinear plasto-viscoelastic (NPVE) approach was successfully used to estimate the total irrecoverable strain and study the nonlinear response of asphalt bitumen. However, a small difference was found between the non-recoverable creep compliance values determined using the conventional MSCR analysis approach and the NPVE approach. The NPVE analysis showed that Sasobit helped in reducing the hardening behaviour of the polymer-modified bitumen and lowering its non-recoverable strain.

The development of permanent strain in the bitumen with the application of loading cycles causes bitumen hardening and coupling between volumetric strain and applied shear stresses. However, the fixed-gap height between the testing plates does not allow normal strains to develop, which led to normal stresses being generated by the plates on the bitumen. The development of permanent strain and normal stresses causes the decrease of the g_2 parameter with an increase in loading cycles.

3.3. Summary and Conclusions

The implementation of WMA technology in Qatar would contribute to the national goals of having eco-friendly construction practices. However, implementation of WMA technology still encounters a lack of adequate studies that cover different aspects of its performance. In this thesis, a thorough investigation was conducted into the WMA technology in order to achieve a complete – and comprehensive – description of its behaviour. However, conducting advanced studies on the WMA material requires a preliminary understanding of its basic properties and behaviour.

In this chapter, the preliminary assessment of the bituminous binders mixed with WMA additives started by evaluating the rheological properties and viscosity using the dynamic shear rheometer and the rotational viscometer by following standard

testing protocols. The results showed that addition of Sasobit has a noticeable effect on the performance grading (PG) of the asphalt bitumen while Advera has no effect. Based on that, it was necessary to check the impact of stiffness elevation on the permanent deformation. Hence, the MSCR test was conducted on asphalt bitumen and analysed using nonlinear viscoelastic and plasto-viscoelastic approaches. The inclusion of the nonlinear plasto-viscoelastic approach in this section was meant to capture any viscoplastic damage that might have occurred in the asphalt bitumen. The results confirmed that the Sasobit additive increased bitumen stiffness and improved permanent deformation resistance, especially with the unmodified bitumen. The results from implementing the nonlinear plasto-viscoelastic approach revealed the same conclusions, while using the viscoelastic approach showed the full deformation of the asphalt bitumen.

Since Sasobit additive have increased the stiffness of the asphalt binder, it could also affect the performance of the asphalt mix against fatigue cracking. Using the parameter of fatigue factor from bitumen testing can underestimate the effect of stiffness increase on the asphalt mix performance. So, the next chapter presents an advanced testing and analysis procedure to examine the fatigue resistance of the asphalt mix using fine aggregate mixtures prepared with WMA additives.

4. Fatigue Characterisation of Fine Aggregate Warm Asphalt Mixtures

Fatigue cracking is one of the main distresses in asphalt pavements that affect its service life. Investigating fatigue cracking has attracted the attention of many researchers for many years because of its complexity and importance in decisions regarding the rehabilitation or replacement of the entire pavement (Bolotin, 1999; Shen and Carpenter, 2007; Hesp *et al.*, 2009). A more robust understanding of the factors that affect fatigue cracking would advance the design of long-lasting pavements.

The resistance of asphalt mixtures to fatigue failure in the laboratory experiments is affected by various factors such as temperature, loading frequency, loading mode, sample type and geometry. Evaluation of fatigue resistance can be performed by applying a repeated load test using an Asphalt Mixture Performance Machine (AMPT) apparatus on full mixture field-cut or lab-fabricated specimens. However, the heterogeneity of full asphalt mixture specimens causes high variability in fatigue testing results, which makes it difficult to predict the field performance with reasonable reliability (Masad *et al.*, 2006; Sadek, 2015). An alternative is to test Fine Aggregate Mixture (FAM) specimens that contain the fine portion of the mixture. FAM specimens have higher uniformity and yield less variability in fatigue testing results than full mixture-sized samples (Howson *et al.*, 2007).

Several analytical approaches have been used to evaluate the performance of asphalt mixtures against fatigue damage; however, the Viscoelastic Continuum Damage (VECD) approach that implements Schapery's theory is the most developed one (Schapery, 1987). The main principle of VECD is calculating the dissipated pseudo-

strain energy (DPSE), which is based on the concept of separating the dissipated energy due to damage from energy dissipated because of viscoelastic behaviour. Masad *et al.* (2008) used that concept and identified three main components for DPSE that are associated with a change in phase angle between load cycles, change in phase angle within a single cycle and change in stiffness between cycles. Masad *et al.* (2008) showed that the VECD approach could unify the predictions from the strain- and stress-controlled loading modes.

This section includes an analysis of the fatigue-cracking resistance of fine aggregate mixtures (FAM) modified with different WMA additives (W-FAM). A shear stress oscillation test was performed on a control FAM mixture without WMA additive and W-FAM modified with three additives (Advera, Sasobit, and Rediset). The test results were analysed using the VECD approach to determine the number of cycles to fatigue failure.

4.1. Testing Materials and Methodologies

In order to examine the influence of WMA additives on the fatigue damage resistance of asphalt mixtures, Fine Aggregate Mixture (FAM) samples were fabricated (12 mm diameter and 50 mm height) in the laboratory using 'Gabbro' aggregate and polymer-modified PG76-22 bitumen. Gabbro, which is imported from the United Arab Emirates, is an igneous rock that has been used in road construction for a long time in the Arabian Gulf region. The PG76-22 bitumen was mixed with three WMA additives, Sasobit, Advera, and Rediset, using a high shear mixer at dosages of 2%, 5% and 0.5% of bitumen's weight, respectively.

The fatigue testing was conducted using the Dynamic Shear Rheometer (DSR), shown in Figure 34, from Malvern (Kinexus Pro model). The instrument has a special tool

for mounting FAM samples, as shown in Figure 34(a). The upper part rotates while the lower one is fixed. The maximum shear force the machine can reach is 600 kPa. In addition, the machine is provided with a temperature chamber (Figure 34(b)) that keeps the temperature uniform at 25°C during the test.

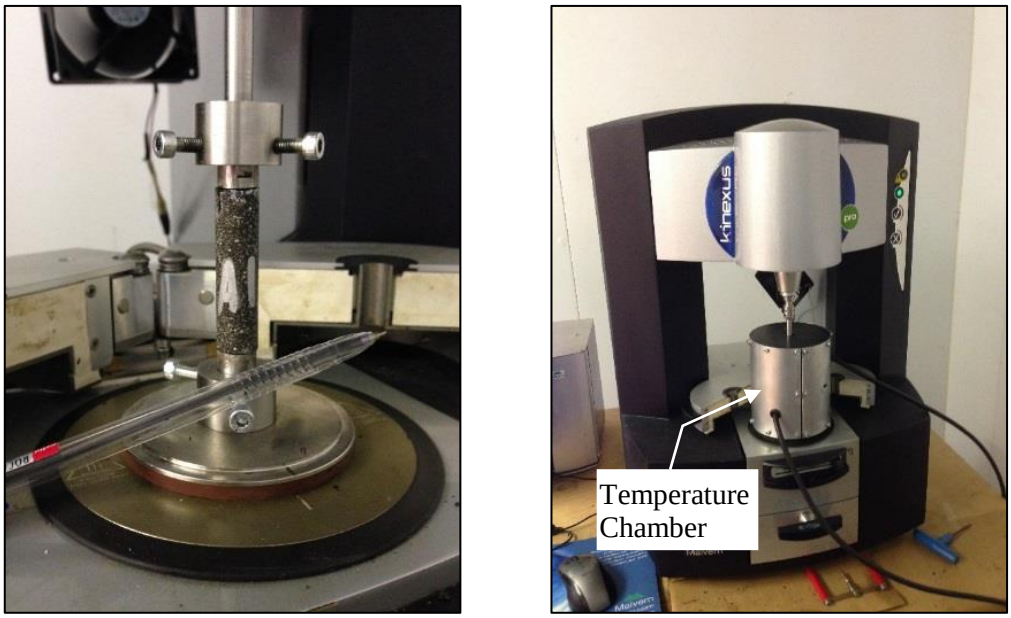

(a) (b)

Figure 34: (a) Special fixation for the cylindrical FAM samples (b) DSR used for fatigue testing with the temperature chamber

The aggregate gradation for the FAM design is based on the proportional ratio of Job Mix Formula (JMF) from the full HMA gradation (Branco *et al.*, 2008; Castelo Branco *et al.*, 2008; Sousa *et al.*, 2011). The HMA mix design used in this study was obtained from a local company that prepared it for base course layer using nominal maximum aggregate size of 25mm. This mix design is using the same exact material used in preparation of the FAM samples. Table 6 shows the JMF gradation from the mix design where the FAM gradation was calculated starting from 1.18 (N16) sieve size by dividing the retained value of all sieves from 0.6 (N30) sieve by the passing percentage of 1.18 (N16) sieve size.

Table 6: Aggregate gradation of control mix design and fine aggregate mix design

Sieve Size, mm (in)	Control Mix Design		FAM Mix Design	
	% Passing	% Retained	% Passing	% Retained
37.5 (1 1/2")	100.0%	0	--	--
25 (1")	98.6%	1.4%	--	--
19 (3/4")	88.2%	10.4%	--	--
12.5 (1/2")	76.9%	11.3%	--	--
9.5 (3/8")	68.9%	8.0%	--	--
4.75 (N4)	47.1%	21.8%	--	--
2.36 (N8)	26.5%	20.6%	--	--
1.18 (N16)	15.8%	10.7%	100%	0.0%
0.6 (N30)	10.5%	5.3%	66.5%	33.5%
0.3 (N50)	7.9%	2.6%	50.0%	16.5%
0.15 (N100)	6.1%	1.8%	38.6%	11.4%
0.075 (N200)	4.2%	1.9%	26.6%	12.0%
Pan	0.0%	4.2%	0.0%	26.6%
Total		100.00%		100.00%

The bitumen content was estimated for the FAM design by burning the bitumen from a loose HMA sample using the ignition oven. The loose HMA mix, which had 3.9% of binder content, was separated and then sieved to obtain the portion of the mix with particles passing sieve 1.18 mm (N16). This fine mix was placed in the ignition oven to burn the bitumen and determine its weight. The results showed that the bitumen content of the fine mix part was 7.3%.

The Gabbro aggregate was collected from a local contractor in Qatar and delivered in five different sizes: 0-5 mm, 5-10 mm, 10-14 mm, 14-20 mm and 20-32 mm. Enough material was taken from the smallest aggregate size barrel (0-5 mm) to perform sieve analysis based on the required sizes in Table 6 (1.18, 0.6, 0.3, 0.15 and 0.075 mm).

The sieved aggregates were mixed and heated overnight at the mixing temperature mentioned in Table 7. Then, the heated aggregate was mixed with 7.3% of polymer-modified bitumen PG76-22 heated at the same temperature but for 2 hours only.

Table 7: Mixing and compaction temperatures for HMA and WMA

Temperature	Original mix	Sasobit mix	Advera mix	Rediset mix
Mixing, °C	163	145	145	145
Compaction, °C	135	116	116	116

The mixing was performed using a mechanical mixer, until a homogenous mixture was achieved. After that, the mixture was heated again for 2 extra hours at the mixing temperature listed in Table 7. Finally, an amount of 3.7 kg was used to compact the mixture using the Superpave gyratory compactor (IPC Servopac Brand). The gyratory software was monitored to achieve a constant height for the sample, which was usually after 250 to 300 gyratory cycles. Three samples of 150 mm diameter were prepared for each additive type and then left for a minimum of one day to cool before the coring and cutting processes.

A total of six cylindrical finger specimens (replicates) were extracted from the compacted samples for each mix by coring and cutting them to 12 mm diameter and 50 mm height, as shown in Figure 35. A drilling machine (Cardi brand) was used with a 12 mm inner diameter coring bit to core the specimens from each mixture sample. Then, a cutting machine (Control Brand) was used to cut the upper and lower part of the specimen to obtain the 50 mm height with flat ends.

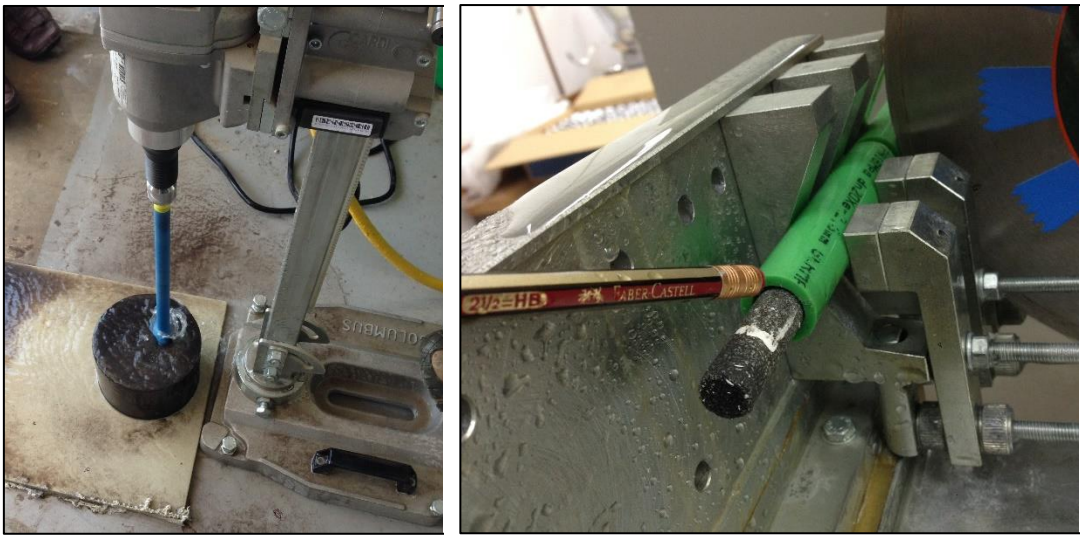

(a) (b)

Figure 35: (a) FAM sample coring (b) FAM sample cutting

In general, mixing and compacting the asphalt mixtures at lower temperatures than the HMA reduces the ageing that could occur in the material due to heating. The WMA mixtures were mixed at 145°C based on the common practice and previous knowledge with polymer-modified bitumen with WMA additives. The specimens were compacted at 116°C following the recommendations of the NCHRP 763 report, and it also meets the typical criteria for compacting the WMA samples at least 15°C below the HMA compaction temperature (Herb and Velasquez, 2006; Martin *et al.*, 2014).

Air voids were measured according to the AASHTO T 166 method. The FAM specimens were measured in water, surface saturated and dried to calculate the bulk specific gravity (G_{mb}). On the other hand, the maximum theoretical specific gravity (G_{mm}) was measured by following the AASHTO T 209 method. Then, the air void percentage was calculated using equation (16):

$$Air\ Voids\ (\%) = \left(\frac{G_{mm} - G_{mb}}{G_{mm}}\right) \times 100 \quad \textbf{(16)}$$

On average, the percentage of air voids for original mix was about 3% in the cylindrical samples.

The differences between the full HMA mixtures and the FAM are in aggregate sizes, binder content and air voids. The aggregate sizes were proportionally reduced to obtain a representative mix that was based on the original HMA mix. The high percentage of binder content (7.3%) in the FAM means that this sample is rich with bitumen, which makes it more viscous than the full HMA mix. In addition, the percentage of air voids in the FAM samples (3.0%) is found to be lower than in the full HMA mix (around 4.6% by the JMF), while the FAM has better interlocking between the aggregate particles than the full HMA mix.

4.1.1. Stress Sweep Test

Categorising the linear and nonlinear viscoelastic properties of the tested materials was achieved by performing the stress sweep test (D'Angelo *et al.* 2007; Branco *et al.* 2008). The test was started from an oscillation value of 1 kPa amplitude (peak-to-peak) and increased by 25 kPa every 20 seconds until it reached 589 kPa before termination.

Experimental data were analysed by calculating the strain slope at each stress level. By applying oscillation stress within the linear viscoelastic region, the strain amplitude (peak-to-peak) should stay at a constant level, as shown in Figure 36. However, when the stress amplitude reaches a nonlinear or a damaging level, the strain amplitude starts increasing to indicate a change in the strain response at the same stress level.

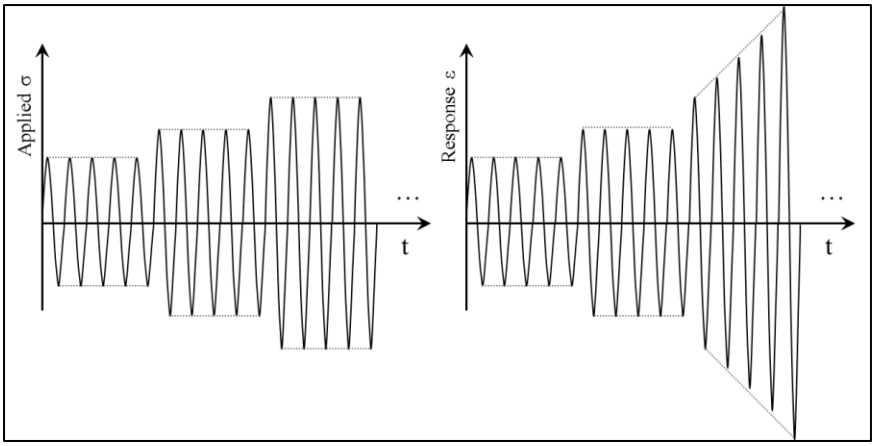

Figure 36: The strain behaviour at different stress levels during the stress sweep test

At each stress level, the strain amplitude was measured for 20 seconds and then fitted with linear equation to calculate its slope. The strain slopes were plotted against the applied stress as shown in Figure 37. The figure shows the average results from the stress sweep test and indicates that any oscillation stress level less than 150 kPa can be considered in the linear viscoelastic region of the materials, while any stress level higher than 150 kPa oscillation stress might expose the material to nonlinearity and then damage. This test was performed at 25°C temperature and 10 Hz frequency.

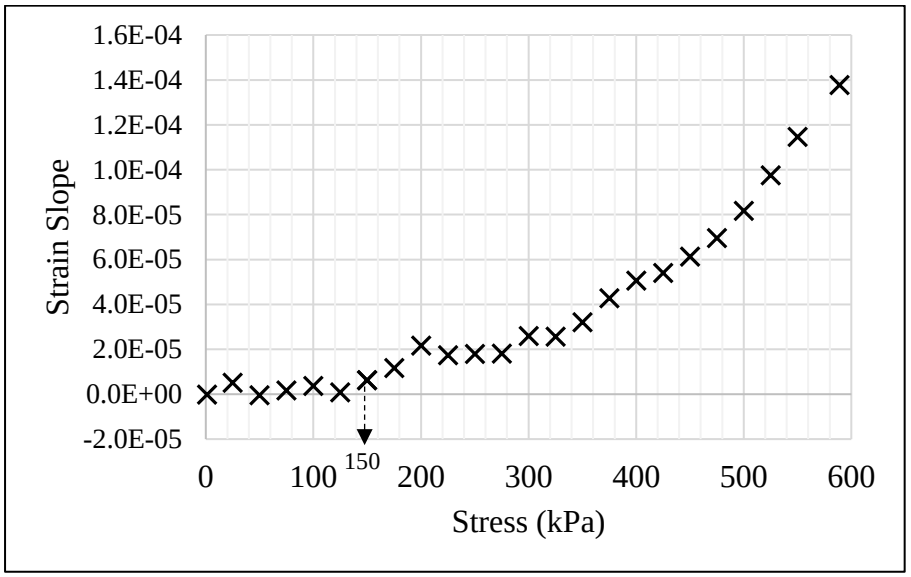

Figure 37: Stress sweep test analysis for defining a linear and nonlinear region in material response

4.1.2. Relaxation Test

The relaxation test, which involves the application of a constant strain for a certain period, was performed to measure the relaxation modulus of the material. The strain amplitude value used in this study was 0.005% and was within the linear viscoelastic region associated with the linear stress level specified by the stress sweep test.

Figure 38 shows the typical results from the relaxation test and the fit curve used to estimate the relaxation modulus parameters G^*_∞, G^*_1 and m of equation (17).

$$G^*_{relaxation} = G^*_\infty + G^*_1 \times t^{-m} \quad \textbf{(17)}$$

where G^*_∞ represents the shear modulus that the material would reach at infinite time, G^*_1 represents the starting shear modulus at the beginning of relaxation test and the 'm' value presents the slope of the relaxation curve (Schapery, 1981). A higher 'm' value indicates a more rapid drop of G^*_1, which initiates a quick reduction in the shear modulus.

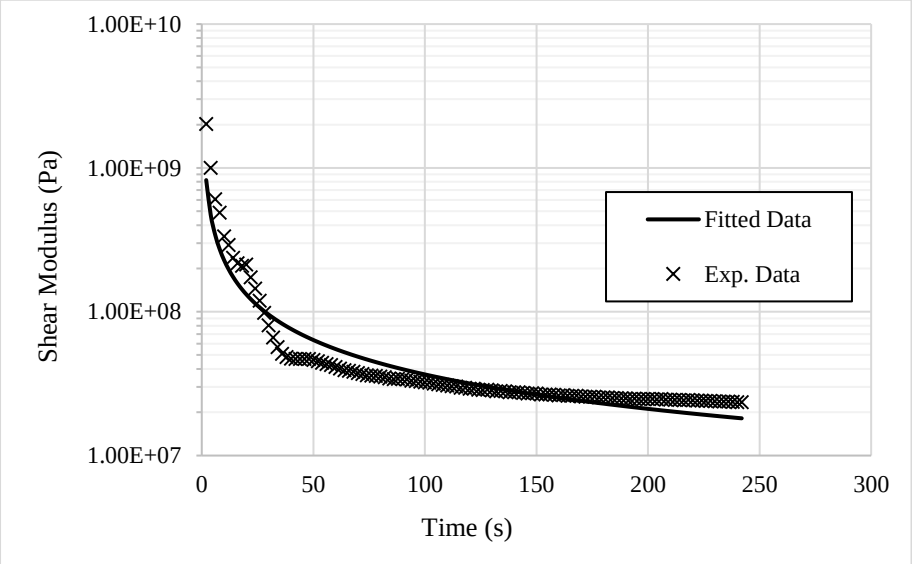

Figure 38: Typical relaxation test data results and fitted curve

4.1.3. Fatigue Test

Two stress amplitudes were applied to the samples: low-stress (75 kPa), which is within the linear viscoelastic response, and high-stress (400 kPa), which causes damage to the specimens. The low-stress level test is applied at 10 Hz for 2 minutes followed by the high-stress level test, which is terminated after 200,000 cycles even if a complete failure does not occur. The failure criterion was chosen to be when the specimen reaches 50% of its starting shear modulus (Kutay *et al.*, 2008).

4.2. Test Results and Discussion

FAM samples were tested at a low-stress level to determine the relaxation modulus, shear modulus and phase angle of the mixtures within the linear viscoelastic range. Tests were performed at a high-stress level to determine the shear modulus and phase angle within the nonlinear viscoelastic range and fatigue damage.

4.2.1. Relaxation Test Results

The instantaneous shear modulus values obtained from the relaxation test experimental data were fitted with the power law relationship shown in equation (17). The 'G^*_∞' values for all mixes were very small compared to the 'G^*_1' values (G^*_∞ is around 1% of G^*_1 values). To simplify the optimisation process, G^*_∞ values were optimised to zero while average values of 'G^*_1' and 'm' are presented in Figure 39.

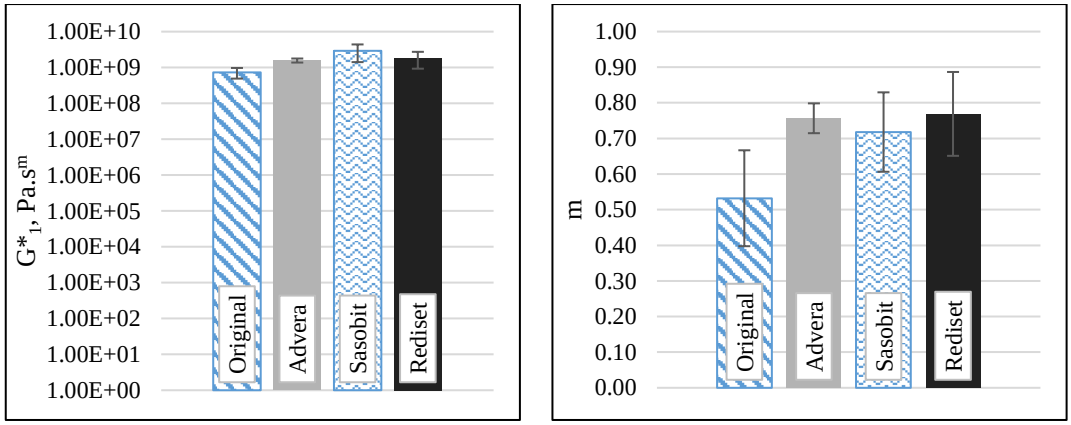

(a) (b)

Figure 39: Relaxation test results (a) G^*_1 and (b) m

As shown in Figure 39(b), the average 'm' value was plotted with the standard error bars (standard deviation divided on the square root of the population) for each mix type and shows considerable variability among replicates. This variability would have a considerable effect on the pseudo-stiffness calculation. The average value of 'm' was used for each mix to emphasise the variability between replicates.

4.2.2. Fatigue Test Results

A stress oscillation test at a low-stress level was conducted to obtain the linear viscoelastic properties of each WMA mix. The experimental data from a number of specimens (6 specimens) were averaged to determine a single shear modulus (|G*|) and phase angle (δ) values for each mix.

Figure 40 shows results from the low-stress oscillation test demonstrating that the addition of Sasobit to asphalt mixtures increased the shear modulus (|G*|) and decreased the phase angle (δ). It is also noticeable that Rediset had a minor influence on the stiffness of the material while the average shear modulus is close to the Original mixture.

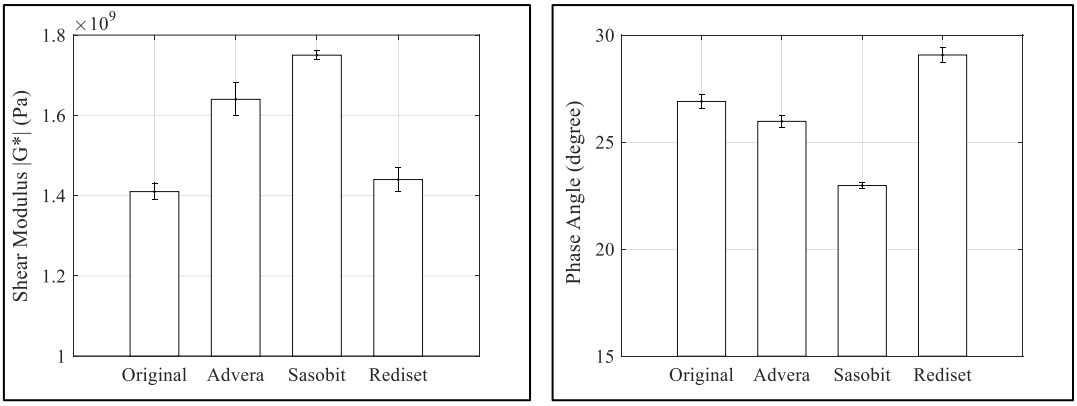

(a) (b)

Figure 40: Average values of (a) shear modulus |G*| (b) phase angle δ for each mix

Fatigue test at the high-stress level was conducted on the same samples after the low-stress level test. The material was allowed to relax for 10 minutes after the low-stress level test to recover any strain that might still exist. The instrument was set to apply an oscillation shear stress of 400 kPa stress level at 10 Hz frequency. The software was configured to capture the shear modulus and phase angle during loading cycles, as shown in Figure 41. Typically, the shear modulus passes through three stages during fatigue testing: rapid reduction within a small number of cycles; steady and slow reduction for many cycles; and finally very rapid reduction leading to failure (Kim *et al.*, 2002). However, in this test, the shear modulus did not reach a total failure or a break at the end of the test.

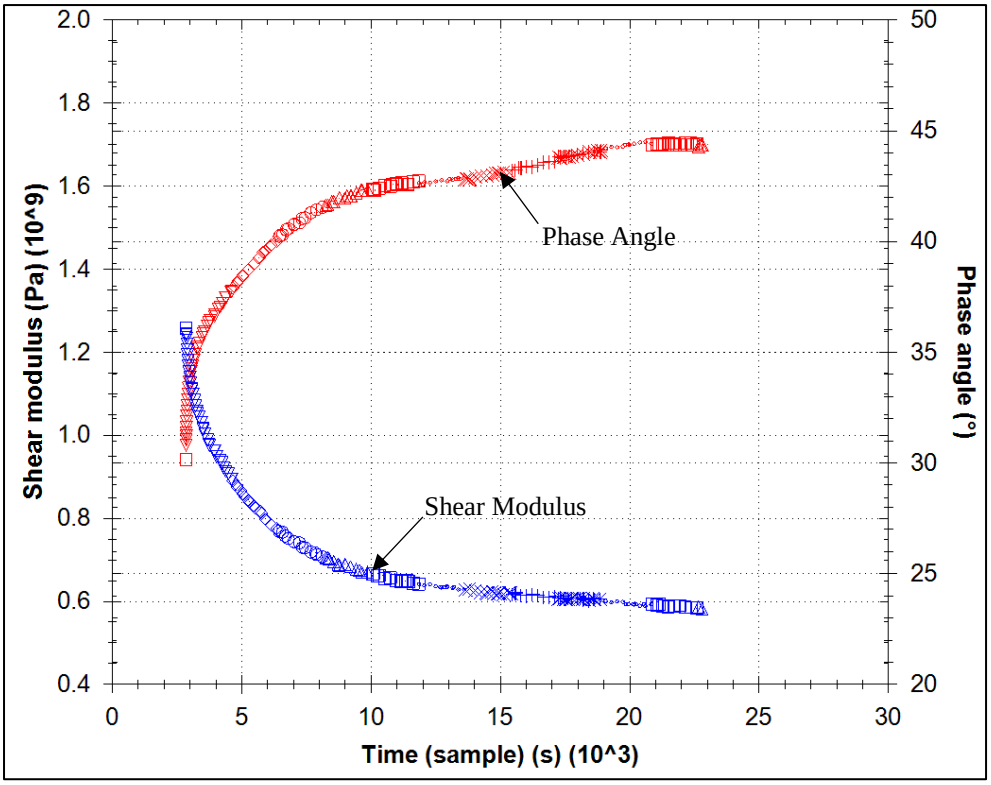

Figure 41: Typical raw experimental data obtained from the instrument software for the high-stress fatigue test

For viscoelastic materials, part of the energy applied during loading dissipates and does not recover upon unloading (Yong-rak Kim *et al.*, 2003; Bhasin *et al.*, 2009). However, viscoelastic materials dissipate even more energy if they are damaged during loading. The dissipated energy associated with damage can be determined by calculating the dissipated pseudo-strain energy (DPSE). Masad *et al.* (2009) proposed that the DPSE can be separated into three components. The first component (W_{R1}) is associated with an increase in the apparent (experimentally measured) phase angle and is calculated as follows:

$$W_{R1} = \pi \frac{\tau_{0F}^2}{G^*_{LVE}} \sin(\delta_{NF} - \delta_{LVE}) \qquad \textbf{(18)}$$

where τ_{0F} is the stress amplitude (Pa) applied to the specimen during the test. The G^*_{LVE} and δ_{LVE} are the linear viscoelastic shear modulus and phase angle values

obtained from the low-stress level test, respectively. Then δ_{NF} is the phase angle at each cycle. The second component of the DPSE method is W_{R2}, which is associated with the change in phase angle within each cycle. Since the phase angle for each cycle is averaged within the stress-strain wave, this component has been ignored in the analysis presented herein. The third component of DPSE (W_{R3}) is the difference between the pseudo-stiffness for undamaged material and the pseudo-stiffness after damage. This component can be calculated using equation (19) as follows:

$$W_{R3} = \frac{1}{2}\tau_{0F}^2\left(\frac{1}{G_{NF}^*} - \frac{1}{G_{LVE}^*}\right) \qquad \textbf{(19)}$$

where G^*_{NF} is the shear modulus at each cycle. Finally, W_{R1} and W_{R3} were summed and plotted against the number of cycles (N), as shown in Figure 42. A higher W_R (W_{R1} + W_{R2}) indicates that the material dissipates more energy during the damage process.

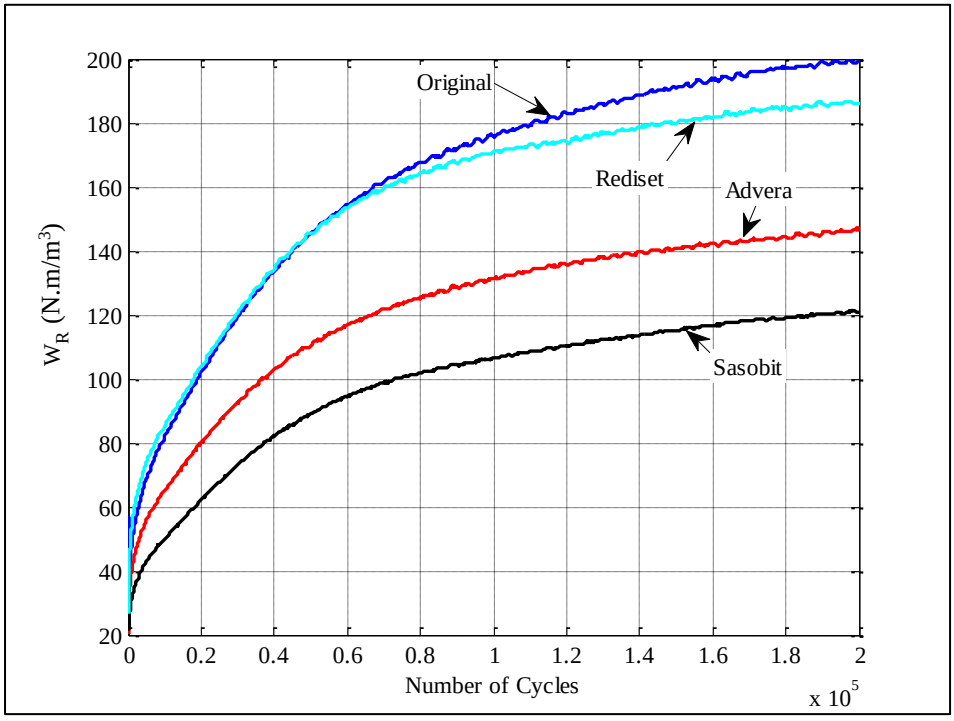

Figure 42: Results of the DPSE method (W_R) for each mix

Results from the DPSE method shown in Figure 42 exhibited trends similar to the linear viscoelastic behaviour. Rediset has a minor influence on the asphalt mixtures and almost matches the Original mixture, particularly at early life. Sasobit presented the lowest dissipated energy of all the mixes. Results indicate that asphalt mixtures mixed with Sasobit dissipated less energy to reach 200,000 cycles than the other materials.

Similarly, by plotting the hysteresis loops after 200,000 cycles for all mixes, as shown in Figure 43, one can see that Sasobit has the smallest hysteresis loop area and the Original mix has the largest. These loops are generated using the experimental data at a specific cycle (200,000 cycles).

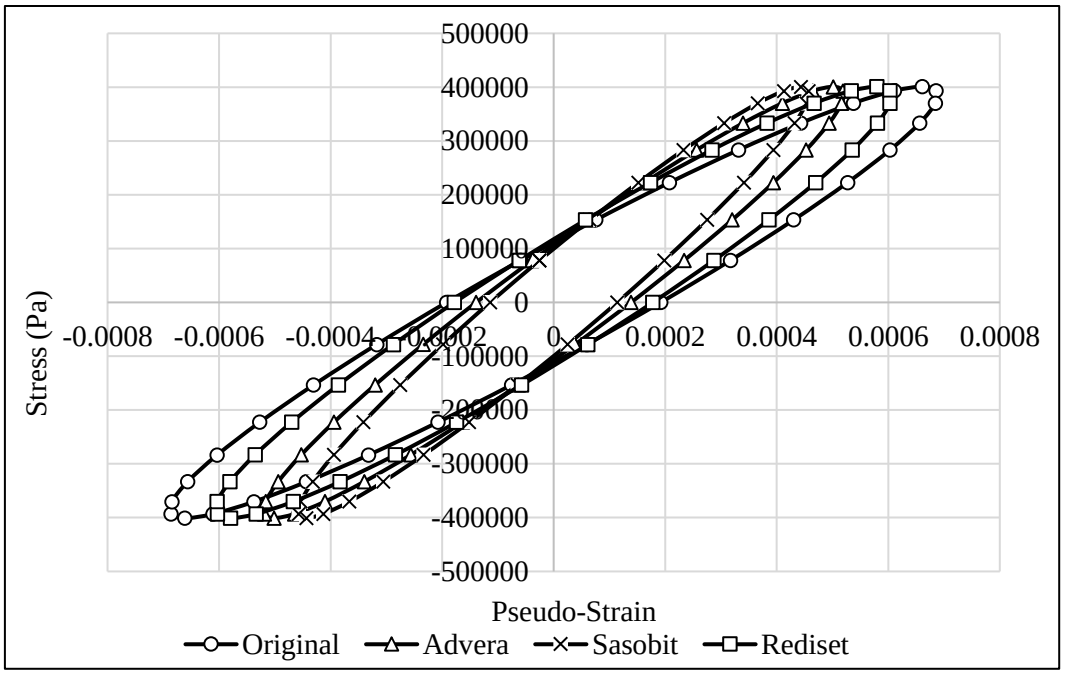

Figure 43: Hysteresis loop after 200,000 cycles for Original, Advera, Sasobit and Rediset mixtures

However, the DPSE alone did not give a full assessment of the resistance to fatigue damage because complete failure did not occur. Although each mixture type had a different dissipated energy, none of the samples exhibited a rapid reduction in the

stiffness. Samples can dissipate less or more energy and fail early or later than other samples. Consequently, the viscoelastic continuum damage (VECD), which incorporates DPSE along with other material properties, is used to quantify the fatigue damage.

Researchers have used various aspects of VECD to analyse the fatigue performance of asphalt mixtures by estimating the number of cycles to failure (N_f). The VECD approach is based on Schapery's elastic-viscoelastic principle that quantifies damage growth inside a specimen (Schapery, 1987; Underwood, 2011). Analysing the fatigue behaviour using this theory is based on calculating pseudo-strain (ε^R), pseudo-stiffness (C) and internal damage parameter (S). Reduction in material properties due to damage is presented by the pseudo-stiffness (C) parameter. Pseudo-stiffness can be calculated as in equation (20).

$$C_N = \frac{G_N^*}{G_{LVE}^*} \qquad \textbf{(20)}$$

The damage parameter, S, presents the damage growth in the material and can be calculated for the stress-controlled test as follows (Kutay *et al.*, 2008):

$$S_{N+\Delta N} = S_N + \left(\frac{\Delta N}{f}\right)^{\frac{1}{1+\alpha}} \left[\frac{0.5}{I}\sigma_N^{R^2}\left(\frac{1}{C_{N+\Delta N}} - \frac{1}{C_N}\right)\right]^{\frac{\alpha}{1+\alpha}} \qquad \textbf{(21)}$$

where 'S_N' is the internal damage at each cycle starting from the initial damage (S_0), 'ΔN' is the difference between a number of cycles, which is fixed to be 2000 cycles in this study, 'f' is the frequency and 'α' is a constant parameter related to the rate of damage growth and depends on failure zone characterisation (Lee and Kim, 1998). The value of the 'α' parameter is considered to be (1/m) where 'm' is the average of the maximum slope obtained from the relaxation test. Finally, 'σ_N^R' is the peak pseudo-

stress calculated by dividing the peak stress at each cycle by the linear viscoelastic shear modulus, as shown in equation (22).

$$\sigma_N^R = \frac{\sigma_N}{G_{LVE}^*} \qquad \textbf{(22)}$$

The value of 'I' in equation (21) is the ratio of the first shear modulus value at the beginning of the test and the linear viscoelastic shear modulus. This assumption was made to eliminate sample-to-sample variability (Kutay *et al.*, 2008). Figure 44 represents the results of C-S curves generated for the tested samples. The C-S curves were presented with the six replicates.

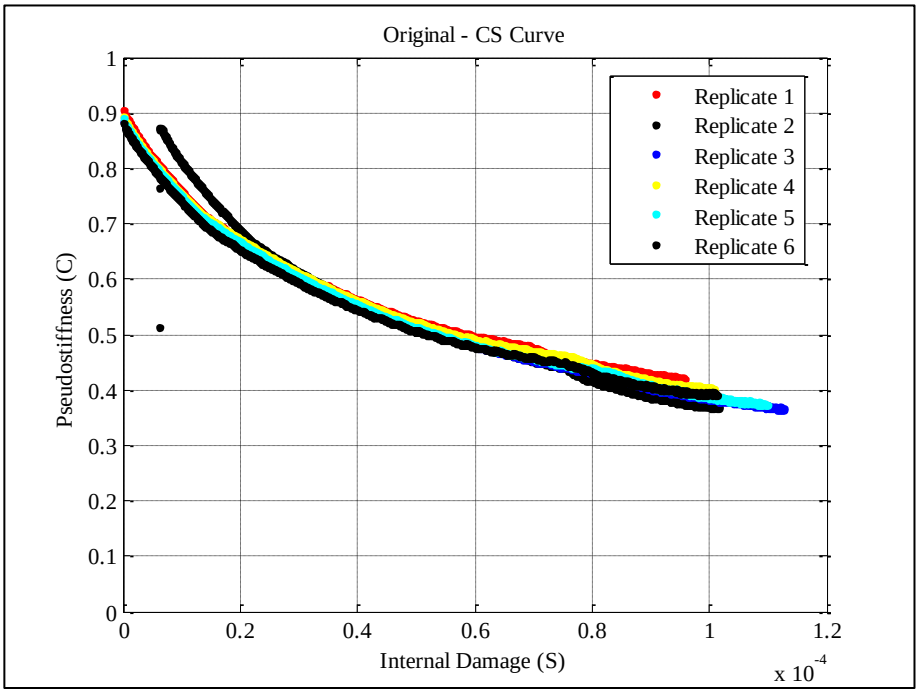

(a) Original

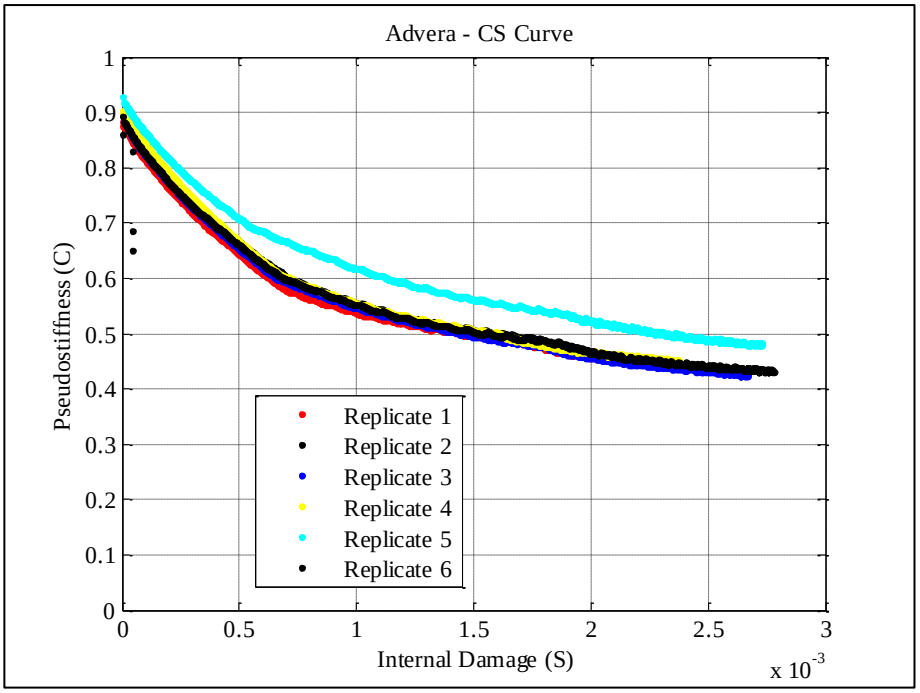

(b) Advera

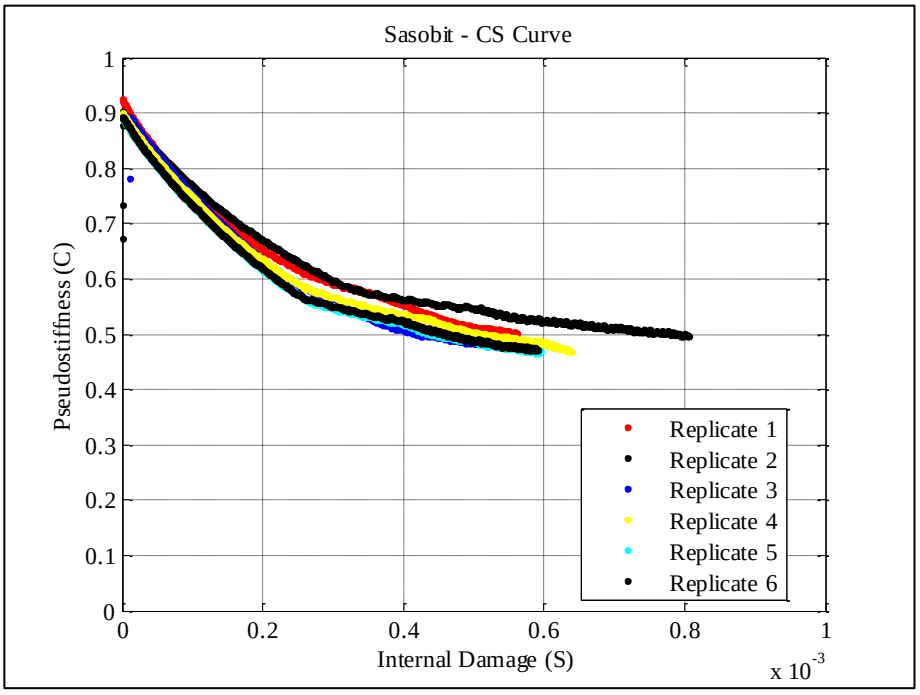

(c) Sasobit

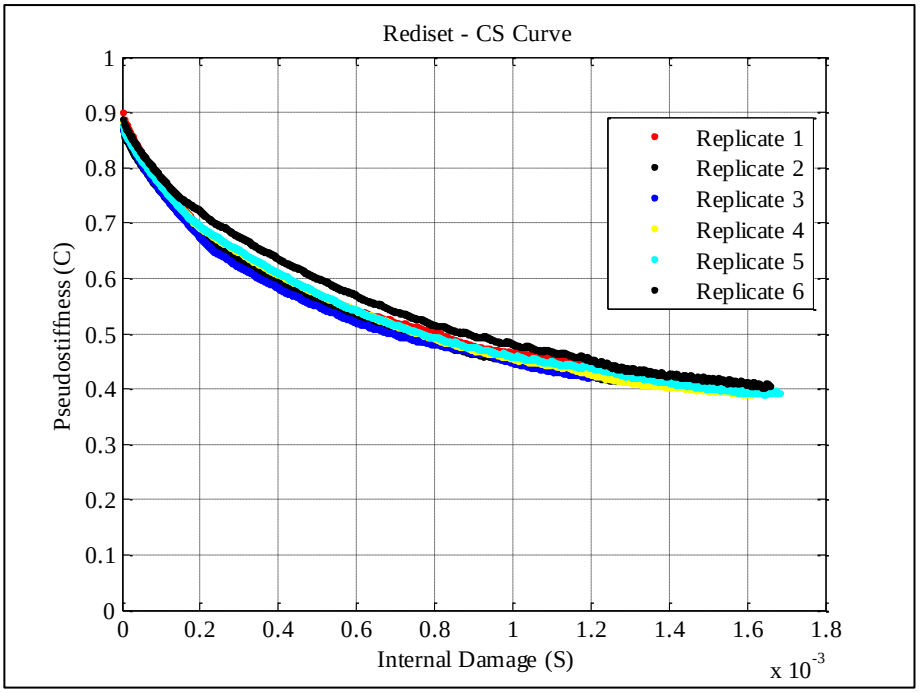

(d) Rediset

Figure 44: Experimental C-S curves for all replicates of (a) Original (control) mix (b) mix with Advera (c) mix with Sasobit (d) mix with Rediset

The results from the experimental C-S curve show the difference between the mixes in terms of internal damage. The curve shows an increase in the internal damage (S) with the reduction of the pseudo-stiffness (C). Using Figure 44, the pseudo-stiffness (C) was chosen to be 0.5, and the internal stresses were compared between mixes. It was found that the internal damages for the Original, Sasobit, Advera and Rediset mixes were: 0.05×10^{-3}, 1.45×10^{-3}, 0.46×10^{-3} and 0.75×10^{-3}, respectively. The lowest internal damage was observed with the Original mix, while the other mixes showed very close results.

Kutay *et al.* (2009) defined the damage because of micro cracks by eliminating the effect of unstable applied stress or strain in the damage analysis. In order to accommodate that, C-S curves presented in Figure 44 are simulated using material behaviour parameters (a and b) which are then used with the true stress value (400

kPa) to calculate the simulated C-S curves. The exponential equation (23) was used to obtain the constant parameters (a and b) and fit the experimental data to simulate C-S curves with the true pseudo-stress value.

$$C_N = \exp(aS_N^b) \quad \textbf{(23)}$$

Values of ‘a’ and ‘b’ obtained by fitting the experimental data are presented in Figure 45. The figure shows the standard error, which is calculated by dividing the standard deviation over the square root of the sample size. It can be noticed that the variability in values of ‘a’ is much higher than for ‘b’. The value of ‘b’ in equation (23) is the parameter that quantifies the rate of reduction in the sample stiffness due to the internal damage growth. The variability can affect the calculation of simulated pseudo-stiffness, which is based on modelling experimental data behaviour.

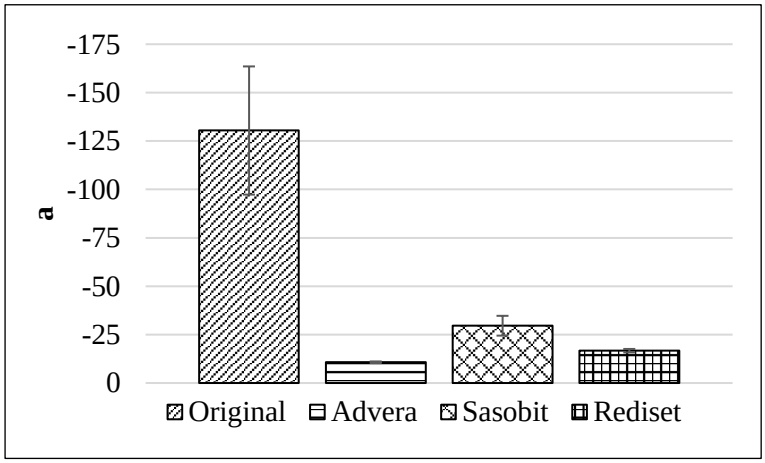

(a)

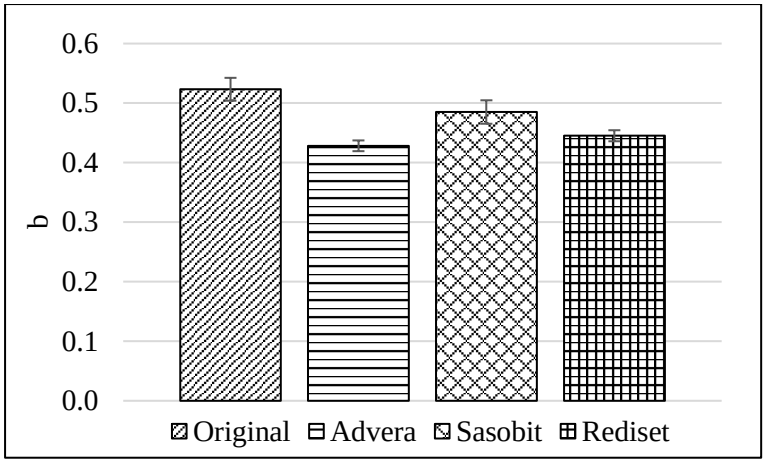

(b)

Figure 45: Average of (a) 'a' and (b) 'b' values for each mix

The simulated damage parameters '$S_{Simulated}$' were then calculated by equation (24) and plotted against simulated pseudo-stiffness '$C_{Simulated}$', which is calculated by equation (25).

$$S_{Simulated}^{N+\Delta N} = S_N + \left(\frac{\Delta N}{f}\right)^{\frac{1}{\alpha}} \left[\frac{0.5}{I}\sigma_T^{R^2}\frac{dC^{-1}}{dS}\right]^{\alpha} \quad \textbf{(24)}$$

$$C_{Simulated} = \exp(aS_{Simulated}^{b}) \quad \textbf{(25)}$$

The term $\frac{dC^{-1}}{dS}$ in equation (24) is computed by a partial derivative of equation (25) to be:

$$\frac{dC^{-1}}{dS} = -(e^{-aS^b})abS^{b-1} \quad \textbf{(26)}$$

Since the machine could not keep the stress amplitude absolutely constant during the whole test due to the fluctuation, σ_N^R is calculated using the true pseudo-stress, as shown in equation (27). By using this technique, creating a simulation analysis of the material's behaviour gives the ability to use any stress amplitude and consequently simulate the material performance, while 'a' and 'b' can be considered as material

properties. In this analysis, the true stress applied (σ_{true}) is considered as 400 kPa for the destructive test.

$$\sigma_T^R = \frac{\sigma_{true}}{G^*_{LVE}} \qquad \textbf{(27)}$$

Failure in a fatigue test can be identified based on several criteria, such as (a) a complete break of the sample, (b) reaching maximum phase angle, (c) drop of 50% of the sample's stiffness or 90% of its complex shear modulus (Ghuzlan and Carpenter, 2000; Zollinger, 2005; Kutay *et al.*, 2008). N_f was calculated by integrating equation (24) from S_0 to S_f while S_0 represents the assumed initial internal damage in the material as in equation (28):

$$N_f = \int_{S_0}^{S_f} \left[\frac{\sigma_T^{R^2}}{2I}\frac{dC^{-1}}{dS}\right]^{-\alpha} f dS \qquad \textbf{(28)}$$

The value of 'S_f' can be obtained by converting equation (23) to measure the number of cycles to failure, 'N_f', by identifying the level of pseudo-stiffness reduction failure criteria, 'S_f', as in equation (29). In this analysis, C_f in all cases was assigned to be 0.5 to calculate the damage parameter (S_f) at 50% reduction in stiffness.

$$S_f = \left(\frac{\ln C_f}{a}\right)^{1/b} \qquad \textbf{(29)}$$

Obtaining 'N_f' requires an assumption about the value of the initial damage (S_0) for the mix and each replicate. The analysis is very sensitive to the initial damage (S_0) value. However, Underwood *et al.* (2012) recommended selecting S_0 to have minimal damage at the beginning of the test and a smooth reduction in pseudo-stiffness with cycles. Each replicate of a mix had a unique initial damage value that ensured to be as close as possible to zero to give a smooth reduction in the pseudo-stiffness with cycles.

The choice of low values was to ensure minimal initial damage since these samples are lab-fabricated samples and have not suffered from damage yet. Based on all the factors mentioned above, Figure 46 shows six replicates of the simulated C-S curves for each mixture.

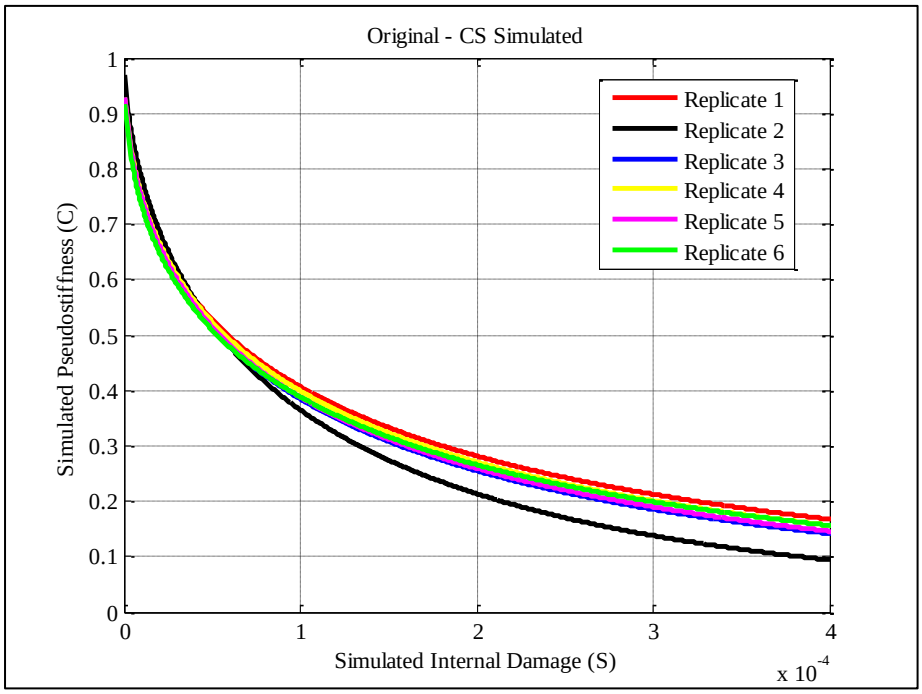

(a) Original

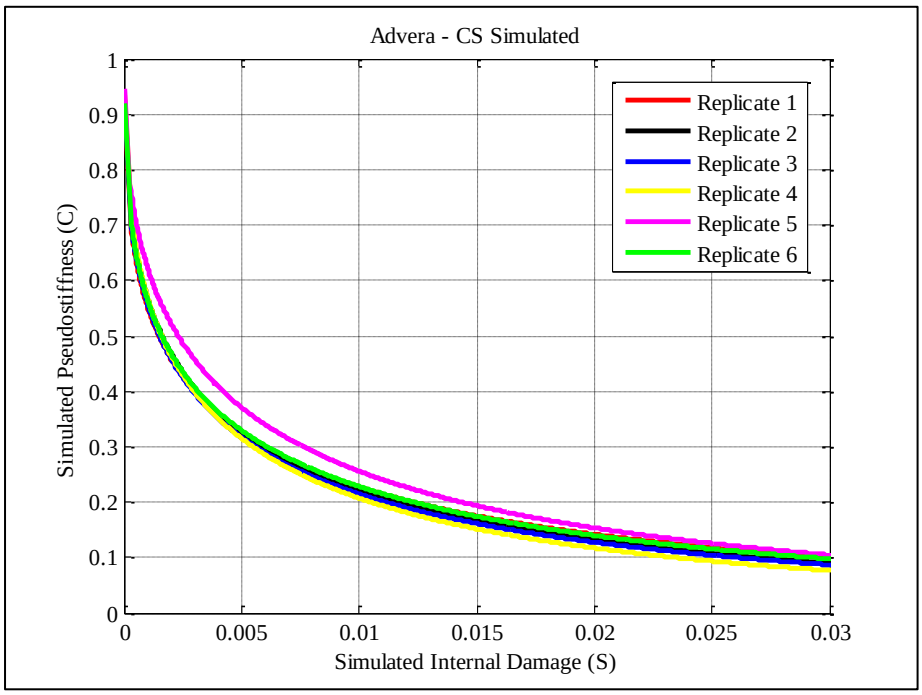

(b) Advera

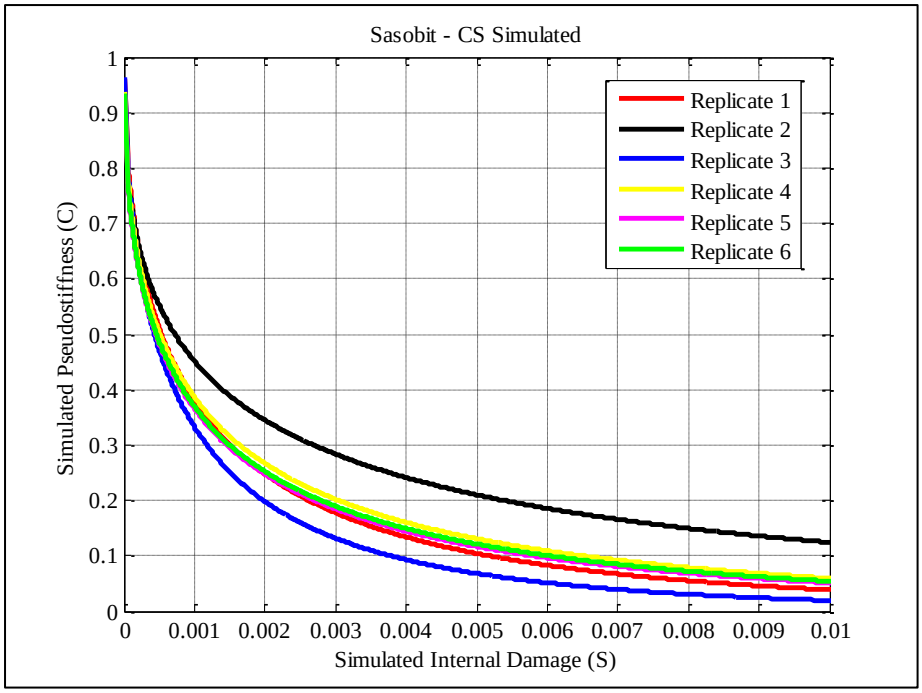

(c) Sasobit

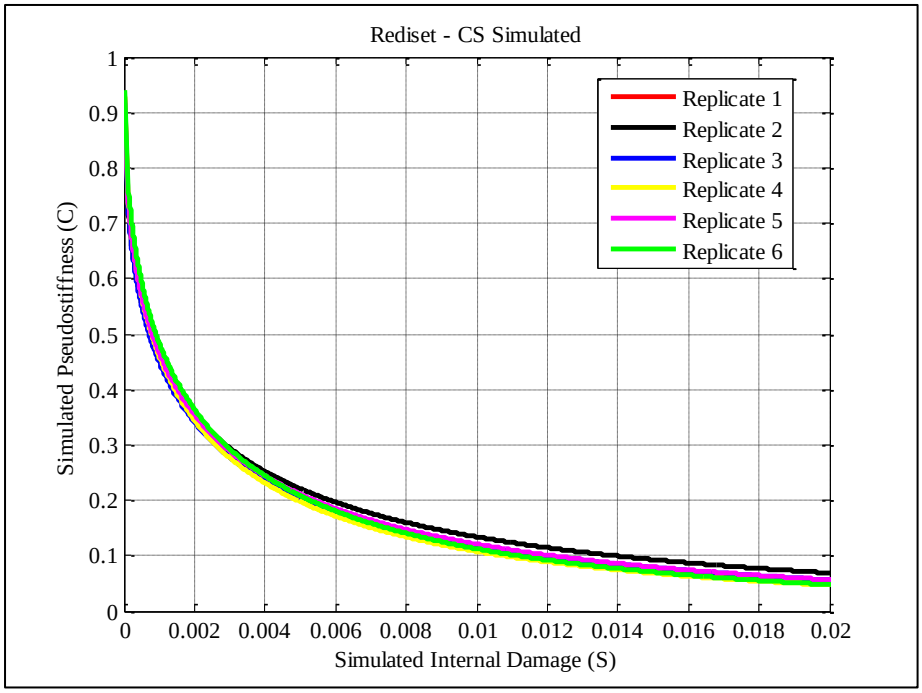

(d) Rediset

Figure 46: Simulated C-S curves for all replicates of (a) Original mix (b) Advera mix (c) Sasobit mix (d) Rediset mix

As shown in Figure 46, replicates are smoother after simulating the experimental data. However, Sasobit had more scattered data than the other mixes which can be referred to as the initial damage assigned for the replicates in the simulation part of the analysis.

The results of the simulated internal damage at 50% of the simulated pseudo-stiffness match the same trend as the experimental results. The Original mix showed the lowest internal damage and the other mixes were close to each other.

By calculating the number of cycles to failure (N_f) for each mixture using equation (28), the average results plotted in Figure 47 show that the Sasobit and Advera mixes have higher variability than the other mixes. The Coefficient of Variance (CoV) for the Sasobit mix is 40%. However, the CoV generated by conducting fatigue testing on FAM samples is still lower than the CoV generated by testing AMPT-sized samples, as per the literature reviewed for similar materials (Sadek, 2015). All mixes showed a relatively short fatigue life – compared to complete number of cycles (200,000 cycles) – with a number of cycles to failure of between 30,000 and 50,000 cycles. This indicates that the fatigue test performed at 400 kPa was high enough to damage the samples at early life.

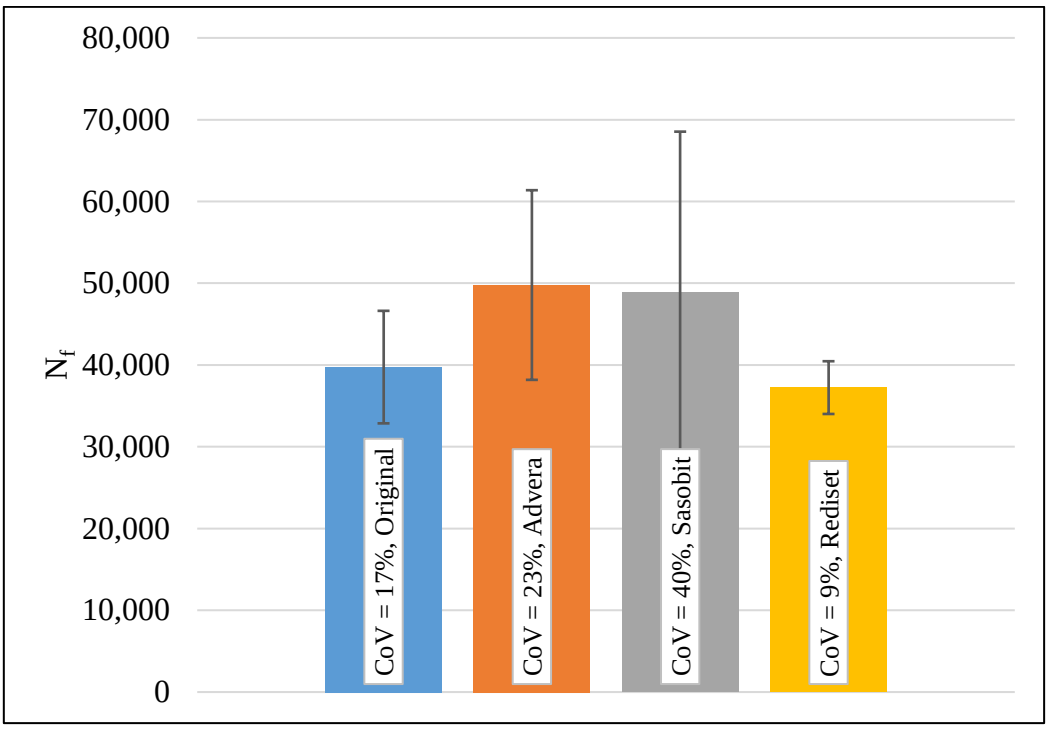

Figure 47: Number of cycles to failure at 50% reduction in material stiffness

It can also be observed from Figure 47 that mixtures prepared with Sasobit and Advera showed a higher number of cycles to failure, which indicated longer service life than the others. On the other hand, the Rediset mix showed almost similar behaviour to the Original mixes. The finding of similar N_f results between the Original mix and Rediset mix supports the claim that Rediset does not affect the mechanical performance of the asphalt mixture (AkzoNobel, 2014). Having Sasobit and Advera mixes with higher N_f confirms that the benefits of using WMA additives are dissipating lower energy and having a longer service life.

In order to evaluate the statistical difference between the mix types, one-way analysis of variance (ANOVA) was used for each analysis method (DPSE and VECD). ANOVA analysis was performed using a statistical significance level of 5% ($\alpha = 0.05$). Assuming that the null hypothesis (no significant difference between mixes) is true, the *p*-value is the probability of finding a test statistic at least as extreme as the one that was truly observed. Based on the results in Table 8, since the *p*-value of the DPSE method is less than 0.05, the null hypothesis was rejected, which indicates that the mixes showed a significant difference in dissipating energy. Having a *p*-value less than 5% means that there is a 95% confidence level that the mean dissipated pseudo-strain energy, W_R, is statistically significant among the mixtures. In other words, the mixes exhibited different behaviour. However, the number of cycles to failure (N_f) in the VECD analysis approach has a *p*-value of more than 0.05, which indicated that, at a 95% confidence level, the mean N_f is not statistically significant among the different mixture types and all mixes are performing similarly.

Table 8: ANOVA results for both analysis methods implemented (α=0.05)

Analysis Parameter	Mix Type	Average	Variance	F_{Value}	$F_{critical}$	*p*-value
DPSE, W_R at 200,000 Cycles	Original	199.27	173.09	70.773	3.098	7.9E-11
	Advera	146.66	40.19			
	Sasobit	120.65	21.40			
	Rediset	186.23	207.89			
VECD, N_f	Original	40,051	48,335,626	1.657	3.098	0.208
	Advera	49,930	134,928,127			
	Sasobit	49,128	388,574,205			
	Rediset	37,396	10,438,174			

In summary, this section aimed to study the fatigue performance of warm fine aggregate mixtures (W-FAM). An oscillatory test was performed on finger-sized samples using a Dynamic Shear Rheometer at a temperature of 25ºC. The linear viscoelastic shear modulus was checked and showed higher values when WMA was used. In addition, W-FAM samples dissipated less energy than the control mixtures when exposed to damaging shear stress. However, since all mixtures completed the test at 200,000 cycles without complete failure, another analysis tool was required to assess the fatigue damage of the W-FAM samples.

The Viscoelastic Continuum Damage (VECD) approach was used in order to estimate the number of cycles to fatigue failure (N_f). There were differences in the N_f of the various mixtures; however, the analysis of variance (ANOVA) tool showed that there was no statistical significance in the estimated N_f among the W-FAM and the control mixture. This finding supports the theory that WMA additives keep the fatigue resistance at a comparable level to that of the hot mix asphalt mixtures.

4.3. Summary and Conclusions

This section aimed to study the fatigue performance of warm fine aggregate mixtures (W-FAM). An oscillatory test was performed on finger-sized samples using a Dynamic Shear Rheometer at a temperature of 25ºC. The linear viscoelastic shear modulus was checked and showed higher values when WMA was used. In addition, W-FAM samples dissipated less energy than the control mixtures when exposed to damaging shear stress. However, since all mixtures completed the test at 200,000 cycles without complete failure, another analysis tool was required to assess the fatigue damage of the W-FAM samples.

The Viscoelastic Continuum Damage (VECD) approach was used in order to estimate the number of cycles to fatigue failure (N_f). There were differences in the N_f of the various mixtures; however, the analysis of variance (ANOVA) tool showed that there was no statistical significance in the estimated N_f among the W-FAM and the control mixture. This finding supports the theory that WMA additives keep the fatigue resistance at a comparable level to that of the hot mix asphalt mixtures.

By conducting fatigue tests on the FAM samples mixed with WMA additives, the results showed that the WMA additives have no significant effect on the fatigue resistance. This indicates that preparing the asphalt mastic samples at the lower temperatures allowed by using WMA additives did not benefit (or harm) the fatigue resistance of the materials. Additionally, the stiffness that was gained from using Sasobit did not affect the fatigue resistance of the asphalt mastic in either a negative or positive way.

It is well known that fatigue cracking is more severe at later stages of the asphalt mixtures' service. During a road's long-term service, the ageing of asphalt mixtures is

highly affected by outdoor factors, such as heat, traffic, weather, etc. Thus, the next chapter introduces a new ageing protocol that adds weathering factors to the ageing process of the FAM samples.

5. Characterisation of Aged Warm Fine Aggregate Mixtures

This chapter documents the investigation into utilising the Accelerated Weathering Machine in simulating the climatic conditions in the State of Qatar to age asphalt mixtures. Ageing is one of the most dominant factors that change the properties of asphalt mixtures in road pavements. The term 'ageing' was originally used to describe the changes occurring in materials exposed to external effects over time, such as heat and sunlight. Naturally, asphalt pavements are exposed to these external effects (sunlight, rain, traffic and temperature) in different dosages, durations and combinations. These combinations depend on location, altitude and/or season. However, simulation of these conditions in the laboratory is essential, with the purpose of being as close as possible to the real atmospheric conditions and simulating their effects. Such simulation combines different ageing factors to bring the material to similar external conditions but obtains results in a much shorter timeframe. Accelerated ageing is necessary to predict the future performance of materials and improve their design.

Ageing of asphalt pavement is a dominant factor in determining its service life. The asphalt pavement is laid down on the road and expected to serve for typically 20 years with a rehabilitation process performed to the surface layer. However, this target is hard to accomplish due to distresses that appear on the pavement's surfaces, which require rehabilitation. Success in the design and construction of asphalt pavement that lasts for the design lifetime is a major goal for infrastructure projects.

The State of Qatar has a dry, subtropical desert climate with low annual rainfall and humid-hot summers (Worldtravelguide.net, 2015). The high temperature in the

summer and high UV index most of the year have a major effect on the asphalt pavement's performance. The current standard techniques used to test asphalt ageing depend on exposing the material to heat and air at different temperatures and pressures to simulate field ageing (ASTM Standard D 6921, 2008; AASHTO - T 240, 2009; Pavement Interactive, 2015). These methods do not include UV light as a cause of ageing to the asphalt material that affects its reliability and performance.

UV light is the part of sunlight that causes physical damage to materials; this is especially the case in countries such as Qatar that have a high UV index most of the year during the day. Direct exposure to UV light results in material degradation. Materials that are not UV-stable may crack or disintegrate due to UV light. Continuous exposure to UV light can be more severe than sporadic exposure, since damage depends on the extent and degree of exposure (Atlas, 2015). In terms of rutting resistance, UV ageing of asphalt pavements can be more serious than thermal ageing (Wu *et al.*, 2009; Liu *et al.*, 2014). Bitumen can be prepared with a UV blocking agent to improve UV ageing resistance, such as Layered Double Hydroxide (LDH) materials. The LDHs are anionic layered materials that act as a shield to prevent UV light affecting the materials (Liu *et al.*, 2015a, 2015b). However, in this study, none of those agents were used.

Weathering machines are intended to reproduce deterioration caused by actual weather. There are two types of weathering machine available on the market, and they are produced by a number of manufacturers. The first type can simulate the full spectra of the sunlight during the testing by exposing the material to all of the sun's irradiation wavelengths (from 300 nm to around 2500 nm), as shown in Figure 48.

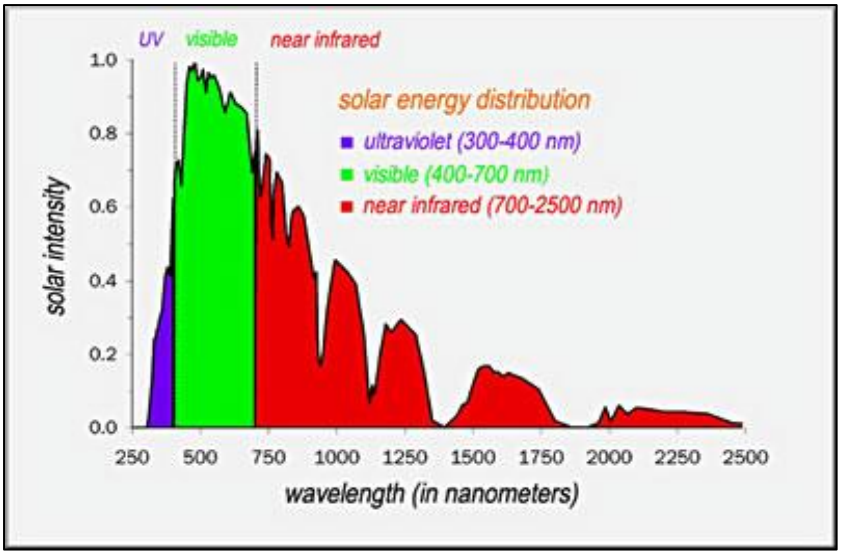

Figure 48: Full spectrum from sunlight (Solar Journey USA, 2016)

These machines are usually used to study the effect of all the light's wavelength range on material degradation. Xenon lamps are usually used with these machines and the samples are mounted against the lamps on a rotating rack, as shown in Figure 49.

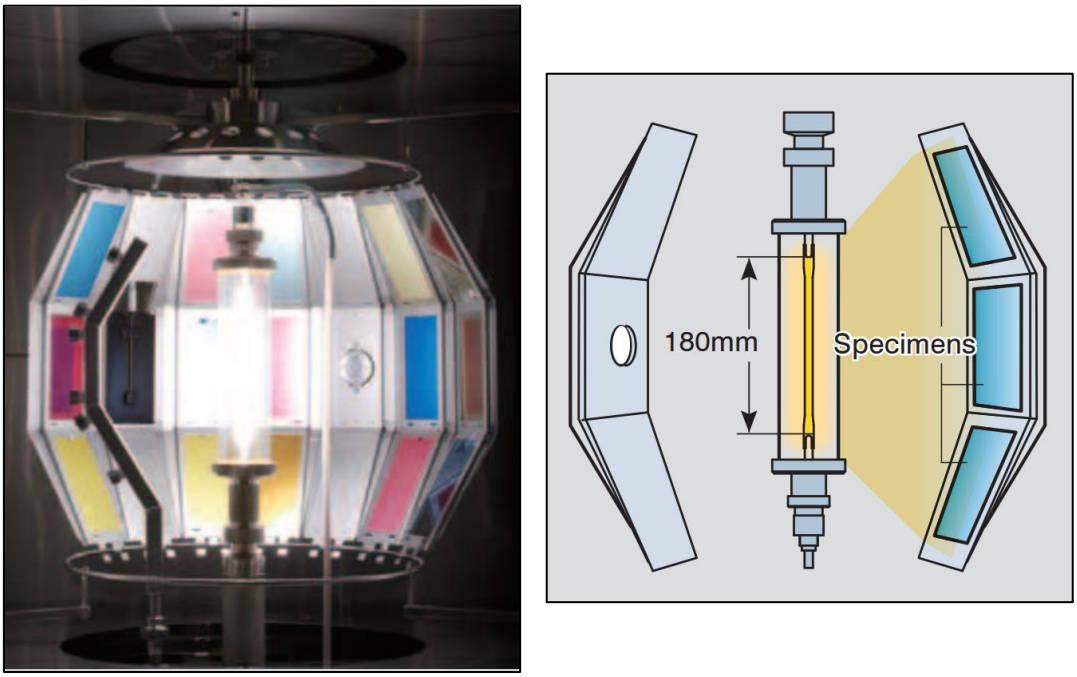

Figure 49: Spherical chamber to hold the specimen for full spectra irradiation (pictures from SUGA Test Instruments, 2011)

The second type of machine only exposes the material to the critical short-wave UV that has a major effect on the material. These machines are usually used for materials whose physical properties and behaviour are affected by the UV light. These machines commonly come with rotating or static panels to handle the samples for continuous exposure. For example, the QUV weathering machine from Q-LAB provides static panels to expose the materials to the critical UV light wavelength, as shown in Figure 50.

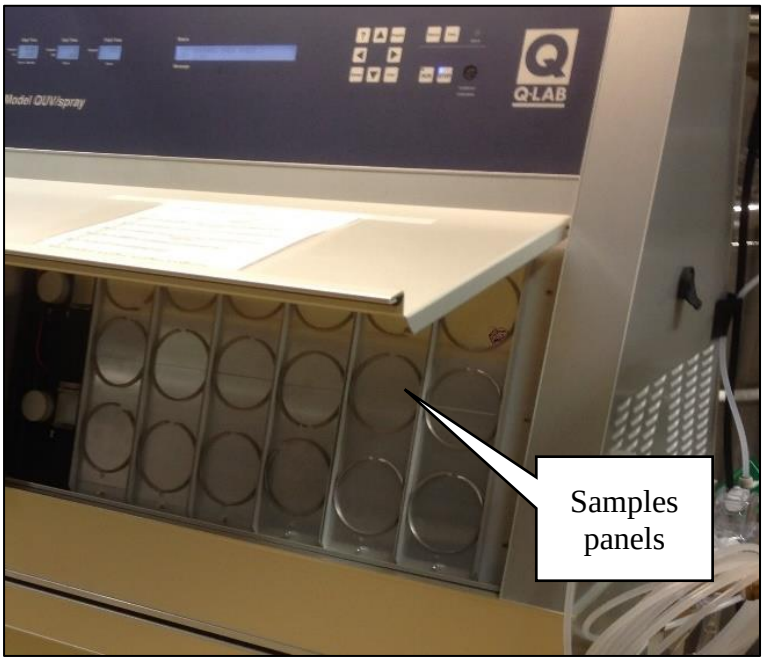

Figure 50: Weathering Machine with static sample panels

The objective of this chapter is to investigate the feasibility of utilising the Accelerated Weathering Machine in simulating the State of Qatar's climatic conditions to age asphalt mixture samples. The QUV model from Q-Lab was used in this study to investigate the ageing of fine aggregate mixtures prepared with WMA additives (as described in Chapter 3). A visual assessment and a mechanical testing were performed on the aged samples to examine the feasibility of using the accelerated weathering

machine (UV light and heat) in ageing the asphalt mixture as per the expected outdoor ageing.

5.1. Accelerated Weathering Machine

The ageing of the W-FAM samples was performed using the Accelerated Weathering Machine from Q-Lab (QUV model). The machine is shaped like a triangular prism that includes UV lamps, heater, water spray nozzles and water pan (Figure 51). The machine has four controllable factors that can be applied to the material in different sets and multiple cycles. The factors are UV light, heat, condensation and water spray. Heat is the only factor that can be combined with other factors. However, the machine can control the factors in pre-set cycles with time periods.

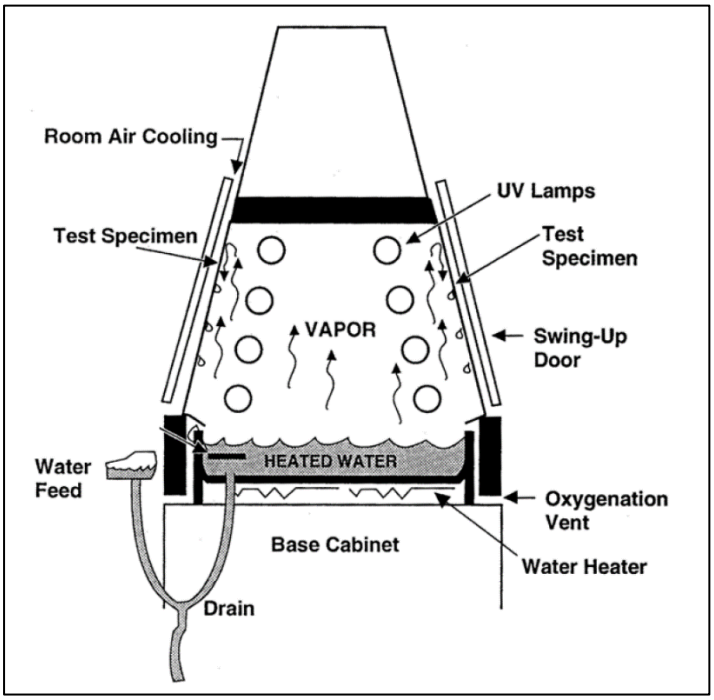

Figure 51: Accelerated Weathering Machine (from Q-Lab) components (Q-Lab Corporation, 2012)

Samples can be heated inside the chamber at temperatures between 40ºC and 80ºC. The machine can control the UV light to be at low intensity, match the sunlight

spectrum, or at high intensity for faster results. Condensation is an on/off option that creates vapour inside the chamber for moisture conditioning. However, the machine does not offer the option of controlling the percentage of condensation; it has to be either 0% or 100%. Finally, the machine has spray nozzles that spray water onto the sample's surface in a controlled volume to simulate rain. Figure 52 shows the accelerated weathering machine with the lamps used in the study.

Figure 52: Accelerated Weathering Machine from Q-Lab and UV lamps

The standard sample form for the Accelerated Weathering Machine is a thin film that can be mounted on the sample panels vertically. These panels were originally used for materials such as polymers or plastic which can be attached to them.

In this study, the new/fresh finger-sized W-FAM samples described in Chapter 3 were used in the ageing protocol. Special sample holders were fabricated at Texas A&M University at Qatar to hold six finger-sized W-FAM samples in one panel inside the weathering machine chamber, as shown in Figure 53. As mentioned earlier, the W-FAM samples were fabricated with a height of 50 mm and diameter of 12 mm. The fabricated holder was designed to cover almost 10 mm of both ends of the samples from the direct UV light. The covered parts were protected in order to keep that parts strong to be glued with the DSR fixations later. Samples were placed inside the

machine for ageing based on the new protocol, which will be described in the coming sections.

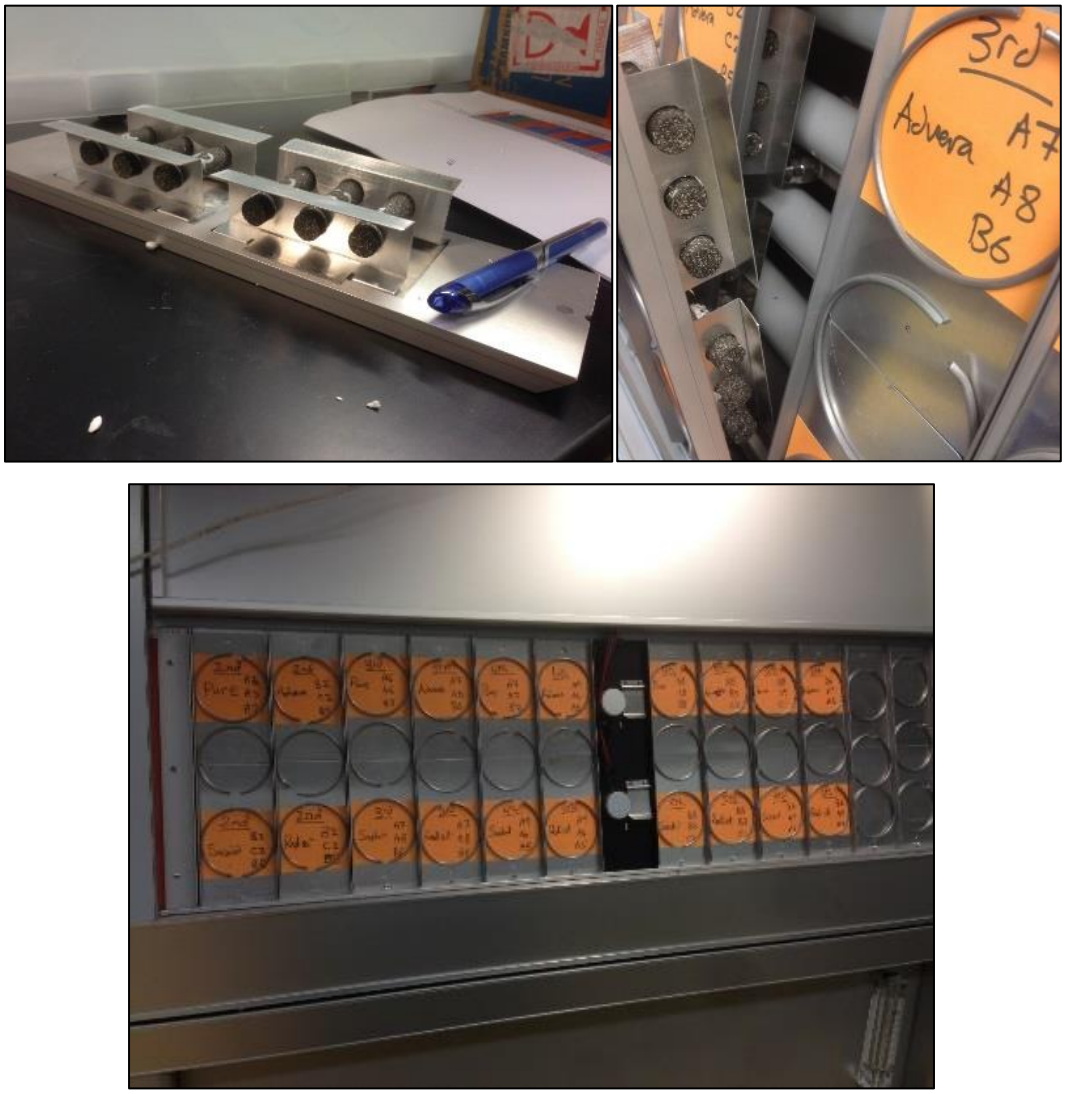

Figure 53: Samples, holders and panels placed in the Accelerated Weathering Machine

A total of 15 samples from each mix (total of four mixes: Original mix, Sasobit mix, Advera mix and Rediset mix) were placed inside the weathering machine and collected at five ageing levels (three replicates of each mix at each level). The total number of samples was 60.

5.2. Ageing Protocol and Methodology

Weathering is the reaction between the material and the climate factors that causes unwanted changes. The significant cost of a material's degradation drives its producers to find ways to keep the product from failure due to environmental causes and increase its durability. As mentioned earlier, the accelerated weathering machine includes three main factors: solar radiation (light energy), temperature and water. The tested material would degrade when the energy absorbed is more than the material's bond energy (Atlas Electric Devices Company, 2001).

In this study, solar energy and temperature were combined in ageing the W-FAM samples while the condensation effect was omitted because it is out of the study's scope.

5.2.1. Solar Radiation

The sun is the primitive source of energy for life on Earth. It sends radiant energy in the form of light (photons) that travels through space and hits Earth's surface. The energy of these photons is inversely proportional to their light wavelength, as shown in equation (30); the shorter the wavelength, the higher the energy and vice versa.

$$E = h\nu = hc/\lambda \quad \textbf{(30)}$$

where 'h' is Planck's constant which is a physical constant that describes the quantum of action and has a value of 6.626×10^{-34} Js, 'ν' is the frequency, 'c' is the velocity of the light wave and 'λ' is the wavelength.

The solar radiation sent to Earth's surface contains a broad spectrum with wavelengths ranging between 280 and 3000 nanometres and can be subdivided into three classes: ultraviolet (UV), visible (VIS) and Infrared (IR), as shown in Figure 54.

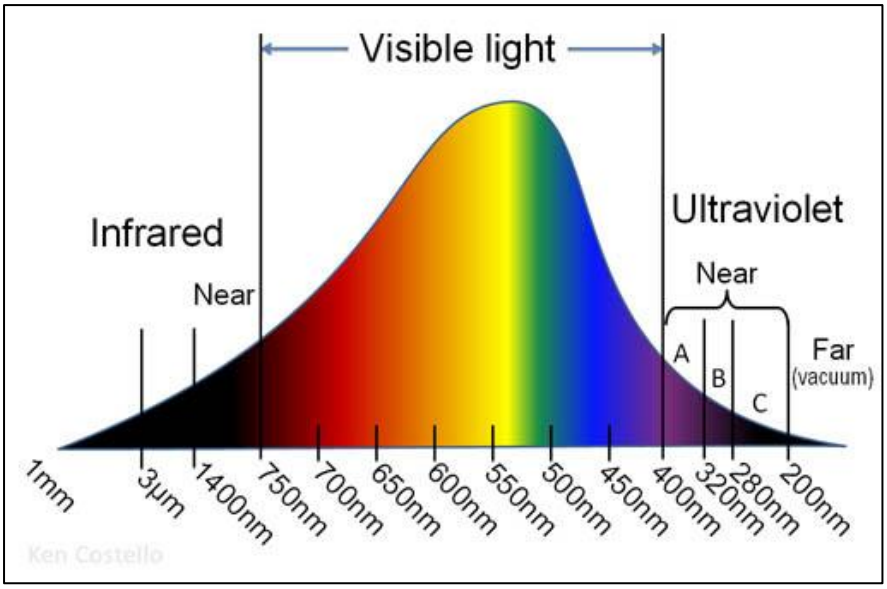

Figure 54: Wavelength distribution within the sunlight spectrum (chemistryland.com, 2015)

UV radiation, for which the wavelength is between 200 and 400nm, represents only 6.8% of the total incident solar radiation (International Commission on Illumination, 1989).

The ozone layer covers the Earth and helps to prevent the UV-C wavelength from passing through. However, the UV-A and UV-B can reach the ground surface in different percentages. Some of the UV-B waves are reflected by the clouds, but all the UV-A passes to the surface and significantly affects human health and causes materials to degrade.

The Accelerated Weathering Machine has UV fluorescent lamps that produce a UV wavelength at a specified intensity. These lamps are identified by 'UVA-340', indicating a UV-A irradiance type, with 340 representing the wavelength that has the maximum irradiance. The UVA-340 lamps can provide similar irradiance to sunlight (UV-A) at 0.68 W/m^2 irradiance intensity, as shown in Figure 55. Using a higher intensity (the maximum irradiance intensity that UVA-340 lamps can provide is 1.55

W/m^2) can accelerate the ageing time, but decreases the possibility of the ageing results being as close as possible to the outdoor ageing results.

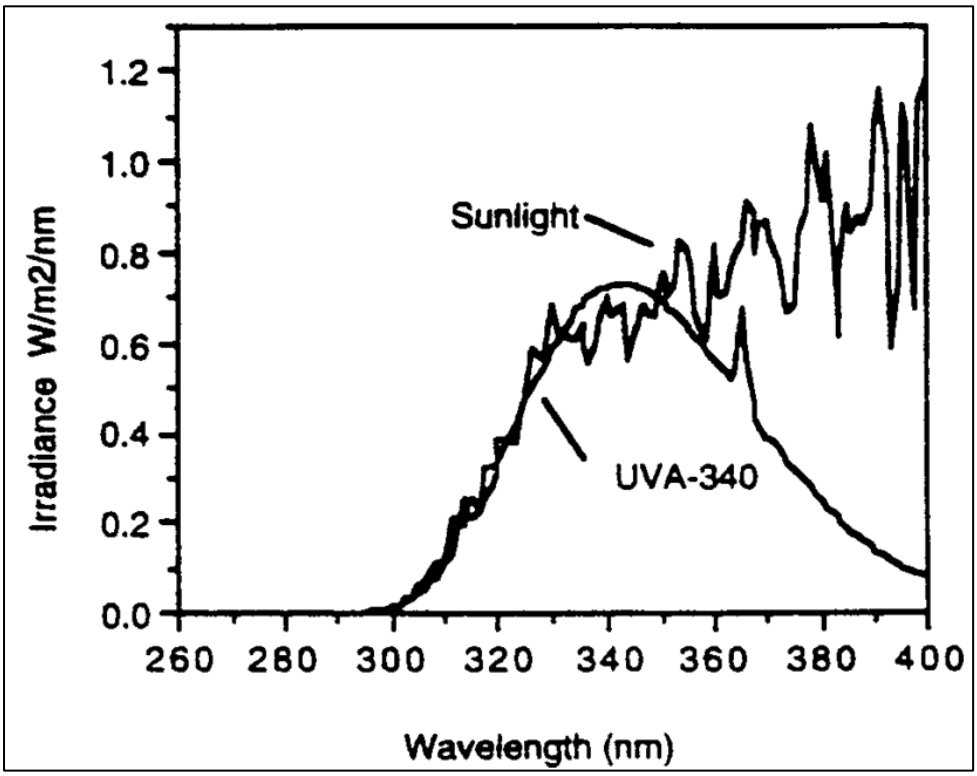

Figure 55: UV lamps compared to sunlight (ASTM - G154 - 12, 2012)

The Global Horizontal Irradiance (GHI) is a measured parameter in the solar energy that indicates the total amount of radiation received by the horizontal surface of the Earth. It is calculated by adding the Direct Normal Irradiation (DNI) and Diffuse Horizontal Irradiation (DHI). DNI is the irradiation that completely reaches the horizontal surface of the Earth without any loss in the atmosphere, while DHI is the irradiation that reaches the horizontal surface of the Earth but after losing some of its components in the atmosphere, as shown in Figure 56.

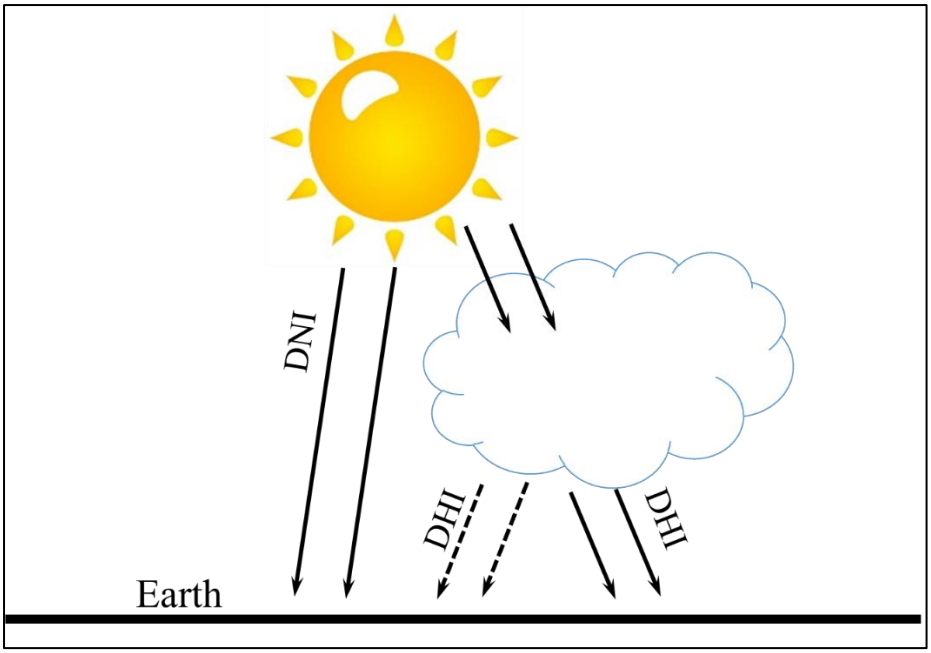

Figure 56: Illustration of Direct Normal Irradiation (DNI) and Diffuse Horizontal Irradiation (DHI)

The Global Horizontal Irradiance (GHI) in the State of Qatar ranges between 2050 kWh/m^2 and 2150 kWh/m^2 per year, as reported on the Solar GIS website (Solargis, 2016). However, this value changes from one year to another. Based on several references, a value of 2140 kWh/m^2 (7704 MJ/m^2/year) was selected for the State of Qatar in this study. The ageing protocol was meant to simulate one year of outdoor ageing inside the laboratory. Simulating more than a year will result in a long laboratory ageing period, which was not reasonable within the study's timeframe.

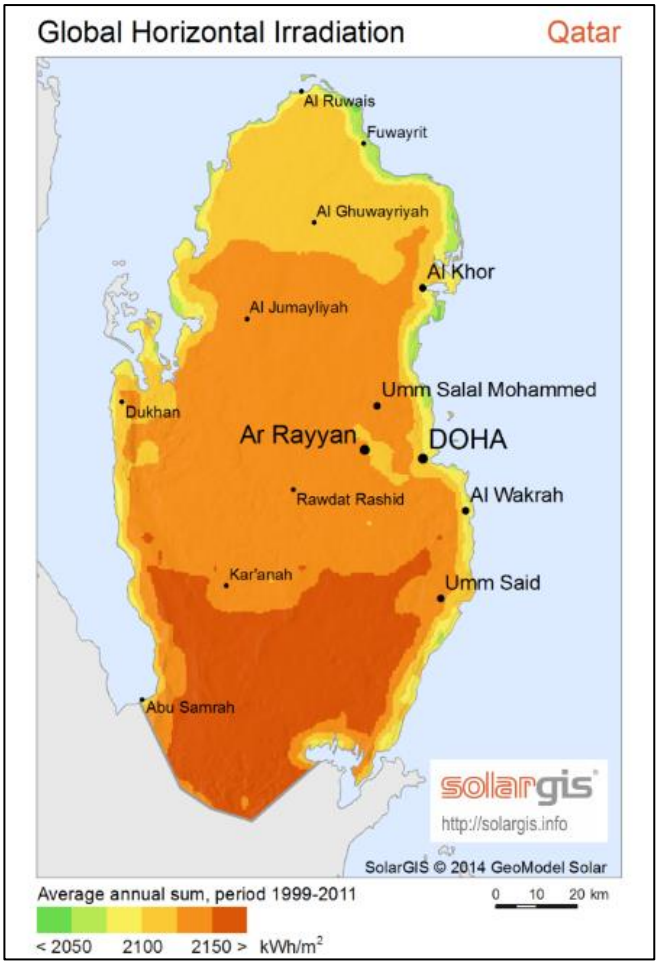

Figure 57: Global Horizontal Irradiance in the State of Qatar (Solargis, 2016)

Since the UV light is around 6.8% of the total solar radiation, as mentioned earlier, the UV radiation would be around 145 kWh/m^2 (524000 kJ/m^2/year). The UV lamps installed in the weathering machine are operative at a single wavelength (340 nm), and the energy contained in a single wavelength range (340 nm) is almost 1% of the total UV-A range (295-385 nm) (Atlas Electric Devices Company, 2001). 524000 kJ/m^2/year at total UV-A (295-385 nm) equals 5240 kJ/m^2 at 340 nm, which will be used in the calculation of the total ageing duration inside the weathering machine.

Since there is still no specific standard to be followed to age asphalt mixtures using the weathering machine, an ASTM general standard was followed to be as close as possible to a standardised ageing protocol for reasonable results. ASTM G 154 titled

'Operating Fluorescent Ultraviolet (UV) Lamp Apparatus for Exposure of Nonmetallic Materials' was used to follow common exposure conditions with pre-set cycles for ageing (ASTM - G154 - 12, 2014). Selecting the intensity of the irradiation is a key factor in defining the ageing period for the sample inside the weathering machine to simulate one year of outdoor real sunlight ageing. Setting the irradiance intensity to 0.68 W/m^2 would offer a more realistic condition with a long ageing period. However, choosing the intensity recommended by the ASTM G 154, 0.89 W/m^2, would still produce comparable results within a much shorter timeframe. The protocol recommended adding dark cycles after the UV light cycles, simulating day and night, for more sensible outcomes (Grossman, 2011). By following these outlines, total UV exposure hours were calculated by dividing the total GHI (5240 kJ/m^2) by intensity (0.89 W/m^2/nm) as follows:

$$t(hr) = \frac{5240\ kJ/m^2}{0.89\ W/m^2/nm \times 3.6} = 1635\ hrs \quad \textbf{(31)}$$

where the 3.6 value is used to convert from seconds to hours. By following the ASTM G154, it is recommended to have 8 hours of continuous UV light. The total number of hours (1635 hrs) was divided by the number of UV light hours (8 hours) to calculate the total number of ageing cycles as follows:

$$\frac{1635\ hrs}{8\ hrs/cycle} \approx 205\ cycles \quad \textbf{(32)}$$

Since the dark cycles will be added to the ageing protocol, the number of dark hours (4 hours as recommended by ASTM G154) was multiplied by the total number of

cycles (205 cycles) to calculate the total number of dark hours required for this ageing protocol as follows:

$$205\ cycles \times 4\ hrs\ dark = 820\ hrs \quad \textbf{(33)}$$

By adding the hours of light (1635 hrs) and dark (820 hrs) cycles, the total ageing period is 2455 hours.

The FAM samples were mounted inside the weathering machine and remained there for the calculated time and ageing cycles (light and dark). The exposure time intervals of the FAM samples were defined originally as shown in Table 9. However, the exposure time was subsequently modified to be a reasonable day and time.

Table 9: Exposure intervals and times for the FAM samples

Collection No. (Ageing Levels)	Original Exposure Time (hrs)	Performed exposure time after modification (hr)
1st collection	0 (Unaged)	0 (Unaged)
2nd collection	300	312
3rd collection	600	600
4th collection	900	936
5th collection	2455	2455

5.2.2. Ageing Temperature

Information about the warmest four months in Qatar (May, June, July and August) was obtained from the Weather Underground website for the year of 2014. The average of the maximum and minimum air temperature of those months is 41°C and 36°C, respectively (Weather Underground, 2014).

Since these temperatures represent air temperature, a model was needed to predict the pavement surface temperature in order to use it as a sample temperature in the machine. There are several models to convert the air temperature to the pavement

surface temperature (Lukanen *et al.*, 2000; Mohseni *et al.*, 2005; Steven, 2009). In this study, the following model is used (Huang, 2004):

$$M_p = M_a\left(1 + \frac{1}{z+4}\right) - \frac{34}{z+4} + 6 \qquad \textbf{(34)}$$

where 'M_p' is the pavement temperature (in Fahrenheit), 'M_a' is the air temperature (in Fahrenheit), and 'z' is the depth of the pavement structure (in inches). Using equation (34), the depth is assigned to zero to calculate the surface temperature. The results of the pavement surface temperature are 54ºC and 42ºC for the average maximum and minimum temperature, respectively.

First, a thermocouple was attached to the sample and placed inside the chamber and heated to different temperatures and different UV intensity. This was carried out to check the difference between the set temperature inside the chamber and the sample's temperature. In addition, the sample might absorb more heat from the UV electromagnetic waves that has to be considered in the machine set temperature. It was observed that the difference between the set temperature and the sample's surface temperature was affected by the absorption of the UV light, which increased the sample's temperature by 4°C. This increment was considered in specifying the UV ageing temperature. Finally, the ageing protocol used in this study is summarised in Table 10.

Table 10: Summary of the ageing protocol

Step	Duration	UV light	Set Temperature*	Sample Temperature
1	4 hrs	Off	42°C	42°C
2	8 hrs	On	50°C	54°C

* Set temperature in the machine's program

The above ageing protocol was set to repeat 205 times to complete 2455 hrs of ageing. This ageing process took around three and a half months.

5.3. Evaluation Approach and Ageing Results

W-FAM samples were subjected to the mechanical testing using the same set of DSR accessories. The DSR used for the mechanical testing has the same accessory (mentioned earlier in Chapter 3) that allows the testing of solid samples by applying shear stress. Figure 58 shows the accessories attached to the lower and upper parts of the DSR. The testing was conducted at a controlled room temperature of 23ºC.

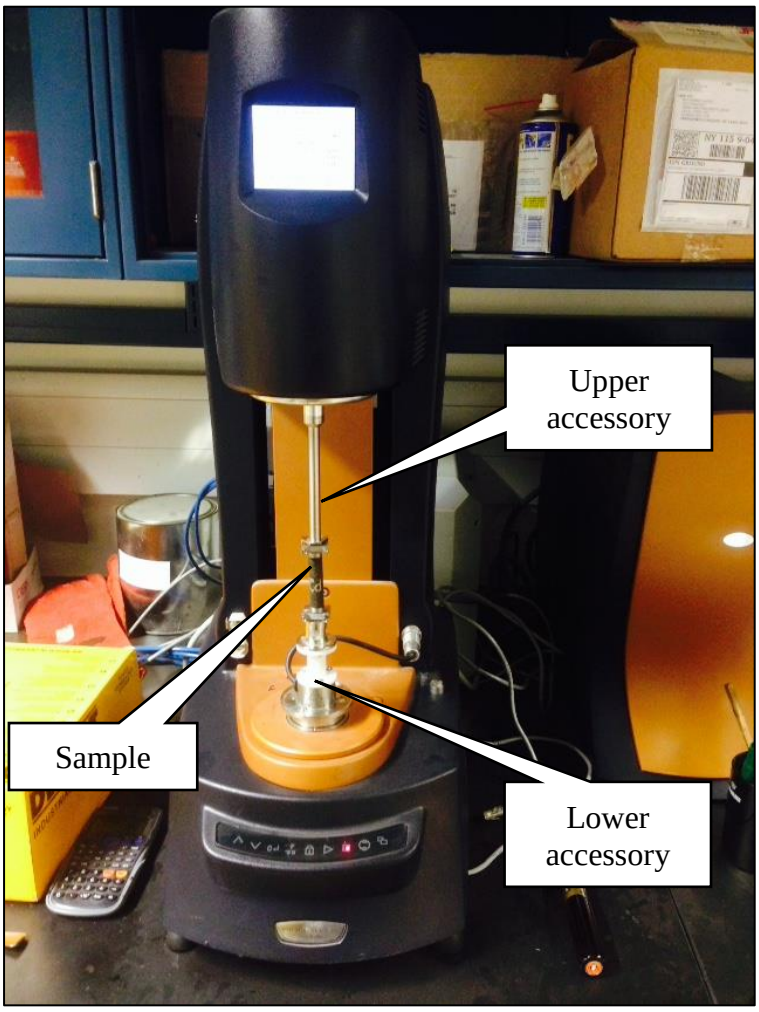

Figure 58: DSR with attached accessory and solid sample

The tests were conducted on three replicates of unaged and fully aged samples to evaluate the effect of the new ageing protocol on W-FAM samples. Samples were subjected to a frequency sweep test starting from 1 Hz until 10 Hz at 75 kPa stress amplitude. The other samples – which were collected at different ageing levels – were kept for further testing, which will be presented in the next chapters. The stress amplitude was selected to be within the linear viscoelastic (LVE) region of the sample behaviour based on the stress sweep test results presented in Chapter 3.

5.3.1. Visual Assessment of UV-aged Samples

Visual assessment was performed on the UV-aged W-FAM samples for different mixtures. Table 11 shows the difference in surface colour with ageing levels. Visual inspection did not show signs of cracks or degradation on the surface of the samples. However, there was clear colour fading in the aged FAM samples.

Table 11: Photographs of the FAM samples were taken after each ageing interval

Ageing Level	Original mix	Sasobit mix	Advera mix	Rediset mix
0 hrs (Unaged)				

312 hrs				
600 hrs				
936 hrs				

2455 hrs (Fully Aged)				

From the photos of the aged samples displayed in Table 11, it can be noticed that the colour fading started at 600 hours of UV ageing. However, it was observed that the end portions of all samples were protected from direct UV light and did not show any physical change on the surface.

It is worth mentioning that the length of the covered part in each sample is different since the sample holders are fixable and did not ensured similar coverage for all samples. This would affect the results since the aged part in the sample is changing from sample to another. However, this variability was ignored since maintaining the same uncovered part length with flexible metal holder was a difficult task.

Since the visual assessment could not detect any physical damage (crack or deformation) on the samples after UV ageing, sample ageing needed to be validated using a mechanical testing, as presented in the next section.

5.3.2. Ageing Feasibility Evaluation

A frequency sweep test was performed using the DSR in order to evaluate the effect of UV ageing on the material stiffness. Figure 59 shows the average and standard deviation (as error bars) of the shear modulus (|G*|) and phase angle (δ) measurements at frequency 10 Hz. It can be noticed that ageing the W-FAM samples using the new

ageing protocol has increased the stiffness (i.e. shear modulus) of the materials as expected. The percentage of increase is presented in white boxes in Figure 59. The Sasobit mix showed the smallest increase between aged and unaged samples, which indicates that using the Sasobit WMA additive can lower the effect of UV light ageing.

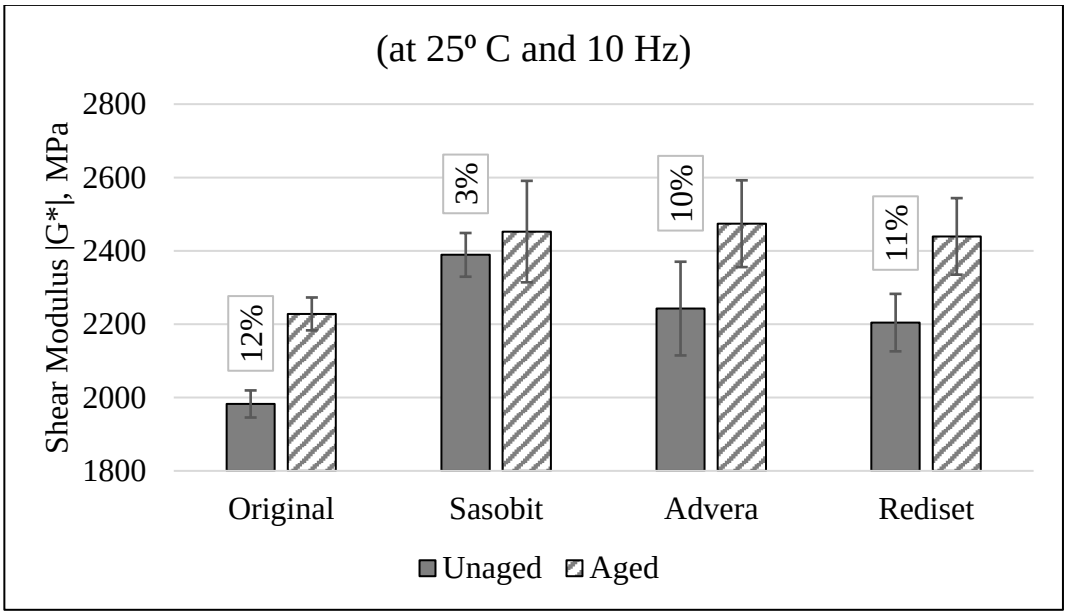

(a)

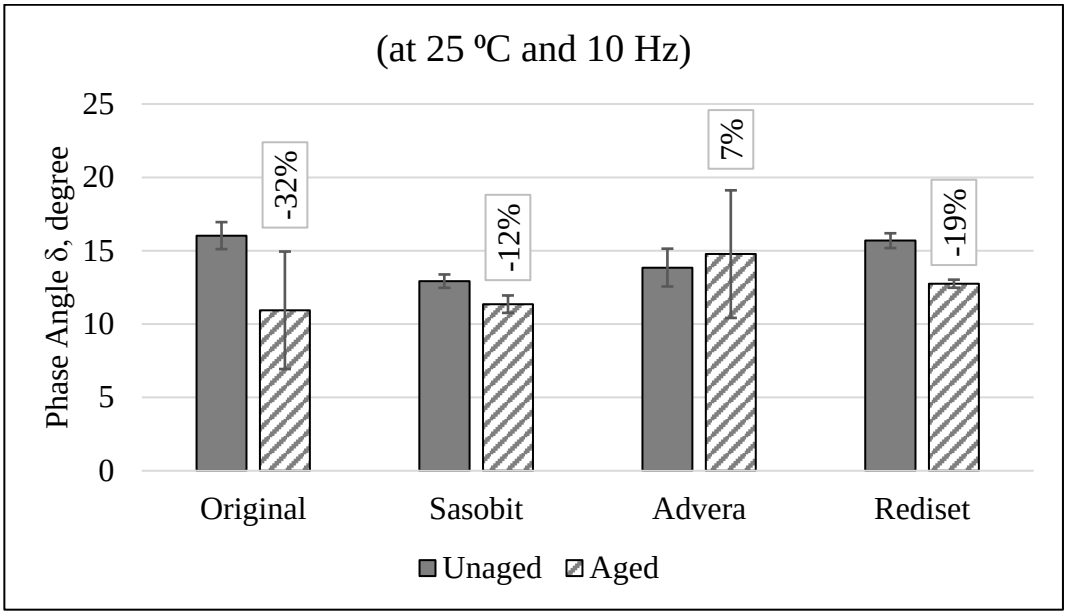

(b)

Figure 59: Average (a) shear modulus (|G*|) and (b) phase angle (δ) at 10 Hz (and 25ºC) for unaged and aged W-FAM samples with percentage of increase/decrease due to ageing

UV ageing reduced the phase angle of all W-FAM samples, indicating a reduction in the viscous component of its response. The Advera additive showed the highest coefficient of variance among the replicates and did not show a significant reduction in phase angle values. This indicates that the addition of Advera elevated the stiffness of the W-FAM samples but did not affect the viscous behaviour of the material.

Moreover, the frequency sweep test results in Figure 60 show that the fully aged samples experienced a higher shear modulus than the unaged samples along with all frequencies. Once more, it can be observed that, for the Sasobit mix, the difference in stiffness between the aged and the unaged samples is smaller than for all the other mixtures.

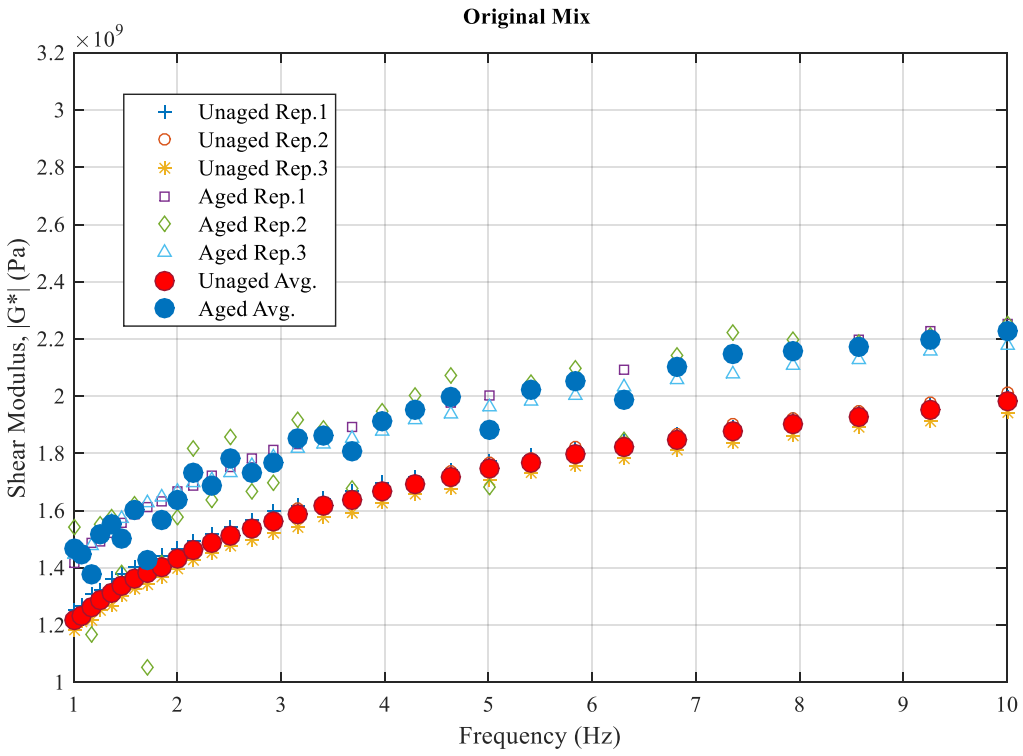

(a)

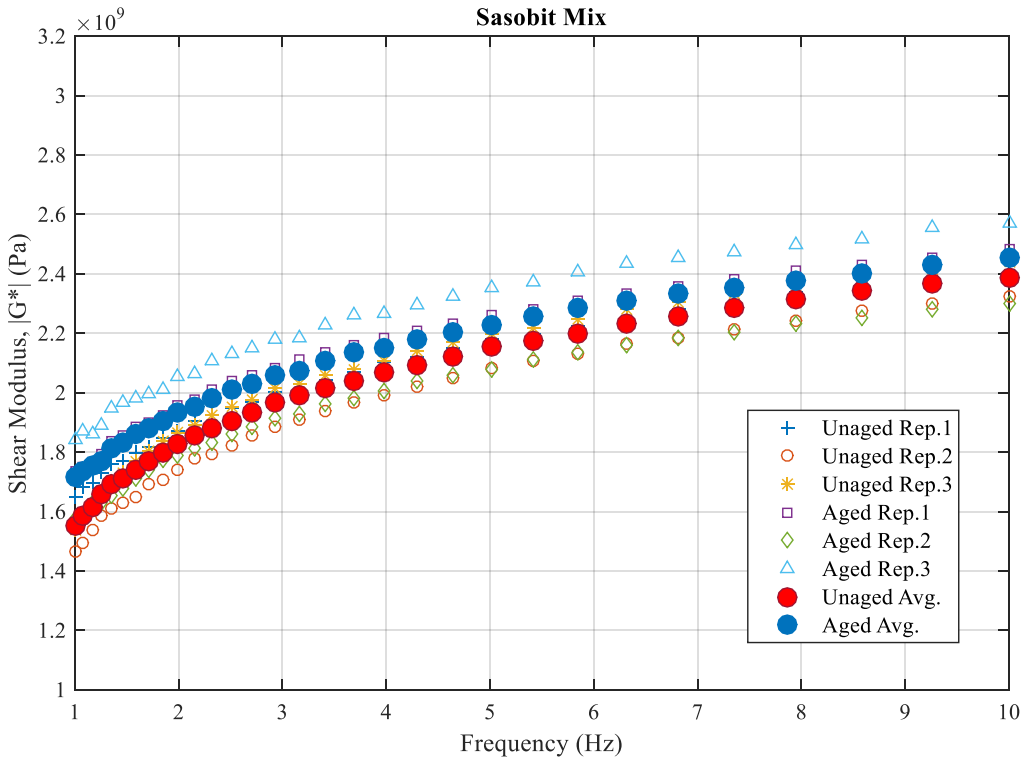
Sasobit Mix
×10^9
Shear Modulus, |G*| (Pa)
Frequency (Hz)
Unaged Rep.1
Unaged Rep.2
Unaged Rep.3
Aged Rep.1
Aged Rep.2
Aged Rep.3
Unaged Avg.
Aged Avg.

(b)

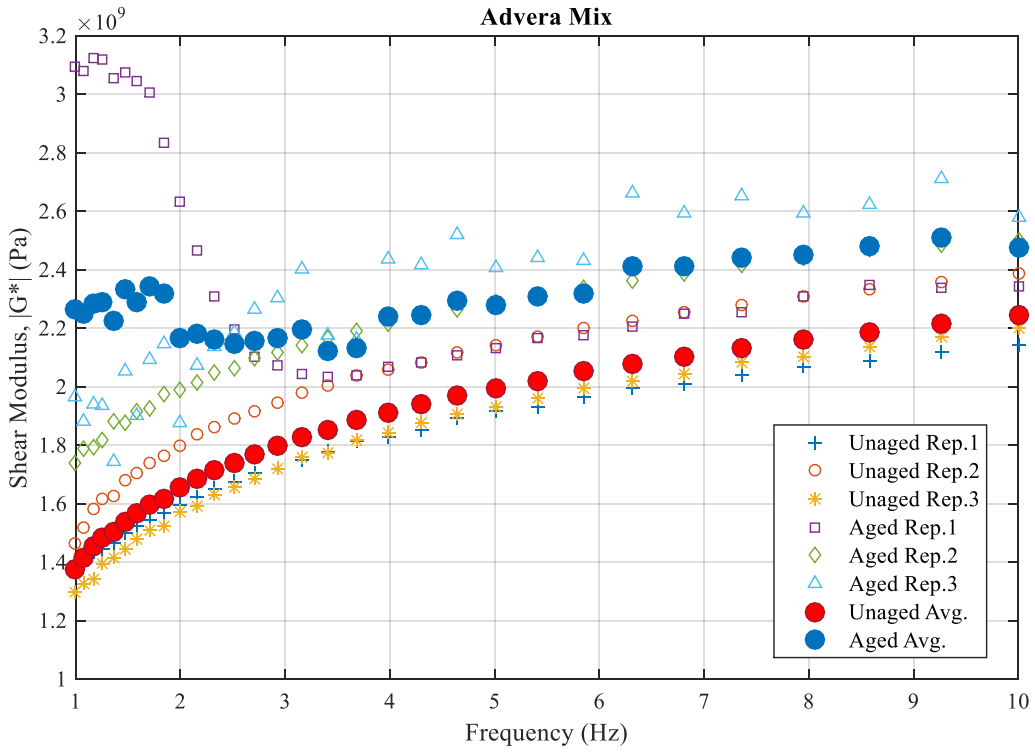
Advera Mix
×10^9
Shear Modulus, |G*| (Pa)
Frequency (Hz)
Unaged Rep.1
Unaged Rep.2
Unaged Rep.3
Aged Rep.1
Aged Rep.2
Aged Rep.3
Unaged Avg.
Aged Avg.

(c)

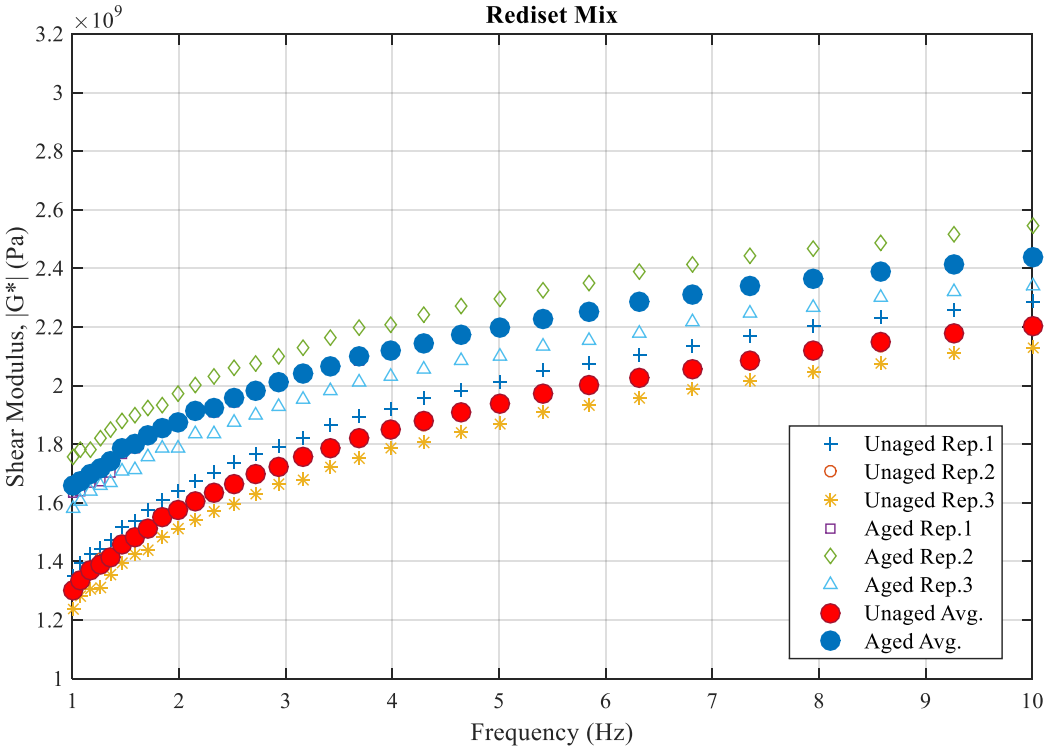

(d)

Figure 60: Frequency sweep test results of the shear dynamic modulus of (a) Original mix, (b) Sasobit mix, (c) Advera mix and (d) Rediset mix

5.4. Conclusions

Ageing is one of the most important factors that influence the performance of asphaltic materials. The State of Qatar has a dry, subtropical desert climate with low annual rainfall and humid-hot summers. The UV index in Qatar is considered high most of the year and adversely affects the physical properties of materials, leading to accelerated degradation. Studying the effect of UV light on the asphalt pavement performance is essential for countries such as Qatar. In this chapter, an accelerated weathering machine was utilised to simulate the equivalent of one year's outdoor ageing. The ageing protocol was designed to expose the material to UV light and heat at pre-set cycles that match Qatar's climate. The weather in Qatar was analysed in order to account for maximum air temperature in the summer and the quantity of

irradiation absorbed by the surface. This information was used to calculate the number of hours of UV light exposure needed to simulate one year of the outdoor service life of asphalt mixture. Warm fine aggregate mixture (W-FAM) samples were placed in the weathering machine for the specified number of hours. All mixes experienced colour fading on the surface after ageing. However, no cracks or degradations were observed on the samples after the ageing.

In addition, samples were tested by the DSR using a frequency sweep test, and the results showed that the combination of UV light and heat ageing elevated the shear modulus and reduced the phase angle of all the W-FAM samples. The Sasobit mix showed the smallest percentage increase in shear modulus (3% only), while the Original mix was the highest with a 12% increment.

The outcomes from the Accelerated Weathering Machine ageing protocol show that the combination of UV light with elevated temperature has an effective influence on the W-FAM ageing. In subsequent chapters, aged samples will be included in a damage and recovery study to evaluate the performance against rutting and fatigue distresses, and correlate the results with the crack enlargement and rearrangement due to loading.

6. Characterisation of the Creep and Recovery Responses of Fine Aggregate Warm Asphalt Mixtures

This chapter documents the characterisation of repeated creep and recovery test responses of FAM samples mixed with WMA additives. The results demonstrate the damage associated with the repeated loading and compare the mixes accordingly.

As discussed in the previous chapters, the performance of the asphalt materials (bitumen or mastic) with WMA additives showed improved rutting resistance compared to the control bitumen/mastic. This is especially true when Sasobit was used. However, the fatigue resistance did not show any significant difference between the Warm Fine Aggregate Mixture (W-FAM) and the control Fine Aggregate Mixture (FAM) samples when tested with an oscillation stress-controlled test.

As mentioned earlier, all the testing procedures and analysis approaches presented in Chapters 2 and 3 investigate the basic performance indicators of WMA materials. Advanced testing and analysis techniques are still required to achieve a solid characterisation of the WMAs' performance. The standard testing of asphalt bitumen or fatigue testing of FAM samples could not explore truly the evolution of damage inside the WMA materials or evaluate the differences in their performance. Unconventional practices should be conducted in order to deeply calculate material damage due to external factors. Since the asphalt pavement behaviour is directly affected by ageing, material must be included in a damage test procedure that considers UV light ageing in the testing matrix. As mentioned earlier, including the UV light ageing in the testing matrix for WMA materials would help in studying the effect of Qatar's climatic conditions in the materials' performance on roads.

The investigation of rutting resistance is typically conducted using a creep loading with relatively slow repeated loads at high temperatures (between 40ºC and 70ºC) to evaluate the permanent deformation, while investigating the fatigue cracking resistance is conducted by applying a relatively fast repeated loading at intermediate and low temperatures (around 25ºC and below) to evaluate the crack propagation and stiffness reduction. However, few studies have investigated the occurrence of the permanent deformation and fatigue cracking at the same time, since the asphalt material experiences a visco-elasto-plastic response (Elber, 1971; Luo, 2012). This response results in the occurrence of the permanent deformation and fatigue cracking at the same time due to a large amount of localised permanent strain around the crack area.

In this chapter, all the W-FAM samples (aged by the accelerated weathering machine) were tested by repeated creep and recovery test. The test was used to characterise the creep and recovery responses of the WMA material and investigate the damage associated with the repeated loading. The results were analysed using a new proposed analysis approach that evaluates the evolution of damage in the W-FAM samples.

6.1. Repeated Creep and Recovery Test

The repeated creep and recovery test protocol was developed to apply consecutive creep and recovery cycles and measure the resultant strain responses. Typically, a step-loading (creep stress) is applied with a specific stress level and loading duration followed by a rest period, as shown in Figure 61. In an ideal situation, the load jumps from zero to the specified stress level and the stress is kept constant for a specified period. Then the stress is released and returns to zero. While the machine needs time

to apply and release the stress on the sample, that stress raise and decay with time during the creep and recovery phases as shown in the dotted line in Figure 61.

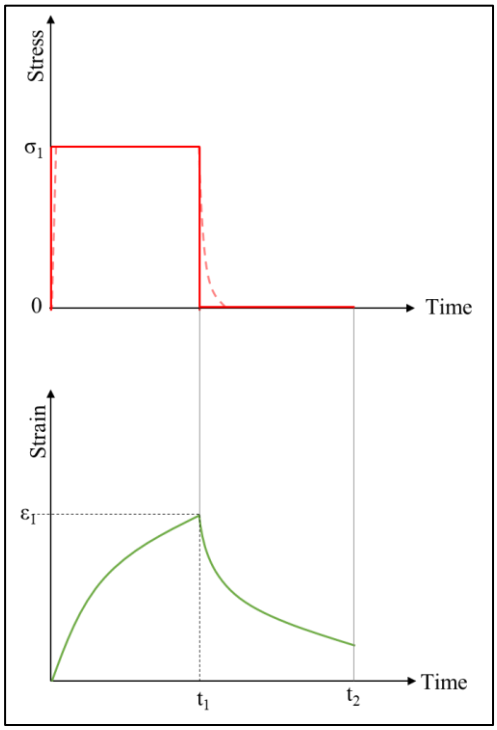

Figure 61: Applied creep stress and recovery and the resultant recovery strain

In the first cycle of the lowest stress level, the material stays in the linear viscoelastic region and no nonlinearity or damage is introduced, while, with more cycles, the material starts to deform more and exhibits damage. There are multiple factors that affect the response of the material, such as creep stress amplitude, duration of the creep loading, duration of the unloading (recovery), number of cycles and ageing level. The amplitude of the creep stress has a major role in the material's behaviour while applying a low creep stress can keep the material in the linear viscoelastic region and it will exhibit no damage. However, applying a high-stress level may cause the damage early in the loading process. Moreover, the duration of the loading and unloading makes a very important contribution to the material's behaviour. With a longer loading

time, the material experiences more damage and permanent deformation, as shown in Figure 62.

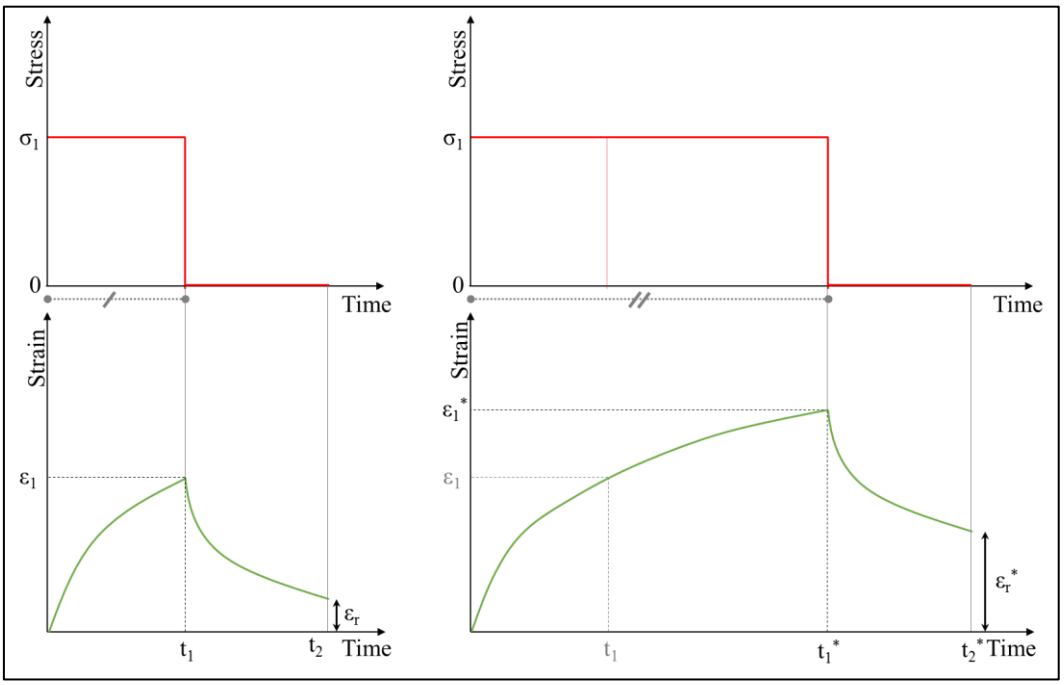

Figure 62: The resultant strain with different creep loading durations

The unloading duration also has a major effect on the overall response of the material at the end of the test cycle. A shorter unloading duration might prevent the material from recovering fully because it has not been given enough time. In this case, the next cycle will add to the unrecovered strain and build the creep response, as shown in Figure 63.

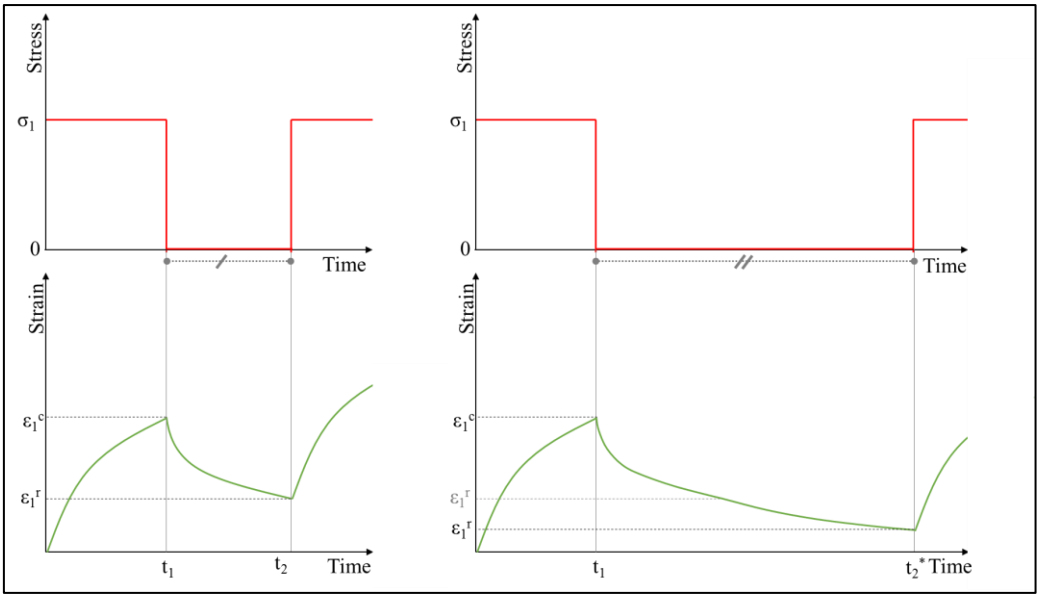

Figure 63: The resultant strain with different recovery durations

The number of cycles also contributes to the material performance in the repeated creep and recovery test. More cycles accumulate more damage and permanent deformation. Alternatively, in the case of high-stress level, the nonlinearity (or even damage) might happen at the first cycle.

In addition, applying repeated cycles of high (i.e. damaging) stress level to the material can show increasing strain amplitude with cycles due to damage generated in the material, as shown in Figure 64. However, applying a small (i.e. non-damaging) stress level keeps the strain amplitude the same because the material's property (modulus) is unchanged during the loading phases.

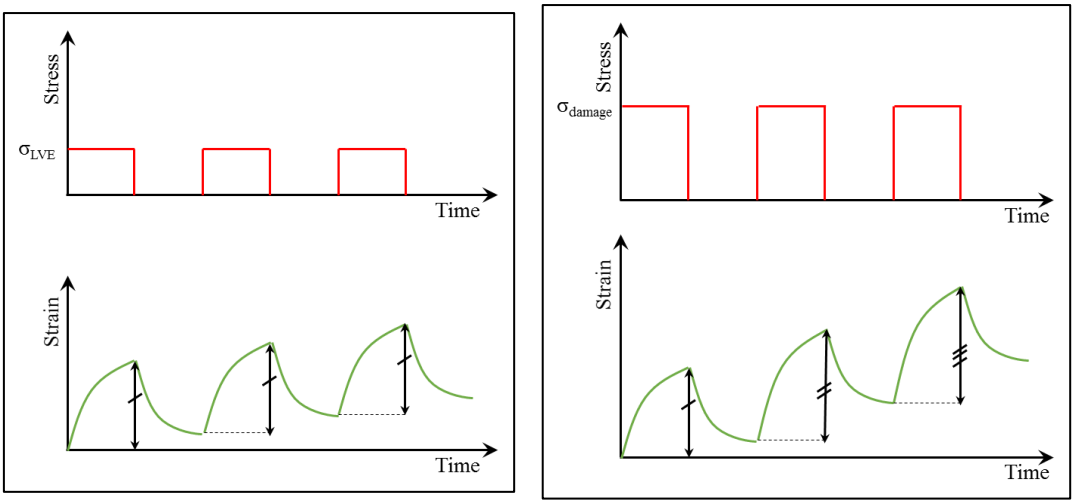

(a) (b)

Figure 64: Repeated creep and recovery cycles and the difference between (a) non-damaging stress level and (b) damaging stress level

6.2. Testing Materials and Apparatus

The Dynamic Shear Rheometer (DSR) was also used to conduct the repeated creep and recovery test. As mentioned earlier, the DSR was fitted with special components to test FAM samples using torsional force. Figure 65 shows the DSR with an attached sample ready for testing.

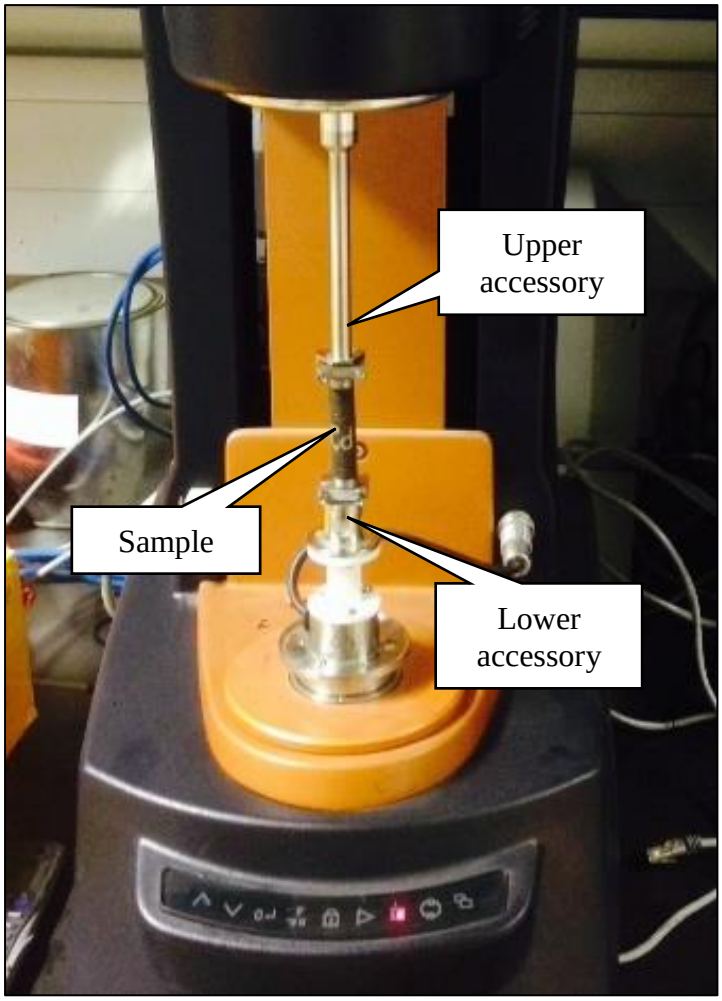

Figure 65: DSR with the attached accessory and solid sample

The testing matrix of this study included the four mix types mentioned earlier (Original mix, Sasobit mix, Advera mix and Rediset mix). All mixes were aged using the accelerated weathering machine with five ageing levels (0, 312, 600, 936 and 2455 ageing hours), as described in Chapter 4. Three replicates were tested from each mix at the five ageing levels, which means that a total of 60 samples were tested. Since the study is concerned with evaluating the crack propagation of the W-FAM samples, all tests were conducted at a controlled room temperature of 25^{o}C.

6.3. Repeated Creep and Recovery Test Protocol

The test protocol followed in this study was designed to investigate two sets of information. The first set is focused on the strain responses during a repeated creep and recovery test. The experimental data were involved in a new proposed analysis approach that investigated damage that evolved through multiple cycles. The second set focused on the internal stresses generated inside the material during the recovery phase of each cycle. The internal stress measurements were implemented based on the same concept presented originally in the strain transient dip test (Ahlquist and Nix, 1971; Teoh *et al.*, 1987), as discussed in Chapter 2. The test was designed to measure both sets of information using the same specimen in the same test.

Prior to applying the repeated creep and recovery test on the W-FAM samples, a one-cycle creep and recovery test was conducted. This test was performed to define the material properties for each mix type at all ageing levels. The one-cycle creep and recovery test was conducted at 75 kPa, which was selected based on the stress sweep test (described in Chapter 3) that ensures the material's behaviour stayed in the LVE region. The test was designed to apply one cycle that consists of 40 seconds of creep loading followed by 85 seconds of recovery (unloading). The duration of the first creep and recovery time was based on the study published by Luo (2012).

6.3.1. Repeated Creep and Recovery Cycles

As mentioned earlier, FAM samples mixed with WMA additives were included in this testing and analysis approach. The repeated creep and recovery test was conducted on the same sample. A minimum of 10 minutes' rest time was given between the one-cycle creep and recovery test mentioned above and the repeated creep and recovery test to ensure full recovery of any remaining strains. The repeated creep and recovery

test was designed to conduct nine cycles of creep and recovery phases. The creep load applied was 400 kPa to guarantee that the material would be introduced to damage. Multiple cycles were included in the test protocol in order to study its effect on the material damage and recovery ability. The test was designed to have constant loading periods (40 seconds). However, the recovery phase duration for each cycle was specified based on an incremental basis. Incremental recovery duration was employed to evaluate the effect of recovery time on the material behaviour. The recovery phase duration was defined by following an exponential trend. The recovery phase of the first cycle was set to 85 seconds to provide enough time to include five step-loadings (related to internal stress measurements, which will be discussed later in this chapter), while it was decided that the duration of the recovery phase in the last testing cycle would be around 3.5 times the first cycle recovery duration. This consideration resulted in using a 300-second duration for the recovery phase of the ninth cycle.

The 85 seconds for the first cycle and 300 seconds for the ninth cycle were used to find the best exponential fit, and the result is shown in equation (35).

$$T_i(sec) = 85e^{0.1579(i-1)} \quad \textbf{(35)}$$

where 'T_i' is the duration of cycle 'i' (i.e. 1 and 9). Then the duration of the in-between cycles (2, 3, 4, ... and 8) was calculated using equation (35). The results were then rounded whilst ensuring that the fitting goodness of the rounded durations should stay high (not less than 99%). The loading and rest durations in this test are summarised in Table 12.

Table 12: Creep and recovery durations for all cycles in the repeated creep and recovery test

Cycle No.	Phase	Duration (sec)
1	Creep	40
	Recovery	85
2	Creep	40
	Recovery	100
3	Creep	40
	Recovery	120
4	Creep	40
	Recovery	135
5	Creep	40
	Recovery	160
6	Creep	40
	Recovery	190
7	Creep	40
	Recovery	220
8	Creep	40
	Recovery	255
9	Creep	40
	Recovery	300

6.3.2. Internal Stresses Concept and Implementation

In 1971, Ahlquist and Nix presented a research work that featured the strain transient dip test. The test applied stress steps (step-loadings) during the recovery phase in order to find a specific stress that overcame the decreasing trend of recovery strain and forced it to remain constant (not increasing or decreasing). The applied stress steps allow the strain responses to be measured during the recovery phase and the rate of change to be calculated. The rate of change for these strain responses is used to find the stress (i.e. internal stress) that makes the rate of strain response equal to zero. The internal stresses in the presented study express the stresses that were generated inside the material to drive it to recover the strain after removing the load. It was called

'internal stress' to differentiate it from the external stress which is equal to zero during the recovery phase.

In this study, the internal stresses concept was used in the proposed testing protocol in order to evaluate the ability of the material to recover the creep load. Small step-loadings were added to each cycle at a decreasing rate to capture the effect of the loading repetitions on the internal stresses' responses. The unloading (recovery) phase during each cycle included five step-loadings at different timing and each step-loading consisted of three sub-steps, as shown in Figure 66.

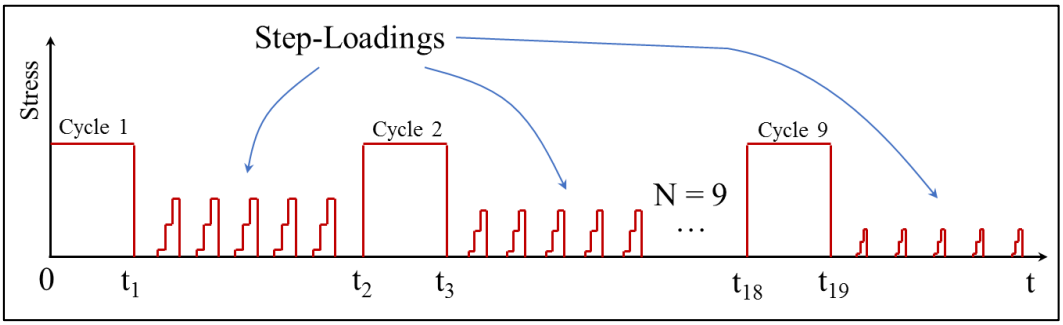

Figure 66: Repeated creep and recovery test protocol with the inclusion of step-loadings in the recovery phase

Each recovery phase included five step-loadings. The first step in the first cycle equals 1% of the creep load, the second step equals 20% of the creep load and the third step equals 50% of the creep load, as shown in Figure 67.

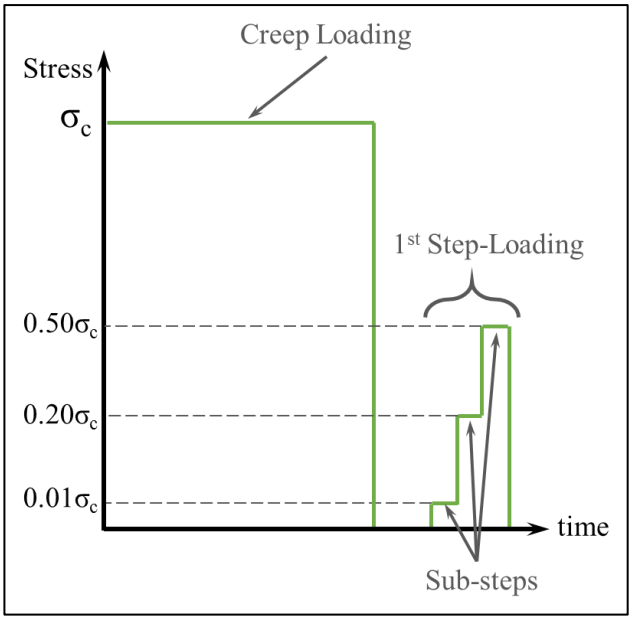

Figure 67: Illustration of the creep stress and the first step-loading stress amplitudes

All five step-loadings followed the same percentages. However, by moving to the second cycle, the first step reduced by 0.1% to be 0.9% of the creep load, the second step reduced by 2% to be 18% of the creep load, the third step reduced by 5% to be 45% of the creep load and so on. The full duration sets are shown in Appendix A.

At the first cycle, the creep phase was designed to last for 40 seconds, while the recovery lasted for 85 seconds. Each step-loading inside the recovery phase was designed to take 2 seconds, as shown in Appendix A. Rest (unloading) duration was assigned to be 1 second after the main creep loading, 4 seconds after the first step-loading, 6 seconds after the second step-loading, 10 seconds after the third step-loading, 14 seconds after the fourth step-loading, and 20 seconds after the fifth step-loading and before the start of the second cycle. The purpose of increasing the rest durations is to give the material sufficient time to follow the undisturbed recovery trend. This practice helped in making the analysis usable for both analysis sets (internal stresses and creep-recovery), since the material becomes weaker with more loading cycles and needs more time to follow the normal recovery trend.

6.4. Analysis Methods and Testing Results

The repeated creep and recovery test results were included in two types of analysis. The first one was to analyse the creep and recovery strain responses using a new proposed approach. The second analysis was to determine the internal stresses that are related to the recovery ability of the material.

6.4.1. Creep and Recovery Analysis Approach

This research proposes a new analysis approach to characterise the damage and recovery behaviour using the repeated creep and recovery test results. The analysis approach is presented in the following sub-sections.

6.4.1.1. Defining the Material Properties from the One-Cycle Creep and Recovery Test

The first step of the analysis approach is to obtain the viscoelastic properties of the W-FAM samples using the results from the low-stress one-cycle creep and recovery test. The viscoelastic model presented in equation (36) was used to represent the material behaviour (Schapery, 1969).

$$\varepsilon = g_0 D_0 \sigma + g_1 \int_0^t \Delta D(\Psi - \Psi^t) \frac{d g_2 \sigma}{d\tau} d\tau \qquad \textbf{(36)}$$

where $\Delta D(\Psi - \Psi^t)$ represents the transient response, while g_0, g_1 and g_2 are the nonlinear parameters discussed earlier in Chapter 3. The first part of equation (36) is responsible for the instantaneous strain at the beginning of the creep and recovery phases, and it is disregarded in this study because the elastic response is not obvious at an intermediate temperature. On the other hand, since the stress is constant during the test, equation (36) can be derived as shown in equation (37) where D(t) can be represented by the Prony Series Model.

$$\varepsilon = g_1 g_2 \sigma \, D(t) \tag{37}$$

As explained in section 3.2, this model was used to separate the viscoelastic strain from the total strain. The nonlinear parameters (g_1 and g_2) were assumed to be unity because the test was performed using one cycle only and at a low-stress level (75 kPa). The Prony Series coefficients were obtained by fitting the recoverable strain ($\Delta\varepsilon(t)$) of the one-cycle creep and recovery test, as shown in Figure 68.

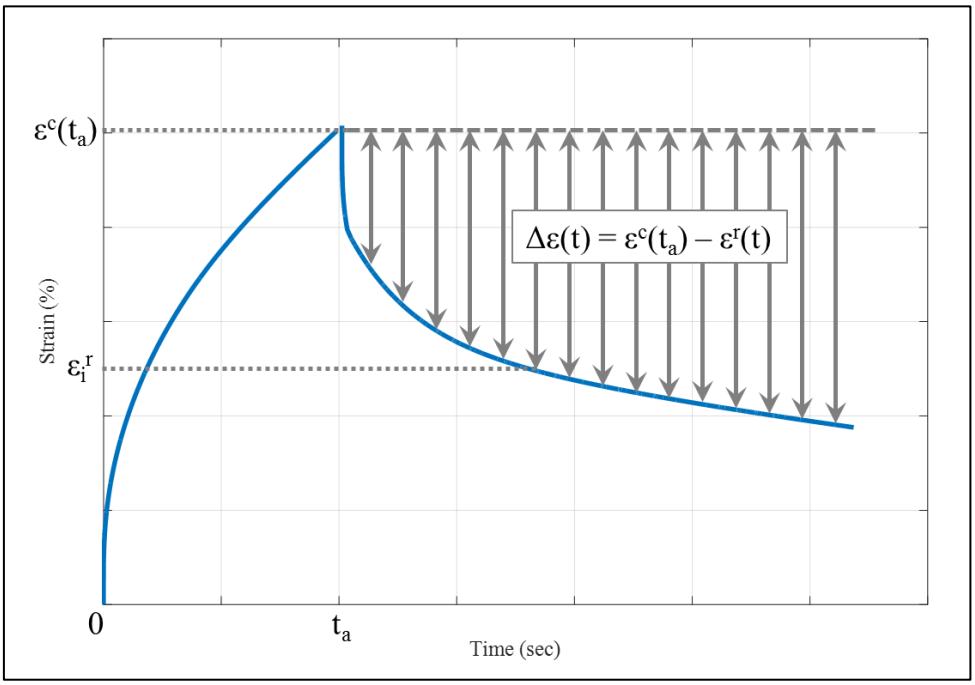

Figure 68: Calculating the recoverable strain (Δε) from the low-stress/one-cycle creep and recovery test

The recoverable strain ($\Delta\varepsilon(t)$) describes the pure viscoelastic behaviour of the material since it represents the recovery response of the material tested by a one-cycle test at a low-stress level and no damage was induced in the material. The material's properties can be represented using a Prony series model that describes its behaviour, as shown in equation (38).

$$D(t) = \sum_{n=1}^{N} D_n(1 - e^{-t\lambda_n}) \quad \textbf{(38)}$$

The recoverable strain ($\Delta\varepsilon(t)$) modelled in equation (39) was used to obtain 'D_n' and 'λ_n' by minimising the error between the experimental data and the model. The time, 't_a', is the duration of the creep phase. The creep and recovery strain models are designated with 'ε^c' and 'ε^r', respectively, and shown in equations (40) and (41). More details about the decoupling process can be found in Masad *et al.* (2009).

$$\Delta\varepsilon = \varepsilon^c(t_a) - \varepsilon_i^r(t) \quad \textbf{(39)}$$

$$\varepsilon^c(t_a) = \sigma_0 \sum_{n=1}^{N} D_n(1 - e^{(\lambda_n t_a)}) \quad \textbf{(40)}$$

$$\varepsilon_i^r(t) = \sigma_0 \sum_{n=1}^{N} D_n(1 - e^{(\lambda_n t_i)}) - \sigma_0 \sum_{n=1}^{N} D_n(1 - e^{(\lambda_n (t_i - t_a))}) \quad \textbf{(41)}$$

σ_0 is the applied creep stress, which is 75 kPa as per the described test.

An optimisation code was developed using MATLAB (2015a) to determine the best representation of Prony Series parameters 'D_n' and 'λ_n'. After several trials, a certain number of Prony Series set (N) was identified to be adequate to provide an accurate simulation of the material behaviour. The number of Prony Series set, 'N', is a key factor in achieving a better fit. The optimisation was developed based on fixing the retardation time (λ_n) values to cover most of the cycle time. This practice made the optimisation more accurate and faster to compute the 'D_n' values. All the Prony Series coefficients obtained in this study are listed in Appendix B.

The Prony Series obtained by this step represents the material behaviour without any damage. These Prony Series coefficients will be used in the next sections in order to always define the undamaged (i.e. pure) material behaviour.

6.4.1.1. Preparation of the Experimental Data

In this step, the experimental data of the repeated creep and recovery test were prepared in order to be useful for creep and recovery damage analysis without the inclusion of the step-loadings fluctuation.

Due to the inclusion of step-loadings during the recovery phase in the repeated creep and recovery test, the strain response exhibited fluctuation. The fluctuation occurs during the recovery phase at the step-loadings and then the strain values return to this original trend. The trend of the recovery phase with and without the step-loadings was compared. The results showed that, due to the low level of applied step-loadings and the very small duration of those steps, the overall recovery trend with the step-loadings matches the trend without step-loadings.

The preparation process of the experimental results obtained from the repeated creep and recovery test starts by selecting specific points in the recovery phase. These points were used to reproduce the undisturbed trend of that phase in order to be fitted with the best curve. Seven points were selected as the last point after the recovery of each step-loading. These points are the critical points where the shape of the curve can be represented as shown in Figure 69.

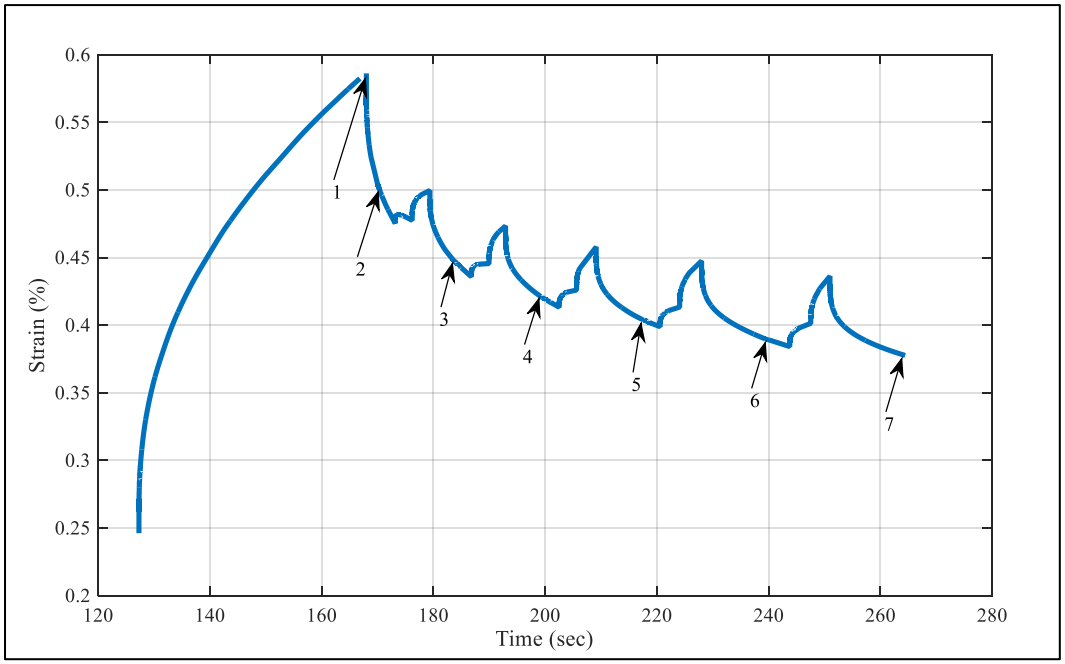

Figure 69: Selected critical points in the original experimental data to be used for generating the recovery trend

Due to the sharp drop at the beginning of the recovery phase, points from 2 to 7 are used to generate the best curve and then the curve was attached to the experimental data between points 1 and 2 to complete the full recovery response. The best fit was found to follow equation (42) by optimising the coefficients 'a', 'b', 'c' and 'd' to simulate the recovery strain ($\varepsilon_r(t)$).

$$\varepsilon_r(t) = ae^{-bt} + ce^{-dt} \quad \textbf{(42)}$$

However, with more cycles, the fitting process became more challenging and did not result in an acceptable goodness. In order to address this issue, the normalisation method was used with the experimental data, which made the fitting of all cycles much easier and more accurate. This was achieved by normalising the time domain of the fitted curve. For each cycle, the mean and standard deviation were calculated for the original time values during the recovery phase, and then equation (43) was used to reproduce normalised time (t_i^{nor}) values where 'i' represents each time value.

$$t_i^{nor} = \frac{t_i^{ori} - mean}{Stdv} \quad \textbf{(43)}$$

By using equation (43), the fitting of the experimental data became more accurate and reproduced the recovery curve without the fluctuation of the step-loadings. Figure 70 shows typical results for the recovery phase after experimental data were reproduced. The reproduced data are used in the coming sections to analyse the repeated creep and recovery test results of the W-FAM samples.

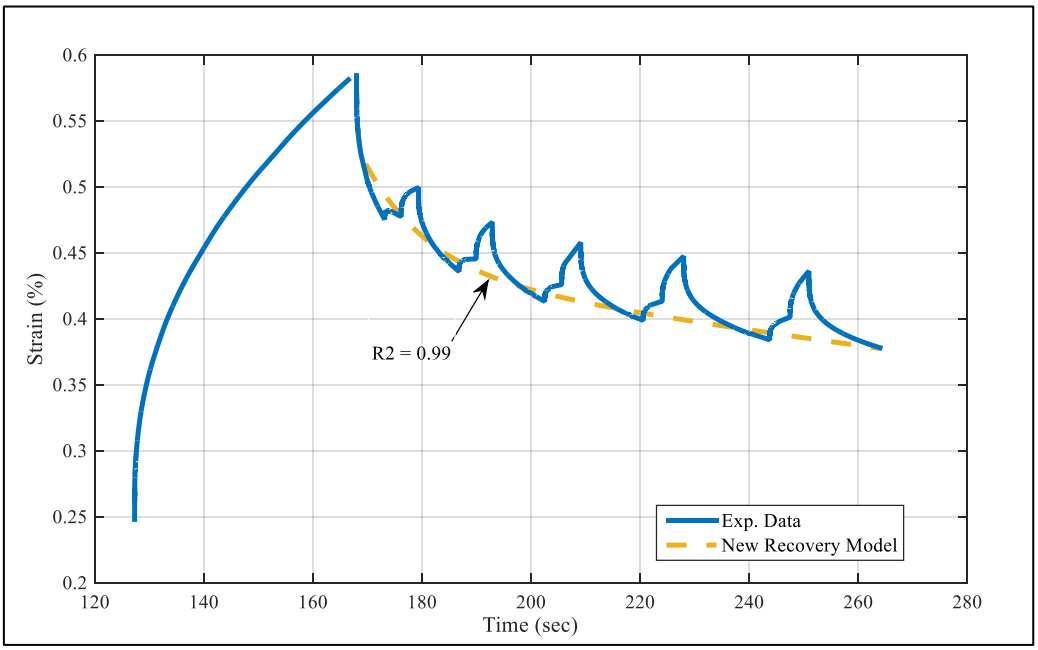

Figure 70: Fitted recovery strain with the model after the normalisation method was applied

The whole reproduced recovery strain for all cycles was used for the creep and recovery damage analysis presented in the next step. It is considered (and titled) as the experimental data.

6.4.1.2. Linear Viscoelastic Response

After preparing the experimental data to be used with the repeated creep and recovery analysis approach, the Prony Series coefficients obtained from the one-cycle creep and recovery test were used to calculate the viscoelastic (VE) strain from the repeated

creep and recovery test. This step was meant to produce the undamaged (i.e. pure) viscoelastic response for the repeated creep and recovery test results.

The superposition principle – as shown in equations (44), (45), (46) and (47) – was implemented to calculate the VE strain with a stress level (σ_0) equal to 400 kPa. The equations below show the creep ($\varepsilon_c^{VE}(t)$) and recovery ($\varepsilon_r^{VE}(t)$) strains of cycles 1 and 2 only.

$$\varepsilon_{c,1}^{VE}(t) = \sigma_0 D(t) \quad \textbf{(44)}$$

$$\varepsilon_{r,1}^{VE}(t) = \sigma_0 D(t) - \sigma_0 D(t - t_a) \quad \textbf{(45)}$$

$$\varepsilon_{c,2}^{VE}(t) = \sigma_0 D(t) - \sigma_0 D(t - t_a) + \sigma_0 D(t - t_b) \quad \textbf{(46)}$$

$$\varepsilon_{r,2}^{VE}(t) = \sigma_0 D(t) - \sigma_0 D(t - t_a) + \sigma_0 D(t - t_b) - \sigma_0 D(t - t_c) \quad \textbf{(47)}$$

Theoretically, the viscoelastic (VE) strain calculated using the (pure) Prony Series represents the material behaviour without viscoplastic deformation and/or damage (cracking). That is the reason behind calling it 'Pure VE Strain (ε_{pure}^{VE})'. Figure 71 shows typical results for the experimental strain and the pure viscoelastic (VE) strain of the material.

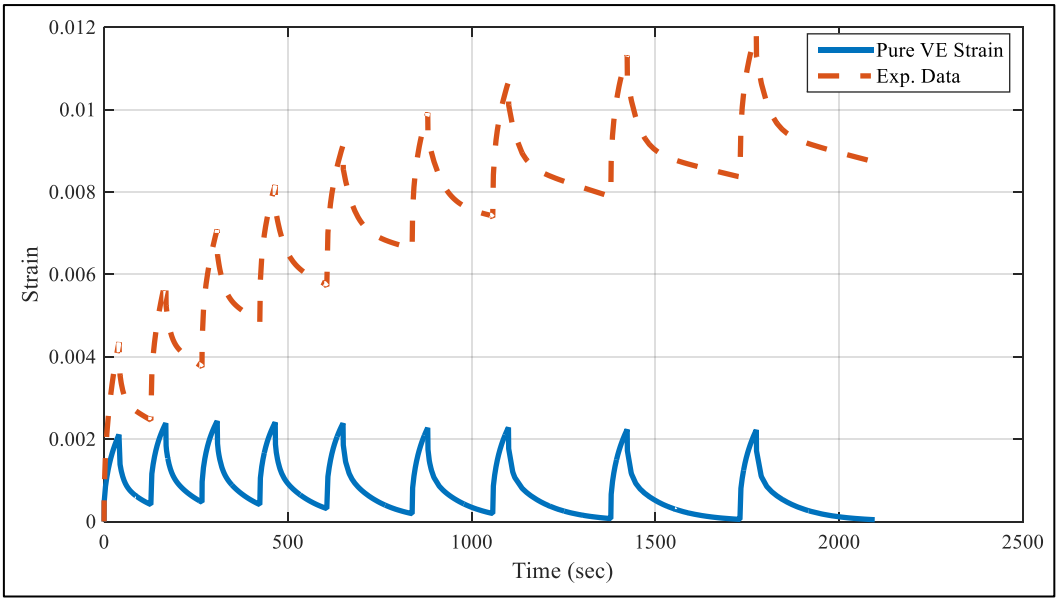

Figure 71: Typical results for the experimental and pure viscoelastic strain from the repeated creep and recovery test

The calculated pure VE strain shown in Figure 71 shows the strain with no damage for all cycles. The Prony Series used in calculating the VE strain for all cycles of the repeated creep and recovery test does not include any damage and represents the pure (i.e. undamaged) behaviour of the material.

6.4.1.3. The True Viscoelastic Response

The method proposed in this section considers generating the viscoelastic response for each cycle of the repeated creep and recovery test separately.

As mentioned earlier, the resultant creep strain amplitude in the damaging stress level test is increasing with cycles. Applying this stress induces damage in the material and deviates the strain response from the viscoelastic response. In fact, the increment of the creep strain amplitude during the creep phase indicates that the cycles incorporate damage with more cycles since the applied load is high enough (400 kPa) to induce damage.

The proposed method is based on treating each cycle of the repeated creep and recovery test as the first cycle. This was achieved by shifting the cycle's experimental data (strain and time) from their original position in the test to zero time and zero strain value, as shown in Figure 72. The shifting was conducted proportionally by subtracting each data point of the strain response from the first data point in each cycle. This was performed to ensure that the cycle's responses shifted without changing the actual trend of the creep and recovery strain responses.

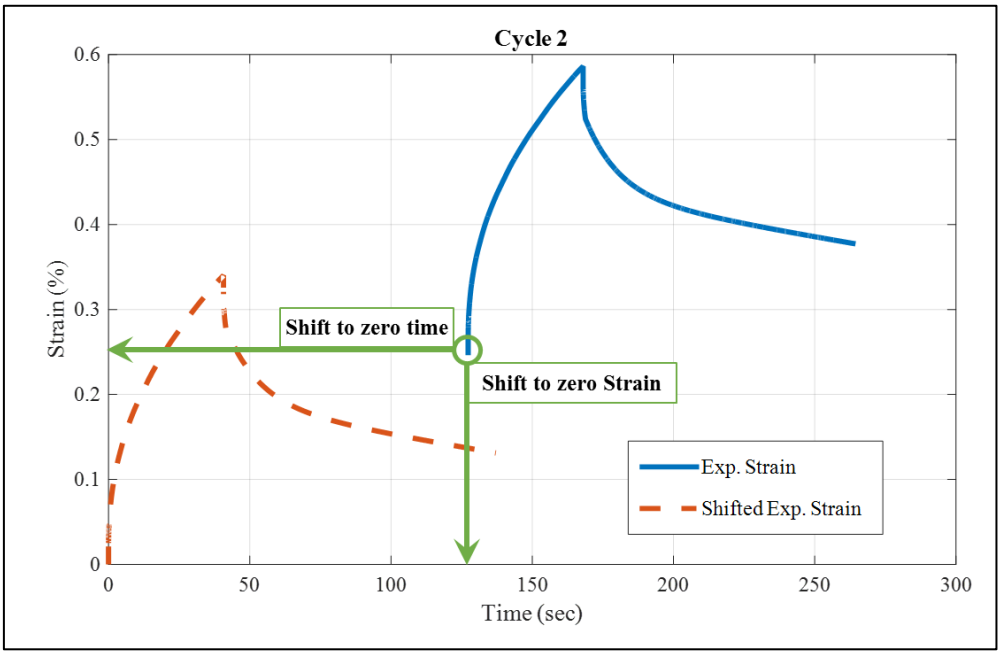

Figure 72: Shifting procedure for cycle 2 of the repeated creep and recovery test

The shifting kept the evolution of strain but with a shift down, and restarted the time but with the same duration. As mentioned earlier, the shifted second cycle – for instance – has a higher strain amplitude in the creep phase compared to the original first cycle due to damage that evolved in the material by loading cycles.

Shifting cycles helped in studying each cycle's behaviour and defining its VE response separately. As mentioned earlier, the second cycle's response contains damage since it is a cycle from a damaging test. Any VE strain that is extracted from this cycle would

include damage since it is not a pure VE strain. To calculate the VE strain of the shifted second cycle, the recoverable strain (Δε) was extracted from the recovery phase, as shown in Figure 73.

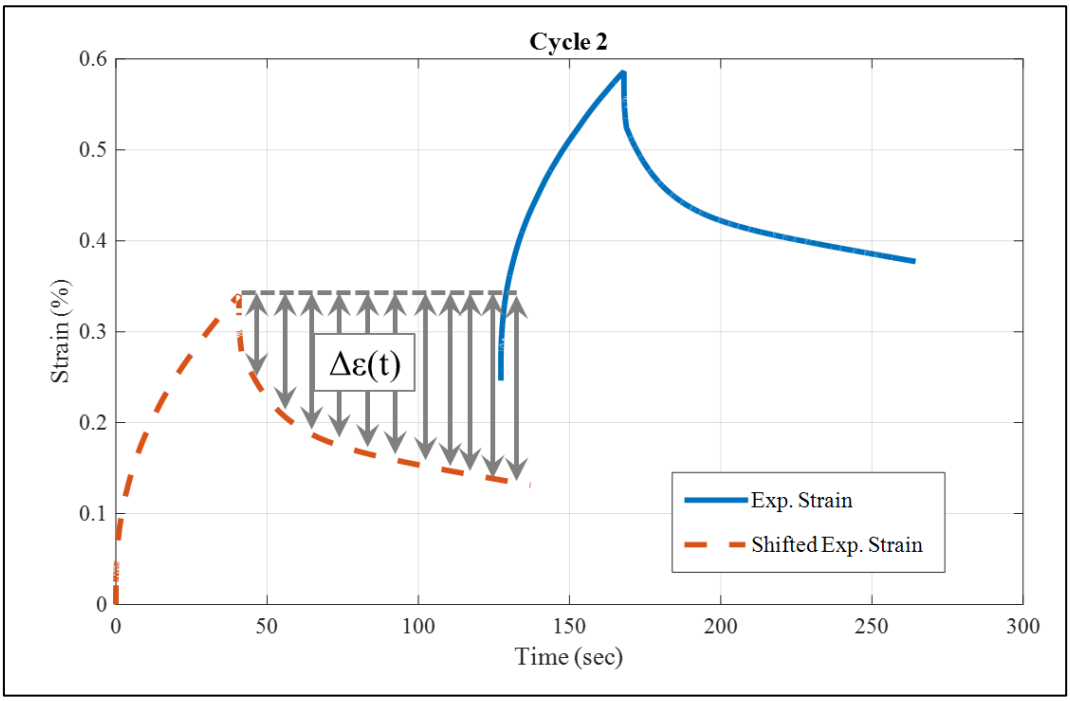

Figure 73: Recoverable strain extracted from the second cycle after shifting

Then, the extracted recoverable strain (Δε) was used to obtain a new set of Prony Series coefficients that represent the material behaviour. Since the Prony Series coefficients were obtained using the recoverable strain (Δε), it is guaranteed that the VE strain calculated for the shifted cycles does not include any viscoplastic deformation. All the viscoplastic deformation is included in the viscoplastic (VP) strain shown in Figure 74.

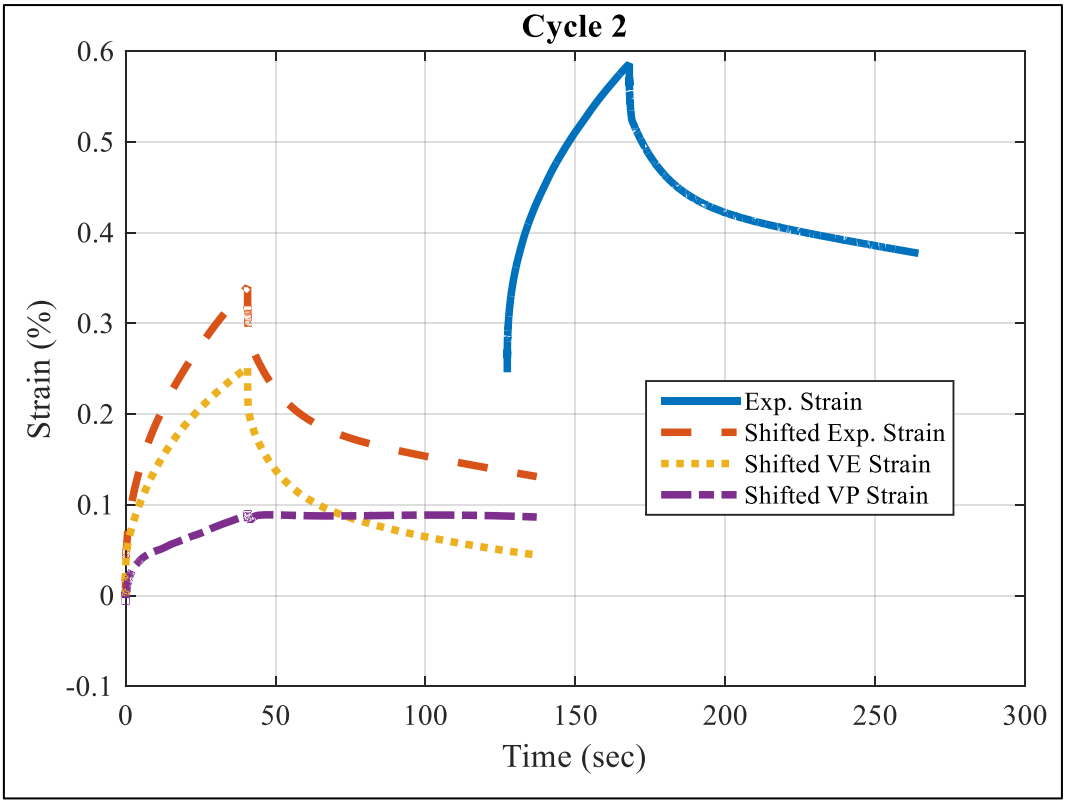

Figure 74: Obtaining the true VE and VP strains of shifted cycle 2 of the repeated creep and recovery test

In this case, the viscoelastic strain (VE) that is generated from the shifted cycles contains only damage that developed inside the material due to repeated loading.

Consequently, the viscoelastic (VE) strain for cycle 2 was shifted back to its original location by adding the first point of the shifted VE strain to the pure VE strain (ε_{pure}^{VE}) calculated for the first cycle. The process was repeated for all other cycles from the third until the ninth cycle. The shifted VE strain of the next cycles were relocated by connecting the first data point of the shifted cycle to the first data point of the pure VE strain (ε_{pure}^{VE}), as shown in Figure 75. All shifted VE strains generated by this step were called 'True VE Strain (ε_{true}^{VE})'.

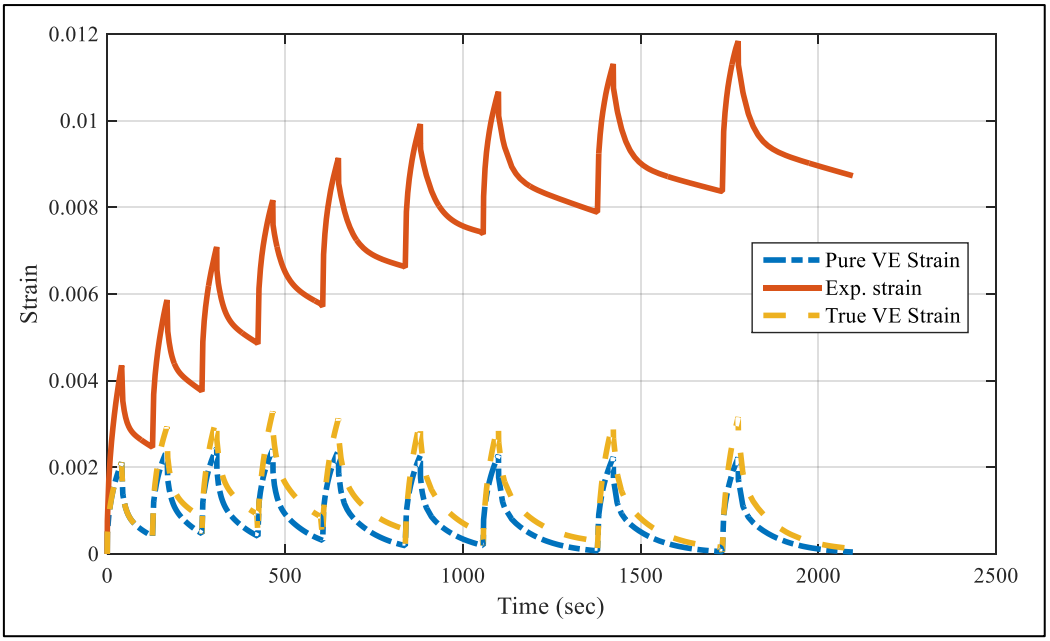

Figure 75: Pure and true VE strains for all cycles for the repeated creep and recovery test

The (ε_{true}^{VE}) indicates the viscoelastic strain calculated by the method of shifting the cycles. It was called 'true' because it is the viscoelastic strain that accounts for the cumulative strain from the damage, while (ε_{pure}^{VE}) is the VE strain that represents the undamaged strain obtained by using the Prony Series coefficients from the lowest stress level. The deviation between the pure VE strain and the true VE strain is due to damage, as shown in Figure 76. If the applied creep stress is a small and non-damaging stress, the pure and the true VE strains would match and no difference would appear between them.

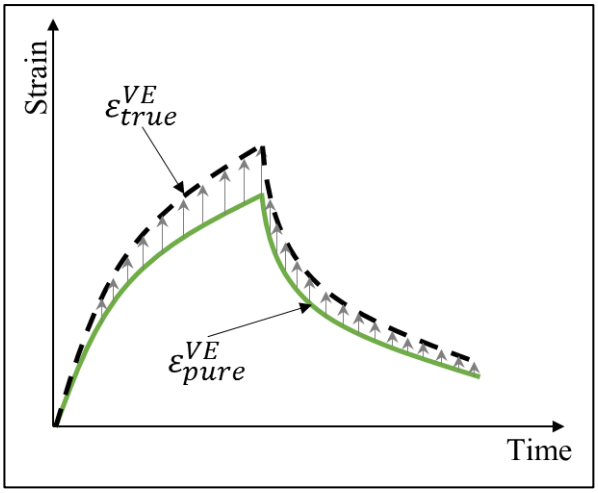

Figure 76: Sketch for the deviation between pure and true VE strains

To obtain a closer look at the meaning of the pure and true viscoelastic strains, a sketch was created, as shown in Figure 76, for the creep and recovery strains of both pure and true VE strains.

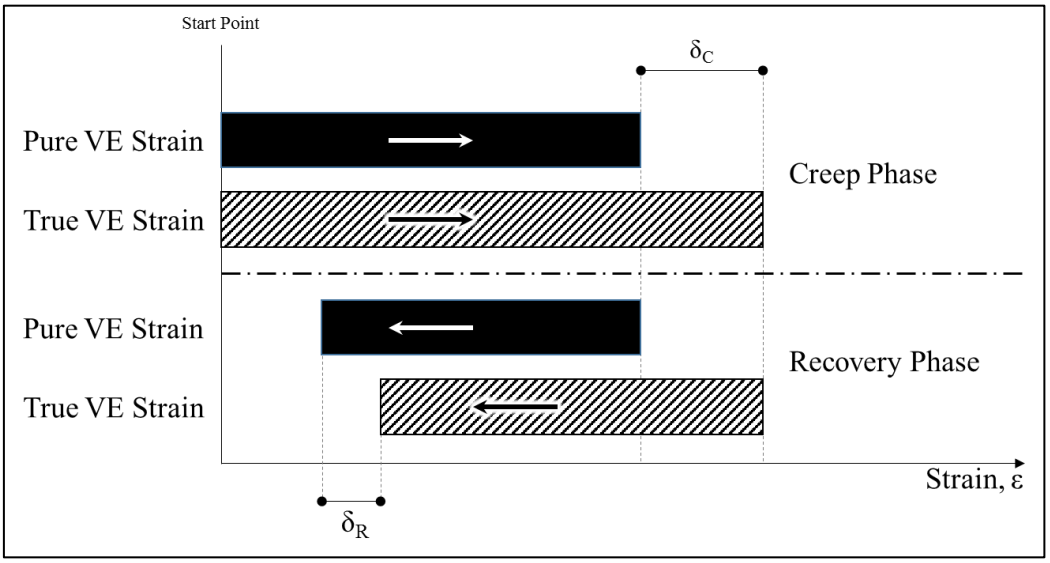

Figure 77: Sketch for the evolving strain during the creep phase and returning strain during the recovery phase for the pure and true VE strains

In Figure 77, the creep strain obtained by the true VE strain deviated from the pure VE strain. The incorporation of more strain indicates a deviation from the undamaged curve and the generation of damage. In the recovery phase, the pure and true VE strains start recovering from different points (where the creep strain stopped) and finish at

different points. The difference between the starting points was originally generated due to different creep strain ends. Hence, the difference generated between the pure and true VE strains during the creep phase was calculated by subtracting the area below the pure VE strain from the area below the true VE strain, as shown in Figure 78.

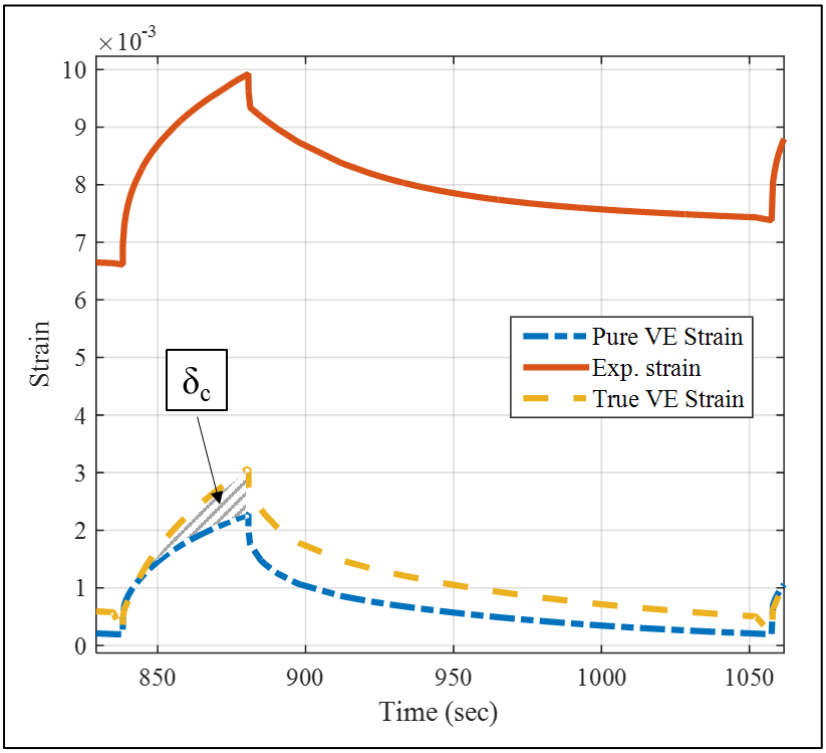

Figure 78: Creep damage area in cycle 6 of the repeated creep and recovery test

Figure 78 shows the experimental strain at cycle 6 obtained from the raw data and the pure viscoelastic strain (ε_{pure}^{VE}) and the true viscoelastic strain (ε_{true}^{VE}) obtained as described above.

The difference between the area under the true VE strain (ε_{true}^{VE}) curve and the pure VE strain (ε_{pure}^{VE}) curve during the creep phase represents the damage that evolved in the material due to the creep loading. The difference was calculated and divided by the area under the true VE strain (ε_{true}^{VE}) curve as shown in equation (48) to normalise the parameter for comparison purposes explained later.

$$\delta_C(\%) = \frac{Area\ Under\ (\varepsilon_{true}^{VE}) - Area\ Under\ (\varepsilon^{VE})}{Area\ Under\ (\varepsilon_{true}^{VE})} \times 100\% \quad \textbf{(48)}$$

The δ_C is called the 'Creep Damage' in this study and it represents the percentage of damage within the true VE strain due to creep loading.

It was found that studying the difference between the ε_{pure}^{VE} and ε_{true}^{VE} using the area under the curve is more representative than studying point-by-point. The area under the curve gave the results a complete overview of the behaviour of material with cycles rather than time, and enabled more comparison of different mixes and ageing levels.

Studying the recovery phase for each cycle of the repeated creep and recovery test was conducted by extracting the recoverable strain (Δε) of the pure and true VE strains, as shown in Figure 79.

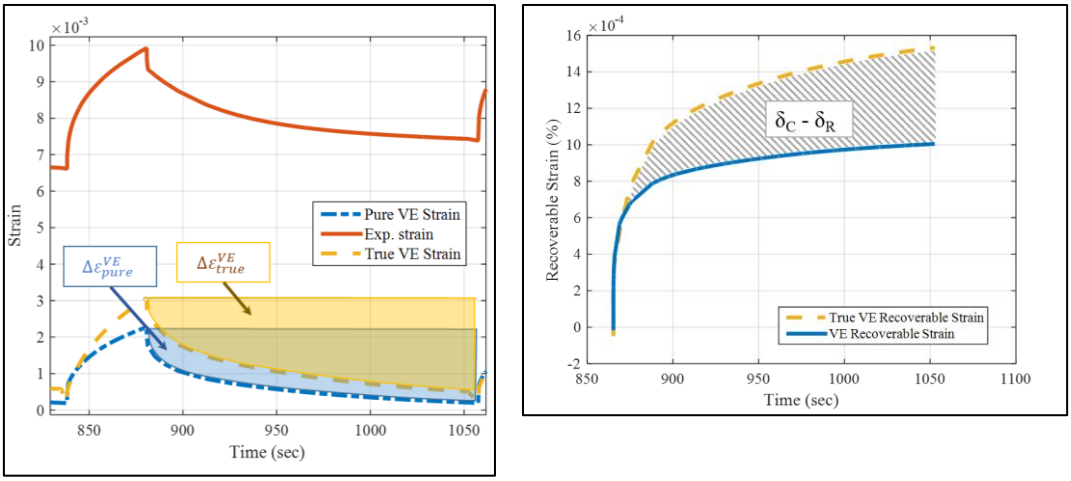

Figure 79: The area used to calculate the recoverable VE strain from the pure and true VE strains

As presented in Figure 79, the true recoverable strain ($\Delta\varepsilon_{true}^{VE}$) shows higher values than the pure VE strain ($\Delta\varepsilon_{pure}^{VE}$). This indicates that the true VE strain recovered more strain than the pure VE strain. This indicates that the material recovered some of the damage that evolved due to creep loading during the recovery phase. The difference

between the pure and true VE recoverable strains ($\Delta\varepsilon_{pure}^{VE}$ and $\Delta\varepsilon_{true}^{VE}$) is designated as the difference between Creep Damage (δ_C) and – as called – Recovery Damage (δ_R); it is calculated as an area under the curve, as shown in Figure 79, and used to calculate the Recovery Damage (δ_R), as shown in equation (49).

$$\delta_C(\%) - \delta_R(\%) = \frac{Area\ Under\ (\Delta\varepsilon_{true}^{VE}) - Area\ Under\ (\Delta\varepsilon^{VE})}{Area\ Under\ (\Delta\varepsilon_{true}^{VE})} \times 100\% \quad \textbf{(49)}$$

The parameter δ_R indicates the percentage of the damage that exists in the recovery phase of the cycle.

By calculating the creep damage (δ_C) from the creep phase, the recovery damage (δ_R) can be calculated by subtracting the area difference result of equation (49) from the creep damage result of equation (48). Figure 80 shows typically calculated results (with standard error as error bars) for the Creep Damage (δ_C) and Recovery Damage (δ_R) from unaged and aged Original mixtures tested with the repeated creep and recovery test protocol.

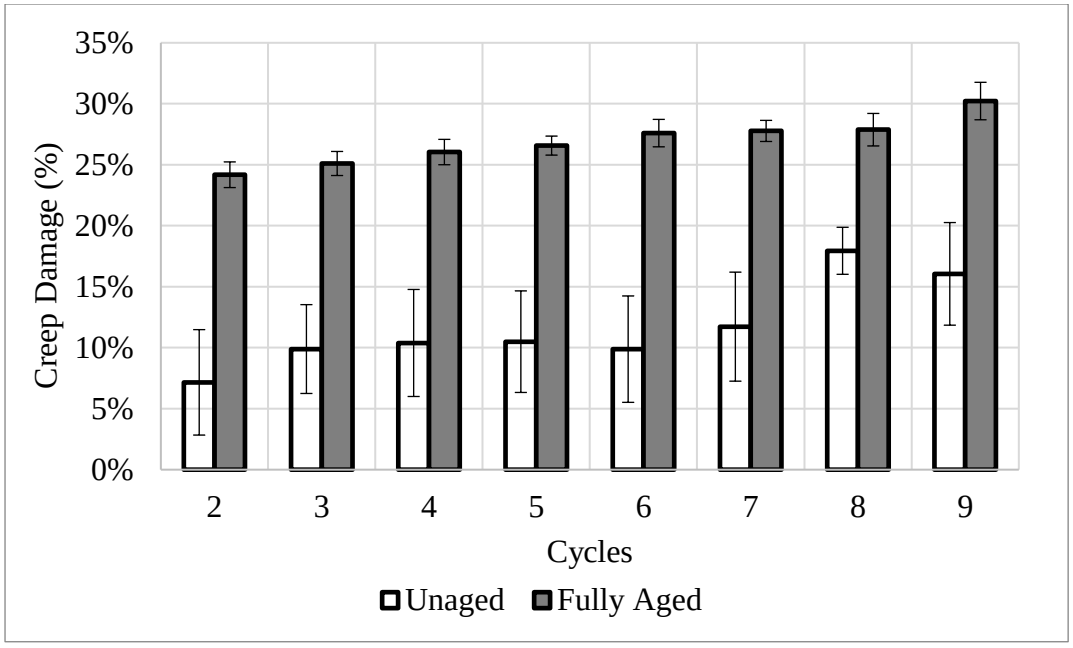

(a)

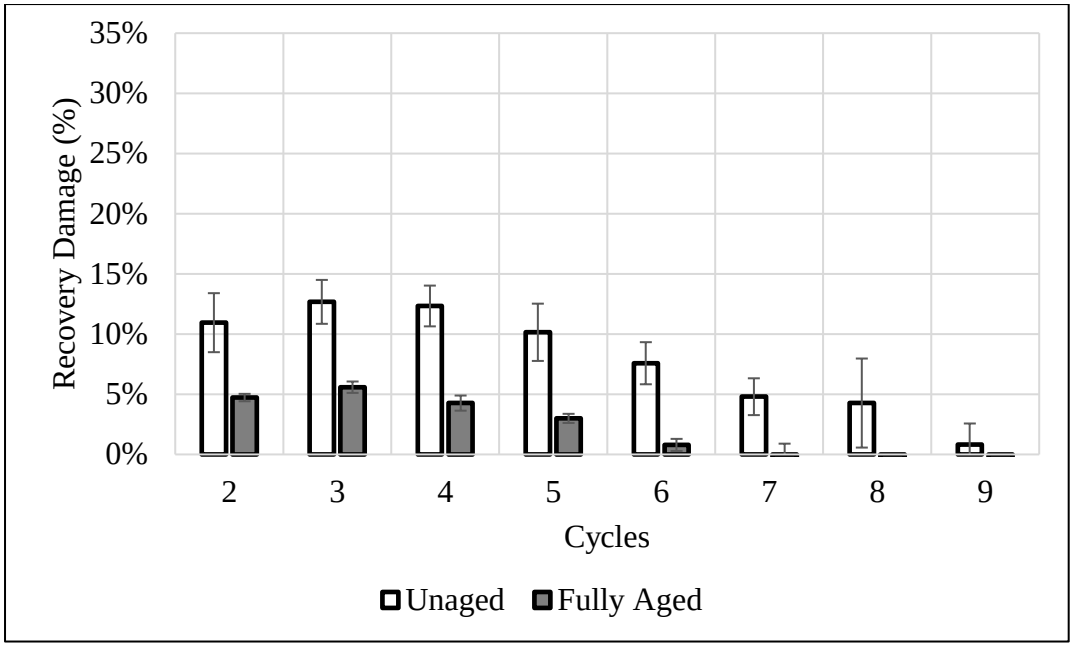

(b)

Figure 80: Typical (a) Creep Damage (δ_C) and (b) Recovery Damage (δ_R) results for the unaged and fully aged Original mix samples

It can be seen from Figure 80 that the creep damage is higher than the recovery damage. Both parameters (creep and recovery damage) became closer with more cycles until the end of the test, indicating that the damage generated during the creep phase was recovered during the recovery phase. The difference between the creep damage and the recovery damage – specifically at the beginning of the test – can be interpreted as the left-over damage that could not be recovered during the recovery phase.

6.4.2. Measurement of Internal Stresses

The repeated creep and recovery test presented in this chapter included applying step-loadings during the recovery phase of each cycle. Applying these step-loadings was intended to measure the internal stresses, as discussed earlier. The internal stresses' analysis required the strain measurements of each step-loading to be extracted with its corresponding time from the experimental data. Each step of the three step-loadings

was analysed separately with its corresponding time to calculate the rate of change (slope), as shown in Figure 81.

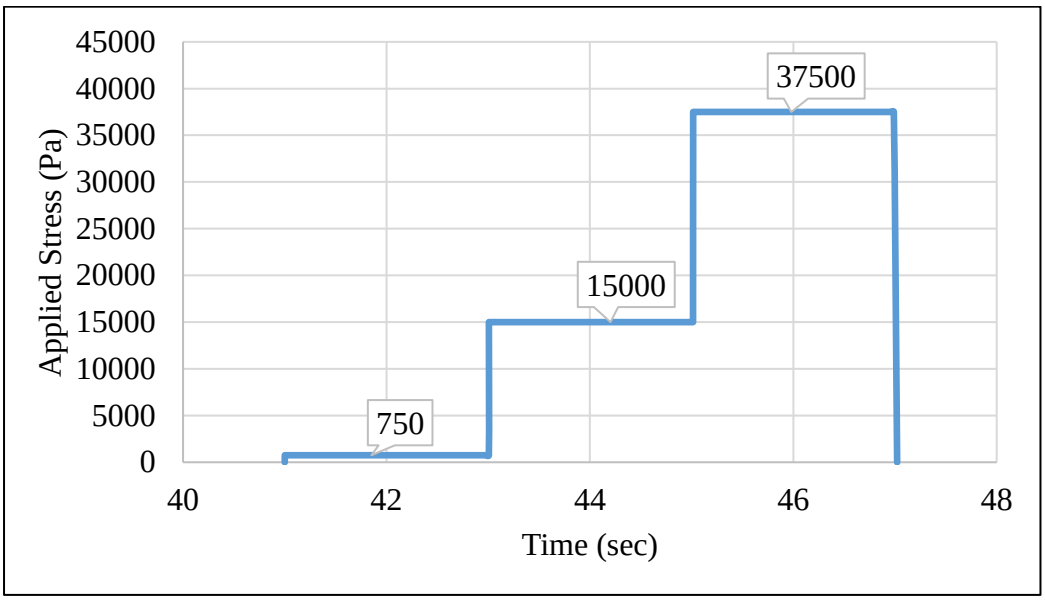

(a)

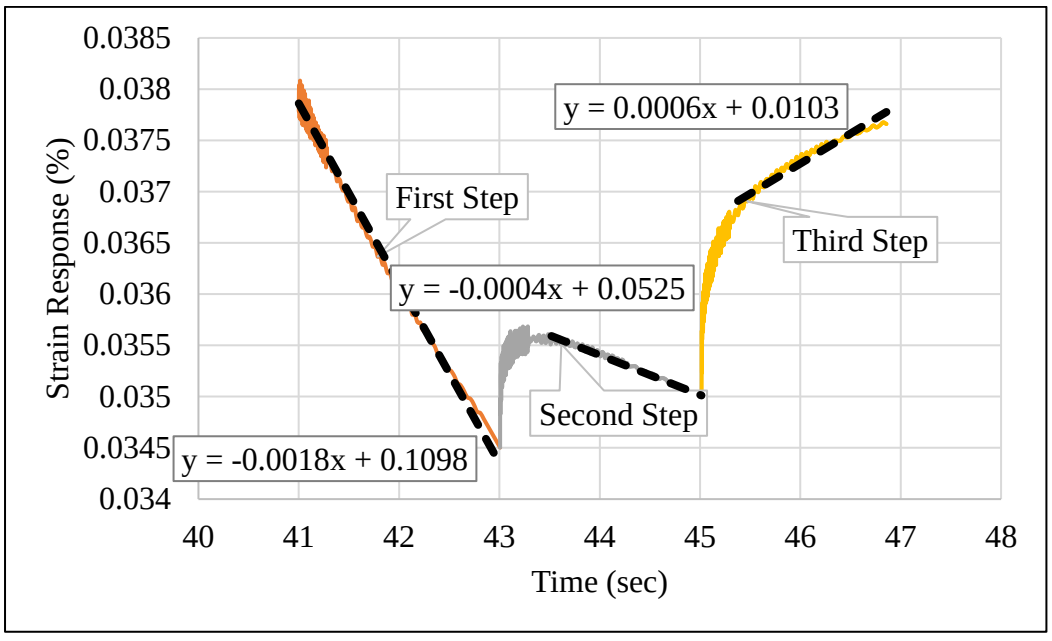

(b)

Figure 81: Example for (a) The applied steps inside a step-loading for the first cycle and (b) the resultant strain and their linear fitting

The strain responses (after excluding the initial machine fluctuation) were fitted with a linear trend to determine the strain slope of each step. As shown in Figure 81, for

instance, the slopes of the linear equation (which is the number associated with the 'x' variable) for the first and second steps are negative values. However, the slope turns into a positive value for the third step. The negative slope indicates that the strain response is decreasing with time during a specific step, which means that the step did not affect the material's recovery enough to reverse its response. However, the positive value of the slope indicates that the applied step affected the recovery response of the material and forced it to anticipate more creep strain during the recovery. The slope results of each step-loading are plotted against the corresponding stress applied and then fitted using a polynomial curve, as shown in Figure 82. The intercept of the polynomial curve with the stress axis is the stress that generates a zero strain rate and is considered as the internal stress of this step-loading at this specific cycle.

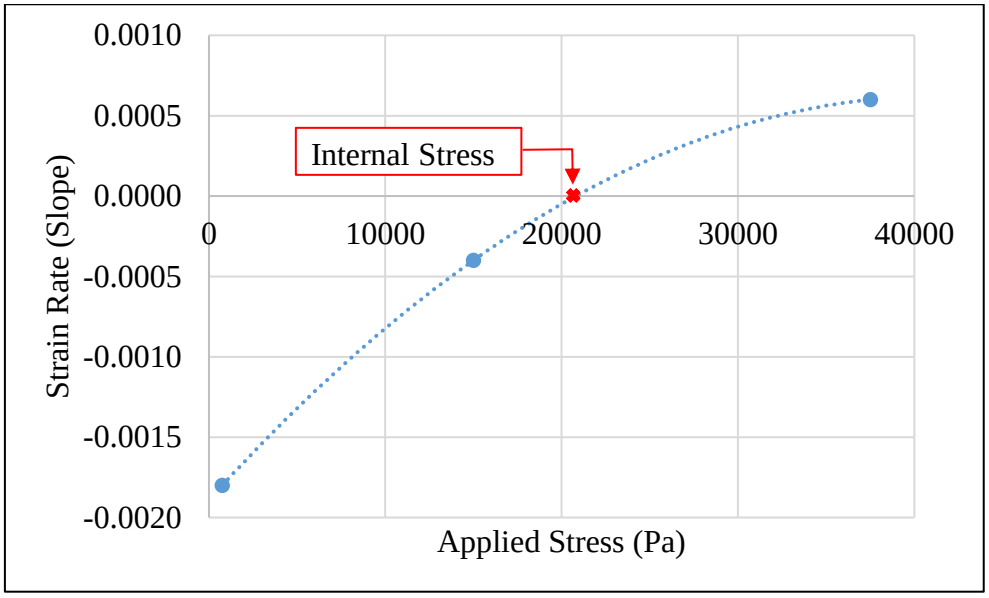

Figure 82: Example for fitting the strain rate with the associated stress to calculate the zero strain rate

The zero strain rate indicates that this stress is equal to (and opposite) the internal stresses inside the material that drive the recovery. The zero strain rate is calculated by obtaining the x-axis intercept of the polynomial equation.

This process is repeated for each step-loading in each cycle. Figure 83 shows typical internal stresses values at all cycles.

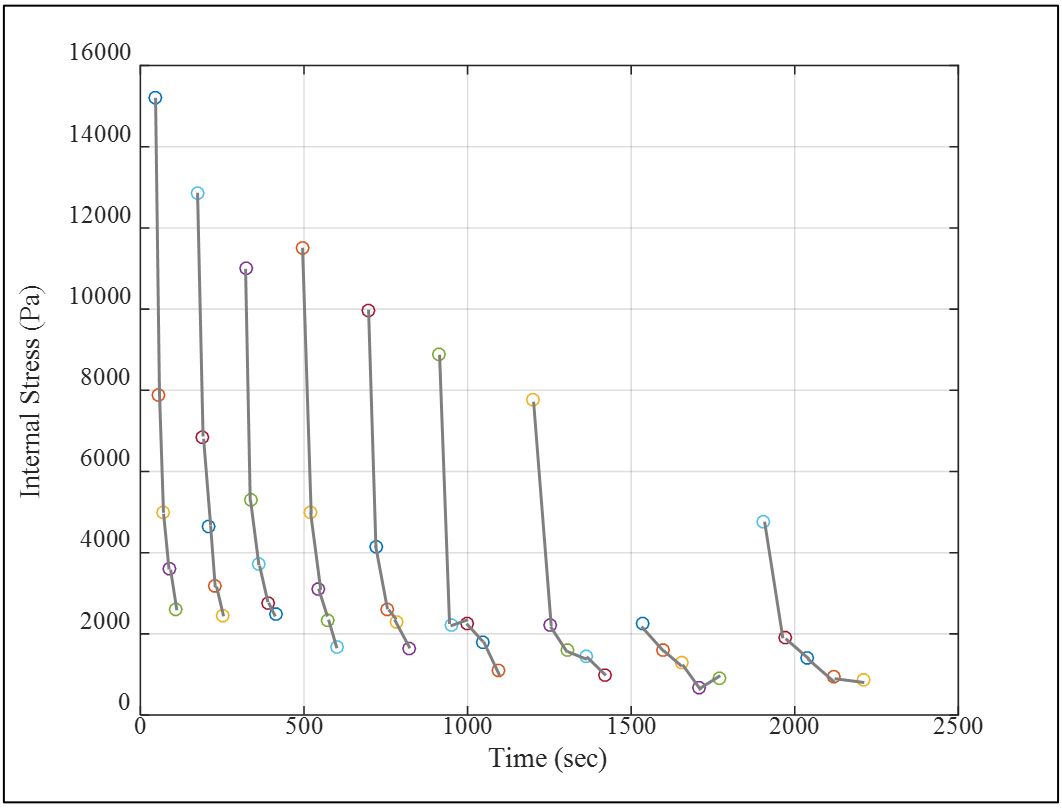

Figure 83: Example for internal stresses values measured from the repeated creep and recovery test for all cycles

It can be noticed that the internal stresses decrease with time (and cycles) during the recovery phase, since the material's ability to recover also decreases with time. Applying higher creep stress to the material generates higher internal stresses which are required to recover the higher strain.

The internal stresses' results were fitted for each cycle using equation (50).

$$\sigma_i(t) = ae^{bt} + ce^{ct} \quad \textbf{(50)}$$

where 'a', 'b', 'c' and 'd' are fitting parameters for the internal stress, 'σ_i', that changes with time, 't'. Then, the fitted internal stresses ($\varepsilon_r(t)$) with the recovery strain

were used to calculate the Recovery Modulus (R_M), as shown in Figure 84. The recovery strain ($\varepsilon_r(t)$) is simulated using equation (42) presented above.

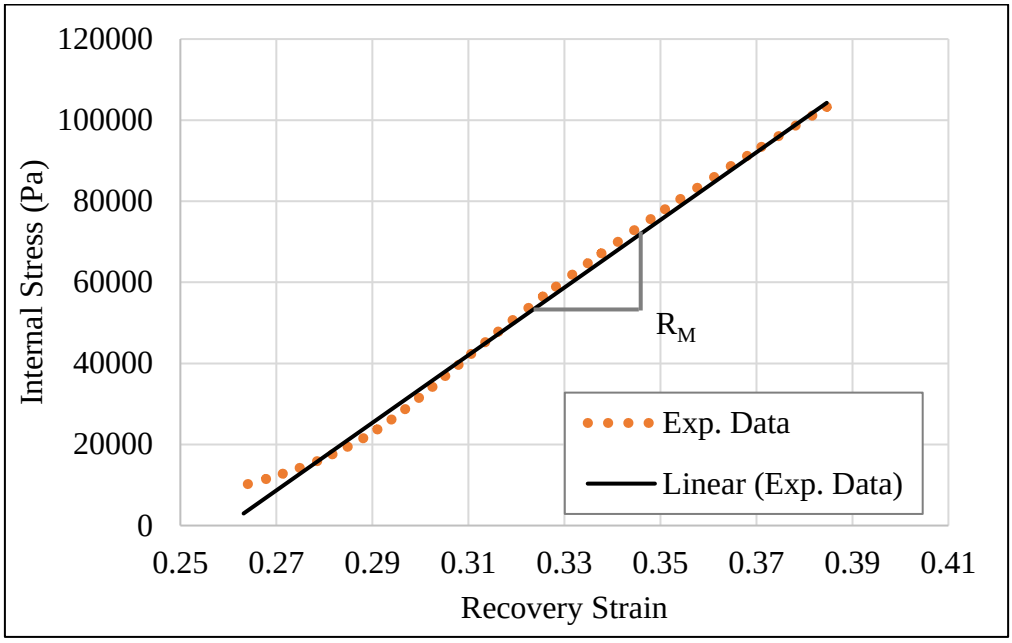

Figure 84: Recovery modulus calculated from internal stresses and recovery strain for the first cycle of the high-stress level test

The recovery modulus was calculated as the slope of the stress-strain curve, and it was noticed that the recovery modulus decreases with more cycles, as shown in Figure 85.

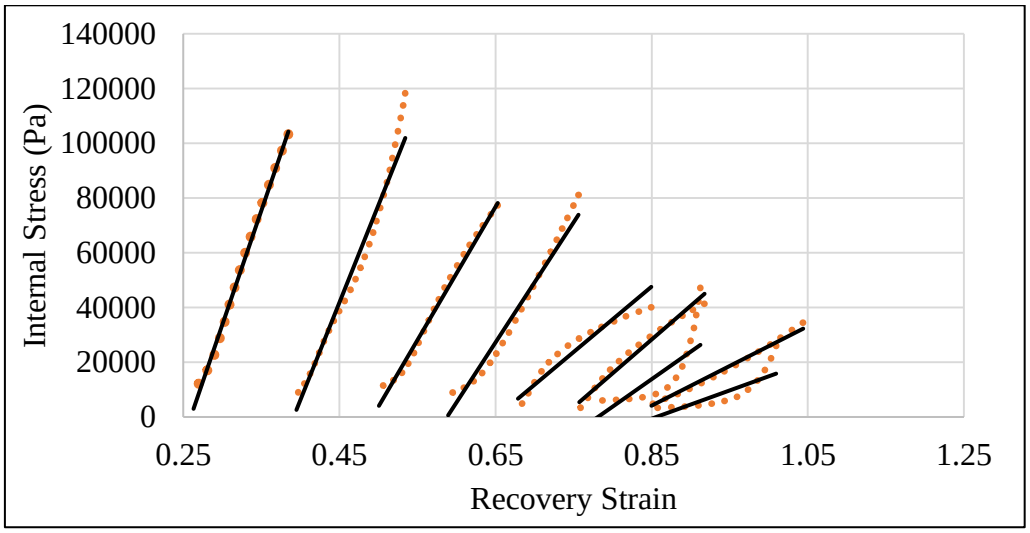

Figure 85: Internal stress vs. recovery strain for all cycles in the high-stress level test

It was expected to have a linear trend for the first few cycles of the test. However, with more cycles, the stress-strain curve started to become nonlinear. For this study, all cycles were simulated with a linear equation, and the recovery modulus was calculated based on that.

6.5. Results and Discussion

As described in the previous section, all W-FAM samples were tested following the repeated creep and recovery testing protocol proposed in this study. The results are presented based on the material type (Original mix, Sasobit mix, Advera mix and Rediset mix) and ageing levels (unaged, 312 hrs ageing, 600 hrs ageing, 936 hrs ageing and 2455 hrs ageing).

6.5.1. Creep and Recovery Damage Results

By following the analysis approach presented in the previous section, the creep and recovery damage parameters (δ_C and δ_R) for each mix were calculated and are shown in Figure 86. The results for 312 hours of aged samples were omitted from the results below since these samples showed high variability compared to the other aged samples.

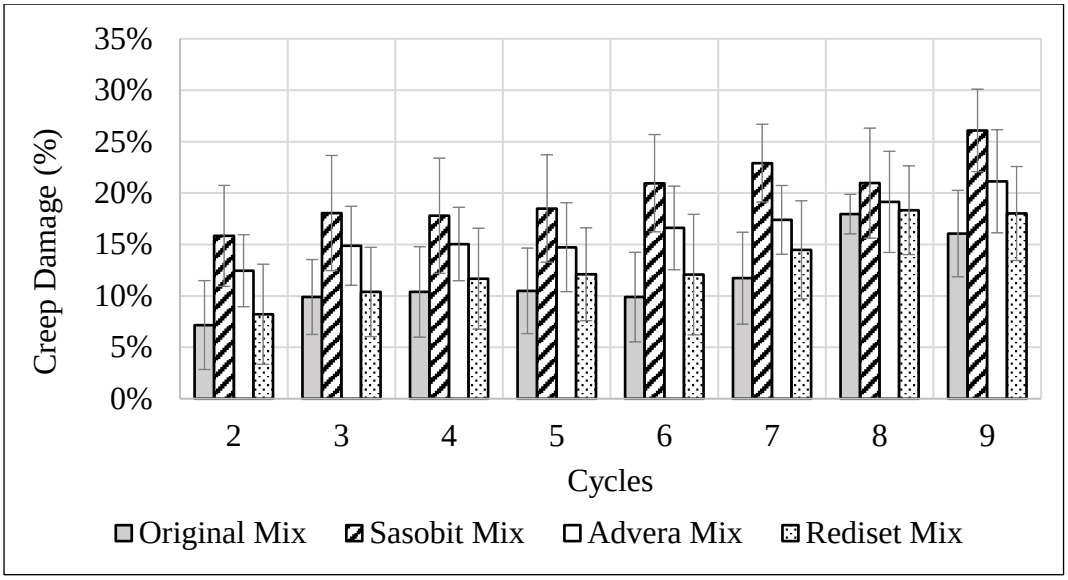

(a) Creep Damage (δ_C)

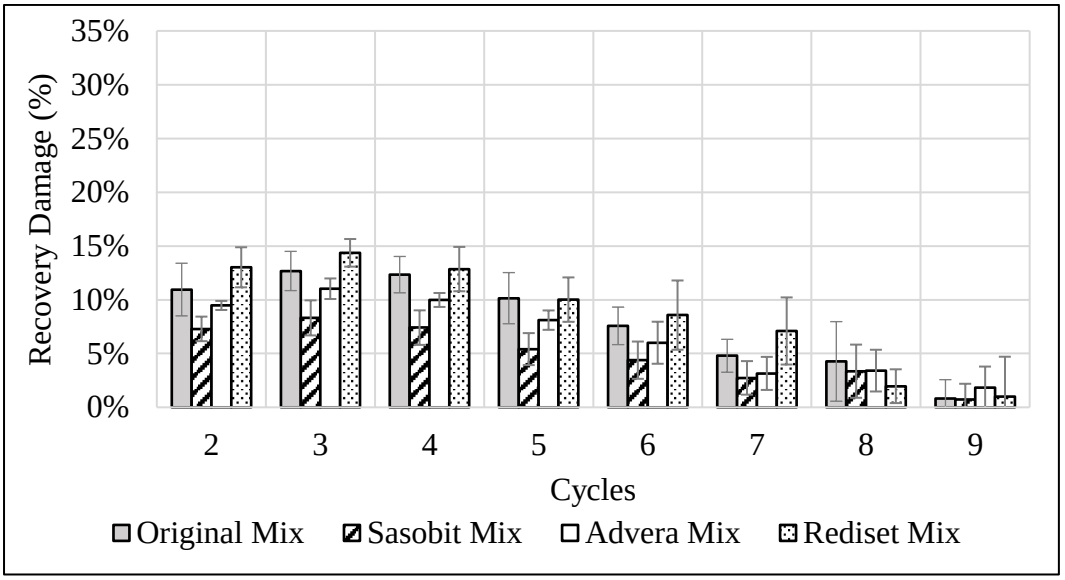

(b) Recovery Damage (δ_R)

Figure 86: (a) Creep and (b) Recovery damage for unaged Original, Sasobit, Advera and Rediset mixes tested with the repeated creep and recovery test

As shown in Figure 86(a), the creep damage values increase with an increase in number of cycles, which confirms that more damage is generated. From the figure, it can be noticed that the highest creep damage is generated in the Sasobit mix. This is followed by Advera, which showed higher creep damage than the Original and Rediset mixes. The increment in the creep damage showed very similar rate of change with

cycles. This is due to having a constant creep stress level and duration, while the effect of stress history was eliminated by the analysis approach.

The error bars shown in Figure 86 are standard error which is calculated by dividing the standard deviation over the square root of the sample size (3 replicates). It can be noticed that the variability in creep damage is higher than the recovery damage which could be related to the material variability, differences in air voids, and/or variation in measurement devices.

The trend of ageing was also captured in this study by testing all the intervals of ageing presented in the previous chapter, as shown in Figure 87. The ageing showed an increasing trend of evolved damage, which confirms the effect of ageing on the damage generated inside the material during creep loading.

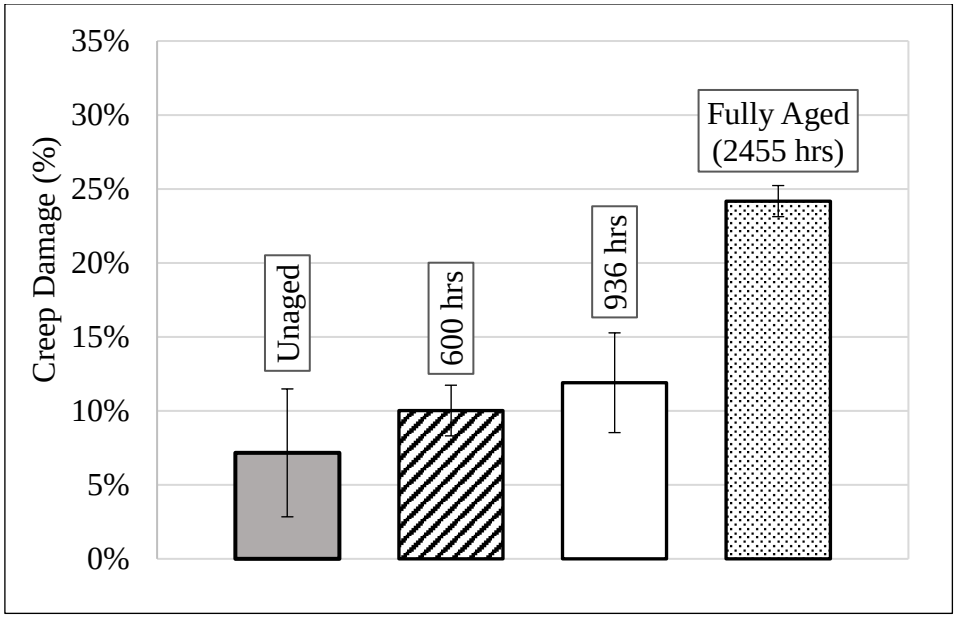

Figure 87: Change in the creep damage with ageing calculated from the second cycle of the Original mix (error bars represent standard error)

It can be noted from Figure 86(b) that the recovery damage results show lower values than the creep damage ones. These results represent the damage left over at the end of the recovery phase. As shown in the figure, the Original and Rediset mixes showed

the highest recovery damage among the mixes, while the Sasobit mix showed the lowest damage. It is also noticeable that the damage during the recovery is decreasing with cycles. This is due to the increase of the recovery duration with cycles, which allowed more recovery to happen.

By comparing the creep damage with the recovery damage, it can be observed that the change between these two parameters explains the ability of the material to recover damage that evolved from the creep phase during the recovery phase. The Sasobit mix has the biggest change (i.e. Reduced Damage) between creep damage and recovery damage, followed by Advera mix and then the Original and Rediset mixes. Figure 88 shows the comparison between the reduced damage of each mix type at the ninth cycle (end of the test) only.

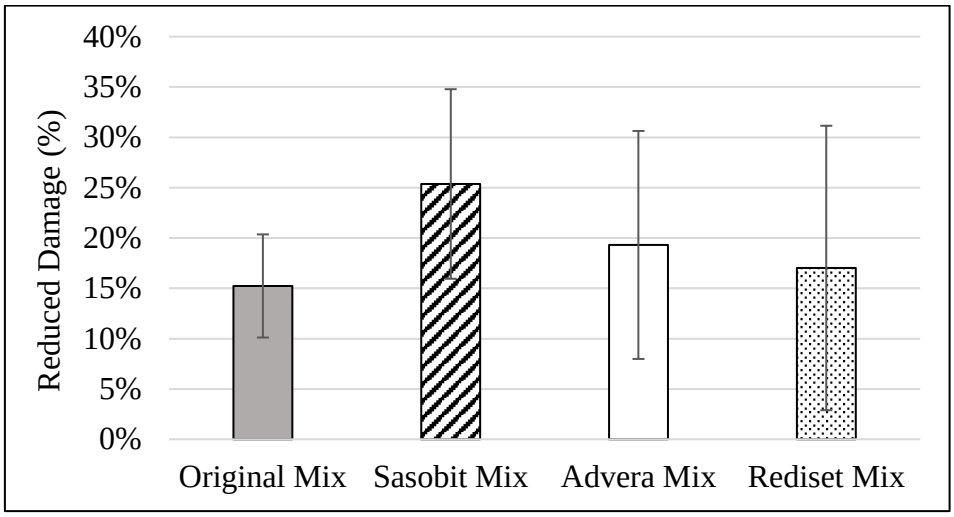

Figure 88: Reduced Damage at the ninth cycle for unaged samples (error bars represent standard error)

On the other hand, ageing also affects the performance of damage in materials during the creep and recovery phases. However, ageing almost overcome the difference in material types (WMA additives) and number of applied cycles, especially in the creep damage results. Figure 89 shows the creep and recovery damage values for the aged samples.

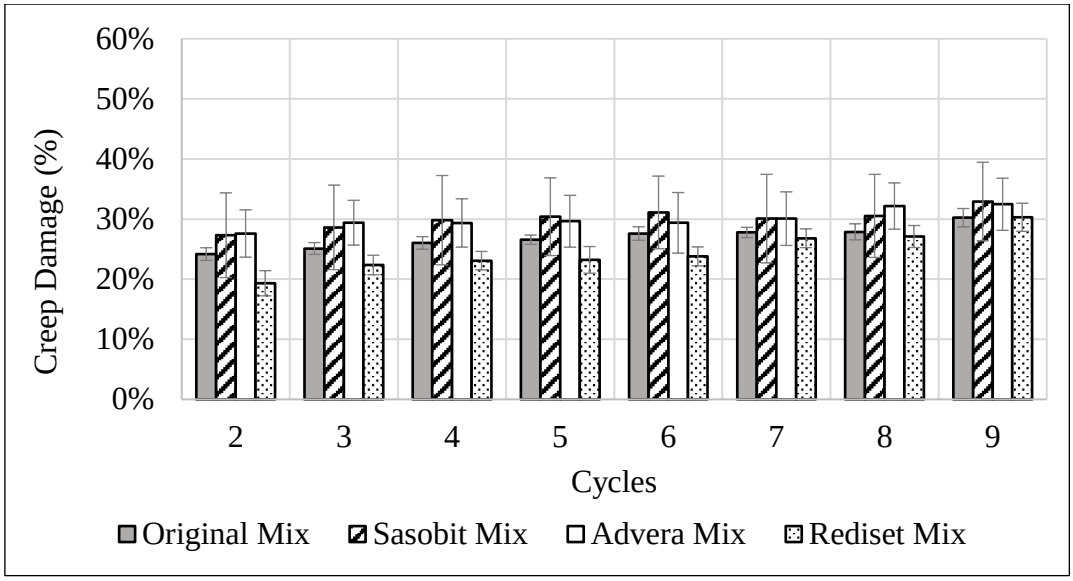

(a) Creep Damage

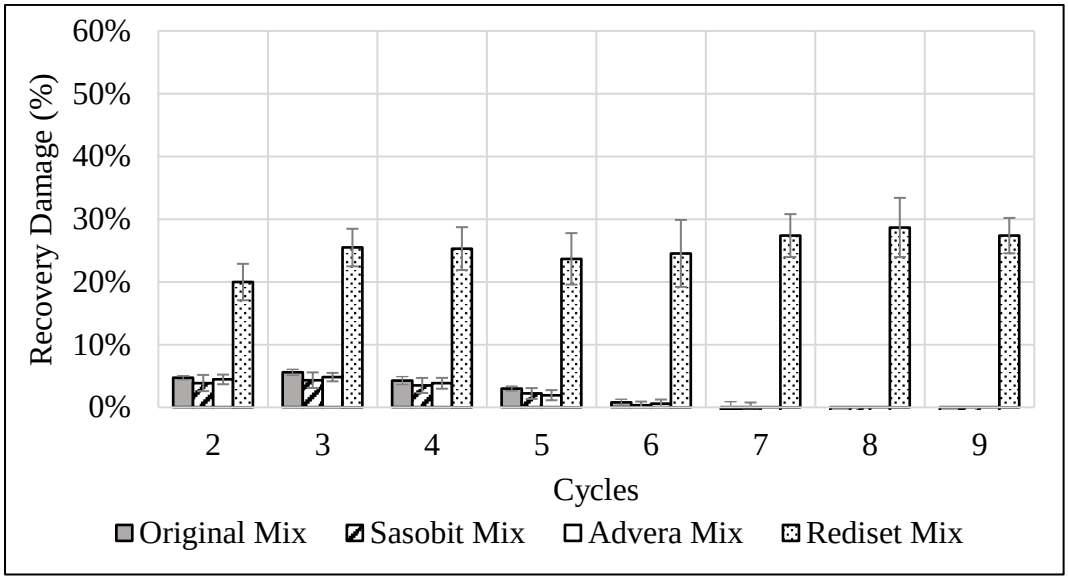

(b) Recovery Damage

Figure 89: (a) Creep and (b) Recovery damage for aged Original, Sasobit, Advera and Rediset mixes tested with the repeated creep and recovery test (error bars represent standard error)

It can be observed from Figure 89 that the Rediset mix has much higher recovery damage than the other mixes. This indicates that the damage generated during the creep phase did not change much in the recovery phase in the Rediset mix. The reduced damage between creep and recovery is presented in Figure 90.

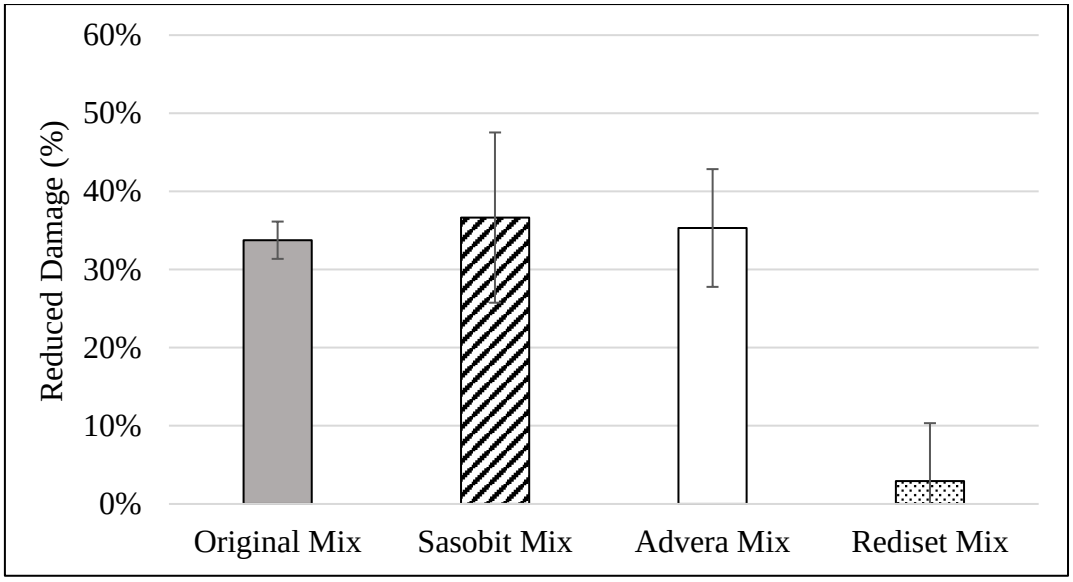

Figure 90: Reduced Damage at the ninth cycle of aged samples (error bars represent standard error)

As shown in Figure 90, the Rediset mix showed the lowest reduced damage among the mixes, which indicates its low ability to recover the damage during the recovery phase.

Hence, samples mixed with the Sasobit additive showed the highest damage during the creep phase but also showed the highest reduced damage during the recovery phase. The ability of the material to recover the damage is investigated through the recovery modulus presented in the next section.

6.5.2. Recovery Modulus Results

As mentioned earlier, all W-FAM samples were tested following the repeated creep and recovery test protocol with the step-loadings included in the recovery phase. The experimental results were used to find the internal stresses, which were used to calculate the recovery modulus (R_M) as the slope between internal stresses and recovery strain. Figure 91 shows the recovery modulus of each mix.

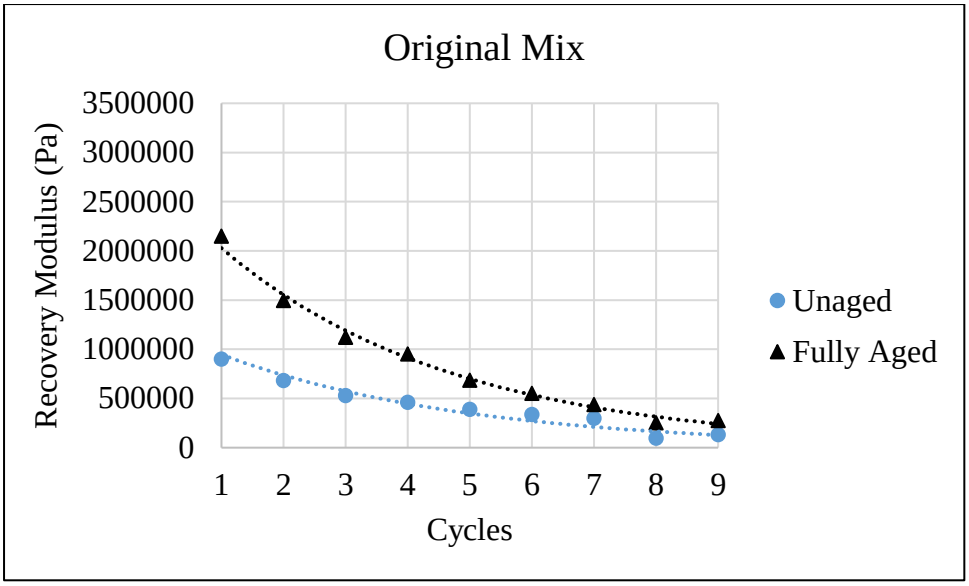
Original Mix
Recovery Modulus (Pa)
3500000
3000000
2500000
2000000
1500000
1000000
500000
0
1
2
3
4
5
6
7
8
9
Cycles
Unaged
Fully Aged

(a)

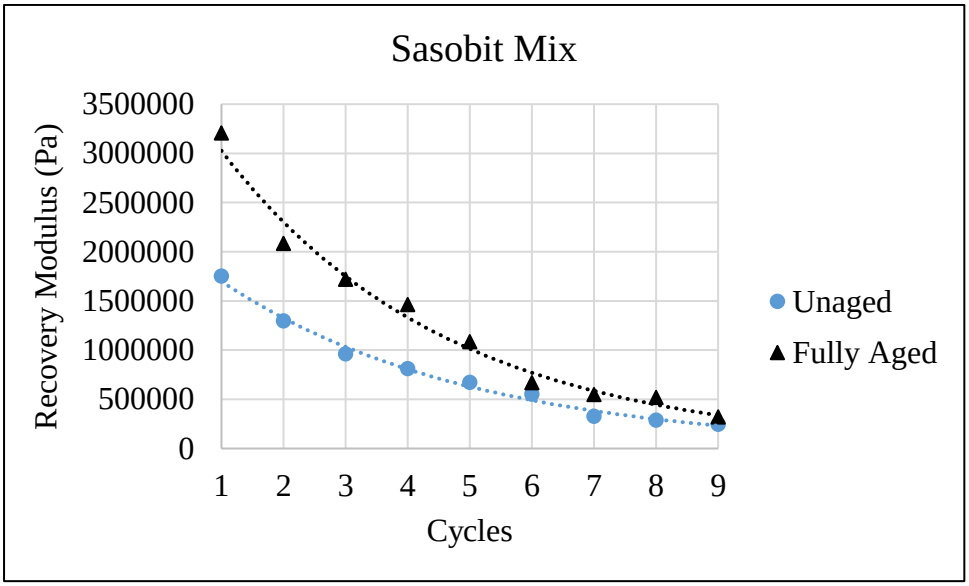
Sasobit Mix
Recovery Modulus (Pa)
3500000
3000000
2500000
2000000
1500000
1000000
500000
0
1
2
3
4
5
6
7
8
9
Cycles
Unaged
Fully Aged

(b)

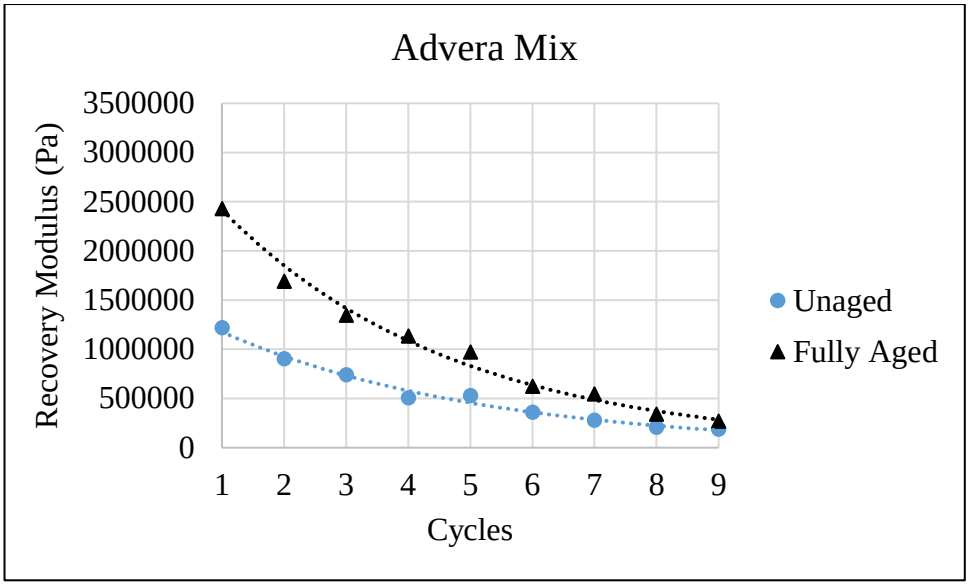

(c)

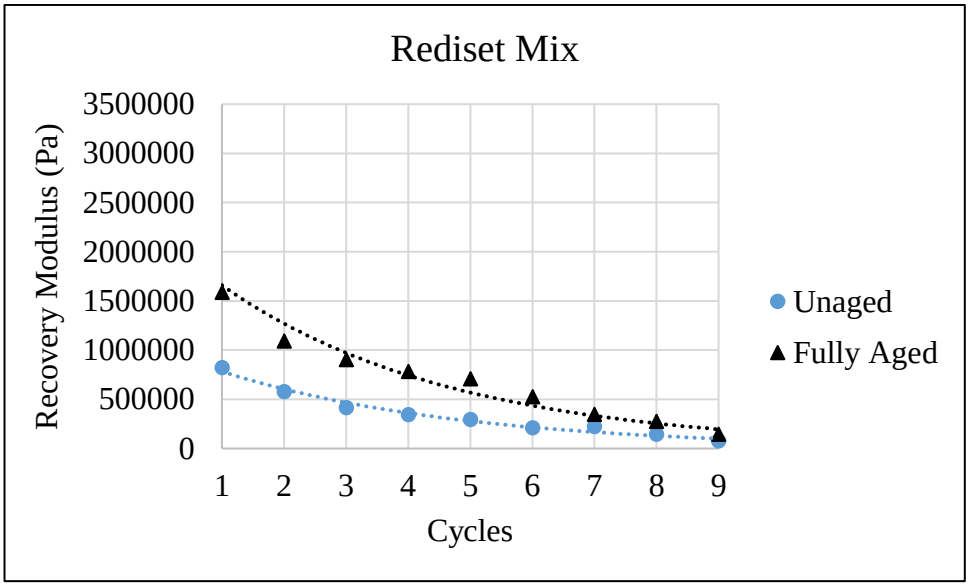

(d)

Figure 91: Recovery modulus for all mixes at unaged and fully aged status

Figure 91 shows that the Sasobit mix has the highest recovery modulus, which gives it the ability to recover the damage more than the other mixes, while the Rediset mix has the lowest recovery modulus compared to the other mixes.

The ageing intervals captured the change in recovery modulus increasing with more hours of UV light exposure. The change is presented in Figure 92.

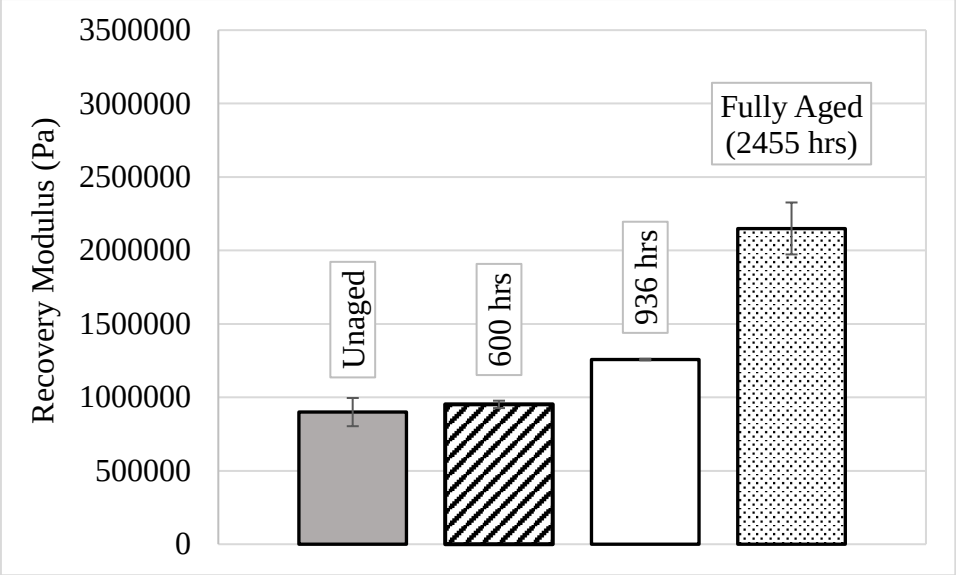

Figure 92: Changing in recovery modulus with ageing captured in the first cycle of the Original mix (error bars represent standard error)

The results for the recovery modulus match the trend of reduced damage results presented in the previous section. The Sasobit has the highest recovery modulus (reached 1.75 MPa of the unaged sample in the first cycle), which indicates its high ability to recover through the internal stresses. The case is similar to the Advera mix, which showed a 1.22 MPa recovery modulus in the first cycle of the unaged samples. The recovery modulus and reduced damage for the ninth cycle of the unaged samples are listed in Table 13.

Table 13: Results of recovery modulus and reduced damage at ninth cycle for all unaged mixes

Mix Type	Recovery Modulus (MPa)	Reduced Damage (%)
Original Mix	0.13	15
Sasobit Mix	0.25	25
Advera Mix	0.19	19
Rediset Mix	0.08	17

As shown in Table 13, the trend of the recovery modulus matched the trend of the reduced damage. The Sasobit mix showed the highest recovery modulus and the

highest reduced damage at the end of the test. The trend is similar to that for the aged samples listed in Table 14. However, ageing almost covered the differences between the Original, Sasobit and Advera mixes, as they showed a close recovery modulus. Additionally, this is reflected in the reduced damage, where all three of them showed a similar percentage for reduced recovery.

Table 14: Results of recovery modulus and reduced damage at ninth cycle for all aged mixes

Mix Type	Recovery Modulus (MPa)	Reduced Damage (%)
Original Mix	0.27	34
Sasobit Mix	0.32	37
Advera Mix	0.27	35
Rediset Mix	0.14	3

The case is different for the Rediset mix since the recovery modulus after ageing showed lower values than the other mixes. The reduced damage is quite small with the Rediset mix, as only 3% of the damage that evolved in the creep test was reduced during the recovery.

It is worth mentioning that the decreasing trend of the recovery modulus with cycles is not related to the change in recovery phase duration. The recovery modulus was calculated as the ratio between the internal stresses and recovery strain for the whole cycle duration, regardless of the duration of the recovery phase. This is in contrast to the recovery damage – explained in the previous section – which is directly affected by the increasing trend of the recovery phase duration that could allow more damage to be recovered. Therefore, having decreasing recovery modulus and decreasing recovery damage with cycles is not contradictory, as recovery damage depends on the recovery duration and recovery modulus does not.

6.6. Conclusions

The characterisation of asphalt mixtures prepared with WMA additives was achieved using fundamental testing procedures and analysis methods. It was found that the current analysis approaches do not explain comprehensibly the resistance of the WMA material to damage and its enhanced ability to recover from it. Additionally, characterisation of damage through standardised ageing techniques had the shortcoming of excluding the effect of UV light from the material damage. Including UV light in the ageing process in a country such as Qatar is essential since the UV index is considered high enough to induce a physical change in the asphalt material's properties.

This chapter presents a new testing and analysis approach that characterises the damage that evolves inside the material due to repeated loading and the recovered damage due to unloading and the material's recovery ability. W-FAM samples were included in a repeated creep and recovery test that applied constant (and damaging) creep stress followed by recovery phase. The creep and recovery phases were repeated in nine cycles during the test and the resultant strain was used for the new proposed analysis approach. In addition, small step-loadings were added to the recovery phase of all cycles to allow measuring of the stress inside the material (i.e. internal stresses) that drives it to recover the creep stress. It was found that the analysis approach can capture material damage during the creep phase. All W-FAM samples showed increasing damage with cycles and ageing during the creep phase. However, damage during the recovery becomes slightly smaller with cycles due to an increase in the recovery phase duration. The analysis approach presented the damage that was reduced during the recovery (i.e. reduced damage) and confirmed the differences between WMA samples in their ability to recover that damage. The trend of the W-

FAM samples' recovery ability was also confirmed by the recovery modulus determined using the internal stresses measured and recovery strain captured during the recovery phase.

Analysis results confirmed that the Sasobit mix would experience the highest damage during the creep phase; however, it has the highest ability to recover that damage during the recovery phase. The Sasobit mix has the highest recovery modulus, which helped in it having the highest reduced damage during the recovery phase. The case is repeated with the Advera mix, which took the second rank after the Sasobit mix. In fact, the Advera mix showed lower damage during the creep phase than the Sasobit mix. However, it reduced that damage during the recovery by less than the Sasobit mix. The case is totally different with the Original and Rediset mixes, which showed low creep damage but did not recover that damage during the recovery phase (especially during the first few cycles). This indicates that the Original and Rediset mixes have a weak ability to recover the damage during the recovery phase since they both have the lowest recovery modulus among the mixes.

It is worth mentioning that ageing has a significant effect on the damage that evolves during the creep phase. Ageing the W-FAM samples almost eliminated the difference between WMA additives in terms of creep damage. The aged Rediset mix has a unique behaviour among the mixes as it showed very small reduced damage during the recovery phase. This indicates that using the Rediset additive prevented the aged material from recovering the damage during the unloading.

Despite the above, the nature (i.e. cause) of the damage captured by the proposed analysis approach is still unclear. Therefore, it is essential to study the crack initiation and/or propagation caused by repeated creep and recovery test. W-FAM samples were

included in an X-Ray CT imaging investigation to examine the effect of repeated loading on the cracks' size. The investigation details are documented in the next chapter.

7. Air Void Measurement for W-FAM Samples using X-Ray Computed Tomography Imaging

This chapter documents the use of X-Ray Computed Tomography (X-Ray CT) to characterise changes in air void in samples subjected to repeated creep and recovery test. The results are then correlated with the material's mechanical response and properties presented in Chapter 5. The samples were prepared with different WMA additives and aged in the accelerated weathering machine, as discussed in Chapter 4. The samples' configuration, digital imaging processing and results analysis are included in this chapter.

7.1. X-Ray Computed Tomography

X-Ray Computed Tomography (CT) is a non-destructive method that produces tomographic images (cross-sectional slices) of a certain object. Slices generated from this machine are used with digital imaging processors to create three-dimensional images for further analysis and investigation (Herman, 2009). In this chapter, the MicroXCT400 machine from XRadia (shown in Figure 93) was used to image FAM prepared with WMA additives (W-FAM).

Figure 93: X-Ray CT Machine used for this study (XRadia MicroXCT-400)

As shown in Figure 94, an X-Ray CT machine consists of an X-Ray source, a detector and a sample holder. The X-Ray CT machine used for this study generates the X-Ray waves using 80 or 140 kilo Voltage (kV) at 10 Watts of power and sends the X-Ray beam through the sample to be received by the detector. Different lenses can be used with the detector to receive the X-Ray beam at different sizes/resolutions. The magnifications (lenses) available with the used X-Ray CT system are 1X, 4X, 10X, 20X and Macro70. The X-Ray beam penetrates the sample at a specified duration of exposure and hits the detector at different intensities. The information received by the detector is then transmitted to the workstation that processes the received intensity into a two-dimensional (2D) image. This process is repeated many times while the sample is rotated through 360 degrees to allow the X-Ray beam to penetrate all its subjected faces.

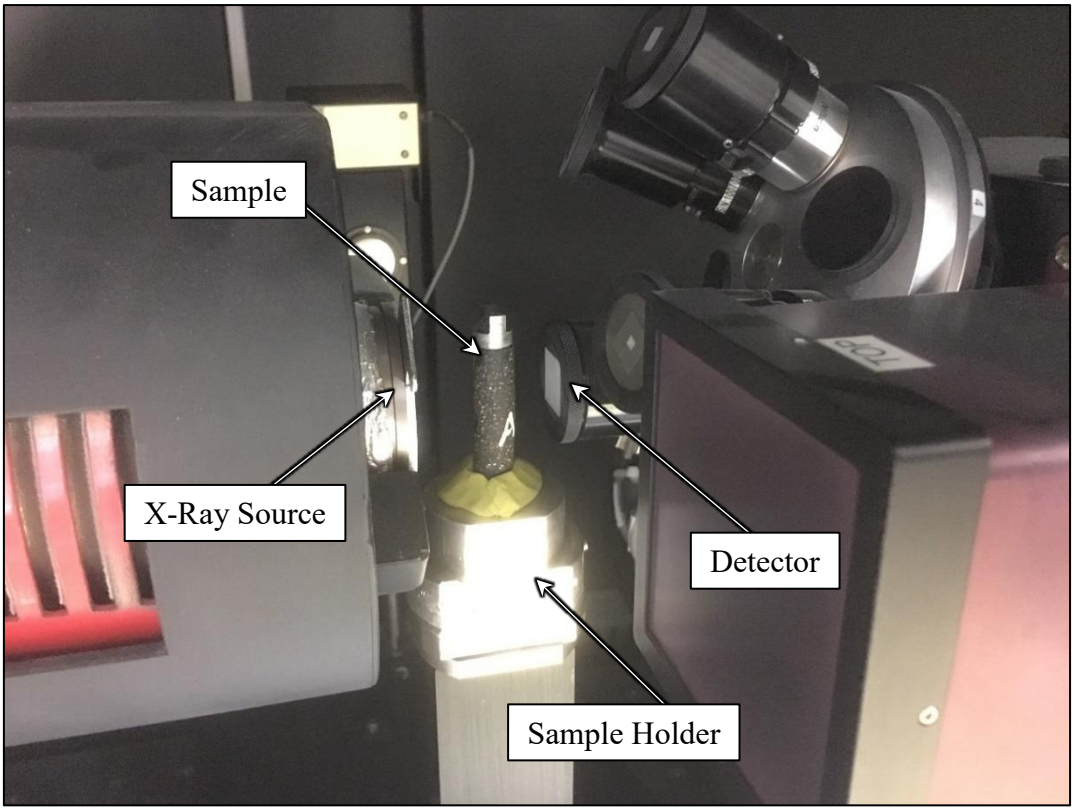

Figure 94: X-Ray CT system indicating its components

Changing the position of the source and the detector has a major role in the resolution of the produced images. In some cases, it is necessary to maintain a wide space between the source and the detector to be able to capture a larger volume of the sample, as shown in Figure 95. However, other times it is preferable to get as close as possible to the sample from both sides (source and the detector) when a small sample or a specific portion of a sample is scanned and the imaging needs to be at high resolution to detect the small parts inside it.

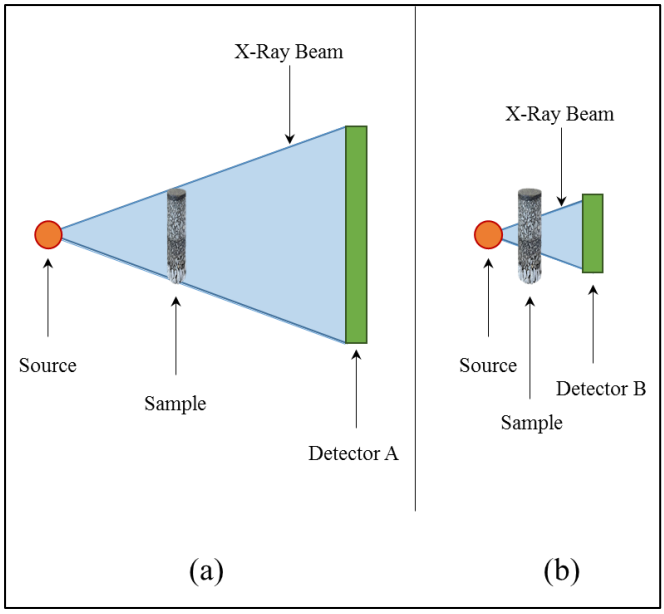

Figure 95: (a) Wider space between the source and the detector to capture the whole sample body (b) bringing the source and the detector as close as possible to capture a specific portion of the sample

Before starting the imaging process, a few trials are required to ensure that the images are produced at the correct intensity. The trials check whether a filter needs to be used with the X-Ray source. The sample is placed in the correct position inside the X-Ray system and an image is taken by the source without any attached filter. Then, the sample is removed and another image is taken without the sample; this is used as a reference image. A transmission value is calculated using both images by dividing the image of the sample over the image without the sample, which produces a new image with transmission values between 0 and 1 (Xradia Inc., 2010; Hsieh, 2012). The transmission value should be compared with a typical list of filters to choose the suitable one to use. The source filters are classified into two types: Low Energy (LE) and High Energy (HE) when using 80kW or 140kW, respectively, as shown in Table 15.

Table 15: Source filter selection based on transmission value (Xradia Inc., 2010)

Transmission @ 80 kV	Transmission @ 140 kV	Source Filter
> 0.63	–	No Filter
0.44 – 0.63	–	LE #1
0.34 – 0.44	–	LE #2
0.28 – 0.34	–	LE #3
0.21 – 0.28	–	LE #4
0.14 – 0.21	–	LE #5
0.08 – 0.14	–	LE #6
–	0.18 – 0.30	HE #1
–	0.08 – 0.18	HE #2
–	0.06 – 0.08	HE #3
–	0.04 – 0.06	HE #4
–	0.03 – 0.04	HE #5
–	< 0.03	HE #6

After performing the practice mentioned above, it was found that the filter labelled ’HE #1’ would generate the best resolution. The source and the detector were kept at specific positions that can cover the whole diameter (12 mm) and the middle 13 mm of the sample, as shown in Figure 96.

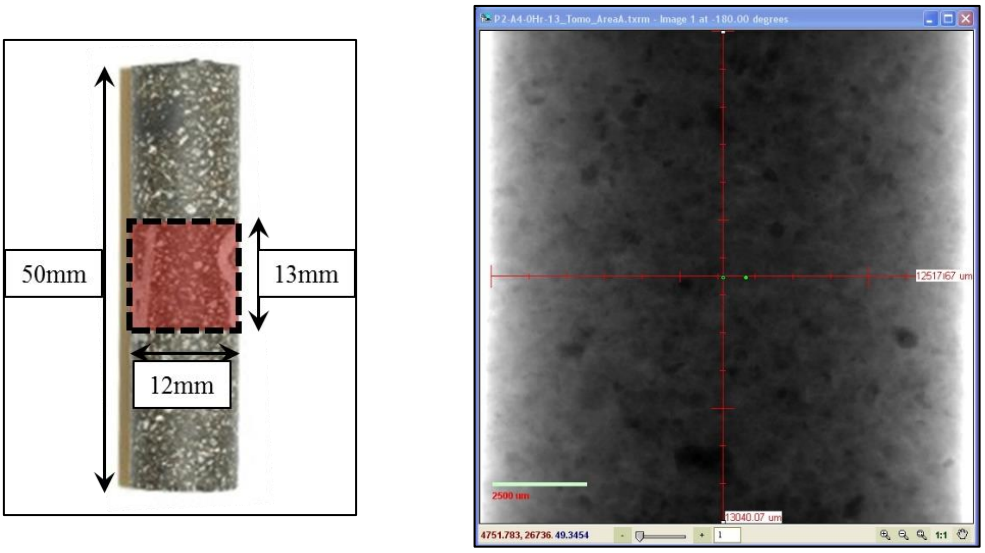

Figure 96: The portion of the sample imaged by the X-Ray CT system

The imaging was performed by focusing on the middle portion of the sample because it is the portion most affected by the applied torsional test. The machine was programmed to take 3600 images of the portion assigned in Figure 96 while the sample rotates 180° clockwise and anticlockwise to capture all faces. Specifying the number of images as 3600 ensured that 10 images would be taken per rotational degree. The machine was set to capture 10 images without the sample after every 400 images with the sample to calibrate the intensity of the produced images. The imaging was set to perform 2 binning of the images captured by 10 seconds of X-Ray exposure. The 2 binning is a procedure that combines four pixels into one single pixel to reduce the noise that might be generated from the imaging process (TIBCO Spotfire, 2015). Imaging with the parameters mentioned above took around 11 hours for the machine to finish a single sample.

7.2. Sample Preparation and Handling

W-FAM samples prepared as discussed in Chapter 3, aged as presented in Chapter 4 and tested as described in Chapter 5 were imaged using the X-Ray CT machine for this study. Slices were generated from the imaging process that allows the air void distribution inside the sample to be inspected and investigates the structural changes due to the mechanical testing (repeated creep and recovery test). The preparation of the four mixes (Original, Sasobit, Advera and Rediset Mix) was discussed in detail in Chapter 3. Table 16 shows the basic information about the preparation and material components.

Table 16: Basic information about the preparation of the Fine Aggregate Mixtures mixed with WMA additives

Parameters	Original Mix	Sasobit Mix	Advera Mix	Rediset Mix
Bitumen type	PG76-22			
Bitumen Content	7.3%			
Aggregate type	Gabbro			
Aggregate Gradation	See Table 6			
Mixing Temperature	163ºC	145ºC	145ºC	145ºC
Compaction Temperature	135ºC	116ºC	116ºC	116ºC
Additive Used	None	Sasobit	Advera	Rediset
Additives Dosage	-	2.0%	5.0%	0.5%

Two replicates of the unaged and the fully aged (2455 hours of UV ageing) W-FAM samples were included in the X-Ray CT imaging. The samples were fixed to the upper and lower DSR fixations and placed with the sample holder inside the X-Ray CT system. The sample holder was designed and fabricated in the machine shop at Texas A&M University at Qatar especially for this study to ensure that the sample was placed at the exact location (in x-, y- and z-axes) before and after testing. Figure 97 shows the sample holder fabricated and used for this study.

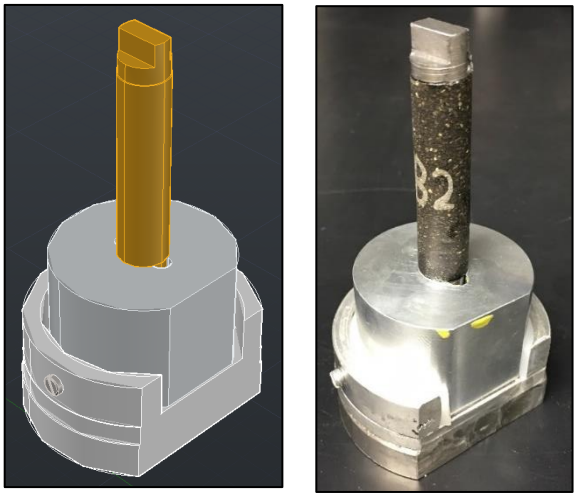

Figure 97: The designed and fabricated sample holder used with the X-Ray CT imaging

Samples were marked in a consistent way to keep the orientation the same to guarantee that comparable images would be obtained both before and after testing. A small amount of paste was placed between the sample and the holder to prevent the sample from vibrating during the imaging due to the rotation. This practice helped in imaging the same portion of the sample before and after the repeated creep and recovery test to evaluate the changes in the crack size and distribution.

7.3. Image Reconstruction

After finishing the imaging by the X-Ray system, slices captured and transmitted to the workstation were processed using special software called 'XMReconstructor'. The images go through two stages of reconstruction: the first is to find the centre shift for all slices and construct the slices without them being blurry. Un-blurry images were produced by specifying a centre factor that was visually selected after running a range of factors (from -10 to 10) and selecting the highest possible focus, as shown in Figure 98. The factor was selected by ±0.1 accuracy to ensure the best results.

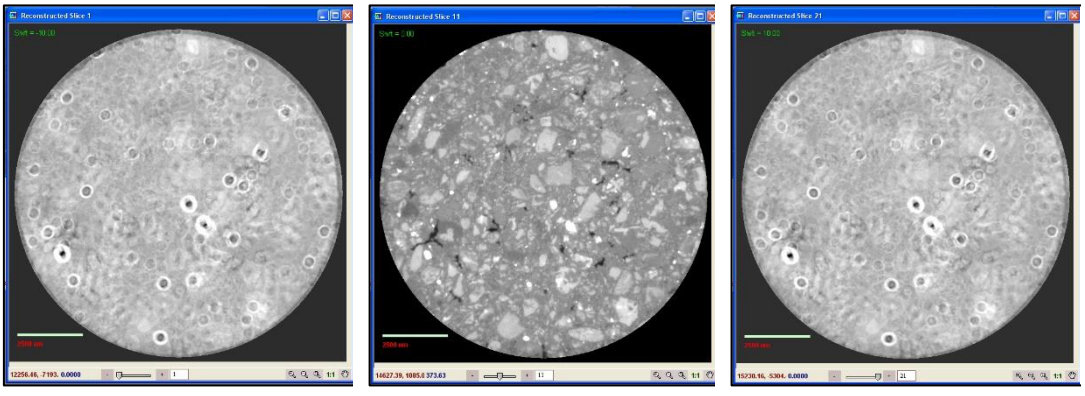

(a) -10 Centre Factor (b) 0 Centre Factor (c) 10 Centre Factor

Figure 98: Specifying the centre factor (from -10 to 10) for the imaged sample during the slices' reconstruction using XMReconstructor software

When the images are transmitted to the workstation for processing, the 'XMReconstructor' software assumes that the X-Ray spectrum is linear and affects

the whole cross-section of the sample at the same level of energy. However, the low level of the X-Ray spectrum is usually absorbed by the sample, which results in reconstructed images that have brighter colours at the edges than the inner part (even if the sample is homogenous). This phenomenon is called 'beam hardening (BH)' (Rana *et al.*, 2015; Tolley and Yue, 2016). The 'XMReconstructor' software provides the user with a tool (shown in Figure 99) to equalise the beam hardening for the images by defining a correction factor. This factor corrects the image's colour intensity and finds the best distribution through the whole cross-section of the sample. This factor alters the intensity of the images and has to be chosen carefully for further image-processing techniques. For comparable results, the beam hardening was fixed for the sample imaged before and after testing, while the centre factor had to be selected carefully each time the sample was imaged because the sample could change its position slightly due to the use of paste.

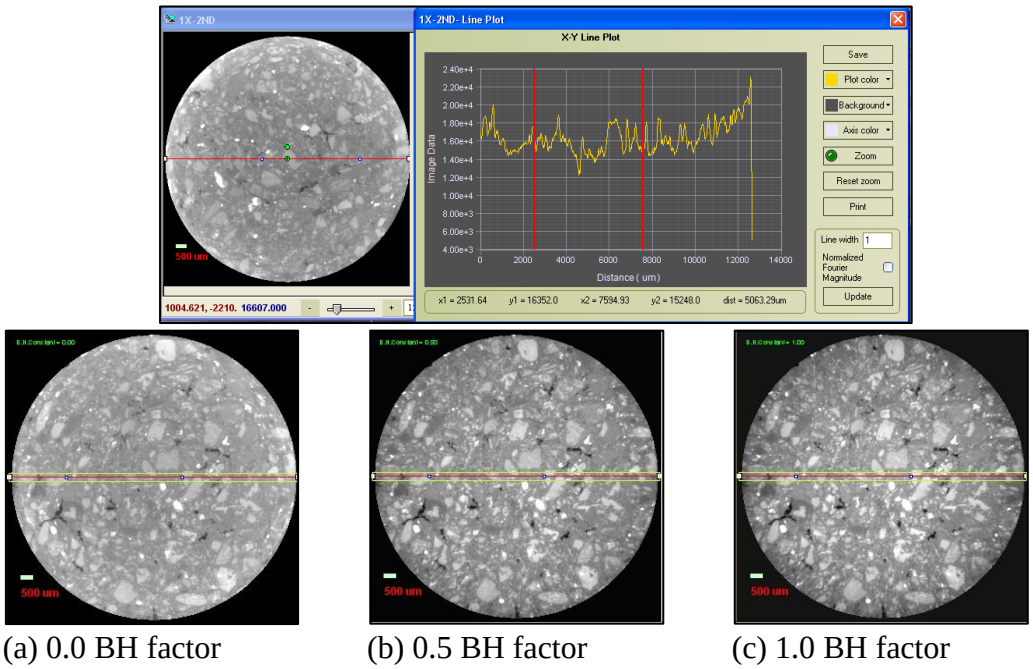

(a) 0.0 BH factor (b) 0.5 BH factor (c) 1.0 BH factor

Figure 99: Specifying the beam-hardening (BH) correction factor for imaged slices using the XMReconstructor software

After selecting the best centre and beam-hardening correction factor, the images were reconstructed to generate 634 slices for each sample. As shown in Figure 100, the side view shows that the imaging covered 12999.89-micrometre height of the sample. The size of the cross-sectional view (consist of the cross-section of the sample and the black area around it) imaged by the X-Ray CT system was measured and found to be 13039.96 micrometres by 12678.81 micrometres. The images captured by the system were converted to a computerised image format (tiff) to be opened using the normal Windows operating system. The image sizes were also converted to pixels instead of micrometres and this showed that all the images were 650 pixels in height and 628 pixels in width. By dividing the actual micrometres dimension of the images (i.e. the height by the width of the tiff image), the results show 20μm resolution. This value (i.e. 20μm) is considered as the resolution of the imaging.

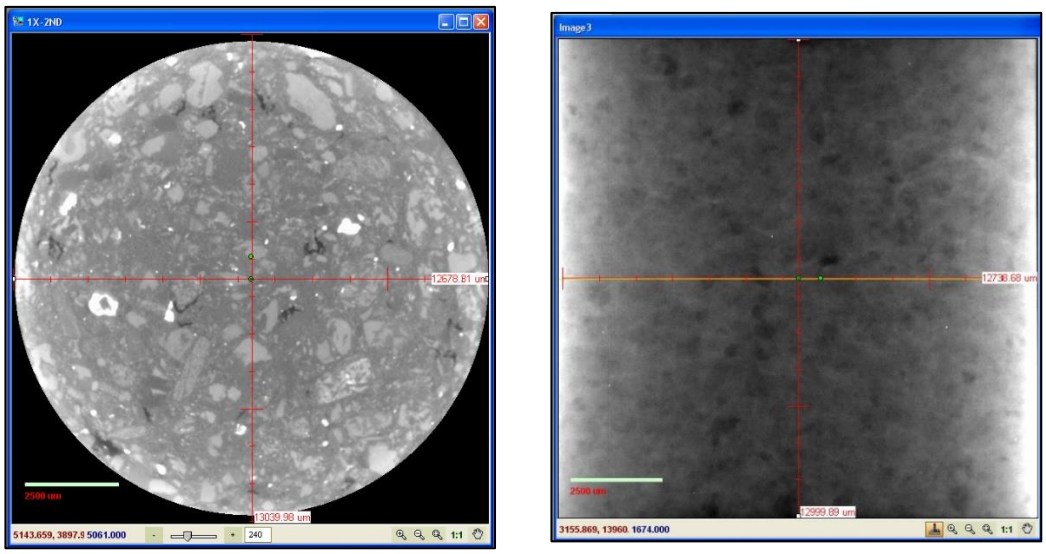

(a) (b)

Figure 100: (a) Cross-sectional view of the imaged sample with diameter measurements (b) Side view with width and height measurements

As shown in Figure 100, the image is produced in the greyscale, where the light grey indicates the aggregate particles, the dark grey is the bitumen and the black parts are the air voids (i.e. cracks) as shown in Figure 101.

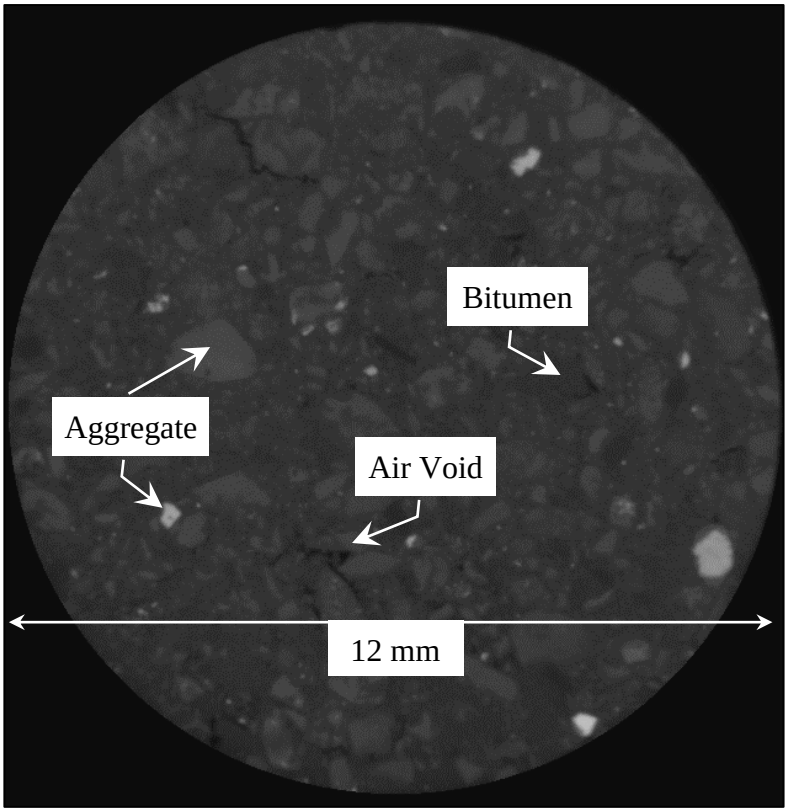

Figure 101: An imaged slice with annotated components showing the aggregate particles, bitumen and air voids

7.4. Air Void Area Measurement

In order to measure the air void changes in the imaged samples, the slices obtained from the reconstructed images were digitally processed. Digital Image Processing (DIP) was made in this study by using MATLAB (2015a) imaging process techniques. The code was developed to convert the images produced by the X-Ray CT software (tiff format) to a quantifiable format. Two thresholding techniques were performed for each slice of the imaged samples. The two thresholding techniques were used to enhance the accuracy of the segmentation of the images into the required regions. The regions were segmented to separate the air void area and measure its distribution in the slices. The code processes the images through four steps, which are explained in detail in the following sections.

7.4.1. Deleting the Unclear Slices

At the beginning of the image processing, all images were evaluated in terms of quality and clearness. It was found that the first and the last imaged portions generated unclear slices, as shown in Figure 102. They were very dark, especially at the edges.

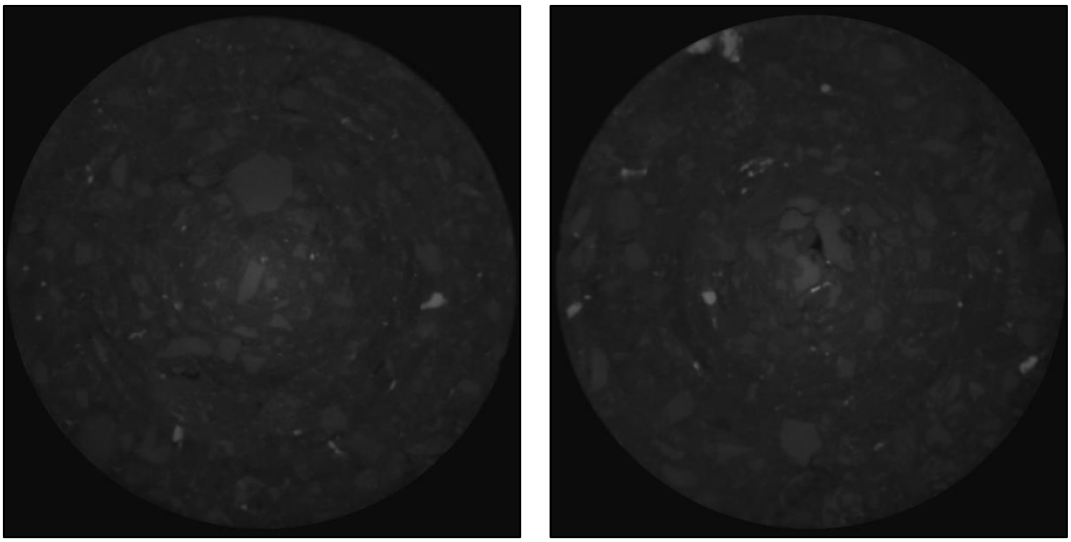

(a) (b)

Figure 102: (a) First slice of the imaging process (b) last slice of the imaging process

The reason behind this unclear portions is related to the X-Ray beam shape to which the sample was subjected during the imaging – the beam can be described as a cone. The cone hits the sample body in a conical shape, and it results in uncovered areas of the sample, as shown in Figure 103. The uncovered areas are reflected on the detector as dark portions similar to the air voids, which are reflected as complete black.

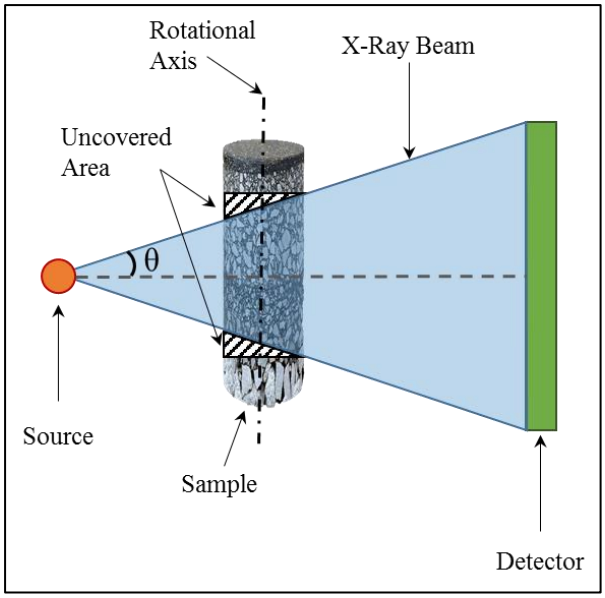

Figure 103: The portion of the sample imaged by the conical X-Ray beam and the uncovered areas

Consequently, several slices had to be removed from the analysis process so that only the clear and sharp slices were processed with the analysis method. To specify the number of slices that should be removed from the study, a simple calculation was conducted using equation (51) (ZEISS Group, 2015).

$$N = \frac{FOV}{2\tan(\theta)} \quad \textbf{(51)}$$

where 'N' is the number of slices that should be ignored by the analysis, 'FOV' is the field of view in pixels (e.g. 1000 when 2 binning is used and 2000 when 1 binning is used) and 'θ' is the cone angle, which is calculated using equation (52).

$$\theta = \arctan\left(\frac{0.0005 \times n \times ps}{sra}\right) \quad \textbf{(52)}$$

where 'n' is the image size (which is in this study 650 pixels), 'ps' is the pixel size (which is the imaging resolution and equals 20μm) and 'sra' is the distance between the source and the rotational axis (centre of the sample rotation axis). It was found by following the above calculation that the first and last 71 slices would have the unclear

issue, however, after several checks it was decided to remove 150 slices from the top and the bottom parts of the sample analysis to ensure that all unclear slices were eliminated.

7.4.2. Segmentation of the Image using Otsu's Method

The first thresholding technique used in this study is Otsu's method. This method is used to segment the colour histogram of the image into several levels and define the best thresholds of each level by dividing it into two parts: background and foreground.

The functions use the image information in each pixel to generate a histogram plot for the colour intensity. The histogram can be divided into a specific number of bins, as shown in Figure 104.

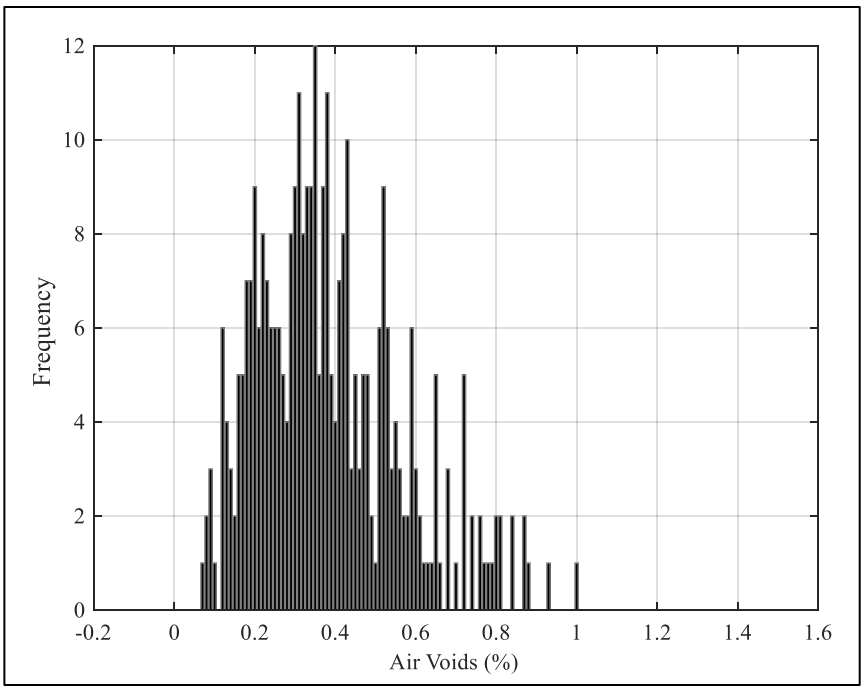

Figure 104: Air void histogram of imaged slice

In this study, Otsu's method is implemented. For best results, 20 levels of thresholding were used to obtain the maximum accuracy possible from each slice. Each threshold divides the histogram into two parts: background and foreground. In each bin before

the threshold (background bins), the function uses the histogram counts to calculate the weight of all bins before the threshold in terms of the image size, as shown in equation (53) and (54).

$$Background\ Weight = W_b = \frac{\sum_{i=0}^{n} freq_i}{Image\ Size} \quad \textbf{(53)}$$

$$Foreground\ Weight = W_f = \frac{\sum_{i=n}^{B} freq_i}{Image\ Size} \quad \textbf{(54)}$$

where '*i*' is the bin number, '*n*' is the last bin before the threshold, '*B*' is the last bin of the histogram, '*freq*' is the frequency of each bin and '*Image Size*' is the area of the image (height x width) in pixels. Also, the counts are used to calculate the mean and variance of the counts, as shown in equations (55) and (56).

$$Background\ Mean = \mu_b = \frac{\sum_{i=0}^{n}(i \times freq)_i}{\sum_{i=0}^{n} freq_i} \quad \textbf{(55)}$$

$$Foreground\ Mean = \mu_f = \frac{\sum_{i=n}^{B}(i \times freq)_i}{\sum_{i=n}^{N} freq_i} \quad \textbf{(56)}$$

Then, the variance is calculated as shown in equations (57) and (58).

$$Background\ Variance = \sigma_b^2 = \frac{\sum_{i=0}^{n}[freq \times (i - \mu_b)]_i}{\sum_{i=0}^{n} freq_i} \quad \textbf{(57)}$$

$$Foreground\ Variance = \sigma_f^2 = \frac{\sum_{i=n}^{B}[freq \times (i - \mu_f)]_i}{\sum_{i=n}^{N} freq_i} \quad \textbf{(58)}$$

Finally, the weight and the variance of both background and foreground are used to calculate the 'Within Class Variance' (σ_W^2), as shown in equation (59).

$$\sigma_W^2 = W_b\sigma_b^2 + W_f\sigma_f^2 \quad \textbf{(59)}$$

The Matlab code tries all thresholds available to obtain the lowest results of the within-class variance. The threshold that produces the lowest within-class variance is considered the best threshold that separates that histogram portion of the image into two parts (Greensted, 2010).

As mentioned above, using a higher number of thresholding levels in Otsu's method ensures a more accurate thresholding process. For example, the Otsu's method was used with one of the imaged slices by applying 2, 7, 15 and 20 levels, and the results are presented in Figure 105.

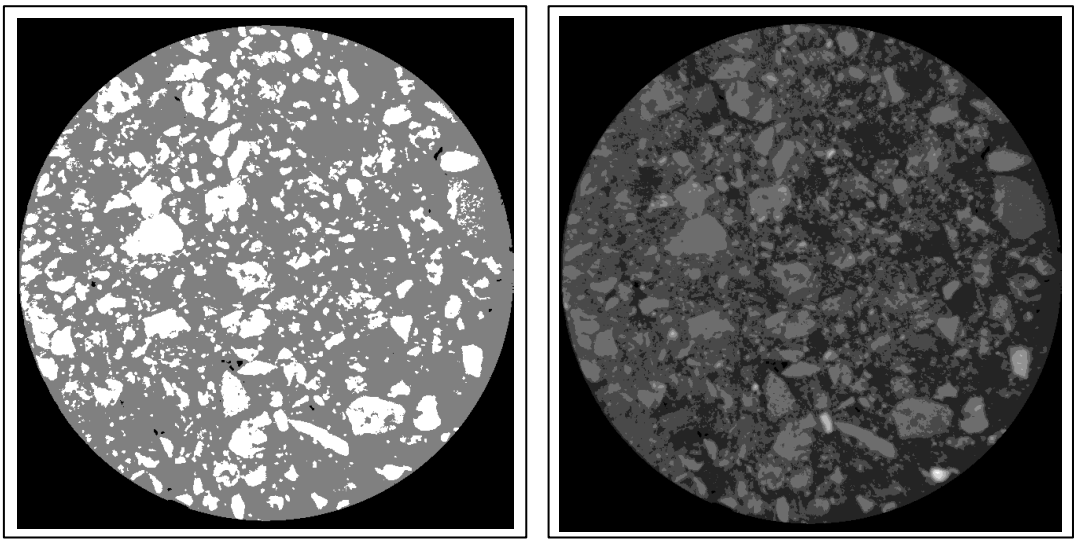

(a) Level = 2 (b) Level = 7

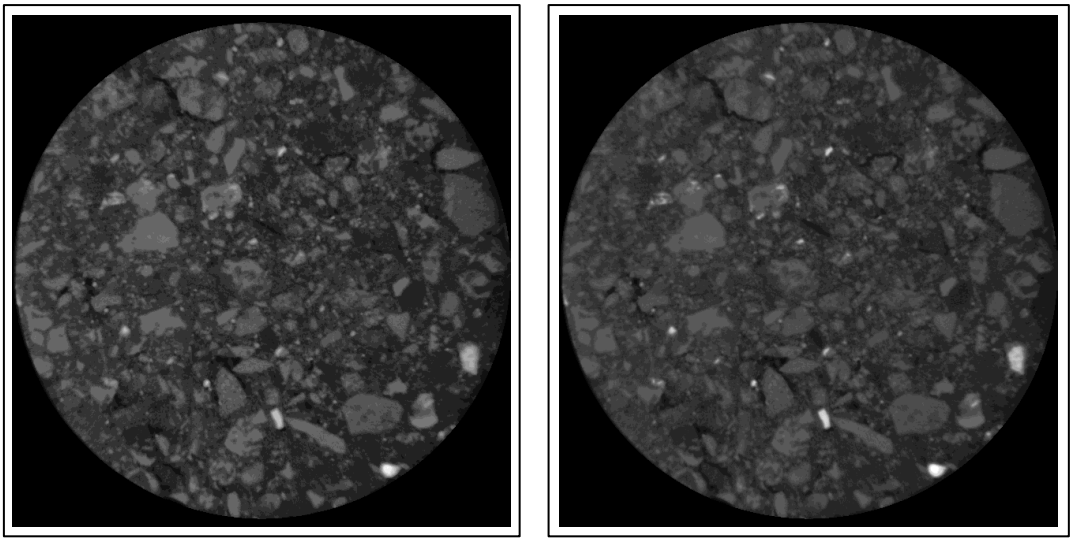

(c) Level = 15 (d) Level = 20

Figure 105: Segmented image using Otsu's method with different levels of segmentation (2, 7, 15 and 20)

As shown in Figure 105, the more levels used, the better the quality and the separation of the image, and more levels of segmentation can be defined, which increases the accuracy of the results.

7.4.3. Performing the Minimum Error Threshold (MET) Method

The second thresholding technique used in this study is the 'Minimum Error Threshold' presented originally by Kittler and Illingworth (1986). The method depends on computing the relative histogram of the image. Similar to Otsu's method, the intensity of the grey level (values between 1 and 255) is investigated by splitting the histogram into two parts: the background and the foreground. The mean and the variance were calculated for each part, as shown in equations (53) to (58), and included in determining the criterion function (J(T)), as shown in equation (60).

$$J(T) = 1 + 2\big(W_b \log(\sigma_b) + W_f \log\big(\sigma_f\big)\big) - 2\big(W_b \log(W_b) + W_f \log\big(W_f\big)\big) \quad \textbf{(60)}$$

W_b and W_f are the weights of the background and the foreground, respectively, in terms of the total image size, while the σ_b and σ_f are the standard deviation also for

the background and foreground histogram counts, respectively. The criterion function investigates each threshold (T), from 1 up to 255. The code keeps on investigating the criterion function and picking the minimum results obtained to be used as the best threshold for that slice. The full MATLAB code developed and used for this analysis is available in Appendix C.

After that, the threshold (T) that produces the minimum criterion function is used to split the image into the two regions mentioned earlier (background and foreground). All values below the threshold (T), which is related to the black colour, are considered as background and all values above (T) are considered as foreground. Then, the image is separated from the foreground by removing all pixels that have greyscale above the threshold (T). The results from that separation process are shown in Figure 106.

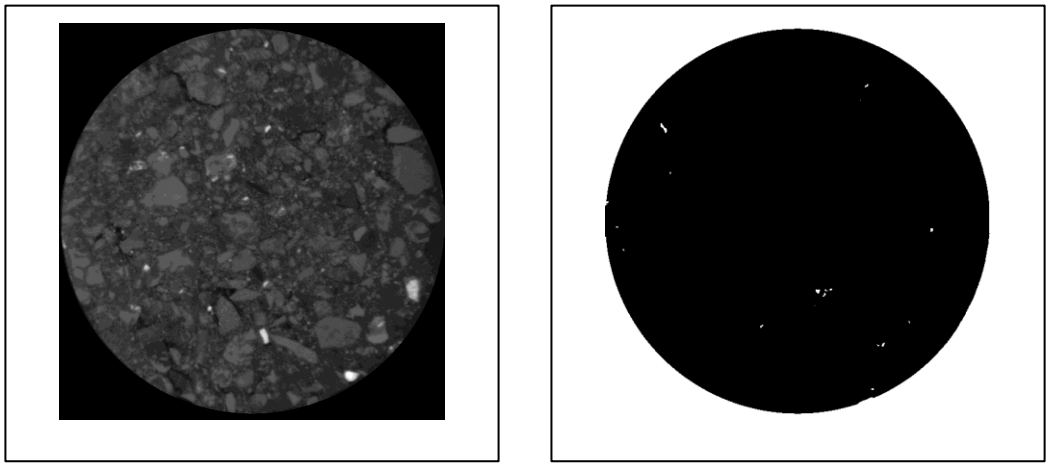

(a) (b)

Figure 106: The image (a) after applying Otsu's thresholding and (b) after applying the minimum error thresholding method

As shown in the above figure, the image on the right has two colours only: black and white. This image is used then in a regionalising technique in order to extract information from each region using the colours.

The two thresholding techniques were able to separate the image's colours smoothly without losing any details. Figure 107 shows a zoom-in shot of one of the slices and specifically shows an aggregate particle and an air void. The figure shows the steps of thresholding and the level of separation performed by each step.

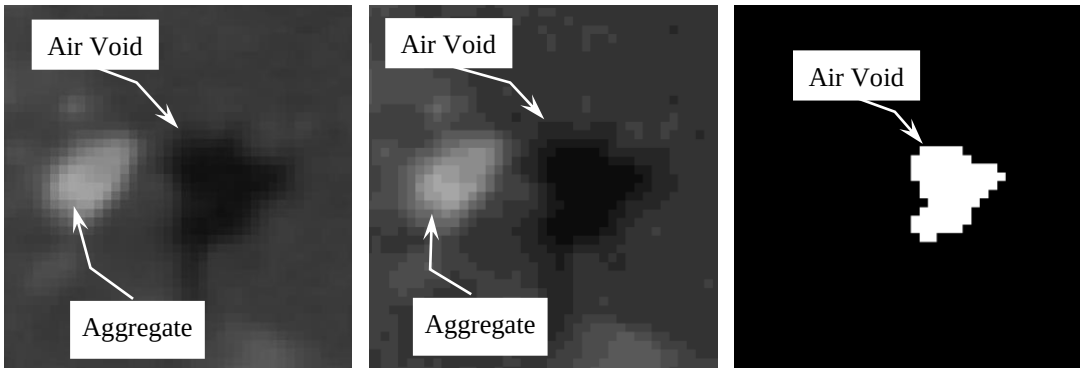

(a) Original Image (b) After Otsu's Method (c) After MET Method

Figure 107: The process of thresholding starting from (a) original image, (b) after Otsu's method and (c) after applying the minimum error thresholding (MET) method showing an aggregate particle and an air void

7.4.4. Regionalisation of the Image

After using the threshold that separates the image/slice into background and foreground, the analysis method ignored the foreground colours, as mentioned earlier, and focused on the white spots (air voids) in order to extract informative data from them. The regionalisation method starts by labelling each white spot area to be considered as a separated region. Then, all the properties of those regions are listed in a structural array. Properties such as area, centroid, axis length, axis width, orientation, etc., are stored in that array. The only information used in this study is the area property of the regionalised image. However, since the image has an empty (white) area surrounding the actual sample, this area has to be dropped from the analysis since it is not an air void. In order to remove this area, a simple criterion was enforced in the code to omit any region that has an area property of more than 500 square pixels.

7.4.5. Calculation of the Air Void Area

To calculate the air void area inside a single image/slice, the white regions captured from the slice were summed after omitting any region bigger than 500 square pixels. The summation of all regions was then multiplied by the resolution of the image 0.02 mm x 0.02 mm (= 0.0004 mm^2) to convert the area from square pixel to mm^2. Then, by having the area of each air void region in a single slice, the total area of air voids in that slice can be calculated by summing all regions together. The total area of air voids inside each slice is used to calculate the air void percentage, as shown in equation (61).

$$Air\ Voids_k\ (\%) = \frac{\sum_{i=1}^{n} Void\ Area_i}{Cross-section\ area} \times 100\% \quad \textbf{(61)}$$

where '*n*' is the number of air voids in each slice, and the area of the whole slice is in mm^2, and '*k*' is the number of the slice (total of 636 slices). Then, all air void percentage (Figure 108) results were studied before and after testing.

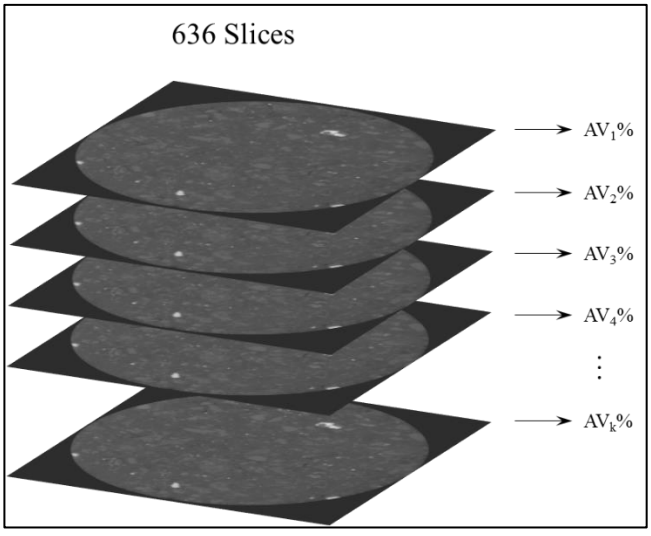

Figure 108: Air voids summed together to calculate the air void percentage of each slice

7.5. Results and Discussion

As discussed in the previous section, the percentage of air voids (AV%) was measured after going through the thresholding process. The measurements were used in calculating the percentage of air voids in each slice. The air void percentages were then evaluated using statistical tools to study the air void size changes before and after applying the repeated creep and recovery test presented in Chapter 5. The results also compared the unaged with fully aged (2455 hrs of ageing) samples to evaluate the effect of UV ageing presented in Chapter 4 on the air void sizes after testing.

The air void percentages of all slices were plotted before and after the repeated creep and recovery testing and are presented in Figure 109.

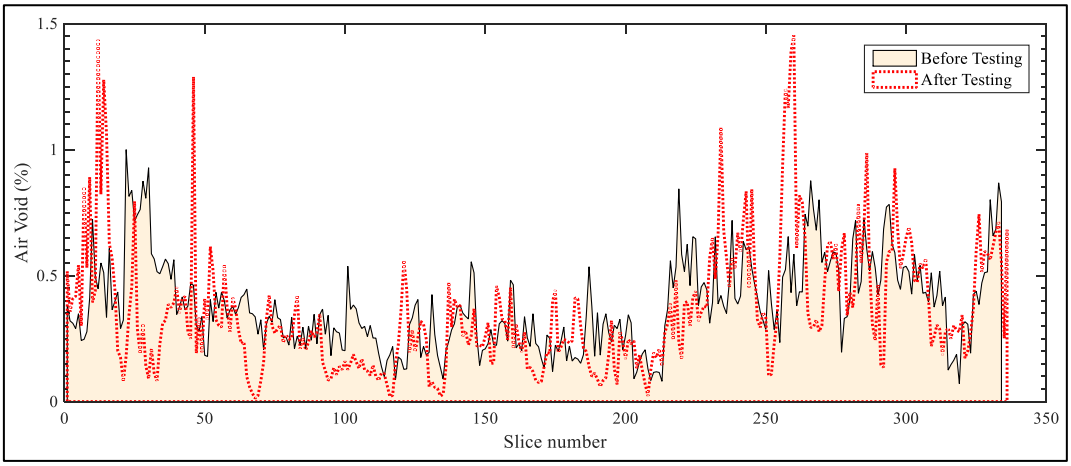

(a) Original Mix

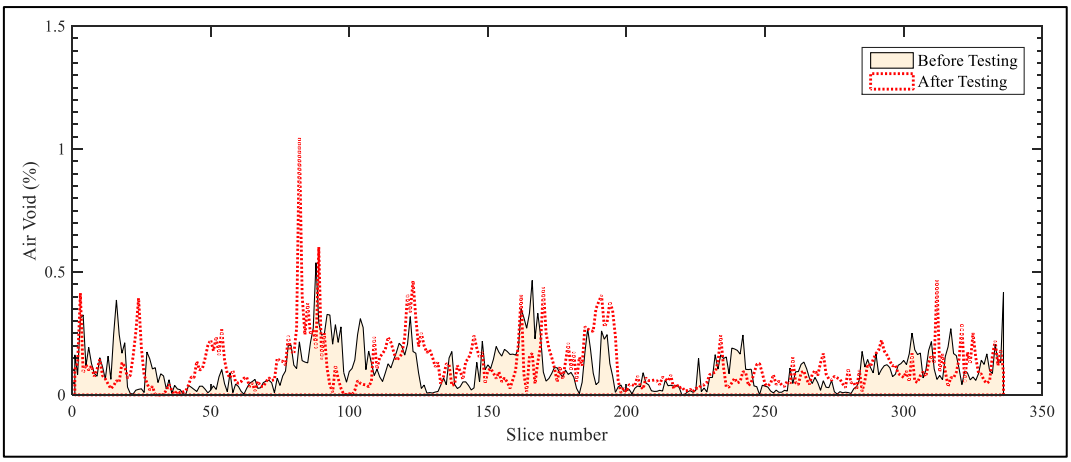

(b) Sasobit Mix

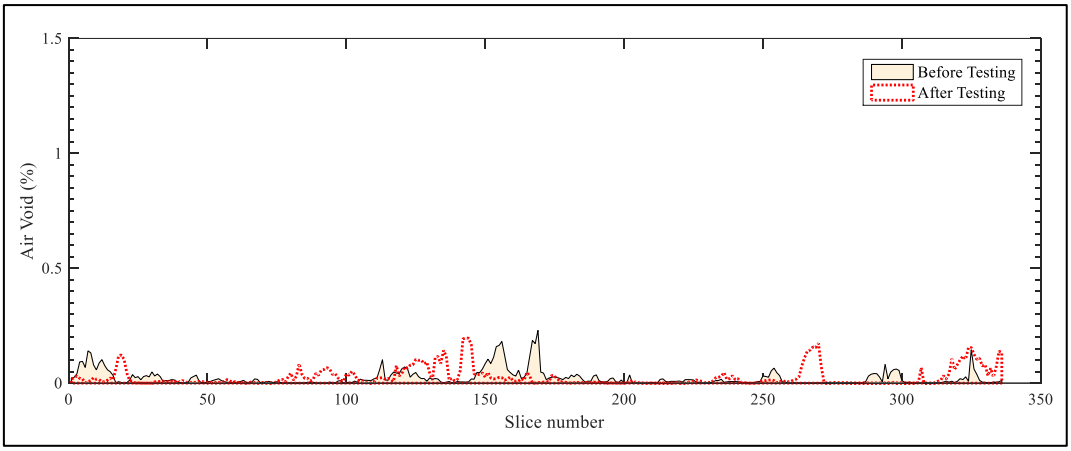

(c) Advera Mix

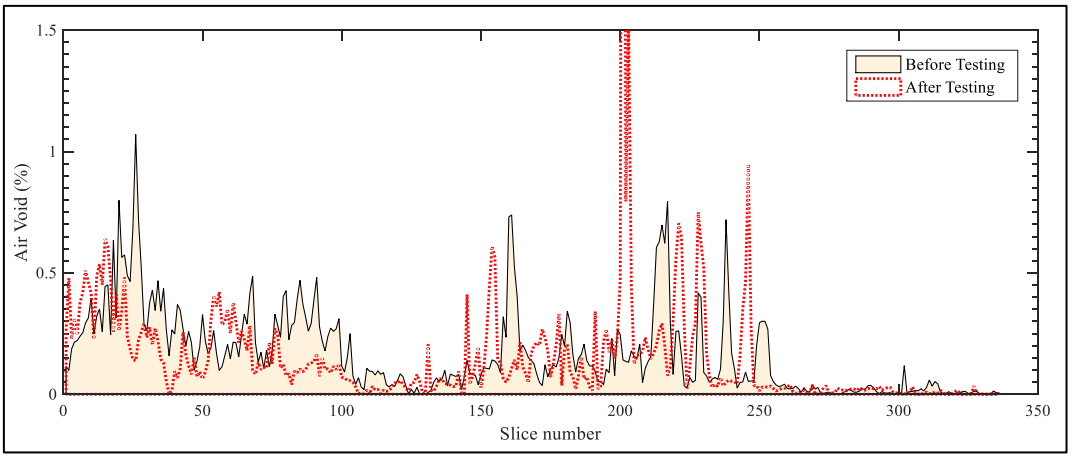

(d) Rediset Mix

Figure 109: Air void distribution of each mix along the length of the imaged samples

From Figure 109, it can be noticed that, although all mixes were prepared using the same aggregate gradation, compaction procedure and bitumen content, the air voids in the Original and Rediset mixes were higher than in the Sasobit and Advera mixes. The difference in the air voids between mixes was generated because different additives were used since, even within the W-FAM (Sasobit, Advera and Rediset mixes), the difference is noticeable. Also, the results of the Advera mix showed the lowest air voids among the mixes. However, the variability between slices is too high and calculating the average will have noteworthy uncertainty. Thus, the air void results were used to generate the empirical cumulative distribution function (ecdf) to study and compare the material according to the 50% (2^{nd}) quantile of the air void values.

Figure 110 shows the ecdf plot for each mix before and after the repeated creep and recovery test.

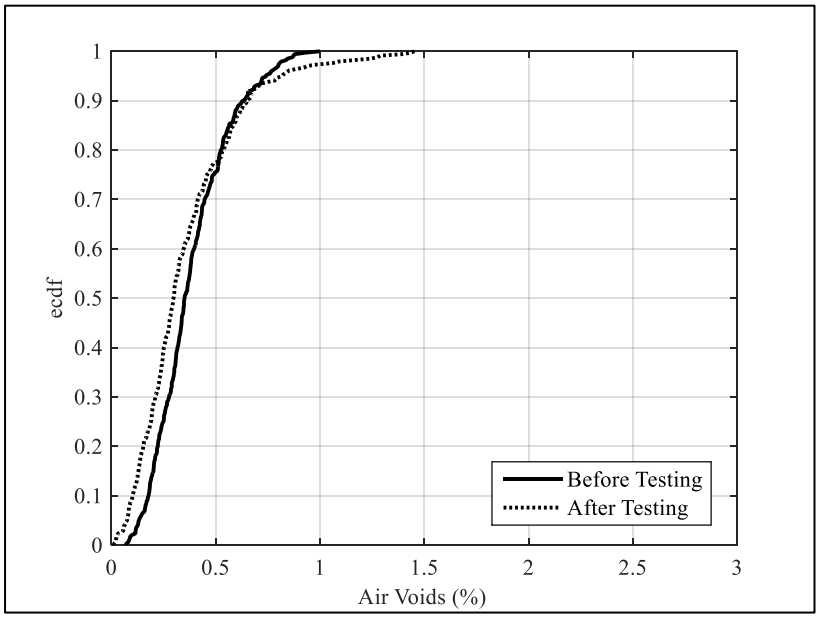

(a) Original Mix

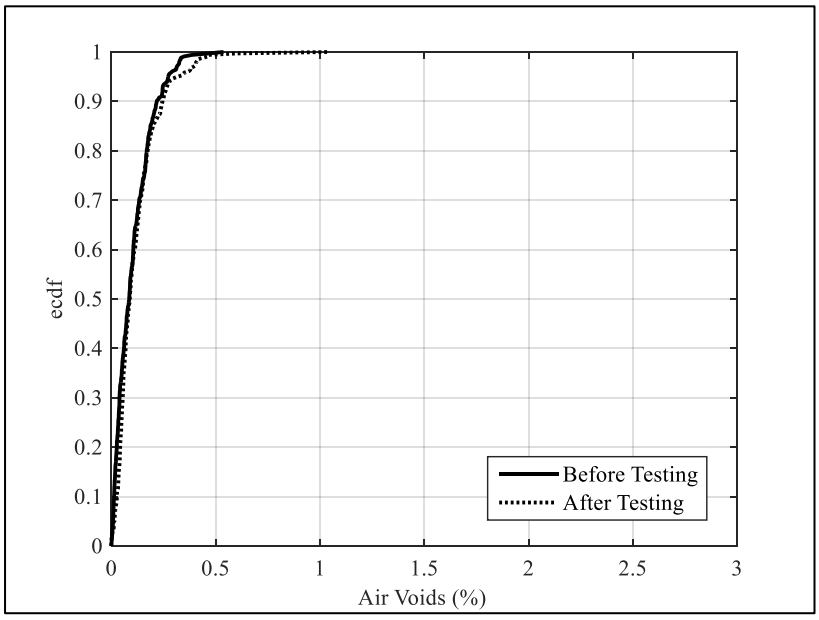

(b) Sasobit Mix

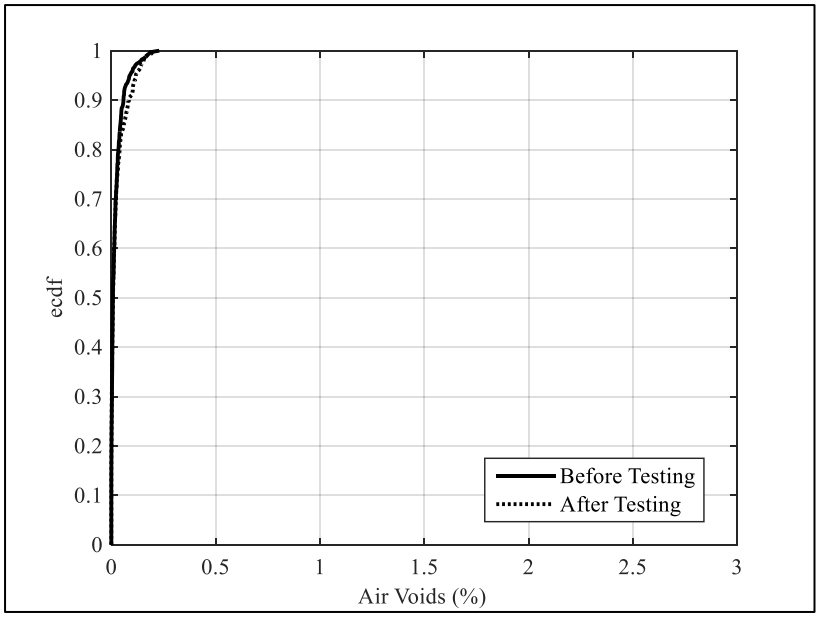

(c) Advera Mix

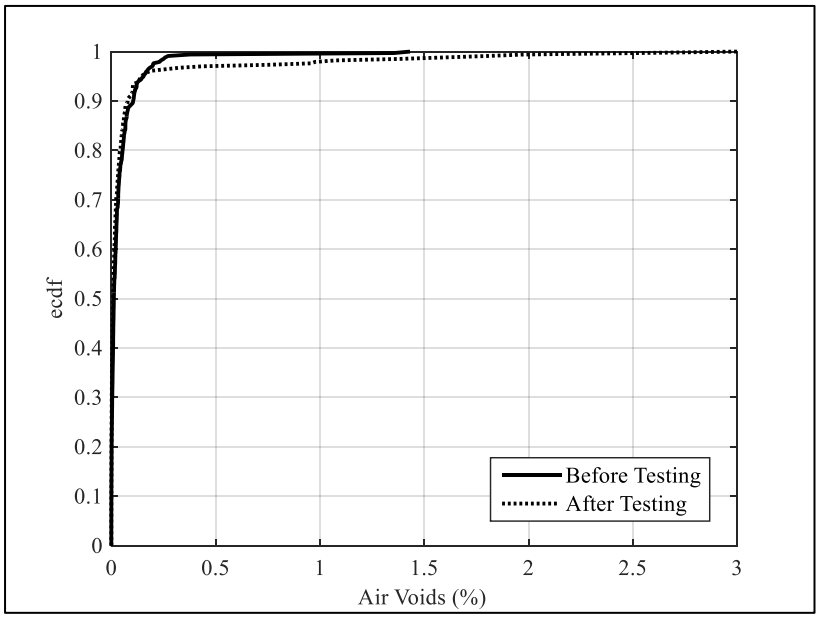

(d) Rediset Mix

Figure 110: The empirical cumulative distribution function of the air void percentage for unaged mixes

Figure 110 presents the air void (%) in ecdf curves which order the sizes in ascending order. As shown in Figure 110(a) for the Original mix, it can be noticed that small air void percentages (0.5% and below) were visible in almost 80% of the slices and they became smaller after testing. However, the other 20% of the slices which show air void percentages of 0.5% and above, became bigger after testing. The biggest air void

percentage before testing was 1% while after testing it reached 1.45%. There are two possible interpretations that can explain the behaviour of the Original mix cracking restructure. The first one is that the small-sized air voids merged after testing and generated bigger voids, as shown in the upper part of Figure 110(a). This phenomenon could be true if the voids were close to each other (or even touching) and generated an open channel between them which made them count as one big crack. The other interpretation is that the small-sized cracks were closed due to a certain force while the big cracks were opened wider. The phenomenon could be true if the certain force (i.e. stress) was in the direction of closing the small cracks and opening the big cracks. If the second interpretation is true, it indicates that the small cracks were closed due to one of the following stresses: the material might use the internal stresses to close the small-sized cracks by forcing the material to recover. The second stress the material might use is the – external – applied creep loading that pushed the material to close its small cracks by bringing their surfaces together again. To check if the first interpretation (i.e. cracks merging) is true, the study looked more deeply at the crack counts before and after testing. It was found that it is almost impossible to specify the effect of the loading on the same exact slice before and after testing, as the sample could shift up or down more than the imaging resolution (20μm). Even when performing the X-Ray CT imaging using the sample holder that ensured the position of the sample, a comparison cannot be made between a specific slice before and after the test because the slice thickness is very small and can move up or down with the repositioning. Several trials were made to specify a unique slice that can be used as a reference to shift the other slices according to it, but the testing changed the whole structure of the material's composition, and it became impossible to recognise the slice after the test. In this case, it was not possible to study the change in the number of

cracks before and after the test on each slice separately. However, it was observed that all mixes experienced an entire composition restructuring due to the mechanical testing which made it impossible to predict if the crack was closed due to external or internal stresses.

On the other hand, the empirical cdf curves of the W-FAM samples (Sasobit, Advera and Rediset mixes) did not show a significant difference before and after testing at all air void sizes. However, the tail of the curve in the Sasobit and Rediset mixes showed that the biggest air void percentages (which are less than 5% of the slices) became significantly bigger after testing. This indicates that the testing of the Sasobit mix and the Rediset mix affected the big air voids only and the small-sized air voids stayed the same. This conclusion might indicate that those additives enforced the bond inside the material not to generate more cracks, but this enforcement is weak when big-sized air voids are present.

The Advera mix showed the lowest change before and after testing. This indicates that the Advera mix had the lowest air voids among the mixes and it prevented more cracks being generated after testing. Another claim that can be made is that the repeated creep and recovery test can significantly affect the material with the high air voids, while this test has a very low effect on the congested material that has low air voids.

On the other hand, ageing affected the empirical cdf curve of the tested samples differently, as shown in Figure 111.

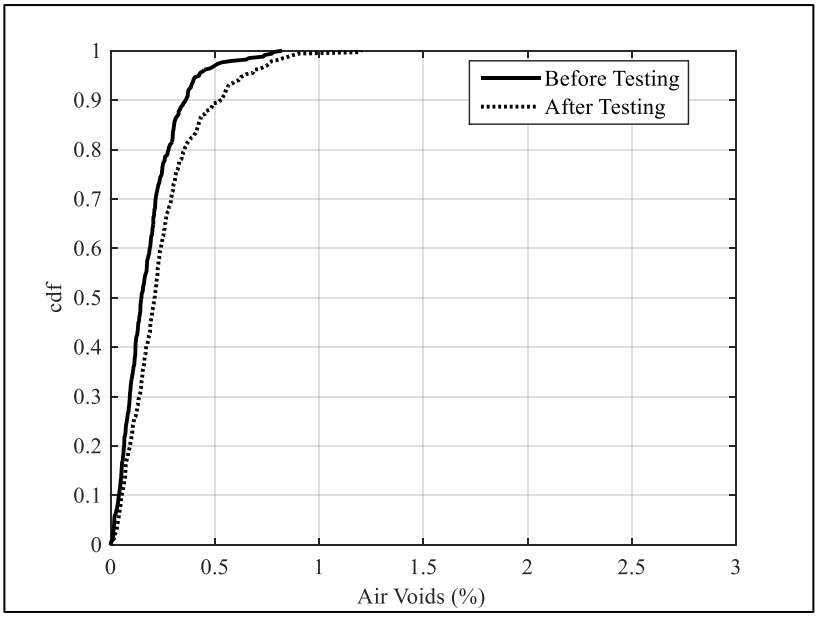

(a) Original Mix

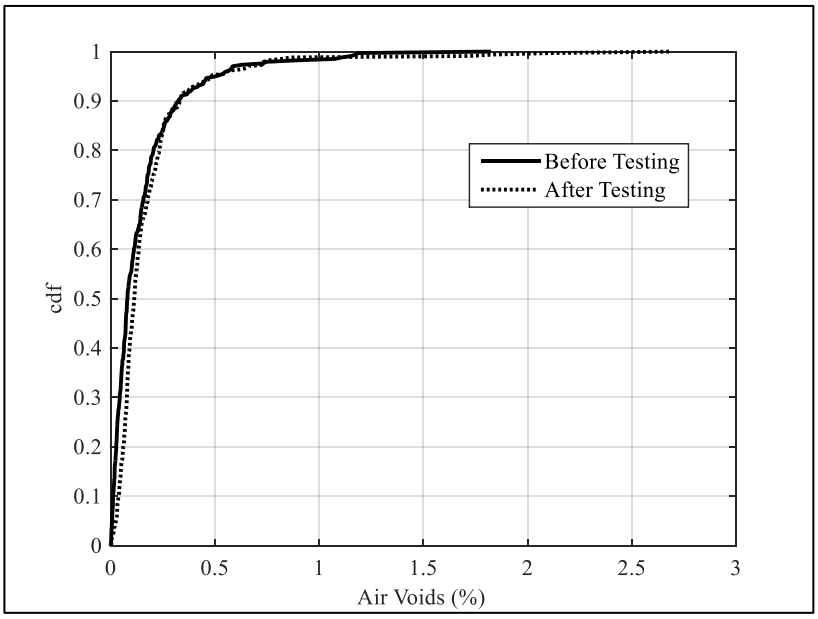

(b) Sasobit Mix

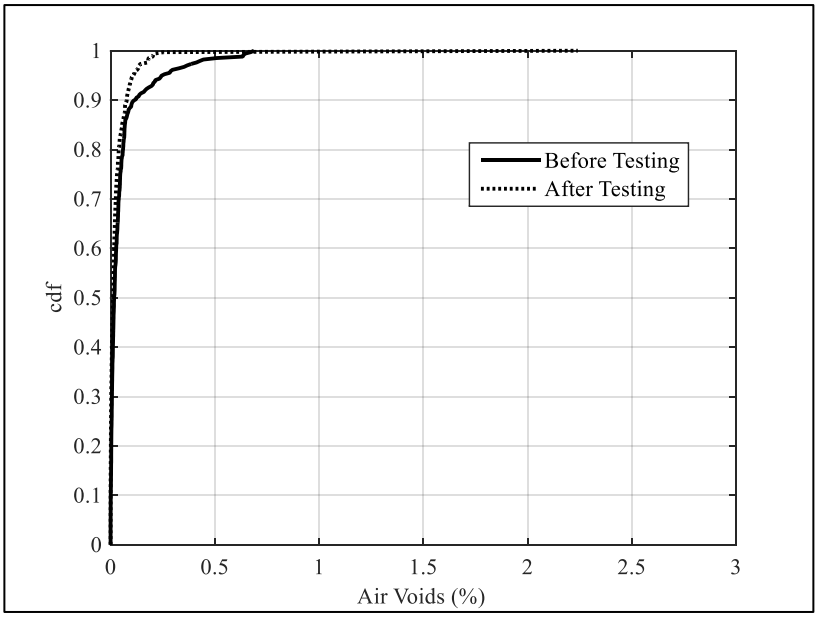

(c) Advera Mix

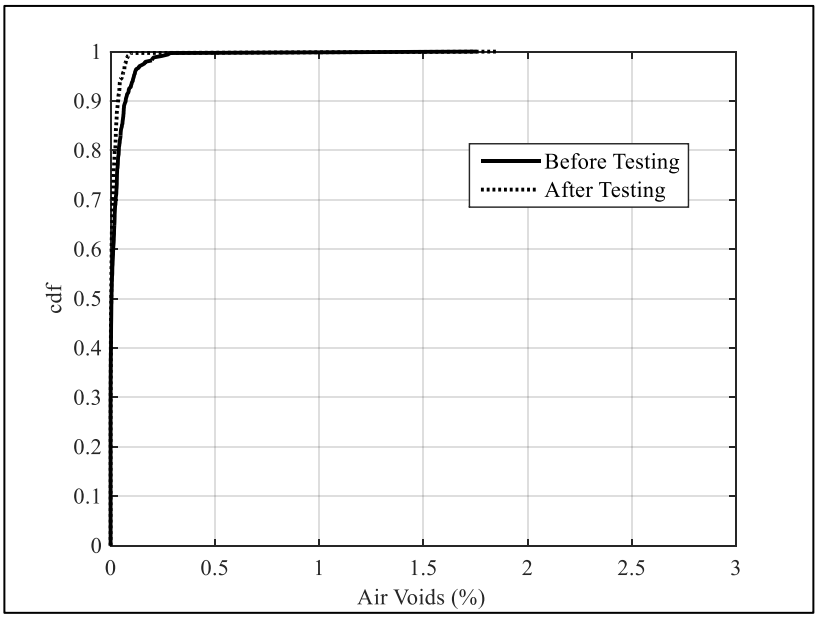

(d) Rediset Mix

Figure 111: The empirical cumulative distribution function of the air void percentage for aged mixes

The Original mix crack restructuring behaved differently with ageing. The whole curve shifted to the left, expressing a higher air void percentage covering the cross-sectional area of the slices. Unlike the unaged sample, the small and big cracks grew bigger with mechanical testing, which indicates that none of the interpretations mentioned above are applicable here. The cracks propagated after testing and

increased in size within the material after applying repeated loading. However, with the Sasobit mix, the air voids (%) did not change after the testing – except for cracks that occupied 1% and more of the cross-sectional slice area. The case is similar with the Advera and Rediset mixes, which increased the percentage of air voids of 0.5% and above.

The above results were looked at more closely by extracting the second (50%) quantile of the ecdf for the unaged samples, as presented in the bar chart in Figure 112.

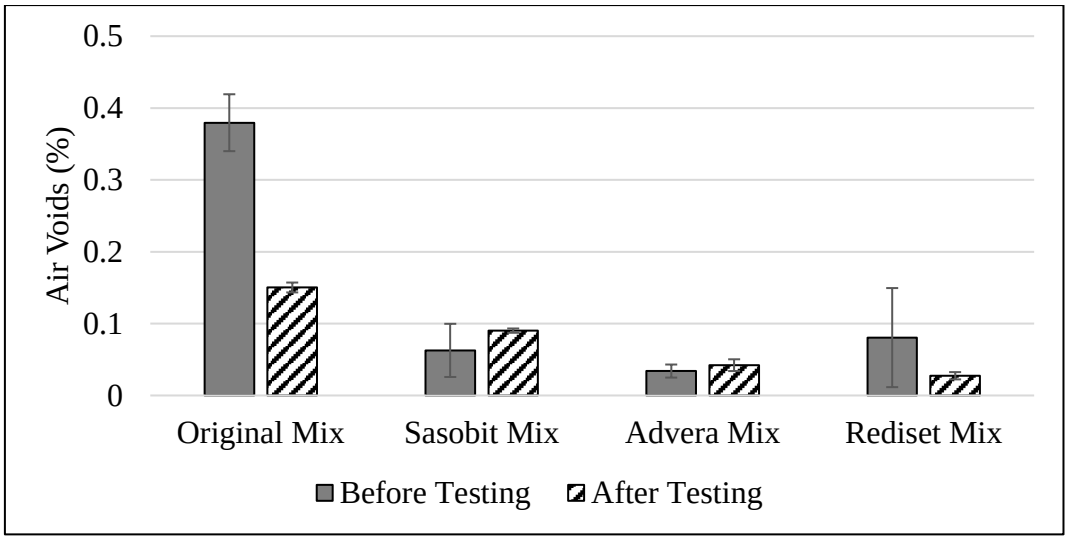

Figure 112: The air void (%) changes at 50% quantile before and after the repeated creep and recovery test for unaged mixes

As shown in Figure 112, before testing the Original mix, 50% of the slices had 0.38% or less of their cross-sectional area as cracks. However, after testing, 50% of the slices had 0.15% or less of their cross-sectional area as cracks. The error bars presented in Figure 112 are the standard deviation calculated by two replicates for each sample. The results significantly show the difference between the air void percentage before and after the repeated creep and recovery test of the Original mix. Also, it shows that the other mixes have much lower air voids (%). The difference between air voids (%) before and after testing of the Sasobit and Advera mixes can be considered as

insignificant. However, it can be noticed that, even with small air voids (%) of the Rediset mix, there is a significant difference between air void sizes before and after testing.

To evaluate the effect of ageing on the air void distribution, the second (50%) quantile was also calculated for the ecdf curves of the imaged slices and is presented in Figure 113.

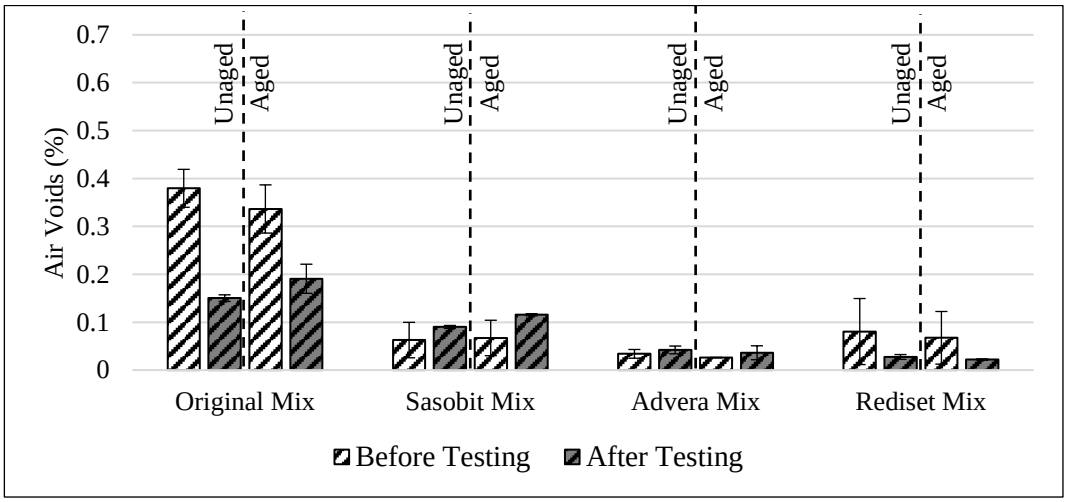

Figure 113: The air void (%) changes before and after testing at 50% quantile with unaged and aged samples of each mix

The results in Figure 113 show that the ageing of the asphalt sample did not affect the air void distribution even after testing, while the reduction in the air void sizes before and after testing was not changed significantly by ageing. The air voids (%) became lower after testing with the Original mix, as mentioned earlier. However, the ageing of the W-FAM samples did not affect the air void (%) change. This could indicate that the ageing of the asphalt material has a minor effect on the performance of air voids (%) with repeated loading while the loading has the major effect. The usage of WMA additives lowered the effect of repeated loading on the air void enlargement or contraction.

The summary of all the analysis procedure results is presented in Table 17.

Table 17: Summary of analysis procedure results for all mixes

Analysis Procedures		Original Mix	Sasobit Mix	Advera Mix	Rediset Mix
Air Void Measurements	Air Voids (%)	High	Low	Lowest	Highest
	Difference between Air Voids (%) before and after testing	Significant Difference	Insignificant Difference	Insignificant Difference	Significant Difference
Recovery Modulus		Low	Highest	High	Lowest
Reduced Damage		Low	Highest	High	Lowest

From Table 17, it can be noticed that the recovery modulus and reduced damage ranking results matched the air void measurements in all the trends. The Original and Rediset mixes had the lowest recovery modulus and reduced damage, which resulted in high air void percentages. This is also noticeable with the air void changes with testing, as the difference is significant. Alternatively, the Sasobit and Advera mixes showed the highest recovery modulus and reduced damage, which resulted in low air voids.

7.6. Summary and Conclusions

The investigation of the W-FAM samples' performance against loading damage was continued in this chapter. The damage captured during the creep and reduced during the recovery of the repeated creep and recovery test results had to be clarified in terms of crack changes. The crack study was meant to correlate the material's susceptibility to damage with the crack size changes.

In this study, W-FAM samples exposed to repeated creep and recovery test were included in an imaging study using the X-Ray CT system. The imaging was performed on the samples before and after testing in order to capture the change in the crack sizes and distribution. The imaging produced cross-sectional slices of the W-FAM samples with a 20μm resolution, which are adequate to obtain air void measurements. The slices went through several steps of digital processing techniques in order to quantify the air void sizes in each slice. These techniques segmented the slices produced by the X-Ray CT imaging and measured the air voids as a percentage of the total slice cross-sectional area.

The results of the imaging process showed clearly the differences between the FAM samples prepared with different WMA additives. The differences were generated through using different additives and preparing them at different temperatures, while all other preparation parameters were unchanged. The difference between mixes was very clear in terms of air voids, where the Advera mix showed the lowest percentage among the mixes. However, all W-FAM samples showed lower air voids than the Original mix, indicating that, when using the WMA additives, the mix design should always be amended to ensure the designed air voids are met.

The addition of WMA additives showed its benefits in controlling the change in air void enlargement and contraction due to repeated loading, while the Original mix intensively changed the air voids after the repeated creep and recovery test was applied. However, the ageing of the FAM samples using the weathering machine showed insignificant difference in terms of air void changes. Although fatigue testing – presented in Chapter 3 – showed that there is no significant difference between the Original and the W-FAM mixes regarding fatigue resistance, the results from X-Ray

CT imaging showed the differences clearly between the mixes regarding air void distribution and change in cracks after testing.

Furthermore, the recovery modulus and reduced damage for each mix at different ageing levels were compared with the cracking behaviour. The results showed good correlation between the cracks in the samples. The controlled mix (Original mix) and Rediset mix showed the highest tendency to change the air void sizes after being exposed to repeated loading. The mixes prepared with Sasobit and Advera additives showed higher control of the mix air voids and showed minor changes after the loading. It can be concluded that material's properties such as the Recovery Modulus can be used to predict the air void behaviour, where having a high recovery modulus can control the air void sizes and limit their changes due to loading. In addition, it was found that addition of WMA additives reduced the air void sizes in the mix that would affect the mix design.

8. Conclusions and Recommendations

8.1. Conclusions

This thesis focused on evaluating the performance and responses of asphalt materials mixed with warm mix asphalt (WMA) technologies and study the feasibility of using these technologies in the State of Qatar. The emphasis is the development of a new approach for analysis of damage based on the results of creep and recovery test. In addition, the thesis evaluated a new ageing protocol that incorporates the effect of heat and ultraviolet (UV) light. All experiments utilised materials that are available for road construction in the State of Qatar.

The literature review showed that only a few studies were conducted on WMA in the Middle East region. These studies attempted to review basic properties and did not address performance against major distresses such as fatigue cracking and performance deformation. In addition, current ageing methods do not include the effect of UV light, which is a concern for the ageing of construction materials in climates such as that in the State of Qatar.

The implementation of WMA technology in the State of Qatar would contribute to the national goals of having eco-friendly construction practices. However, this is not feasible without conducting research studies to evaluate WMA using local materials and prevailing climatic conditions. In this thesis, a thorough investigation was conducted on the WMA technology in order to achieve a comprehensive understanding of its behaviour.

The study started by evaluating the rheological properties of asphalt binders modified using different warm mix additives. The WMA additives were mixed with bitumens

that are used in the asphalt construction industry. The results showed that the addition of Sasobit has a noticeable effect on the performance grading (PG) of the asphalt bitumen while Advera has no effect. The Multiple Stress Creep Recovery (MSCR) test was conducted on asphalt bitumen and the results were analysed using a nonlinear viscoelastic and plasto-viscoelastic approach. The Sasobit additive increased bitumen stiffness and improved permanent deformation resistance.

The resistance to fatigue cracking was evaluated using dynamic mechanical testing of Fine Aggregate Mixtures (FAM), which consist of asphalt binder and fine aggregate particles. Overall, the results showed that using WMA additives had no significant effect on the fatigue resistance. The stiffness gained from using Sasobit did not adversely affect fatigue resistance.

In order to account for the influence of ageing on WMA performance, this study utilised a new ageing protocol that employs UV light and heat as sources of ageing. The Qatar's climate was simulated in an accelerated weathering machine. The UV index in Qatar is considered high most of the year and adversely affects the physical properties of materials leading to their accelerated degradation. The combination of UV light and heat ageing caused an increase the shear modulus and reduced the phase angle of all FAM samples. The Sasobit mix exhibited the smallest percentage increase in shear modulus (3% increase), while the original mix without a warm mix additive experienced the highest increase in modulus (12% increase).

This research study developed a new testing and analysis approach that characterises damage due to repeated loading and recovered damage during unloading. As expected, samples experienced an increase in damage with more loading cycles during the creep phase. The analysis approach was able to detect differences in damage and recovery

among the various WMA materials. The results showed that the Sasobit mix experienced the highest damage during the creep phase; however, it had the highest ability to recover that damage during the recovery phase. Advera mix showed lower damage during the creep phase than the Sasobit mix did; however, the Advera mix had less ability to recover damage during unloading. The Original and Rediset mixes, which showed low creep damage, but they did not recover that damage during the unloading phase. This is especially true during the first few cycles.

X-Ray CT imaging was conducted on the samples before and after applying the test in order to examine the effect of repeated loading test on the W-FAM material's damage. It was noticed that air void sizes decreased dramatically when WMA additives were used indicating that WMA mixes have better compactability than HMA mixes. The repeated creep and recovery test caused an increase in air void sizes in the Original mix without warm mix additives. However, there was little change in air void sizes in the Sasobit and Advera mixes after it was subjected to loading. The Rediset mix also showed a significant change in the air void sizes after loading, but air voids were still smaller than the Original mix. In addition, the ageing of the asphalt material did not show a noteworthy difference in the air void percentages.

The results of the recovery modulus matched the trend of the crack measurements obtained by the X-Ray CT imaging. The mixes that had the lowest recovery modulus also experienced the highest change in air void percentages and vice versa.

The benefits of using WMA additives are clear and significant. It could be a game changer in the market of modified bitumens and road construction in the Middle East. The State of Qatar can avail from the implementation of WMA in the local projects

by reducing energy utilised during construction, minimising the environmental impact of road construction, and reducing the construction cost.

8.2. Recommendations

This thesis has developed several promising analysis approaches and tools. Future studies can focus on further enhancements of certain aspects of these outcomes. First, the ageing protocol proposed in this study can be improved by simulating several years of ageing in the accelerated weathering chamber. It can also be compared with actual outdoor ageing and conventional lab ageing (i.e. PAV). The effect of UV light can be further discerned by comparing the effects of heat cycles with others that involve both heat and UV light.

The proposed repeated creep and recovery test procedure can be refined by excluding the step-loadings for the measurement of internal stresses and focusing on the strain responses during the creep and recovery phases. The suggested 'reduced damage' parameter can be investigated further during the unloading stage as it could be related to material healing potential.

Finally, the proposed imaging procedure with the X-Ray CT system can be used to study a full mixture (not only FAM samples). In addition, other tools (such as Avizo software) can be used to verify the air void measurements obtained using MATLAB in order to fully investigate air void change as a result of repeated loading. The air voids measurements performed in this thesis focused on a specific portion of the sample and presented air voids percentage based on the area of voids in each slice. These measurements can be verified with actual volume of air voids and compared with lab density measurements of the same samples.

Publications

[1] M. Sadeq, E. Masad, H. Al-Khalid, O. Sirin, I. Menapace, and M. d'Eurydice, "New Protocol Utilising the Accelerated Weathering Tester to Age Fine Asphalt Mixtures with Warm Mix Asphalt Additives," *7th International European Asphalt Technology Association Conference*, Zurich, June 2017.

[2] M. Sadeq, H. Al-Khalid, E. Masad, and O. Sirin, "Comparative evaluation of fatigue resistance of warm fine aggregate asphalt mixtures," *Construction and Building Materials*, vol. 109, pp. 8–16, Apr. 2016.

[3] M. Sadeq, E. Masad, H. Al-Khalid, O. Sirin, and D. Little, "Rheological Evaluation of Short- and Long-Term Performance for Warm Mix Asphalt (WMA) Binders," in *8th RILEM International Symposium on Testing and Characterization of Sustainable and Innovative Bituminous Materials*, vol. 11, F. Canestrari and M. N. Partl, Eds. Dordrecht: Springer Netherlands, 2016, pp. 129–139.

[4] M. Sadeq, E. Masad, H. Al-Khalid, O. Sirin, and L. Mehrez, "Linear and nonlinear viscoelastic and viscoplastic analysis of asphalt binders with warm mix asphalt additives," *International Journal of Pavement Engineering*, vol. 8436, no. August, pp. 1–8, 2016.

[5] M. Sadeq, E. Masad, H. Al-Khalid, and O. Sirin, "Assessment of linear and nonlinear viscoelastic responses of warm-mix asphalt binders," in *6th International Conference Bituminous Mixtures & Pavements*, 2015, pp. 27–32.

References

AASHTO - M 320 (2009) ‘Performance-Graded Asphalt Binder’, in. American Association of State Highway and Transportation Officials.

AASHTO - T 240 (2009) ‘Effect of Heat and Air on a Moving Film of Asphalt Binder (Rolling Thin-Film Oven Test)’, in. USA: American Association of State Highway and Transportation Officials.

AASHTO - T 315 (2009) ‘Determining the Rheological Properties of Asphalt Binder Using a Dynamic Shear Rheometer (DSR)’, in. American Association of State Highway and Transportation Officials.

AASHTO - TP 70 (2009) ‘Multiple Stress Creep Recovery (MSCR) Test of Asphalt Binder Using a Dynamic Shear Rheometer (DSR)’, in. American Association of State Highway and Transportation Officials.

Abu Al-Rub, R. K., Darabi, M. K., Little, D. N. and Masad, E. a. (2010) ‘A micro-damage healing model that improves prediction of fatigue life in asphalt mixes’, *International Journal of Engineering Science*. Elsevier Ltd, 48(11), pp. 966–990. doi: 10.1016/j.ijengsci.2010.09.016.

Adorjányi, K. and Füleki, P. (2011) ‘Performance evaluation of bitumens at high temperature with multiple stress creep recovery test’, *Hungarian journal of industrial chemistry veszprém*, 39(2), pp. 195–199.

Ahlquist, C. N. and Nix, W. D. (1971) ‘The measurement of internal stresses during creep of al and Al-Mg alloys’, *Acta Metallurgica*, 19(4), pp. 373–385. doi: http://dx.doi.org/10.1016/0001-6160(71)90105-2.

Ahmed, T. M. and Khalid, H. A. (2015) ‘A new approach in fatigue testing and evaluation of hot mix asphalt using a dynamic shear rheometer’, in *6th International Conference Bituminous Mixtures & Pavements*. Thessaloniki: Taylor & Francis Group, pp. 351–359.

Airey, G. D. (2003) ‘State of the art report on ageing test methods for bituminous pavement materials’, *International Journal of Pavement Engineering*, 4(December), pp. 165–176. doi: 10.1080/1029843042000198568.

AkzoNobel (2014) *Rediset LQ - AkzoNobel Asphalt Applications*. Available at: http://sc.akzonobel.com/en/asphalt/Pages/new-product-rediset-LQ.aspx.

Al-Rawashdeh, A. (2008) *Performance assessment of warm mix asphalt (WMA) pavements*. Available at: http://scholar.google.com/scholar?hl=en&btnG=Search&q=intitle:Performance+Assessment+of+Warm+Mix+Asphalt+(WMA)+Pavements#0 (Accessed: 12 September 2013).

Arega, Z. a. Z., Bhasin, A. and Kesel, T. D. T. (2013) ‘Influence of extended aging on the properties of asphalt composites produced using hot and warm mix methods’, *Construction and Building Materials*. Elsevier Ltd, 44, pp. 168–174. doi: 10.1016/j.conbuildmat.2013.02.081.

Arega, Z. and Bhasin, A. (2012) *Final Report: Binder Rheology and Performance in*

Warm Mix Asphalt. Texas, USA: Texas Department of Transportation. Available at: http://trid.trb.org/view.aspx?id=1225677 (Accessed: 7 September 2013).

Arega, Z., Bhasin, A., Motamed, A. and Turner, F. (2011) 'Influence of Warm-Mix Additives and Reduced Aging on the Rheology of Asphalt Binders with Different Natural Wax Contents', *Journal of Materials in Civil Engineering*, 23(10), pp. 1453–1459. doi: 10.1061/(ASCE)MT.1943-5533.0000315.

Artamendi, I. and Khalid, H. (2005) 'Characterization of fatigue damage for paving asphaltic materials', *Fatigue & Fracture of Engineering Materials and Structures*, 28(12), pp. 1113–1118. doi: 10.1111/j.1460-2695.2005.00949.x.

ASTM - G154 - 12 (2012) 'Standard Practice for Operating Fluorescent Ultraviolet (UV) Lamp Apparatus for Exposure of Nonmetallic Materials'. doi: 10.1520/G0154-12.

ASTM - G154 - 12 (2014) *Operating Fluorescent Ultraviolet (UV) Lamp Apparatus for Exposure of Nonmetallic Materials*. doi: 10.1520/G0154-12.

ASTM Standard D 6921 (2008) 'Standard Practice for Accelerated Aging of Asphalt Binder Using a Pressurized Aging Vessel (PAV)', *Www.Astm.Org*, pp. 1–6. doi: 10.1520/D6521-08.Copyright.

Ates, M., Temel, S., Öz, P. H. and Köroglu, H. J. (2015) 'Investigating rheological effects of WMA additives by means of a viscometer and a newly designed workability device', in *6th International Conference Bituminous Mixtures & Pavements*. Thessaloniki: Taylor & Francis Group, pp. 61–64.

Atlas (2015) *63 Years of UV Exposure in 1 Year*. Available at: http://atlas-mts.com/news-events/news/news-detail/?tx_ttnews%5Btt_news%5D=33&cHash=dc84f987bfaf5e20cbde39f5f48c6107.

Atlas Electric Devices Company (2001) *Weathering Testing Guidebook*.

Bahia, H., Hanson, D., Zeng, M. and Zhai, H. (2001) *Characterization of modified asphalt binders in superpave mix design*. NATIONAL COOPERATIVE HIGHWAY RESEARCH PROGRAM. Available at: http://trid.trb.org/view.aspx?id=692511 (Accessed: 1 October 2013).

Beake, B. (2006) 'Modelling indentation creep of polymers: a phenomenological approach', *Journal of Physics D: Applied Physics*, 39(20), p. 4478. Available at: http://stacks.iop.org/0022-3727/39/i=20/a=027.

Bhasin, A., Castelo Branco, V. T., Masad, E. and Little, D. N. (2009) 'Quantitative Comparison of Energy Methods to Characterize Fatigue in Asphalt Materials', *Journal of Materials in Civil Engineering*, 21(2), pp. 83–92. doi: 10.1061/(ASCE)0899-1561(2009)21:2(83).

Bhasin, A., Little, D. N., Bommavaram, R. and Vasconcelos, K. (2008) 'A Framework to Quantify the Effect of Healing in Bituminous Materials using Material Properties', *Road Materials and Pavement Design*, 9(sup1), pp. 219–242. doi: 10.1080/14680629.2008.9690167.

Bhasin, A., Palvadi, S. and Little, D. N. (2011) 'Influence of Aging and Temperature on Intrinsic Healing of Asphalt Binders', *Transportation Research Record: Journal of*

the Transportation Research Board, 2207(1), pp. 70–78. doi: 10.3141/2207-10.

Bocci, M. and Cerni, G. (2000) 'The ultraviolet radiation in short-and long-term aging of bitumen', in *PROCEEDINGS OF THE PAPERS SUBMITTED FOR REVIEW AT 2ND EURASPHALT AND EUROBITUME CONGRESS, HELD 20-22 SEPTEMBER 2000, BARCELONA, SPAIN. BOOK 1-SESSION 1*.

Bolotin, V. V. (1999) *Mechanics of Fatigue*. Mechanical. Edited by CRC Mechanical Engineering Series. Minneaplies: CRC Press.

Bommavaram, R. R., Bhasin, A. and Little, D. N. (2009) 'Determining Intrinsic Healing Properties of Asphalt Binders', *Transportation Research Record: Journal of the Transportation Research Board*, 2126(1), pp. 47–54. doi: 10.3141/2126-06.

Branco, C., Franco, V. and BRANCO, V. T. F. C. (2008) *A unified method for the analysis of nonlinear viscoelasticity and fatigue cracking of asphalt mixtures using the dynamic mechanical analyzer*. Texas A&M University. Available at: http://repository.tamu.edu/handle/1969.1/ETD-TAMU-3136 (Accessed: 3 March 2014).

Braz, D., Lopes, R. . and Motta, L. M. . (2004) 'Research on fatigue cracking growth parameters in asphaltic mixtures using computed tomography', *Nuclear Instruments and Methods in Physics Research Section B: Beam Interactions with Materials and Atoms*, 213, pp. 498–502. doi: 10.1016/S0168-583X(03)01610-0.

Breen, J. J. and Stephens, J. E. (1967) *The Glass Transition Temperature and the mechanical properties of asphalt*.

Brinson, H. F. and Brinson, L. C. (2008) *Polymer engineering science and viscoelasticity*. Springer.

Button, J., Estakhri, C. and Wimsatt, A. (2007) 'A synthesis of warm mix asphalt', 7(2). Available at: http://swutc.tamu.edu/publications/technicalreports/0-5597-1.pdf (Accessed: 12 September 2013).

Butz, T., Rahimian, I. and Hildebrand, G. (2001) 'Modification of road bitumens with the Fischer-Tropsch paraffin Sasobit (R)', *Journal of Applied Asphalt Binder Technology*, 1(2).

Cao, D. and Ji, J. (2011) 'Evaluation of the Long-term Properties of Sasobit Modified Asphalt', 4(6), pp. 384–391.

Caro, S., Beltrán, D. P., Alvarez, A. E. and Estakhri, C. (2012) 'Analysis of moisture damage susceptibility of warm mix asphalt (WMA) mixtures based on Dynamic Mechanical Analyzer (DMA) testing and a fracture mechanics model', *Construction and Building Materials*. Elsevier Ltd, 35, pp. 460–467. doi: 10.1016/j.conbuildmat.2012.04.035.

Castelo Branco, V. T. F., Masad, E., Bhasin, A. and Little, D. N. (2008) 'Fatigue Analysis of Asphalt Mixtures Independent of Mode of Loading', *Transportation Research Record: Journal of the Transportation Research Board*, 2057(1), pp. 149–156. doi: 10.3141/2057-18.

chemistryland.com (2015) *chemistryland.com*. Available at: http://www.chemistryland.com/.

Cheung, C. and Cebon, D. (1997) ‘Deformation Mechanisms of Pure Bitumen’, *Journal of Materials in Civil Engineering*, 9(3), pp. 117–129. doi: 10.1061/(ASCE)0899-1561(1997)9:3(117).

Cheung, C. and Cebon, D. (1997) ‘Thin Film Deformation Behavior of Power-Law Creeping Materials’, *Journal of Engineering Mechanics*, 123(11), pp. 1138–1152. doi: 10.1061/(ASCE)0733-9399(1997)123:11(1138).

Chowdhury, A. and Button, J. (2008) *A Review of Warm Mix Asphalt*. College Station, TX: Texas Transportation Institute.

D’Angelo, J. and Dongre, R. (2002) ‘Superpave binder specifications and their performance relationship to modified binders’, in. Canadian Technical Asphalt Association.

D’Angelo, J., Harm, E., Bartoszek, J., Baumgardner, G. and Corrigan, M. (2008) *Warm-Mix Asphalt: European Practice*. Washington, D.C.: Federal Highway Administration.

D’Angelo, J., Kluttz, R. and Dongre, R. (2007) ‘Revision of the Superpave High Temperature Binder Specification: The Multiple Stress Creep Recovery Test (With Discussion)’, *Journal of the …*. Available at: http://trid.trb.org/view.aspx?id=839413 (Accessed: 9 February 2014).

D’Angelo, J., Kluttz, R., Dongre, R. and Stephens, K. (2007) ‘Revision of the Superpave High Temperature Binder Specification: The Multiple Stress Creep Recovery Test (With Discussion)’, *Journal of the Association of Asphalt Paving Technologists*, 76, pp. 123–162. Available at: http://trid.trb.org/view.aspx?id=839413 (Accessed: 22 October 2014).

Darabi, M. K., Abu Al-Rub, R. K. and Little, D. N. (2012) ‘A continuum damage mechanics framework for modeling micro-damage healing’, *International Journal of Solids and Structures*. Elsevier Ltd, 49(3–4), pp. 492–513. doi: 10.1016/j.ijsolstr.2011.10.017.

Darabi, M. K., Abu Al-Rub, R. K., Masad, E. a. and Little, D. N. (2013) ‘Constitutive modeling of fatigue damage response of asphalt concrete materials with consideration of micro-damage healing’, *International Journal of Solids and Structures*. Elsevier Ltd, 50(19), pp. 2901–2913. doi: 10.1016/j.ijsolstr.2013.05.007.

Das, P. K., Tasdemir, Y. and Birgisson, B. (2012) ‘Low temperature cracking performance of WMA with the use of the Superpave indirect tensile test’, *Construction and Building Materials*, 30, pp. 643–649. doi: 10.1016/j.conbuildmat.2011.12.013.

Davidson, R. R., Bullin, J. A., Glover, C. J., Jr., B. L. B., Jemison, H. B., Kyle, A. L. G. and Cipione, C. A. (1989) *Development of Gel Permeation Chromatography, Infrared and Other Tests to Characterize Asphalt Cements and Correlate with Field Performance*. College Station, Texas: Texas Transportation Institute. Available at: internal-pdf://216.174.164.44/458-1F-V1.pdf.

Van Dijk, W. and Visser, W. (1977) ‘Energy approach to fatigue for pavement design’, in *Association of Asphalt Paving Technologists Proc*.

Van Dijk, W. and Visser, W. (1977) ‘The Energy Approach to Fatigue for Pavement’, *Asphalt Paving Technology*, 46, pp. 1–40.

Dongre, R. and D'Angelo, J. (2003) 'Evaluation of Different Parameters for Superpave High Temperature Binder Specification Based on Rutting Performance in the Accelerated Loading Facility at FHWA', *82nd Annual Meeting of Transportation Research Board*, (August 2002), pp. 39–46. Available at: https://www.scopus.com/inward/record.uri?eid=2-s2.0-1642476671&partnerID=40&md5=20b1324f00d42ac262966dbc9d8d2725.

Edler, A. C., Hattingh, M. M., Servas, V. P. and Marais, C. P. (1985) 'USE OF AGING TESTS TO DETERMINE THE EFFICACY OF HYDRATED LIME ADDITIONS TO ASPHALT IN RETARDING ITS OXIDATIVE HARDENING (WITH DISCUSSION)', in *Association of Asphalt Paving Technologists Proc*.

Elber, W. (1971) *Damage Tolerance in Aircraft Structures*. Edited by M. Rosenfeld. 100 Barr Harbor Drive, PO Box C700, West Conshohocken, PA 19428-2959: ASTM International. doi: 10.1520/STP486-EB.

Feipeng, V. S. P. and Bradley, X. (2012) 'Effects of long-term aging on moisture sensitivity of foamed WMA mixtures containing moist aggregates', pp. 251–264. doi: 10.1617/s11527-011-9763-4.

Felhos, D., Xu, D., Schlarb, A. K., Váradi, K. and Goda, T. (2008) 'Viscoelastic characterization of an EPDM rubber and finite element simulation of its dry rolling friction', *Express Polymer Letters*, 2(3), pp. 157–164. doi: 10.3144/expresspolymlett.2008.21.

Fernández-Gómez, W. D., Rondón Quintana, H. A., Daza, C. E. and Reyes Lizcano, F. A. (2014) 'The effects of environmental aging on Colombian asphalts', *Fuel*, 115, pp. 321–328. doi: 10.1016/j.fuel.2013.07.009.

Franck, A. J. (2014) *Normal stresses in shear flow*, *TA Instruments*. AN007.

Ghuzlan, K. A. and Carpenter, S. H. (2000) 'Energy-derived, damage-based failure criterion for fatigue testing', *Transportation Research Record*, (1723), pp. 141–149.

Ghuzlan, K. and Carpenter, S. (2000) 'Energy-Derived, Damage-Based Failure Criterion for Fatigue Testing', *Transportation Research Record*, 1723(1), pp. 141–149. doi: 10.3141/1723-18.

Gie, Y. and Chan, B. (1984) 'Non-newtonian shear viscosity, normal stress coefficients and corresponding states in rheology', *Physics Letters*, 101A(7), pp. 7–11. Available at: http://www.sciencedirect.com/science/article/pii/037596018490851X (Accessed: 19 August 2014).

Golalipour, A. (2011) *Modification of Multiple Stress Creep and Recovery Test Procedure and Usage in Specification*. University of Wisconsin – Madison. Available at: http://144.92.161.87/handle/1793/56398 (Accessed: 22 October 2013).

Gordon, A., Rahimzadeh, B. and Collop, A. (2002) 'linear viscoelastic limits of bituminous binders'. Asphlt paving technology, pp. 89–115.

Gordon, A., Rahimzadeh, B. and Collop, A. C. (2004) 'Linear Rheological Behavior of Bituminous Paving Materials', *Journal of Materials in Civil Engineering*, 16(3), pp. 212–220. doi: 10.1061/(ASCE)0899-1561(2004)16:3(212).

Greensted, A. (2010) *Otsu Thresholding*, *The Lab Book Pages*. Available at:

http://www.labbookpages.co.uk/software/imgProc/otsuThreshold.html (Accessed: 17 February 2017).

Grossman, G. W. (2011) *Correlation of Laboratory to Natural Weathering*. Available at: Technical Bulletin LU-0824.

Gutierrez-Lemini, D. (2014) 'Constitutive Equations in Hereditary Integral Form', in *Engineering Viscoelasticity*. Boston, MA: Springer US, pp. 23–52. doi: 10.1007/978-1-4614-8139-3_2.

Haggag, M. M., Mogawer, W. S. and Bonaquist, R. (2011) 'Fatigue Evaluation of Warm-Mix Asphalt Mixtures', *Transportation Research Record: Journal of the Transportation Research Board*, 2208(1), pp. 26–32. doi: 10.3141/2208-04.

Hagos, E. (2008) *The effect of aging on binder properties of porous asphalt concrete*. Delft University of Technology. Available at: http://www.ct.tudelft.nl/fileadmin/Faculteit/CiTG/Over_de_faculteit/Afdelingen/Afdeling_Bouw/-_Secties/Sectie_Weg_en_Railbouwkunde/-_Nieuws/-_Colloquia/doc/presentation_Hagos.pdf (Accessed: 26 August 2014).

Hamzah, M. O., Golchin, B., Jamshidi, A. and Chailleux, E. (2014) 'Evaluation of Rediset for use in warm-mix asphalt: a review of the literatures', *International Journal of Pavement Engineering*, 8436(June 2015), pp. 1–23. doi: 10.1080/10298436.2014.961020.

Harold L. Von Quintus, Chuck S. Hughes and James A. Scherocman (1992) 'NCHRP Asphalt-Aggregate Mixture Analysis System', *Transportation Research Record*, pp. 90–99.

Herb, W. and Velasquez, R. (2006) *Simulation and characterization of asphalt pavement temperatures, Minnesota Department of Transportation (MNDOT)*. Available at: http://www.tandfonline.com/doi/abs/10.1080/14680629.2009.9690190 (Accessed: 19 May 2014).

Herman, G. T. (2009) *Fundamentals of computerized tomography: image reconstruction from projections*. Springer Science & Business Media.

Hesp, S. a. M., Soleimani, A., Subramani, S., Phillips, T., Smith, D., Marks, P. and Tam, K. K. (2009) 'Asphalt pavement cracking: analysis of extraordinary life cycle variability in eastern and northeastern Ontario', *International Journal of Pavement Engineering*, 10(3), pp. 209–227. doi: 10.1080/10298430802343169.

Howson, J., Masad, E. and Bhasin, A. (2007) 'System for the Evaluation of Moisture Damage Using Fundamental Material Properties', 7(2). Available at: http://d2dtl5nnlpfr0r.cloudfront.net/tti.tamu.edu/documents/0-4524-1.pdf (Accessed: 12 September 2013).

Hsieh, C. H. (2012) *Procedure and Analysis of Mineral Samples Using High Resolution X-Ray Micro Tomography*. The University of Utah.

Hu, G., Tay, A. A. O., Zhang, Y., Zhu, W. and Chew, S. (2006) 'Characterization of viscoelastic behaviour of a molding compound with application to delamination analysis in IC packages', *2006 8th Electronics Packaging Technology Conference*, pp. 53–59. doi: 10.1109/EPTC.2006.342690.

Huang, C.-W., Abu Al-Rub, R. K., Masad, E. A. and Little, D. N. (2011) 'Three-

Dimensional Simulations of Asphalt Pavement Permanent Deformation Using a Nonlinear Viscoelastic and Viscoplastic Model', *Journal of Materials in Civil Engineering*, 23(1), pp. 56–68. doi: 10.1061/(ASCE)MT.1943-5533.0000022.

Huang, Y. H. (2004) *Pavement Analysis and Design*. Second Edi. Pearson Education.

Hurley, G. and Prowell, B. (2005) 'Evaluation of Sasobit® for use in warm mix asphalt', *NCAT report*, (June). Available at: http://www.ncat.us/files/reports/2005/rep05-06.pdf (Accessed: 3 July 2013).

Hurley, G. and Prowell, B. (2006a) 'Evaluation of Evotherm for use in warm mix asphalt', *NCAT report*, (June). Available at: http://www.structural-engineering-courses.bece.auburn.edu/research/centers/ncat/files/reports/2006/rep06-02.pdf (Accessed: 1 December 2013).

Hurley, G. and Prowell, B. (2006b) 'Evaluation of potential processes for use in warm mix asphalt', *Journal of the Association of Asphalt Paving Technologists*. Available at: http://www.warmmix.net/submissions/10_20071127_Evaluation_of_Potential_Processes.pdf (Accessed: 12 September 2013).

Inanc, F., Gopalakrishnan, K. and Ceylan, H. (2007) 'Using X-ray computed tomography to study paving materials', *Proceedings of the ICE - Construction Materials*, 160(1), pp. 15–23. doi: 10.1680/coma.2007.160.1.15.

International Commission on Illumination (1989) *CIE 085-1989 Solar Spectral Irradiance*.

Jamshidi, A., Hamzah, M. and You, Z. (2013) 'Performance of warm mix asphalt containing Sasobit®: state-of-the-art', *Construction and Building Materials*, 38, pp. 530–553. Available at: http://www.sciencedirect.com/science/article/pii/S0950061812005983 (Accessed: 7 September 2013).

Kane, M., Zhao, D., Chailleux, E., Delarrard, F. and Do, M. T. (2013) 'Development of an accelerated pavement test reproducing the effect of natural ageing on skid resistance', *Road Materials and Pavement Design*, 14(1), pp. 126–140. doi: 10.1080/14680629.2012.749804.

Karki, P., Li, R. and Bhasin, a. (2014) 'Quantifying overall damage and healing behaviour of asphalt materials using continuum damage approach', *International Journal of Pavement Engineering*, 16(4), pp. 350–362. doi: 10.1080/10298436.2014.942993.

Khan, R. and Collop, A. C. (2010) 'The Use of X-Ray Computed Tomography to Characterize Microdamage in Asphalt', *Road Materials and Pavement Design*, 11(January 2015), pp. 89–109. doi: 10.1080/14680629.2010.9690328.

Khodaii, A., Tehrani, H. K. and Haghshenas, H. F. (2012) 'Hydrated lime effect on moisture susceptibility of warm mix asphalt', *Construction and Building Materials*. Elsevier, 36, pp. 165–170.

Kim, B. and Roque, R. (2006) 'Evaluation of healing property of asphalt mixtures', *Transportation Research Record: Journal of the Transportation Research Board*, 1970, pp. 84–91. Available at:

http://trb.metapress.com/index/q291148864545wgn.pdf (Accessed: 20 June 2014).

Kim, H., Lee, S.-J. and Amirkhanian, S. N. (2010) 'Effects of warm mix asphalt additives on performance properties of polymer modified asphalt binders', *Canadian Journal of Civil Engineering*, 37(1), pp. 17–24. doi: 10.1139/L09-118.

Kim, Y., Little, D. and Lytton, R. (2002) 'Use of Dynamic Mechanical Analysis (DMA) to Evaluate the Fatigue and Healing Potential of Asphalt Binders in Sand Asphalt Mixtures', *Asphalt Paving Technology*, 71, pp. 176–206. Available at: http://144.171.11.39/view.aspx?id=698742 (Accessed: 25 November 2014).

Kim, Y., Little, D. N. and Lytton, R. L. (2003) 'Fatigue and Healing Characterization of Asphalt Mixtures', *Journal of Materials in Civil Engineering*, 15(1), pp. 75–83. doi: 10.1061/(ASCE)0899-1561(2003)15:1(75).

Kim, Y., Song, I. and Little, D. (2003) 'Use of Dynamic Mechanical Analysis to Predict Damage in Asphalt Mastic', *Proc., 11th Annual International Center for …*. Available at: http://aftre.nssga.org/Symposium/2003-10.pdf (Accessed: 19 February 2014).

Kittler, J. and Illingworth, J. (1986) 'Minimum error thresholding', *Pattern Recognition*, 19(1), pp. 41–47. doi: 10.1016/0031-3203(86)90030-0.

Kutay, E., Gibson, H. and Youtcheff, J. (2008) 'Use of Pseudistress and pseudostrain concepts for characterization of asphalt fatigue tests', *Mechanisms, Modeling, Detection, Testing and Case Histories Kutay*, 5(19), pp. 305–314. doi: 10.1201/9780203882191.

Kutay, E., Gibson, N. and Youtcheff, J. (2008) 'Conventional and Viscoelastic Continuum Damage (VECD)-Based Fatigue Analysis of Polymer Modified Asphalt Pavements', *Asphalt Paving Technology*, 77, pp. 395–433. Available at: http://trid.trb.org/view.aspx?id=890260 (Accessed: 17 May 2014).

Kutay, E., Gibson, N., Youtcheff, J. and Dongré, R. (2009) 'Use of Small Samples to Predict Fatigue Lives of Field Cores', *Transportation Research Record: Journal of the Transportation Research Board*, 2127, pp. 90–97. doi: 10.3141/2127-11.

Kutay, M. E. and Aydilek, A. H. (2010) 'Accuracy of the Two Common Semi-Analytical Equations in Predicting Asphalt Permeability', *Advances in X-ray Tomography for Geomaterials*, pp. 301–307. doi: 10.1002/9780470612187.ch30.

Lancaster, I. M. and Khalid, H. A. (2015) 'Viscoelastic continuum damage analysis of polymer modified asphalt in the cyclic semi-circular bending test', in *6th International Conference Bituminous Mixtures & Pavements*. Thessaloniki: Taylor & Francis Group, pp. 21–26.

Lee, H. and Kim, Y. (1998) 'Viscoelastic continuum damage model of asphalt concrete with healing', *Journal of Engineering Mechanics*, (Schapery 1990), pp. 1224–1232. Available at: http://ascelibrary.org/doi/abs/10.1061/(ASCE)0733-9399(1998)124:11(1224) (Accessed: 18 September 2014).

Liu, P. F., Zheng, J. and Wu, S. P. (2014) 'UV Aging Performance of Asphalt Containing LDHs', *Key Engineering Materials*, 599, pp. 265–270. doi: 10.4028/www.scientific.net/KEM.599.265.

Liu, Q., Schlangen, E. and Ven, M. (2012) 'Characterization of the material from the

induction healing porous asphalt concrete trial section', *Materials and Structures*, pp. 831–839. doi: 10.1617/s11527-012-9936-9.

Liu, T., Zhang, X., Li, Z. and Chen, Z. (2014) 'Research on the homogeneity of asphalt pavement quality using X-ray computed tomography (CT) and fractal theory', *Construction and Building Materials*. Elsevier Ltd, 68, pp. 587–598. doi: 10.1016/j.conbuildmat.2014.06.046.

Liu, X., Wu, S., Liu, G. and Li, L. (2015a) 'Effect of Ultraviolet Aging on Rheology and Chemistry of LDH-Modified Bitumen', *Materials*, 8(8), pp. 5238–5249. doi: 10.3390/ma8085238.

Liu, X., Wu, S., Liu, G. and Li, L. (2015b) 'Optical and UV-Aging Properties of LDH-Modified Bitumen', *Materials*, 8(7), pp. 4022–4033. doi: 10.3390/ma8074022.

Lukanen, E., Stubstad, R. and Briggs, R. (2000) *Temperature predictions and adjustment factors for asphalt pavement - Part A*. Available at: http://trid.trb.org/view.aspx?id=653890 (Accessed: 19 May 2014).

Luo, X. (2012) *Characterization of Fatigue Cracking and Healing of Asphalt Mixtures*. Texas A&M University. Available at: http://repository.tamu.edu/bitstream/handle/1969.1/ETD-TAMU-2012-05-10924/LUO-DISSERTATION.pdf?sequence=2&isAllowed=y (Accessed: 18 February 2015).

Luo, X., Ph, D., Luo, R., Asce, M., Lytton, R. L. and Asce, F. (2015) 'Energy-Based Crack Initiation Criterion for Viscoelastoplastic Materials with Distributed Cracks', pp. 1–14. doi: 10.1061/(ASCE)EM.1943-7889.0000830.

Manahiloh, K., Muhunthan, B., Kayhanian, M. and Gebremariam, S. (2012) 'X-Ray Computed Tomography and Nondestructive Evaluation of Clogging in Porous Concrete Field Samples', *Journal of Materials in Civil Engineering*. American Society of Civil Engineers, 24(8), pp. 1103–1109. doi: 10.1061/(ASCE)MT.1943-5533.0000484.

Martin, A. E., Arambula, E., Yin, F., Cucalon, L. G., Chowdhury, A., Lytton, R., Epps, J., Estakhri, C. and Park, E. S. (2014) *Evaluation of the Moisture Susceptibility of WMA Technologies, Transportation Research Board*. College Station, TX.

Masad, E., Castelo Branco, V. T. F., Little, D. N. and Lytton, R. (2006) *An Improved Method for the Dynamic Mechanical Analysis of Fatigue Failure of Sand Asphalt Mixtures, Federal Highway Administration*. Texas Transportation Institute, Texas A&M University (FHWA/473630).

Masad, E., Castelo Branco, V. T. F., Little, D. N. and Lytton, R. (2008) 'A unified method for the analysis of controlled-strain and controlled-stress fatigue testing', *International Journal of Pavement Engineering*, 9(4), pp. 233–246. doi: 10.1080/10298430701551219.

Masad, E., Huang, C., D'Angelo, J. and Little, D. (2009) 'Characterization of asphalt binder resistance to permanent deformation based on nonlinear viscoelastic analysis of multiple stress creep recovery (MSCR) test', in *Asphalt Paving Technology 2009, AAPT*. Minneapolis, United states: Association of Asphalt Paving Technologist, pp. 535–562. Available at: http://trid.trb.org/view.aspx?id=918744 (Accessed: 23 January 2014).

Masad, E., Jandhyala, V. K., Dasgupta, N., Somadevan, N. and Shashidhar, N. (2002) 'Characterization of Air Void Distribution in Asphalt Mixes using X-ray Computed Tomography', (May 2012), pp. 122–129.

Masad, E., Kassem, E. and Little, D. (2011) 'Characterization of Asphalt Pavement Materials in the State of Qatar: A Case Study', *Road Materials and Pavement …*, 12(4), pp. 739–765. doi: 10.3166/rmpd.12.739-765.

Masad, E. and Somadevan, N. (2002) 'Microstructural finite-element analysis of influence of localized strain distribution on asphalt mix properties', *Journal of engineering mechanics*, (October), pp. 1105–1114. Available at: http://ascelibrary.org/doi/abs/10.1061/(ASCE)0733-9399(2002)128:10(1106) (Accessed: 10 April 2014).

Menapace, I. and Masad, E. (2016) 'Evolution of the microstructure of unmodified and polymer modified asphalt binders with aging in an accelerated weathering tester', *Journal of Microscopy*, 0(0), pp. 1–16. doi: 10.1111/jmi.12405.

Menapace, I., Masad, E., Papavassiliou, G. and Kassem, E. (2015) 'Evaluation of Aging in Asphalt Cores at Room Temperature Using Low Field Nuclear Magnetic Resonance', in *6th International Conference on Bituminous Mixtures and Pavements*. Thessaloniki.

Mogawer, W., Austerman, A., Mohammad, L. and Kutay, M. E. (2013) 'Evaluation of high RAP-WMA asphalt rubber mixtures', *Road Materials and Pavement Design*, 14(sup2), pp. 129–147. doi: 10.1080/14680629.2013.812846.

Moghadas Nejad, F., Azarhoosh, A., Hamedi, G. H. and Roshani, H. (2014) 'Rutting performance prediction of warm mix asphalt containing reclaimed asphalt pavements', *Road Materials and Pavement Design*. Taylor & Francis, 15(1), pp. 207–219.

Mohseni, A., Carpenter, S., D'Angelo, J., McGennis, R. B., Rowe, G., Monismith, C., Dunning, R. and Coulter, M. (2005) 'Development of SUPERPAVE High-Temperature Performance Grade (PG) Based on Rutting Damage', in *Asphalt Paving Technology: Association of Asphalt Paving Technologists*. Long Beach, CA, United states: Association of Asphalt Paving Technologist, pp. 197–253.

Molenaar, A. A. A. (1983) *Structural performance and design of flexible road constructions and asphalt concrete overlays*. Delft University of Technology.

Monismith, C. L., Epps, J. A. and Finn, F. N. (1985) 'Improved Asphalt Mix Design', in *Asphalt Paving Technology*. San Antonio, Texas, pp. 347–406.

Montepara, A. and Giuliani, F. (2000) 'PERFORMANCE TESTING AND SPECIFICATIONS FOR BINDER AND MIX. COMPARISON BETWEEN AGEING SIMULATION TESTS OF ROAD BITUMEN', in *PROCEEDINGS OF THE PAPERS SUBMITTED FOR REVIEW AT 2ND EURASPHALT AND EUROBITUME CONGRESS, HELD 20-22 SEPTEMBER 2000, BARCELONA, SPAIN. BOOK 1-SESSION 1*.

Montepara, A., Santagata, E. and Tosi, G. (1996) 'Photochemical degradation of pure bitumen by UV radiation', in *EURASPHALT & EUROBITUME CONGRESS, STRASBOURG, 7-10 MAY 1996. VOLUME 3. PAPER E&E. 5.133*.

Mouillet, V., Farcas, F., Chailleux, E. and Sauger, L. (2014) 'Evolution of bituminous

mix behaviour submitted to UV rays in laboratory compared to field exposure', *Materials and Structures*, pp. 1287–1299. doi: 10.1617/s11527-014-0258-y.

National Center for Asphalt Technology (2005) 'NCAT evaluates warm mix asphalt', *National Center for Asphalt Technology, Auburn University*, pp. 1–16.

Newcomb, D. E., Arambula, E., Yin, F., Zhang, J., Bhasin, A., Li, W. and Arega, Z. (2015) *REPORT 807: Properties of Foamed Asphalt for Warm Mix Asphalt Applications*. WASHINGTON, D.C.

Pacheco, J. E. L., Bavastri, C. A. and Pereira, J. T. (2015) 'Viscoelastic relaxation modulus characterization using Prony series', *Latin American Journal of Solids and Structures*, 12(2), pp. 420–445. doi: 10.1590/1679-78251412.

Pang, L., Jiang, H., Wu, S. S. and Wu, S. S. (2012) 'Self healing capacity of asphalt binders', *Journal Wuhan University of Technology, Materials Science Edition*, 27(4), pp. 794–796. doi: 10.1007/s11595-012-0550-z.

Pang, L., Wan, L., Wu, S. P. and Lu, L. (2011) 'Effect of UV aging on the rheological properties of asphalt mortar', in *Advances in Heterogeneous Material Mechanics*. Shanghai, China, pp. 539–542.

Park, S. W. and Schapery, R. a. (1999) 'Methods of interconversion between linear viscoelastic material functions. Part I—a numerical method based on Prony series', *International Journal of Solids and Structures*, 36(11), pp. 1653–1675. doi: 10.1016/S0020-7683(98)00055-9.

Pauls, J. T. and Welborn, J. Y. (1952) 'Studies of the hardening properties of asphaltic materials', in *Assoc Asphalt Paving Technol Proc*.

Pavement Interactive (2015) *Pressure Aging Vessel*. Available at: http://www.pavementinteractive.org/article/pressure-aging-vessel/.

Petersen, J. C., Barbaar, F. A. and Dorrence, S. M. (1974) 'Catalysis of asphalt oxidation by mineral aggregate surfaces and asphalt components', in *Association of Asphalt Paving Technologists Proc*.

PQ Corporation (2014) *Advera Warm mix asphalt*. Available at: http://www.adverawma.com/wma.html.

Pronk, A. C. (2006) 'Partial Healing: A New Approach for the Damage Process during Fatigue Testing of Asphalt Specimen', in *GEOTECHNICAL SPECIAL PUBLICATION*. Baton Rouge, LA, United states: American Society of Civil Engineers, pp. 83–94. doi: 10.1061/40825(185)9.

Public Works Authority (2017) *The Expressway Programme*. Available at: http://www.ashghal.gov.qa/en/Projects/Pages/The-Expressway-Programme.aspx (Accessed: 1 August 2017).

Q-Lab Corporation (2012) *Accelerated Weathering Machine - Technical Manual*.

Qiu, J. (2012) *Self Healing of Asphalt Mixtures*. Delft University of Technology.

Rahimzadeh, B. (2002) *Linear and Non-Linear Viscoelastic Behaviour of Binders and Asphalts*. University of Nottingham.

Rana, N., Rawat, D., Parmar, M., Dhawan, D. K., Bhati, A. K. and Mittal, B. R. (2015)

‘Evaluation of external beam hardening filters on image quality of computed tomography and single photon emission computed tomography/computed tomography’, *Journal of Medical Physics / Association of Medical Physicists of India*. India: Medknow Publications & Media Pvt Ltd, 40(4), pp. 198–206. doi: 10.4103/0971-6203.170790.

Al Raya newspaper (2010) ‘23 ,’خلطة إسفلتية باردة لصيانة حفر الشوارع June. Available at: http://www.raya.com/news/pages/4c3d0fbb-4f07-4e11-801d-3826cb0ed2de.

Sadek, H. A. S. (2015) *Mechanistic-Based Characterisation of Fatigue Resistance of Alternative Mix Designs*. University of Liverpool.

Sadeq, M., Masad, E., Al-Khalid, H. and Sirin, O. (2015) ‘Assessment of linear and nonlinear viscoelastic responses of warm-mix asphalt binders’, in *6th International Conference Bituminous Mixtures & Pavements*. Ancona, Italy: Taylor & Francis Group, London, pp. 27–32.

Sadeq, M., Masad, E., Al-Khalid, H., Sirin, O. and Little, D. (2016) ‘Rheological Evaluation of Short- and Long-Term Performance for Warm Mix Asphalt (WMA) Binders’, in Canestrari, F. and Partl, M. N. (eds) *8th RILEM International Symposium on Testing and Characterization of Sustainable and Innovative Bituminous Materials SE - 11*. Springer Netherlands (RILEM Bookseries), pp. 129–139. doi: 10.1007/978-94-017-7342-3_11.

Safaei, F., Lee, J., Nascimento, L. A. H. Do, Hintz, C. and Kim, Y. R. (2014) ‘Implications of warm-mix asphalt on long-term oxidative ageing and fatigue performance of asphalt binders and mixtures’, *Road Materials and Pavement Design*, 15(sup1), pp. 45–61. doi: 10.1080/14680629.2014.927050.

Sasol (2014) *Recommended Dosage of Sasobit®*.

Sasol Wax (2014) *Sasobit - Sasolwax US*. Available at: http://www.sasolwax.us.com/.

Schapery, R. (1969) ‘On the characterization of nonlinear viscoelastic materials’, *Polymer Engineering & Science*, 9(4), pp. 295–310. Available at: http://onlinelibrary.wiley.com/doi/10.1002/pen.760090410/abstract (Accessed: 9 February 2014).

Schapery, R. (1987) ‘Deformation and fracture characterization of inelastic composite materials using potentials’, *Polymer Engineering & Science*, (7). Available at: http://onlinelibrary.wiley.com/doi/10.1002/pen.760270110/abstract (Accessed: 18 September 2014).

Schapery, R. A. (1981) ‘Nonlinear Fracture Analysis of Viscoelastic Composite Materials Based on a Generalized J Integral Theory’, in *Proceedings Japan-U.S.* Tokyo, Japan. Scott: Conference on Composite Materials.

Schapery, R. A. (1984) ‘Correspondence principles and a generalized J integral for large deformation and fracture analysis of viscoelastic media’, *International Journal of Fracture*, 25(3), pp. 195–223. doi: 10.1007/BF01140837.

Scholz, T. V (1995) *Durability of Bitumenous Paving Mixtures*. University of Nottingham.

Shaheen, M., Al-Mayah, A. and Tighe, S. (2016) ‘A novel method for evaluating hot mix asphalt fatigue damage: X-ray computed tomography’, *Construction and Building*

Materials. Elsevier Ltd, 113, pp. 121–133. doi: 10.1016/j.conbuildmat.2016.03.030.

Shan, L., Tan, Y. and Richard Kim, Y. (2013) 'Establishment of a universal healing evaluation index for asphalt binder', *Construction and Building Materials*. Elsevier Ltd, 48, pp. 74–79. doi: 10.1016/j.conbuildmat.2013.06.039.

Shen, S. and Carpenter, S. H. (2007) *Dissipated Energy Concepts for HMA Performance: Fatigue and Healing*.

Shen, S., Chiu, H.-M. and Huang, H. (2010) 'Characterization of Fatigue and Healing in Asphalt Binders', *Journal of Materials in Civil Engineering*, 22(September), pp. 846–852. doi: 10.1061/(ASCE)MT.1943-5533.0000080.

Shirodkar, P., Mehta, Y., Nolan, A., Dahm, K., Dusseau, R. and McCarthy, L. (2012) 'Characterization of creep and recovery curve of polymer modified binder', *Construction and Building Materials*. Elsevier Ltd, 34, pp. 504–511. doi: 10.1016/j.conbuildmat.2012.02.018.

Solar Journey USA (2016) *How Solar Works 1: Sunlight*. Available at: http://solarjourneyusa.com/sunlight.php (Accessed: 6 January 2017).

Solargis (2016) *Global horizontal irradiation (GHI), GeoModel Solar*. Available at: http://solargis.info/doc/free-solar-radiation-maps-GHI#Q (Accessed: 20 June 2002).

Sorvari, J. and Hämäläinen, J. (2010) 'Time integration in linear viscoelasticity—a comparative study', *Mechanics of Time-Dependent Materials*, 14(3), pp. 307–328. doi: 10.1007/s11043-010-9108-7.

Sorvari, J. and Malinen, M. (2007) 'On the direct estimation of creep and relaxation functions', *Mechanics of Time-Dependent Materials*, 11(2), pp. 143–157. doi: 10.1007/s11043-007-9038-1.

Sousa, P., Kassem, E., Masad, E. and Little, D. N. (2011) 'New Design Method of Fine Aggregate Mixtures and Automated Method for Analysis of Dynamic Mechanical Analysis Data', *Presented at the Annual Meeting of the Transportation Research Board*.

Steven, B. (2009) 'Friction Testing of Pavement Preservation Treatments: Temperature Corrections and Operator/Machine Variability', (April). Available at: http://trid.trb.org/view.aspx?id=1127098 (Accessed: 11 July 2013).

Stuart, K. D., Mogawer, W. S. and Romero, P. (1999) 'Validation of asphalt binder and mixture tests that measure rutting susceptibility using the accelerated loading facility', *Rep. No. FHWA-RD-99-204*, (November). Available at: http://trid.trb.org/view.aspx?id=690565.

SUGA Test Instruments (2011) *GX75*.

Tan, Y., Shan, L., Richard Kim, Y. and Underwood, B. S. (2012) 'Healing characteristics of asphalt binder', *Construction and Building Materials*. Elsevier Ltd, 27(1), pp. 570–577. doi: 10.1016/j.conbuildmat.2011.07.006.

Taniguchi, S., Nishizaki, I., Ogawa, K. and Otani, J. (2012) 'New X-ray ct evaluation method of engineering characteristics of asphalt mixture', *Advances in Transportation Geotechnics II*, pp. 400–406.

Taniguchi, S., Otani, J. and Kumagai, M. (2014) ‘A study on characteristics evaluation to control quality of asphalt mixture using X-ray CT’, *Road Materials and Pavement Design*, 15(4), pp. 892–910. doi: 10.1080/14680629.2014.944204.

Teoh, S. H., Chuan, C. L. and Poo, A. N. (1987) ‘Application of a modified strain transient dip test in the determination of the internal stresses of PVC under tension’, *Journal of Materials Science*, 22(4), pp. 1397–1404. doi: 10.1007/BF01233140.

The Green Construction Board (2016) *Infrastructure Carbon Review*. Available at: http://www.greenconstructionboard.org/index.php/resources/infrastructure (Accessed: 1 May 2016).

Tia, M., Ruth, B. E., Charai, C. T., Shiau, J. M., Richardson, D. and Williams, J. (1988) ‘Investigation of original and in-service asphalt properties for the development of improved specifications-Final phase of testing and analysis’, *Final Report, Engineering and Industrial Experiment Station, University of Florida, Gainesville, FL*.

TIBCO Spotfire (2015) *What is Binning?* Available at: https://docs.tibco.com/pub/spotfire/7.0.1/doc/html//bin/bin_what_is_binning.htm (Accessed: 20 June 2008).

Tolley, G. and Yue, S. (2016) *Beam hardening – What is it and how to reduce it?*, *North Star Imaging Inc.* Available at: http://4nsi.com/blog/2016/02/12/beam-hardening/ (Accessed: 2 March 2017).

ttv gmbh (2017) *Optical Filters*. Available at: https://www.go-ttv.com/optical-filters/ (Accessed: 27 March 2017).

Tzikang, C. (2000) ‘Determining a Prony Series for a Viscoelastic Material From Time Varying Strain Data’, *Nasa*, (May).

Underwood, B. (2011) *Multiscale Constitutive Modeling of Asphalt Concrete*. Available at: http://adsabs.harvard.edu/abs/2011PhDT14U (Accessed: 25 August 2013).

Underwood, B. S., Baek, C. and Kim, Y. R. (2012) ‘Simplified Viscoelastic Continuum Damage Model as Platform for Asphalt Concrete Fatigue Analysis’, *Transportation Research Record: Journal of the Transportation Research Board*, 2296(1), pp. 36–45. doi: 10.3141/2296-04.

Vaiana, R., Iuele, T. and Gallelli, V. (2013) ‘Warm Mix Asphalt with Synthetic Zeolite: a Laboratory Study on Mixes Workability.’, *International Journal of Pavement Research and Technology*, 6(5), pp. 562–569. Available at: http://search.ebscohost.com/login.aspx?direct=true&profile=ehost&scope=site&authtype=crawler&jrnl=19971400&AN=90253259&h=GYzDJozqTI4qpflMKyoosa8Twf6rlsU5z9N97z8w50tkWmBfsYCB9JHAXbbQlxwIUnRjyB39qVL%2FDU91kTV2sw%3D%3D&crl=c (Accessed: 14 January 2014).

Wang, L. B., Frost, J. D., Voyiadjis, G. Z. and Harman, T. P. (2003) ‘Quantification of damage parameters using X-ray tomography images’, *Mechanics of Materials*, 35(8), pp. 777–790. doi: 10.1016/S0167-6636(02)00206-5.

Weather Underground (2014) *Weather History for Doha, Qatar*, *Weather History for Doha*. Available at: http://www.wunderground.com/.

Worldtravelguide.net (2015) *Qatar Weather, climate and geography*. Available at: http://www.worldtravelguide.net/qatar/weather-climate-geography.

Wu, J. (2009) *The influence of mineral aggregates and binder volumetrics on bitumen ageing*. University of Nottingham.

Wu, S. P., Zhu, G. J., Liu, G. and Pang, L. (2009) 'Laboratory Research on Thermal Behavior and Charac- Terization of the Ultraviolet Aged Asphalt Binder', 95, pp. 595–599.

Xiao, F. and Amirkhanian, S. N. (2010) 'Effects of liquid antistrip additives on rheology and moisture susceptibility of water bearing warm mixtures', *Construction and Building Materials*. Elsevier Ltd, 24(9), pp. 1649–1655. doi: 10.1016/j.conbuildmat.2010.02.027.

Xiao, F., Newton, D., Putman, B., Punith, V. S. and Amirkhanian, S. N. (2013) 'A long-term ultraviolet aging procedure on foamed WMA mixtures', *Materials and Structures*, 46(12), pp. 1987–2001. doi: 10.1617/s11527-013-0031-7.

Xie, Z., Fan, W., Wang, L. and Shen, J. (2013) 'The Effectiviness of Warm Mix Asphalt (WMA) Additives Affected by The Type of Aggregate and Binder.', *International Journal of …*, 6(5), pp. 554–561.

Xradia Inc. (2010) *MicroXCT-200 and MicroXCT-400 User's Guide*. Concord, USA. Available at: http://www.xradia.com/products/support.php.

ZEISS Group (2015) *Technical Procedure : Vertical Stitching*. Oberkochen, Germany. Available at: www.zeiss.com.

Zelelew, H. M. and Papagiannakis, A. T. (2011) 'A volumetrics thresholding algorithm for processing asphalt concrete X-ray CT images', *International Journal of Pavement Engineering*, 12(6), pp. 543–551. doi: 10.1080/10298436.2011.561345.

Zelelew, H., Paugh, C., Corrigan, M., Belagutti, S. and Ramakrishnareddy, J. (2013) 'Laboratory evaluation of the mechanical properties of plant-produced warm-mix asphalt mixtures', *Road Materials and Pavement Design*, 14(1), pp. 49–70. doi: 10.1080/14680629.2012.735799.

Zeng, W., Wu, S., Wen, J. and Chen, Z. (2015) 'The temperature effects in aging index of asphalt during UV aging process', *Construction and Building Materials*. Elsevier Ltd, 93, pp. 1125–1131. doi: 10.1016/j.conbuildmat.2015.05.022.

Zollinger, C. (2005) *Application of surface energy measurements to evaluate moisture susceptibility of asphalt and aggregates*. Texas A&M University. Available at: http://repository.tamu.edu/handle/1969.1/2320 (Accessed: 24 February 2014).

Appendices

Appendix A

Repeated creep and recovery test program for all cycles

Cycle 1			Cycle 2			…	Cycle 9		
Loading Type	**Stress (%)**	**Time (sec)**	**Loading Type**	**Stress (%)**	**Time (sec)**	**…**	**Loading Type**	**Stress (%)**	**Time (sec)**
Loading	100	40	Loading	100	40	…	Loading	100	40
Unloading	0	1	Unloading	0	1	…	Unloading	0	1
Step-Load 1.1.1	1	2	Step-Load 2.1.1	0.9	2	…	Step-Load 9.1.1	0.2	2
Step-Load 1.1.2	20	2	Step-Load 2.1.2	18	2	…	Step-Load 9.1.2	4	2
Step-Load 1.1.3	50	2	Step-Load 2.1.3	45	2	…	Step-Load 9.1.3	10	2
Unloading	0	4	Unloading	0	5	…	Unloading	0	19
Step-Load 1.2.1	1	2	Step-Load 2.2.1	0.9	2	…	Step-Load 9.2.1	0.2	2
Step-Load 1.2.2	20	2	Step-Load 2.2.2	18	2	…	Step-Load 9.2.2	4	2
Step-Load 1.2.3	50	2	Step-Load 2.2.3	45	2	…	Step-Load 9.2.3	10	2
Unloading	0	6	Unloading	0	9	…	Unloading	0	35
Step-Load 1.3.1	1	2	Step-Load 2.3.1	0.9	2	…	Step-Load 9.3.1	0.2	2
Step-Load 1.3.2	20	2	Step-Load 2.3.2	18	2	…	Step-Load 9.3.2	4	2
Step-Load 1.3.3	50	2	Step-Load 2.3.3	45	2	…	Step-Load 9.3.3	10	2
Unloading	0	10	Unloading	0	12	…	Unloading	0	50
Step-Load 1.4.1	1	2	Step-Load 2.4.1	0.9	2	…	Step-Load 9.4.1	0.2	2
Step-Load 1.4.2	20	2	Step-Load 2.4.2	18	2	…	Step-Load 9.4.2	4	2
Step-Load 1.4.3	50	2	Step-Load 2.4.3	45	2	…	Step-Load 9.4.3	10	2
Unloading	0	14	Unloading	0	18	…	Unloading	0	70
Step-Load 1.5.1	1	2	Step-Load 2.5.1	0.9	2	…	Step-Load 9.5.1	0.2	2
Step-Load 1.5.2	20	2	Step-Load 2.5.2	18	2	…	Step-Load 9.5.2	4	2
Step-Load 1.5.3	50	2	Step-Load 2.5.3	45	2	…	Step-Load 9.5.3	10	2
Unloading	0	20	Unloading	0	25	…	Unloading	0	95

Appendix B

Prony Series Parameters for all mixes

D_n

Original Mix

λ_n	0 hrs			312 hrs			600 hrs			936 hrs			2455 hrs		
	Repl. 1	Repl. 2	Repl. 3	Repl. 1	Repl. 2	Repl. 3	Repl. 1	Repl. 2	Repl. 3	Repl. 1	Repl. 2	Repl. 3	Repl. 1	Repl. 2	Repl. 3
0.01	7.34E-06	1.09E-05	6.96E-06	6.88E-06	3.80E-06	3.84E-06	6.21E-06	6.02E-06	6.65E-06	3.53E-06	5.07E-06	5.26E-06	1.83E-06	3.48E-06	2.38E-06
0.1	1.48E-06	2.01E-06	2.08E-06	1.60E-06	1.50E-06	1.42E-06	1.78E-06	1.84E-06	1.86E-06	2.98E-07	1.19E-06	1.04E-06	7.19E-07	9.14E-07	8.48E-07
1	3.48E-07	4.05E-07	5.13E-07	4.51E-07	4.24E-07	7.14E-07	4.38E-07	5.27E-07	4.16E-07	6.75E-07	4.71E-07	5.89E-07	5.41E-07	2.45E-07	2.27E-07
10	5.50E-07	7.20E-07	6.29E-07	5.89E-07	5.25E-07	3.66E-07	6.26E-07	6.02E-07	6.76E-07	9.96E-08	3.99E-07	3.24E-07	2.38E-07	3.80E-07	3.96E-07
500	2.18E-12	2.48E-12	2.22E-14	6.40E-08	1.15E-12	2.44E-07	7.61E-13	5.02E-13	3.23E-13	1.96E-08	6.74E-12	1.25E-07	1.09E-07	8.73E-08	7.59E-13
1000	2.80E-07	2.43E-07	4.45E-07	2.22E-14	3.71E-07	2.25E-07	3.46E-07	4.98E-07	4.85E-07	4.09E-14	3.88E-07	5.26E-12	3.18E-14	2.22E-14	3.39E-07
10000	9.82E-08	1.08E-07	4.34E-08	3.55E-14	5.55E-08	4.24E-08	7.64E-08	1.80E-08	1.45E-08	1.60E-11	1.91E-07	1.84E-07	3.39E-07	2.11E-08	4.05E-08
100000	9.65E-08	1.07E-07	2.24E-11	1.65E-07	5.47E-08	2.22E-14	7.42E-08	1.75E-08	1.37E-08	3.12E-07	1.89E-07	1.84E-07	2.22E-14	7.59E-08	3.95E-08

Sasobit Mix

λ_n	0 hrs			312 hrs			600 hrs			936 hrs			2455 hrs		
	Repl. 1	Repl. 2	Repl. 3	Repl. 1	Repl. 2	Repl. 3	Repl. 1	Repl. 2	Repl. 3	Repl. 1	Repl. 2	Repl. 3	Repl. 1	Repl. 2	Repl. 3
0.01	4.23E-06	4.85E-06	2.17E-06	2.31E-06	4.04E-06	3.25E-06	3.20E-07	2.00E-12	2.80E-06	2.66E-06	1.62E-06	2.93E-06	1.04E-06	1.56E-06	2.00E-06
0.1	9.92E-07	1.18E-06	8.97E-07	8.81E-07	1.50E-09	9.51E-07	1.21E-09	2.92E-14	1.01E-06	9.41E-07	5.41E-07	8.10E-07	3.39E-07	6.32E-07	6.41E-07
1	2.46E-07	2.91E-07	2.51E-07	2.64E-07	1.72E-11	2.64E-07	2.65E-08	1.22E-07	2.79E-07	2.47E-07	4.55E-07	2.27E-07	3.34E-07	2.02E-07	2.07E-07
10	3.78E-07	4.39E-07	3.61E-07	3.40E-07	1.48E-07	3.66E-07	5.96E-08	8.52E-08	3.69E-07	3.78E-07	1.89E-07	3.25E-07	1.07E-07	2.66E-07	2.91E-07
500	2.00E-12	2.22E-14	2.22E-14	4.27E-09	8.21E-08	1.85E-12	1.84E-12	1.25E-12	2.22E-14	2.58E-12	1.29E-07	8.84E-09	6.72E-08	2.22E-14	2.72E-08
1000	2.42E-07	4.16E-07	3.01E-07	3.50E-07	3.24E-14	2.37E-07	1.29E-07	2.16E-07	3.15E-07	2.28E-07	2.09E-12	3.60E-07	2.22E-14	3.51E-07	2.78E-07
10000	9.18E-08	2.52E-08	5.61E-08	6.08E-08	1.31E-07	8.45E-08	9.08E-08	6.27E-08	5.41E-08	8.56E-08	1.85E-07	5.22E-08	2.21E-07	5.23E-08	1.05E-07
100000	9.04E-08	6.16E-11	5.54E-08	1.34E-11	1.31E-07	8.41E-08	9.06E-08	6.22E-08	5.33E-08	8.51E-08	1.85E-07	2.39E-11	2.78E-10	9.00E-12	7.19E-12

Advera Mix

λ_n	0 hrs			312 hrs			600 hrs			936 hrs			2455 hrs		
	Repl. 1	Repl. 2	Repl. 3	Repl. 1	Repl. 2	Repl. 3	Repl. 1	Repl. 2	Repl. 3	Repl. 1	Repl. 2	Repl. 3	Repl. 1	Repl. 2	Repl. 3
0.01	6.46E-06	4.72E-06	4.32E-06	2.27E-14	3.16E-06	4.10E-06	5.08E-06	5.36E-06	N/A	3.41E-06	2.21E-06	2.73E-06	2.81E-06	1.42E-06	2.07E-06
0.1	1.34E-06	1.48E-06	1.42E-06	2.22E-14	1.03E-06	1.07E-06	1.03E-06	9.97E-07	N/A	1.00E-06	8.54E-07	7.34E-07	7.14E-07	5.87E-07	7.95E-07
1	3.12E-07	7.15E-07	3.57E-07	2.28E-14	2.58E-07	2.77E-07	3.27E-07	5.57E-07	N/A	2.76E-07	1.18E-07	2.00E-07	1.96E-07	5.76E-07	2.56E-07
10	4.62E-07	3.18E-07	4.70E-07	5.09E-08	4.29E-07	4.28E-07	3.49E-07	2.79E-07	N/A	3.88E-07	3.89E-07	3.23E-07	3.15E-07	1.49E-07	2.96E-07
500	3.93E-13	1.38E-07	2.22E-14	4.44E-14	1.34E-12	7.73E-13	1.68E-11	2.74E-08	N/A	6.76E-13	2.77E-12	2.22E-14	2.74E-13	2.02E-07	4.42E-14
1000	1.49E-07	2.96E-07	3.52E-07	3.61E-07	3.21E-07	2.50E-07	2.79E-07	4.37E-07	N/A	2.19E-07	1.84E-07	2.78E-07	1.74E-07	2.22E-14	5.17E-07
10000	8.59E-08	6.28E-08	5.25E-08	5.81E-10	7.16E-08	7.07E-08	3.10E-07	4.91E-09	N/A	9.18E-08	1.10E-07	4.99E-08	9.59E-08	2.98E-14	2.24E-14
100000	8.56E-08	2.25E-14	8.36E-11	5.00E-10	7.08E-08	7.02E-08	2.22E-14	3.88E-14	N/A	9.08E-08	1.09E-07	4.93E-08	9.56E-08	3.01E-14	2.22E-14

Rediset Mix

λ_n	0 hrs			312 hrs			600 hrs			936 hrs			2455 hrs		
	Repl. 1	Repl. 2	Repl. 3	Repl. 1	Repl. 2	Repl. 3	Repl. 1	Repl. 2	Repl. 3	Repl. 1	Repl. 2	Repl. 3	Repl. 1	Repl. 2	Repl. 3
0.01	5.44E-06	8.34E-06	8.53E-06	5.48E-06	5.92E-06	5.94E-06	7.08E-06	7.28E-06	7.31E-06	8.61E-06	6.47E-06	5.20E-06	3.12E-06	4.18E-06	4.06E-06
0.1	1.57E-06	2.32E-06	2.44E-06	1.25E-06	1.53E-06	1.03E-06	1.38E-06	1.85E-06	1.84E-06	5.36E-07	1.70E-06	1.50E-06	9.60E-07	1.03E-06	1.34E-06
1	8.77E-07	5.91E-07	5.11E-07	6.70E-07	3.64E-07	8.36E-07	3.32E-07	4.30E-07	4.58E-07	1.33E-07	3.84E-07	3.99E-07	3.74E-07	2.92E-07	3.54E-07
10	2.97E-07	6.19E-07	6.43E-07	3.43E-07	5.19E-07	2.61E-07	5.37E-07	5.98E-07	6.57E-07	2.66E-07	5.47E-07	5.24E-07	3.59E-07	3.87E-07	4.11E-07
500	3.37E-07	2.22E-14	6.17E-13	6.93E-08	1.21E-12	3.49E-07	2.78E-12	1.79E-12	2.22E-14	1.12E-12	2.06E-12	1.45E-12	2.25E-14	6.80E-13	7.28E-08
1000	6.66E-08	4.47E-07	3.18E-07	3.98E-07	3.00E-07	1.50E-07	2.41E-07	2.41E-07	3.06E-07	1.73E-07	2.30E-07	3.31E-07	4.07E-07	2.82E-07	5.88E-12
10000	9.22E-08	4.40E-08	6.26E-08	8.74E-09	6.74E-08	8.00E-08	1.09E-07	8.97E-08	7.32E-08	8.39E-08	9.36E-08	6.59E-08	2.53E-08	6.20E-08	1.01E-07
100000	2.22E-14	2.81E-11	6.07E-08	2.22E-14	6.67E-08	2.22E-14	1.07E-07	8.91E-08	7.14E-08	8.33E-08	9.30E-08	6.51E-08	1.19E-11	6.14E-08	1.01E-07

Appendix C

MATLAB code for X-Ray CT image processing

```
clear all; close all; clc

% To read all images together

tic


% testing files

AAfld={'~\Pure\P2-A4-0Hr-13','~\Pure\P3-A1-0Hr-25','~\Pure\P2-A9-
2472Hr-21','Pure\P3-C1-2472Hr-36','~\Sasobit\S1-A3-0Hr-
38','~\Sasobit\S2-A9-0Hr-63','~\Sasobit\S2-A7-2472Hr-
61','Sasobit\S2-A8-2472Hr-62','~\Advera\A1-A3-0Hr-
74','~\Advera\A2-A9-0Hr-99','~\Advera\A2-A7-2472Hr-97','Advera\A2-
A8-2472Hr-98','~\Rediset\R1-A3-0Hr-110','~\Rediset\R2-A9-0Hr-
135','~\Rediset\R2-A7-2472Hr-133','Rediset\R2-A8-2472Hr-134'};


no_files=length(AAfld);


for F=1:no_files
    close all; clc
    Afld=AAfld{1,F};



    for i=1:2
          if i==1
              fld=[Afld '\Untested\'];
          elseif i==2
              fld=[Afld '\Tested\'];
          end
          srcFiles=dir(fullfile(fld, '*.tiff'));
          fld


    Q=150; % Number of removed slices from the analysis



    for h=Q+1:length(srcFiles)-Q;
```

```
    file_n= strcat(fld,srcFiles(h).name);
          IR=imread(file_n);


    IR=double(IR);


%%%%%%%%%%%%%%%%%%%% Calculate a multi threshold values for the
image.
    [level,metric] = multithresh(IR,20);
    IR = imquantize(IR,level);


    [ T J]=kittlerMinimimErrorThresholding(IR);
     IR1=IR<T;
     bw=bwlabel(IR1); % This is to label each void in the image
     s=regionprops(bw,'all'); % This to get all properties of the
voids


     areas  = cat(1,s.Area); % This is to specify the area from
the properties
     areas1{h-Q,1}=areas(areas<500)*0.000415285; % This to
separate the area from the outer area by size
     AREA(h-Q,1)=(sum(areas1{h-Q,1})./113.1).*100; %Percentage of
Air Voids




     end


    %AREA'
    Fcolor=['y','none'];
    Ecolor(1)='k';
    Ecolor(2)='r';
    LS(1)='-';
    LS(2)=':';
    figure(1)
    X=[1:length(AREA(:))]';
    Y=AREA(:);

area(X,Y,'FaceColor',Fcolor(i),'LineStyle',LS(i),'LineWidth',2,'Ed
geColor',Ecolor(i));
```

```
    %view(90,90)
    ylabel(' Air Void (%)','FontName','Times New
Roman','FontSize',12)
    xlabel('Slice number','FontName','Times New
Roman','FontSize',12)
    set(gca,'FontName','Times New Roman','fontsize',12)
    hleg1=legend('Before Testing','After Testing');
    set(hleg1,'FontName','Times New Roman','FontSize',12);
    set(hleg1,'Location','Best')
    saveas(figure(1),fullfile(Afld,'Area.fig'));
    hold all


    % --- Create a histogram, pdf and cdf of the results
    color(1)='k';
    color(2)='r';
    xbins=0:0.01:1.5;
    [nelements,centers] = hist(AREA,xbins); % 50 bins
    figure (2) % Histogram
    bar(centers,nelements,color(i),'EdgeColor','k')
    xlabel('Air Voids (%)','FontName','Times New
Roman','FontSize',12)
    grid on
    box on
    saveas(figure(2),fullfile(Afld,'hist.fig'));
    hold all


    figure(3)
    [f,x] = ecdf(AREA);
    r=['-',':'];
    plot(x,f,r(i),'LineWidth',2,'Color',[0 0 0]);
    xlabel('Air Voids (%)','FontName','Times New
Roman','FontSize',12)
    set(gca,'FontName','Times New Roman','fontsize',12)
    ylabel('cdf','FontName','Times New Roman','FontSize',12)
    hleg1 = legend('Before Testing','After Testing');
    set(hleg1,'FontName','Times New Roman','FontSize',12);
    set(hleg1,'Location','Best');
```

```
    %set(gca,'xscale','log');
    saveas(figure(4),fullfile(Afld,'cdf.fig'));
    grid on
    box on
    hold all



        if i==1
            Quantile_BT = quantile(x,[.25 .50 .75]);
            filename=([Afld '\Quantile_BT']);
            save(filename,'Quantile_BT')
            AV_BT.mean = mean(AREA);
            AV_BT.std = std(AREA);
            AV_BT.median = median(AREA);
            filename=([Afld '\AV_BT']);
            save(filename,'AV_BT')
        elseif i==2
            Quantile_AT = quantile(x,[.25 .50 .75]);
            filename=([Afld '\Quantile_AT']);
            save(filename,'Quantile_AT')
            AV_AT.mean = mean(AREA);
            AV_AT.std = std(AREA);
            AV_AT.median = median(AREA);
            filename=([Afld '\AV_AT']);
            save(filename,'AV_AT')
        end



    end

end
toc
close all
```